College of Aeronautics Report No.9606
March 1996

Conceptual design synthesis and optimization for new generations of combat aircraft

F.Siegers

ISBN 1 871564 875

£10

The investigation which is the subject of this report was carried out under the terms of Contract ASF/2150/U for the Research Manager, Air Vehicle Performance Department, Defence Research Agency, Pyestock

College of Aeronautics
Cranfield University
Cranfield
Bedford MK43 0AL
England

I. ABSTRACT

A numerical design synthesis methodology for new generations of combat aircraft has been developed. It incorporates advanced technology in the form of design for low observables. Aircraft capable of being modelled with this methodology will have internal or external weapons carriage, side mounted intakes, a straight-tapered trapezoidal wing, aft-mounted tail with the option of single or twin fins, and one or two engines with rectangular or axisymmetric nozzles. The design methodology incorporates sufficiently accurate and realistic algorithms for the calculation of the geometry and the estimation of the aerodynamic, mass and performance properties of the aircraft. The inherent flexibility of the design permits the examination of a wide range of configurations whilst maintaining the accuracy required to examine minor changes in the design requirements. A numerical optimization routine was linked to the synthesis, allowing the determination of optimum aircraft design variables for a given set of mission and performance requirements. Results were obtained showing the usefulness of this design tool for setting up parametric trend studies. The numerical accuracy, flexibility of configuration options and high level of advanced aircraft technology of this synthesis make a significant contribution to the continuing development of automated design tools.

II. ACKNOWLEDGEMENT

The author wishes to thank the United Kingdom Defence Research Agency for its financial support of this investigation, which was performed in part under the terms of Contract ASF/2150/U for Research Manager, Air Vehicle Performance Department, DRA Pyestock.

III. Table of Contents

IV. List of Figures

V. LIST OF TABLES

VI. NOTATION AND LIST OF VARIABLES

Variable	Description	type[1]
AEFN	Fin aspect ratio	ev
AETN	Aspect ratio of net tailplane	ev
AII	Aspect ratio of intake	ev
AIX	Aspect ratio of diffuser at a given station x	dv
AMMX	Maximum airframe design Mach number	ev
AP4	Ratio of nozzle height to width at exit	dv
BB1BI	Width overall of internal weapons bay 1	dv
BB1I	Total width of each store in bay 1	ev
BB1K	Clearance on width of stores in bay 1	ev
BB2BI	Width overall of internal weapons bay 2	dv
BB2I	Total width of each store in bay 2	ev
BB2K	Clearance on width of stores in bay 2	ev
BBBI	General width of a weapons bay	dv
BCH	Minimum width of standard cockpit	ev
BEFN	Fin span	dv
BETN	Net span of tailplane (exposed)	dv
BFA	Width of fuselage at station A	dv
BFAB	Width of bottom part of fuselage at station A	dv
BFAT	Width of top part of fuselage at station A	dv
BFB	Width of fuselage at station B	dv
BFBB	Width of bottom part of fuselage at station B	dv
BFBT	Width of fuselage station B at cockpit side	dv
BFC	Width of fuselage at station C	dv
BFCDH	Maximum fuselage width	dv
BFD	Width of fuselage at station D	dv
BFDB	Width of underside of fuselage station D	dv
BFDT	Width of fus. station D, top part, for spline definition	dv
BFE	Width overall at fuselage station E	dv
BFE1	Auxiliary height for def. of fus. splines at station E	dv
BFEB	Width of fuselage underside at station E	dv
BFF	Width of fuselage at station F	dv
BFFB	Width of fuselage underside at station F	dv
BFFT	Aux. variable for splines around eng. bay at statn. F	dv
BFG	Width of fuselage at station G	dv
BFG1	Width of engine plus clearance at fuselage station G	dv
BFH	Width of fuselage at station H	dv
BFH1	Width of engine plus clearance at fuselage station H	dv
BID	Width of the diffuser at fuselage station D	dv
BIE	Width of the intake diffuser at fuselage station E	dv

[1]This column was compiled by considering three types of variable: 1. ev (external variables) are set as input data. 2. dv (dependent variables) are assigned a value as a result of a calculation within the synthesis code. 3. iv (independent variables) are set as input values, but may be modified by an optimizer linked to the synthesis code.

BII	Width of intake	dv
BIIB	Width of intake projected into horizontal	dv
BP3	Width of two-dimensional nozzle at nozzle entrance	dv
BP4	Width of two-dimensional nozzle at exit	dv
BUMG	Width of main undercarriage wheel incl. clearances	dv
BUMW	Width of main undercarriage wheel	dv
CAVC	Constant factor in expression for cost of aircraft avionics	ev
CEFB	Fin root chord	dv
CEFM	Mean aerodynamic chord of fin	dv
CENG0	Constant in expression for cost of aircraft propulsion system	ev
CENG1	Constant factor in expression for cost of aircraft propulsion systme	ev
CEQP	Constant factor in expression for cost of aircraft equipment	ev
CETB	Chord of tailplane at body side	dv
CETM	Mean aerodynamic chord of tailplane	dv
CF1	Weighting for unit production cost in objective function	ev
CF2	Weighting for turning performance parameter in objective function	ev
CSTR	Constant factor in expression for cost of aircraft strcture	ev
CWMA	Aerodynamic mean chord of wing	dv
CWMG	Geometric mean chord of the wing	dv
DAR	Diameter of the radar dish	ev
DFC	Equivalent fuselage diameter at station C	dv
DIE	Diameter of the intake at the exit	dv
DP1	Diameter of engine at compressor front face	dv
DP1R	Diameter of reference engine at compressor front face	ev
DP2	Diameter of engine at front of reheat fuelling section	dv
DP2R	Diameter of ref. engine at front of reheat fuelling section	ev
DP3	Diameter of engine at entrance to nozzle	dv
DP3R	Diameter of reference engine at entrance to nozzle	ev
DP4	Diameter of engine at nozzle exit	dv
DP4R	Diameter of reference engine at nozzle exit	ev
DUMG	Diameter of main undercarriage wheel incl. clearances	dv
EBP1	Engine bay width clearance at the compressor face	dv
EBP1H	Maxi. engine bay width clearance at the compressor face	ev
EBP1S	Min. engine bay width clearance at the compressor face	ev
EBP2	Eng. bay width clearance at entrance to reheat fuelling	dv
EBP2H	Max. width clearance at entrance to reheat fuelling	ev
EBP2S	Min. width clearance at entrance to reheat fuelling	ev
EBP3	Engine bay width clearance at entrance to nozzle	dv
EBP3H	Max. width clearance at entrance to nozzle	ev
EBP3S	Min. width clearance at entrance to nozzle	ev
EDAR	Clearance on the diameter of the radar dish	ev
EHCS	Dist. between seat back and rear cockpit bulkhead	ev
EHP1	Engine bay height clearance at the compressor face	dv
EHP1H	Max. eng. bay height clearance at the compressor face	ev
EHP1S	Min. eng. bay height clearance at the compressor face	ev
EHP2	Eng. bay height clearance at entrance to reheat fuelling	dv
EHP2H	Max. height clearance at entrance to reheat fuelling	ev
EHP2S	Min. height clearance at entrance to reheat fuelling	ev
EHP3	Engine bay height clearance at entrance to nozzle	dv
EHP3H	Max. height vlearance at entrance to nozzle	ev

EHP3S	Min. height clearance at entrance to nozzle	ev
ELCT	Increment in length between front and rear cockpit	ev
ELUP	Dist. between main u/c pintle and rear or front of u/c bay	ev
EMFBI	Mass increment due to internal weapons bays	dv
FBP1K	Width clearance factor on eng. diam. at the compressor face	ev
FBP2K	Width clearance factor on engine diameter at reheat fuelling	ev
FBP3K	Width clearance factor on engine diameter at nozzle entrance	ev
FBUMW	Clearance factor on the main u/c wheel width	dv
FDBH	Store release disturbance factor	ev
FFS	Factor on the fuselage width for the chine	ev
FHP1K	Height clearance factor on eng. diameter at compressor face	ev
FHP2K	Height clearance factor on eng. diameter at reheat fuelling	ev
FHP3K	Height clearance factor on engine diameter at nozzle entrance	ev
FHWBF	Factor on height of wing box to allow for carry-through struct.	ev
FLP1K	Factor in correlation for scaling of LP12R	ev
FLP2K	Factor in correlation for scaling of LP22AR	ev
FLP3K	Factor in correlation for scaling of LP2B3R	ev
FLP4K	Factor in correlation for scaling of LP34R	ev
FMBBI1	Factor in correlation for the weapons bay door mass	ev
FMBBI2	Exponent in correlation for the weapons bay door mass	ev
FMBBI3	Exponent in correlation for the weapons bay door mass	ev
FMBBI4	Factor in correlation of weapons bay roof mass	ev
FMBBI5	Factor in correlation of weapons bay roof mass	ev
FMBI	Factor for the mass of the weapons bay structural surroundings	dv
FMF2	Materials factor on average skin/stringer combination weight	dv
FMTSWL	Limiting value of wing mass loading at take-off	ev
FYID	Coefficient in calculation of y-coordinate of diffuser centreline	dv
FZCR	Array of coefficients for cubic of top of rear canopy section	dv
FZID	Coefficient in calculation of z-coordinate of diffuser centreline	dv
G1	Gradient used in calculation of curve fits	dv
G2	Gradient used in calculation of curve fits	dv
GCCANR	Gradient in the calculation of the canopy z-coordinate cubic	dv
GOF1	Gradient of fuselage cross-sectional area distribution at radome	ev
GRFNH	Mximum allowable boat tail angle at rear of fusleage	ev
GTCPH	Maximum G-force that pilot can sustain	ev
HB1BI	Height overall of internal weapons bay 1	dv
HB1I	Total height of each store in bay 1	ev
HB1K	Clearance on height of stores in bay 1	ev
HB2BI	Height overall of internal weapons bay 2	dv
HB2I	Total height of each store in bay 2	ev
HB2K	Clearance on height of stores in bay 2	ev
HC1	Distance between thighpoint and eyepoint in standard cockpit	ev
HC2	Distance between thighpoint and heel point in standard cockpit	ev
HC3	Distance between thigh point and seat back in standard cockpit	ev
HC4	Distance between eyepoint and canopy in standard cockpit	ev
HC5	Front bulkhead height above cockpit floor	dv
HC6	Clearance in cockpit for ejection seat escape path	ev
HC7	Height of pilot's eyepoint above cockpit side	dv
HCCANR	Height of the canopy above the cockpit floor at rear	dv
HCCANS	Maximum height of cockpit canopy above cockpit floor	dv

HCEYE	Height of the pilot's eyepoint above the cockpit floor	dv
HCSEAT	Pilot's seat point above floor measured along the seat back	ev
HCT	Increment in height between front and rear cockpit	dv
HCWSC	Height of the top of the windscreen above the cockpit floor	dv
HFA	Height of fuselage at station A	dv
HFAB	Height used to define bottom splines at station A	dv
HFAT	Height used to define top spline at station A	dv
HFBB	Height of bottom part of fuselage at station B	dv
HFBT	Height of fuselage side (cockpit side) above chine at station B	dv
HFC	Height of fuselage at station C	dv
HFCDH	Maximum fuselage height	dv
HFD	Height of fuselage at station D	dv
HFDC	Height of fuselage station D from top of wing box to underside	dv
HFDT	Height of fuselage top part for spline definition	dv
HFE	Height of fuselage station E	dv
HFEC	Height of fuselage station E from underside to wing centreline	dv
HFET	Height of fuselage station E, top part	dv
HFFC	Fuselage height at centreline, station F	dv
HFG	Overall height of fuselage station G	dv
HFG1	Height of fuselage station G above wing plane	dv
HFG2	Height of fuselage station G below wing plane	dv
HFGC	Height of fuselage station G at centreline	dv
HFH	Overall height of fuselage station H	dv
HFH1	Height of fuselage station H above wing plane	dv
HFH2	Height of fuselage station H below wing plane	dv
HIDBX	Height of diffuser at a given station x	dv
HIE	Height of intake diffuser at fuselage station E	dv
HII	Height of intake	dv
HIIB	Projection of the intake intake height HII into vertical plane	dv
HP3	Height of two-dimensional nozzle at nozzle entrance	dv
HP4	Height of two-dimensional nozzle at exit	dv
HWBE	Height of wing box at fuselage station E	dv
HWBF	Height of wing box at station F	dv
HWBG	Height of wing or tailplane box at fuselage station G	dv
HWBH	Height of taiplane or wing box at fuselage station H	dv
HWD	Height of the wing box at fuselage station D	dv
KPP1	Constant for use in point performance calculations	ev
KPP2	Constant for use in point performance calculations	ev
LB1BI	Length overall of internal weapons bay 1	dv
LB1I	Total length of each store in bay 1	ev
LB1K	Clearance on length of stores in bay 1	ev
LB2BI	Length overall of internal weapons bay 2	dv
LB2I	Total length of each store in bay 2	ev
LB2K	Clearance on length of stores in bay 2	ev
LBBI	General length of a weapons bay	dv
LCCAN	Total length of the cockpit canopy	ev
LCCANS	Length of cockpit canopy minus windscreen	dv
LCEYE1	Horiz. dist. between cockpit front bulkhead and pilot's eyepoint	dv
LCEYE2	Distance of rear pilot's eyepoint from front cockpit bulkhead	dv
LCFL1	Floor length of front cockpit	dv

LCFL2	Floor length of rear cockpit	dv
LCFOOT	Horizontal dist. between cockpit front bulkead and heel point	dv
LCT	Distance of rear cockpit aft of front cockpit bulkhead	dv
LCWSC	Length of windscreen from front bulkhead	dv
LEFCQM	Fin moment arm measured from wing mean quarter chord point	ev
LETCQM	Distance between mean ¼ chord points of wing and tail	ev
LIDG	Total length of intake diffuser	dv
LP12	Length of engine gas generator	dv
LP12R	Length of engine gas generator for reference engine	ev
LP22A	Length of reheat fuelling section of engine	dv
LP22AR	Length of reheat fuelling section of reference engine	ev
LP22B	Engine length between gas generator and transition section	dv
LP2A4	Length of reheat burning section of engine	dv
LP2A4R	Length of reheat burning section of reference engine	ev
LP2B3	Length of transition section for two-dimensional nozzles	dv
LP2B3R	Length of reference transition section for two-dimensional nozzles	ev
LP34	Nozzle length	dv
LP34R	Reference nozzle length	ev
LPG	Overall length of engine including nozzle	dv
LT	Total length of aircraft	dv
LTTH	Maximum distance for take-off ground roll	ev
LUMB	Length of main undercarriage bay	dv
MBBID	Mass of the internal weapons bay doors	dv
MBBIR	Mass of weapons bay roof to carry shear loads	dv
MBI	Total mass of internal stores in a given bay	dv
MFXAVG	Average weight of skin/stringer combination of fuselage	dv
MLI	Total mass of launchers in a given bay	dv
NBB1I	Number of store stations in width of internal bay 1	ev
NBB2I	Number of store stations in width of internal bay 2	ev
NENG	Number of engines (1 or 2)	ev
NFIN	Number of fins (1 or 2)	ev
NHB1I	Number of store stations vertically in internal bay 1	ev
NHB2I	Number of store stations vertically in internal bay 2	ev
NLB1I	Number of store stations lengthwise in internal bay 1	ev
NLB2I	Number of store stations lengthwise in internal bay 2	ev
NPP	Number of point performance calculations to be done	ev
NWEPB	Number of internal weapons bays	ev
OB1BI	Area of cavity for internal weapons bay 1	dv
OB2BI	Area of cavity for internal weapons bay 2	dv
OBBI	General area of a weapons bay cavity	dv
OF1	Cross-sectional area of fuselage at rear of radome	dv
OFA	Cross-sectional area required by fairing curve at station A	dv
OFAS	Cross-sectional area at station A	dv
OFB	Cross-sectional area required by fairing curve at station B	dv
OFBS	Cross-sectional area at fuselage station B	dv
OFC	Cross-sectional area at station C required by fairing curve	dv
OFCS	Cross-sectional area at station C	dv
OFD	Cross-sectional area required by fairing curve at fus. station D	dv
OFDS	Cross-sectional area at fuselage station D	dv
OFE	Cross-sectional area required by fairing curve at fus. station E	dv

OFES	Cross-sectional area at fuselage station E	dv
OFF	Cross-sectional area required by fairing curve at station F	dv
OFFS	Cross-sectional area at fuselage station F	dv
OFG	Cross-sectional area required by fairing curve at fus. station G	dv
OFGS	Cross-sectional area at fuselage station G	dv
OFH	Cross-sectional area required by fairing curve at fus. station H	dv
OFHS	Cross-sectional area of fuselage station H	dv
OIE	Cross-sectional area of intake exit	dv
OII	Cross-sectional area of intake streamtube	dv
OISX	Area of enclosing parallelogram at diffuser station x	dv
OIX	Cross-sectional area of inlet at a given x-position	dv
OIXD	Cross-sectional area of intake diffusers at fuselage station D	dv
OIXE	Cross-sectional area of intake diffusers at fuselage station E	dv
OP1B	Cross-sectional area of engine bay at compressor face	dv
OP2B	Cross-sectional area of engine bay at entrance to reheat fuelling	dv
OP2BB	Cross-sectional area of engine bay at entrance to transition section	dv
OP3B	Cross-sectional area of engine bay at nozzle entrance	dv
OPN	Nozzle exit area	dv
OVI	Cross sectional area of boundary layer diverter at station C	dv
PFAB1	Bezier control points for bottom spline 1 at B	dv
PFAB2	Bezier control points for bottom spline 2 at B	dv
PFAT1	Bezier conrtol points for top spline 1 at A	dv
PFAT2	Bezier control points for top spline 2 at A	dv
PFBB1	Bezier control points for bottom spline 1 at station B	dv
PFBB2	Bezier control points for bottom spline 2 at station B	dv
PFBT1	Bezier control points for top spline 1 at station B	dv
PFBT2	Bezier control points for top spline 2 at station B	dv
PFC	Perimeter of fuselage at station C	dv
PFCT1	Bezier control points for top spline at station C	dv
PFCT2	Bezier control points for bottom spline at station C	dv
PFD	Perimeter of fuselage at station D	dv
PFDT1	Bezier control points for top spline 1 at station D	dv
PFDT2	Bezier control points for top slpine 2 at station D	dv
PFEB1	Bezier control points for bottom spline 1 at station E	dv
PFEB2	Bezier control points for bottom spline 2 at station E	dv
PFET1	Bezier control points for top spline 1 at station E	dv
PFET2	Bezier control points for top spline 2 at station E	dv
PFET3	Bezier control points for top spline 3 at station E	dv
PFET4	Bezier control points for top spline 4 at station E	dv
PFF	Perimeter of fuselage at station F	dv
PFFB1	Bezier control points for bottom spline 1 at station F	dv
PFFT1	Bezier control points for top spline 1 at station F	dv
PFFT2	Bezier control points for top spline 2 at station F	dv
PFFT3	Bezier control points for top spline 3 at station F	dv
PFFT4	Bezier control points for top spline 4 at station F	dv
PFGB1	Coefficients of superellipse at station G	dv
PFGT1	Coefficients of superellipse at station G	dv
PFGT2	Coefficients of superellipse at station G, twin-engine	dv
PFHB1	Coefficients of superellipse at fuselage station H	dv
PFHT1	Coefficients of superellipse at fuselage station H	dv

PFHT2	Coefficients of superellipse at fuselage station H	dv
PFR	Perimeter of fuselage at rear of radome	dv
PFRT1	Array holding Bezier coefficients at rear of radome	dv
PFRT2	Array holding Bezier coefficients at rear of radome	dv
PNDKG	Conversion factor from pounds into kilogram	ev
QCCAN	Inclination angle of the side of the cockpit canopy	ev
QCEYE1	Pilot's downward vision angle in standard cockpit	ev
QCEYE2	Pilot's upward vision angle in standard cockpit	ev
QCEYE3	Pilot's side and downward vision angle	ev
QCEYE4	Rear cockpit forward downward vision angle	ev
QCFOOT	Angle bet. the line joining the thigh-heel points and horizontal	dv
QCSEAT	Angle to vertical of back of ejection seat	ev
QCWSC	Windscreen inclination angle to horizontal	dv
QEF	Fin cant angle (for twin fins) from vertical	ev
QEFL	Fin leading edge sweep	ev
QETL	Tailplane leading edge sweep	ev
QFC1	Angle of fuselage side at station C, top section	ev
QFD1	Angle between fuselage side and vertical at station D	ev
QFD2	Angle of fus. side above wing plane with horizontal at station D	ev
QFD3	Angle between fus. side at bottom to vertical, fuselage station D	ev
QFE1	Angle between fuselage side and vertical at E, top part	ev
QFE2	Angle between fuselage and horizontal, top part	ev
QFE3	Angle between fuselage side and horizontal at E, bottom part	dv
QFE4	Angle between fuselage side and vertical at E, bottom part	ev
QFG1	Angle between fuselage side and vertical at fuselage station G	ev
QFH1	Angle between fuselage side and vertical at fuselage station H	ev
QFS	Angle to the vertical of the fuselage side	ev
QID1	Angle between vertical and intake side	ev
QID2	Angle between horizontal and bottom of intake	ev
QIX1	Angle between side of diffuser and vertical at station x	dv
QIX2	Angle between bottom of diffuser and the horizontal at station x	dv
RCCAN	Radius of cockpit canopy	ev
REFSW	Vertical tail volume coefficient	dv
RETSW	Horizontal tail volume coefficient	ev
RHHV	Ratio of fus. sections above and below wing plane at centreline	dv
RLUPCW	U/C c.g. pos. aft of mean ¼ chord point as frac. of AMC	ev
ROFAS	Scaling factor on cross-sectional area at station A	dv
ROFBS	Scaling factor on fuselage cross-sectional area at station B	dv
ROFCNS	Scaling factor on net cross-sectional area at station C	dv
ROFDS	Scaling factor on cross-sectional area at fuselage station D	dv
ROFES	Scaling factor on cross-sectional area at fuselage station E	dv
ROFFS	Scaling factor on cross-sectional area at fuselage station F	dv
ROFGS	Scaling factor on cross-sectional area at fuselage station G	dv
ROFHS	Scaling factor on cross sectional area at fuselage station H	dv
ROIDX	Ratio of the area of the enclosing parallelogram to the intake area	dv
RTEF	Fin thickness to chord ratio	ev
RTP	Engine scale factor	iv
SEFN	Fin planform area	dv
SEFNH	Projection of fin planform area into horizontal plane	dv
SEFNV	Projection of the fin planform area into the vertical plane	dv

SETN	Planform area of horizontal stabilizer	dv
SW	Gross wing area	iv
TPGD	Maximum sea-level static thrust of the engine with reheat	dv
UEFF	Factor for the utilization of fin volume for fuel storage	ev
UEFN	Fin taper ratio	ev
UETN	Taper ratio of net tailplane	ev
ULTN	Ultimate load factor	dv
VB1BI	Volume of internal weapons bay 1	dv
VB2BI	Volume of internal weapons bay 2	dv
VD	Design dive speed in knots	ev
VEFF	Volume of fin	dv
VFR	Volume of radome	dv
VP12B	Volume of engine gas generator	dv
VP23B	Volume of engine reheat fuelling and burning section	dv
VP2B3B	Volume of transition section from 2d to rectangular exhaust nozzle	dv
VP34B	Volume of engine exhaust nozzle	dv
VPB	Volume of entire engine	dv
VTLH	Maximum value of landing approach speed	ev
WFR	Wetted area of radome	dv
XEFLB	Distance of fin leading edge at fin root aft of aircraft nose	dv
XEFM	Distance of fin mean ¼ chord point aft of fin leading edge	dv
XETLB	Distance of tailplane l.e. at tailplane root aft of aircraft nose	dv
XETM	Distance of tailplane mean ¼ chord point aft of tailplane l.e.	dv
XFA	X-coordinate of fuselage station A	dv
XFB	X-coordinate of fuselage station B	dv
XFC	X-coordinate of fuselage station C	dv
XFD	X-coordinate of fuselage station D	dv
XFE	X-coordinate of fuselage station E	dv
XFF	X-coordinate of fuselage station F	dv
XFG	X-coordinate of fuselage station G	dv
XFH	X-coordinate of fuselage station H	dv
XFN	Distance of nozzle exit plane aft of aircraft nose	iv
XFR	X-coordinate of fuselage station containing radar dish	dv
XI1	X-coordinate of diffuser centreline at end of forward section	dv
XI2	X-coordinate of diffuser centreline at end of centre section	dv
XI3	X-coordinate of diffuser centreline at end of aft section	dv
XID	X-coordinate of any diffuser station measured from intake front	dv
XII	X-coordinate of intake, measured from aircraft nose	dv
XSI	X-coordinate of rear of front fuselage chine	dv
XUMB	X-coordinate of front of main undercarriage bay	dv
XWCQM	Distance of wing mean quarter chord point from aircraft nose	ev
YFA	Y-coordinate of chine at station A	dv
YI1	Y-coordinate of diffuser centreline at end of forward section	dv
YI2	Y-coordinate of diffuser centreline at end of centre section	dv
YI3	Y-coordinate of diffuser centreline at end of aft section	dv
YID	Y-coordinate of diffuser centreline a station D	dv
YIDC	Y-coor. of intake centre measured from lower inboard corner	dv
YIDX	Y-coordinate of diffuser centreline at any station x	dv
YIXE	Horizontal separation dist. between intake diffusers at station E	dv
YPCH	Separation distance between engine centrelines	dv

YSA	Y-coordinate of fuselage chine at station A	dv
YSB	Y-coordinate of fuselage chine at station B	dv
YSI	Y-coordinate of the rear of the front fuselage chine	dv
ZB1C	Z-coordinate of centre of gravity of weapons bay 1	iv
ZCCANR	Z-Coordinate of canopy top at aircraft centreline	dv
ZDATWB	Datum Z-coordinate used in dimensioning of fuselage station F	dv
ZEFM	Distance along z-axis of mean aerodynamic chord from fin root	dv
ZFD	Z-coordinate of the fuselage top at station D, centreline	dv
ZFE	Z-coordinate of fuselage top centreline at station E	dv
ZFEBP	Z-coord. of fuselage underside at station E, at diffuser centreline	dv
ZFETC	Z-coordinate of fuselage spine at station E	dv
ZFFTC	Z-coordinate of fuselage top at station F, centreline	dv
ZFFTP	Z-coordinate of fuselage top above propulsion bay at station F	dv
ZFLOOR	Z-coordinate of cockpit floor	dv
ZFUS	Array for z-coordinate of fuselage underside between A and C	dv
ZI1	Z-coordinate of diffuser centreline at end of forward section	dv
ZI2	Z-coordinate of diffuser centreline at end of centre section	dv
ZI3	Z-coordinate of diffuser centreline at end of aft section	dv
ZIDC	Z-coord. of intake centre measured from lower inboard corner	dv
ZIDX	Z-coordinate of diffuser centreline at any station x	dv
ZIXE	Z-coordinate of diffuser centreline at fuselage station E	dv
ZPCH	Z-coordinate of engine bay	dv
ZSA	Z-coordinate of chine at station A	dv
ZSB	Z-coordinate of fuselage chine at station B	dv
ZSI	Z-coordinate of rear of front fuselage chine	dv
ZW	Z-coordinate of wing centreline	dv

1. INTRODUCTION

Reductions in the levels of government spending on defence, brought about in part by the ending of the cold war, have forced a rethinking of the priorities behind the procurement of many military systems, including that of combat aircraft. Bearing in mind that modern versions of these types of aircraft have reached an extremely high level of complexity, the implications for both manufacturers and purchasers are far-reaching. For example, it may no longer be feasible to have at the disposal of the armed forces a large variety of aircraft each optimized or designed for a specific mission. Rather, it will become more common to have one aircraft type employed in a variety of roles. Also, reduced procurement budgets mean that fewer aircraft numbers will be purchased, increasing the need for systems which must reconcile the sometimes conflicting objectives of low cost and high lethality.

These conclusions can be drawn when the combat aircraft procurement process is viewed from the perspective of two, sometimes opposing, overall requirements. On the one hand lies the desire to equip the armed forces with the latest in technology to meet what is perceived as the current and future military threat. New aircraft may also be necessary as a replacement for older, less capable and, in terms of operations, more costly equipment. This requirement will lead to the definition of new features deemed to be appropriate for new generations of combat aircraft. Examples currently under consideration by government and industry research and development organizations are low observables, thrust vectoring, unstable control-configured vehicles, the increased use of advanced materials such as composites, and modular avionics systems.

On the other hand lies the desire of the government agencies involved in military systems procurement to obtain this equipment at the lowest possible cost. In some cases, this is justified by the apparent reduction in magnitude of the military threat. The resulting savings can be used to either reduce the overall government budget or to increase spending on other, competing areas whilst reducing spending on defence. Another justification for reductions in expenditure is past experience with aircraft procurement projects. Often, it has been seen that costs have escalated out of control in order to meet specific and unattainable development milestones and performance requirements. Frequently, projects have been cancelled for a variety of technical, political or economic reasons, leading to large expenditures with little or no return.

These two budgetary and technical requirements lead to a conflict because one goal is often contrary to the other. The addition of new technical features to an aircraft is usually fraught with uncertainties because of the lack of experience with that particular technology. At the conceptual design stage, in particular, little is known about the effects on aircraft mass and costs, or indeed reliability and effectiveness, of new features. Frequently this may lead to an

increase in the projected cost of a development program. Yet there is also a clear trend towards reduced military expenditures.

To illustrate this point it is useful to consider one of the most important of the abovementioned technical features of modern combat aircraft: the inclusion of low observables technology. In theory, the benefits are quite clear. Reduced radar signatures should decrease an aircraft's probability of detection and subsequent tracking by radar. This can be used to reduce the radar detection range, but other, less immediately tangible benefits may be obtained. One is the possibility of flying higher low-level penetration legs on ground attack missions, or extending the high altitude cruise portion to within a closer distance of the target. Fuel savings may result, hence reducing aircraft take off mass or allowing increased range or weapons load. Reduced infrared signatures will make an aircraft less vulnerable to attack by infrared-guided missiles, leading to an increase in survivability. On a more general note, the incorporation of low observables technology may reduce the number of combat aircraft required for a given mission requirement, bringing with it reductions in the costs associated with operations and maintenance. However, the benefits in practice have yet to be fully determined, especially when the design and cost uncertainties of this new technology are taken into account.

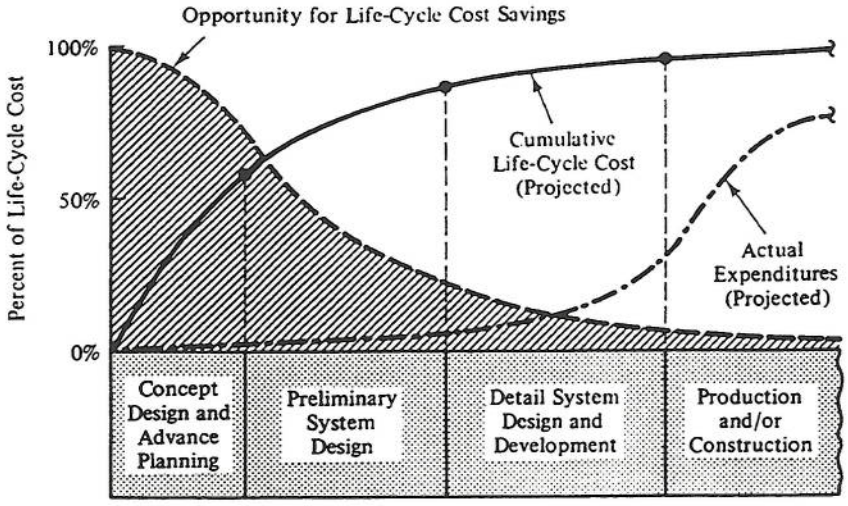

Fig. 1: Commitment of Life Cycle Cost (Blanchard, 1992)

It is widely recognized that the full benefits of new technology will only be obtained when considered from the outset of a development program. Figure 1 illustrates this point for the life cycle costs of a system. They include not only research, development and production, but also operations, maintenance and disposal after the design life of the system has been reached. Clearly, a majority of the total costs are locked in at a very early stage. More than 50% has been commited by the time the concept design and advance planning phase is over, although most of the program expenditure (75%) doesn't occur until production and/or construction begins. A similar logic applies to other areas of system design such as mass or effectiveness gains.

Their magnitude must be estimated at the beginning in order to justify specific design features, but the expected benefits will not actually be obtained until the aircraft has been in service for a number of years.

One of the ways of studying the effects of new technology whilst making an attempt to minimize the risks associated with its inclusion in the aircraft design project is to ensure that a designer has at his finger tips a design synthesis tool which will allow him or her to evaluate a wide range of potential candidate designs within a short period of time. The objective of this research program was to develop such a tool for the conceptual design of new generations of combat aircraft. This thesis will argue that the current engineering, political and economic environment surrounding the combat aircraft design process necessitates the continual development of new, further advanced and more capable design methodologies. Key aircraft geometric features, including those related to low observables, will be identified in the light of present and future requirements and their inclusion as conceptual design methodologies examined.

2. Requirements for the Analysis of Advanced Technology

2.1 Combat Aircraft Stealth Design Considerations

The classification of combat aircraft missions into air superiority, ground attack and interceptor is well known (Hooper, 1979 and Whitford, 1987). Air superiority missions generally occur at medium to low altitude, and the aircraft typically finds its targets (usually other aircraft) through the direction of a ground based or airborne radar. Since this type of aircraft will normally be engaged in air-to-air combat, or dogfighting, only a moderate weapons load of short and medium range air-to-air missiles and a gun will be carried. Furthermore, instantaneous turn rates are of utmost importance, which will require moderate to low wing loadings and low induced drag at high angles of attack. The pilot will normally have very good visibility, obtained by sufficiently raising the seat and canopy above the cockpit side. Since the aircraft will often be operating close to the front line and must have quick turn-around times, good airfield performance is more important than range.

In contrast, an interceptor aircraft will be required to fly longer ranges at high altitude, often at high speeds, while being directed to the target by means of airborne or groundbased radar. High speeds are important to achieve surprise and because of the need to intercept targets which may be escaping from the combat arena. The weapons load will consist of medium to long range missiles. Low wave drag and good lift to drag ratio are essential for this type of aircraft as is a large internal fuel capacity and low fuel consumption for longer range. Turn performance and low speed characteristics are only of secondary importance.

In many ways, the aircraft designed for ground attack lies somewhere in between the interceptor and the air superiority aircraft. High speed performance is important both on the inbound leg (approaching the target area) and the outbound leg. This translates into a design requirement for low drag. On the other hand, a significant amount of maneuvering may need to take place, both while approaching the target area at low levels and while over the actual target to avoid air defenses. This calls for good turn performance and low wing loading. Another significant requirement for ground attack aircraft is the ride quality, which relates to an aircraft's sensitivity to gusts. With a good ride quality, the aircraft is very stable in its flight path, improving the ride comfort over uneven terrain while enhancing the aiming accuracy for weapons delivery. In contrast to the turn performance requirement, a good ride quality requires a relatively high wing loading to alleviate gust sensitivity. This conflict is often the reason why, in the past, dedicated ground attack/bombers such as the Tornado or F-111 have been designed with variable sweep wings.

More recently, interest has begun to focus on aircraft which have the capability of carrying out various missions. There have been examples of such designs in past, a good one being the F-15, which now carries out ground attack

roles despite having been designed exclusively as an air superiority fighter. In contrast, the current discussion centers on aircraft designed from the outset for multiple roles (Burns 1982, O'Neill 1994). Such designs will be required to carry a greater mix of weapons, including air-to-air and air-to-surface. Diverse and frequently conflicting performance constraints will require compromises to be made in the design of the flying surfaces and the aircraft structure.

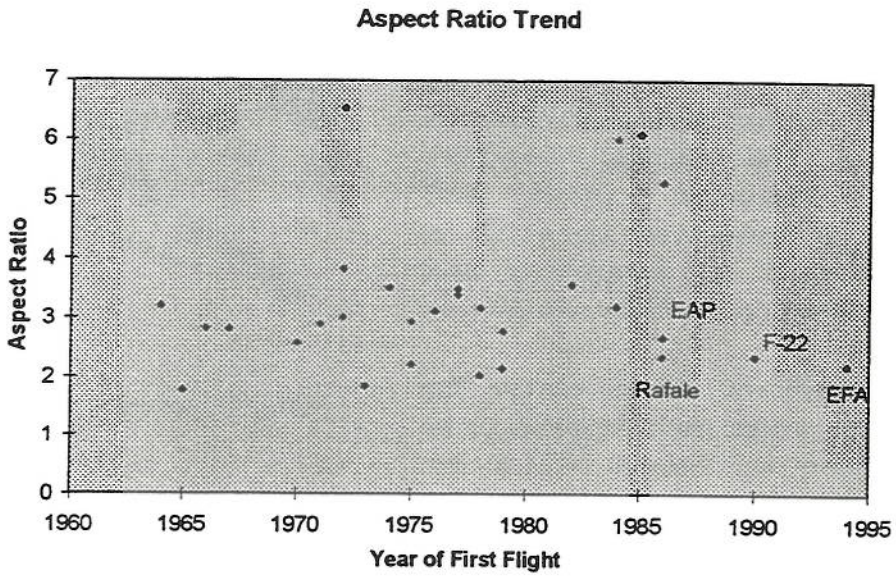

Fig. 2: Aspect Ratio Trend (Woodford, 1995)

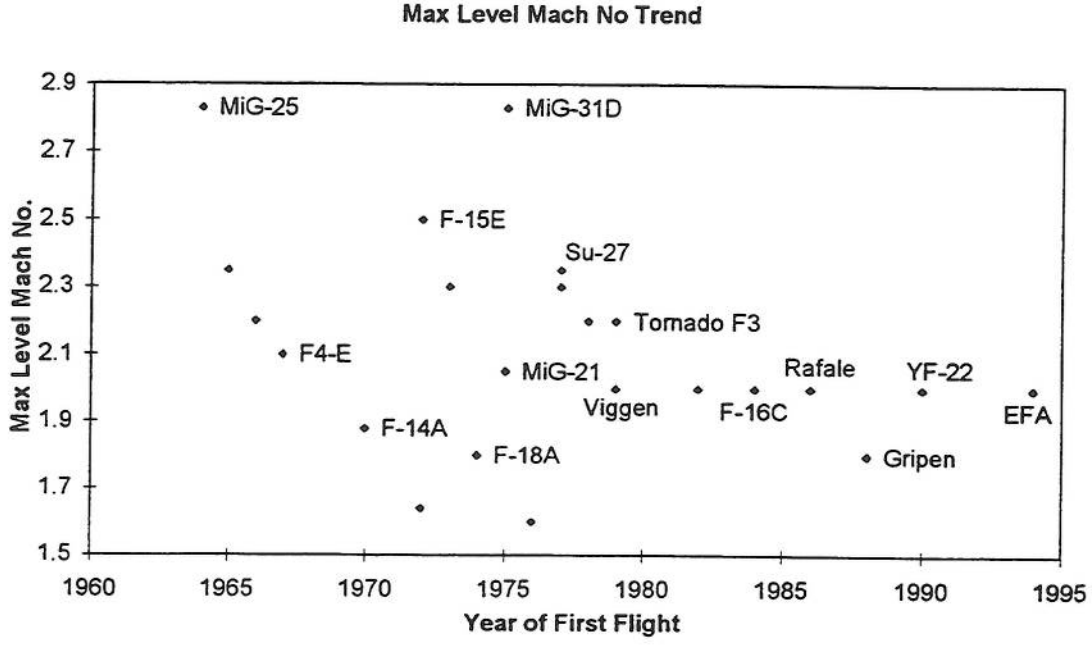

Fig. 3: Max Level Mach Number Trend (Woodford, 1995)

Thus, some of the features expected of multirole aircraft would be moderate aspect ratio and wing loading as a compromise between the necessity for high speed, high altitude performance and low speed combat maneuverability. Figure 2 shows how the newest generation of combat aircraft all have wings designed with similar aspect ratios. The capability of carrying a large weapons load and mix will be essential for ground attack roles, whilst thrust vectoring and advanced fly-by-wire flight controls will enable the aircraft to retain high instantaneous turn rates and carefree handling qualities. Maximum speed will probably be limited to Mach 2.0 in order to avoid the complexity and added weight of variable air intakes (Fig. 3).

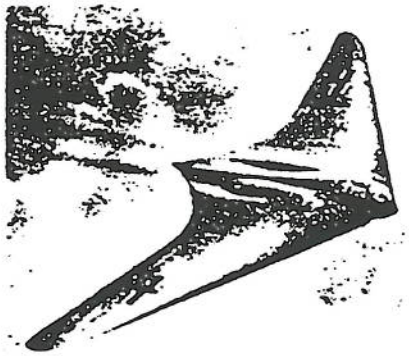

Fig. 4: Germany's Ho IX

A significant design driver for future combat aircraft is expected to be the inclusion of features which are consistent with low observable characteristics. Although such designs are not new (the first dedicated low observable aircraft was perhaps the Ho IX, Fig. 4), only with recent advances in computing power has sufficient progress been made to allow full-scale development of low observable aircraft. Examples include the F-117 Stealth Fighter, the F-22 Advanced Tactical Fighter, and the B-2 Bomber. Even more conventional configurations from the low-observables point of view such as the Eurofighter (EFA) and the Rafale are known to contain significant amounts of such technology in their design (Jane's 1994/95).

The common thread behind all types of low observable technology is the desire to sharply reduce an aircraft's reflectivity and emissivity of optical, infrared, acoustic or radar energy (Howe, 1991). A low observable aircraft will be more difficult for an opponent to detect and track, and there are several means by which this can be achieved. One is to design the surface geometry of the aircraft to appropriately reflect away from the receiver the impinging energy forms. Optical reflections can be reduced through camouflage paint schemes. Infrared emissions depend significantly on the type and shape of the exhaust nozzles as well as the temperature of the exhaust gases themselves. Acoustic emissions similarly depend to a large extent on the engine exhaust characteristics, but aerodynamic noise from flaps and control surfaces may also play a role.

Since radar reflectivity, measured as the cross section equivalent to that of a sphere with the same reflectivity, is usually considered to be the most significant of the four aircraft emissions, most attention is usually paid to reducing this component. Specific measures have been well documented, for example (Ruck et al 1970), (Brown, 1993), (Fuhs, 1982), (Fulghum, 1993), and (Wilson, 1993), and include the elimination of corner reflectors, avoiding flat

surfaces and edges at right angles to the radar receiver, shielding of the engine face, and treatment with radar absorbing material. The electromagnetic phenomena responsible for radar cross section are usually of a very complicated nature. At the conceptual design stage it is therefore difficult to make precise predictions about its characteristics (magnitude, polarization and direction). Instead, one is forced to rely on simple rules of thumb along with, in some cases, quick numerical estimates for certain simplified cases.

Other combat aircraft design features which have gained importance in recent years are related to aircraft performance, and they include supermaneuverability and supercruise. Both can be seen as extensions or enhancements of the traditional aircraft performance envelope. Supermaneuverability refers to aircraft agility, and is quantified by measuring an aircraft's ability to change its attitude at any flight condition. In some cases this can mean that the aerodynamic controls are no longer effective, such as at high angles of attack or at very low speeds. Also known as post-stall maneuvers, these capabilities have bcome possible with the introduction of thrust vectoring nozzles, as described in (Capone, 1981 and 1992), (Herrick, 1988), (Raymer, 1991) and (Gal-Or, 1994). Supercruise denotes an aircraft's ability to cruise supersonically without the assistance of afterburning engines. The requirements for such a configuration are primarily high dry thrust with low fuel consumption, low wave drag, and high lift-to-drag ratios, as described by (Herrick, 1988) and (Hinz and Miller, 1979).

It can be seen that these requirements more often than not will conflict with each other. There is nothing new about this. Any aircraft design process, in particular the conceptual phase, has always involved a large number of trade-offs to be made between conflicting performance and mission requirements and the resulting design features. What is changing is the fact that combat aircraft are moving away from a stage in which they have been designed merely to perform to a given set of requirements, sometimes at any cost. Traditional aircraft performance measures and figures of merit still form very much the basis for any design. Yet as technological enhancements to the systems are made, the complexity of the finished system increases, and hence the cost. Future combat aircraft will be more capable in themselves, but will also be required to perform more roles and more demanding missions with a smaller inventory. In short, they must become more effective. To understand why this is the case, it is useful to examine some of the economical and political considerations involved in combat aircraft development programs, and to show how they affect the choice of technology levels.

2.2 Advanced Technology Procurement Scenario

The difficulties faced by all sectors of the aerospace industry in recent years are graphically demonstrated in Fig. 5. It shows the trends in aerospace employment, exemplified here by the USA, broken down into the categories civil aircraft, military aircraft, missiles and space and other related industries. From a peak of roughly 1.3 million in 1989, total employment has dropped to around 800,000 in 1995, representing a decline of 38%. Even when the twelve

year period from 1983 to 1995 is considered, one can still determine a 20% drop in employment figures.

But the above totals hide other numbers which are of more significance for this research work. As can be seen upon closer examination of Figure 5, the largest overall decline took place in the military aircraft, missiles and space, and other related industries, which in 1983 accounted for 80% of the total employment. From 1983 to 1995, the net loss in aerospace jobs not counting the civil aircraft market was approximately 33%, while a small increase in employment can be seen for the civil aircraft market. Furthermore, civil aircraft employment now accounts for 30% of the total.

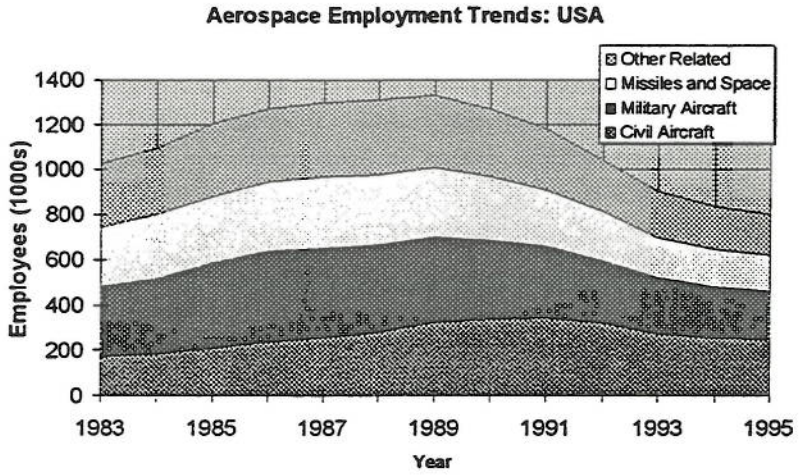

Fig. 5: Aerospace Employment Trends, USA (Foley, T. M., 1995)

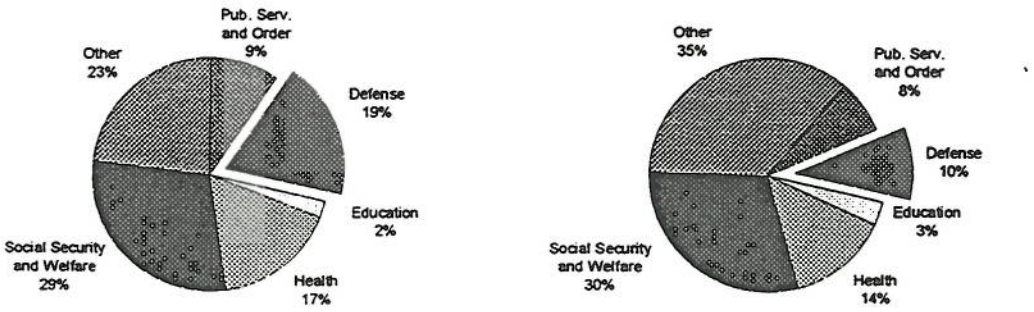

Fig. 6: Typical Breakdown of Government Expenditure
(as percentage of total) Left: USA (1993), Right: UK (1992), (I.M.F., 1994).

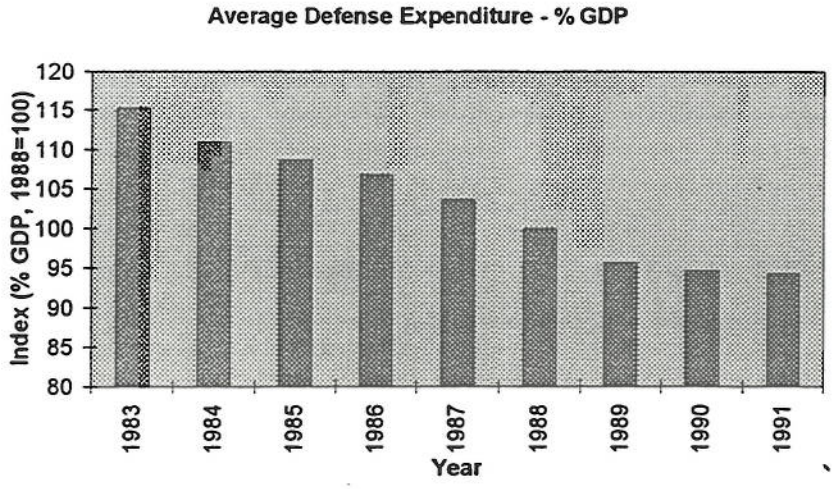

Fig. 7: Average Defense Expenditure (I.M.F., 1994)

These numbers can be explained by comparison with the information given in Figure 7. With the ending of the cold war the perceived necessity of large scale spending on defense has given way to a widely held view that alternative uses for the existing resources could and should be found. This is reflected in the decrease in spending on defense as a percentage of GDP. Worldwide, defence spending dropped from $1.2 trillion in 1985 to $868 billion in 1993 (Economist, 1996, 69-72).

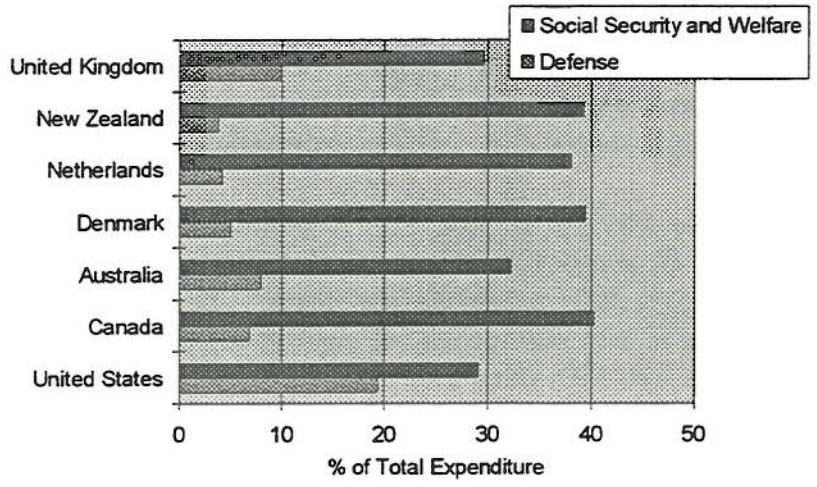

Fig. 8: Competition for government resources
(latest available data, I.M.F., 1994)

Budgetary choices are made by governments based upon the needs of its particular society. Thus, as an example, Figure 6 shows the breakdown of expenditure by category for the United Kingdom and the United States. As can be seen, the proportion spent on defense is significantly higher in the United States, whereas other items such as social security and welfare or public

services and order are roughly similar. The greater the spending on a given sector the larger the effect on the total if it is reduced by a given percentage. Because the share of expenditure by the United States government on defense is such a large proportion of the total, reducing overall expenditure by cuts in defense looks very attractive. However, Figure 8 shows that reductions in social security and welfare would have an even greater effect on the overall budget.

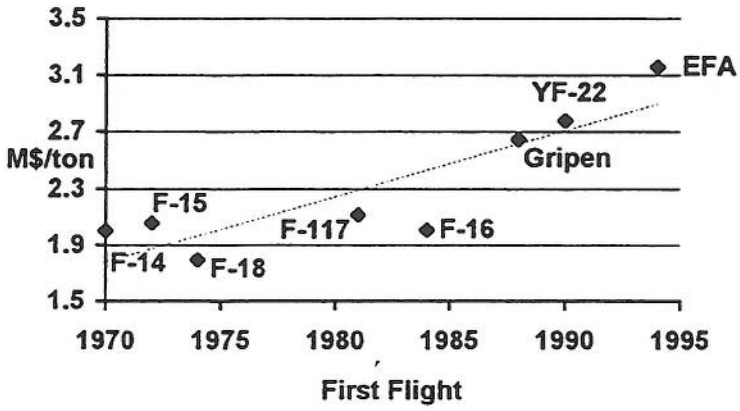

Fig. 9: Flyaway Cost/Unit Weight vs. Year of First Flight (FY94$) (Woodford, 1995)

While defense budgets appear to be decreasing, the actual cost of developing and procuring an aircraft is increasing. Figure 9 shows this trend for a variety of currently or soon to be operational combat aircraft (Woodford, 1995). Shown here is the recurring flyaway cost per unit weight, in this case millions of US dollars per ton of W_{AMPR}. The recurring flyaway cost does not include the cost of research, development testing and evaluation. W_{AMPR} is a weight term similar to the empty mass, but excluding wheels, tyres, tubes and brakes, engines, fuel cells, starters, auxiliary power unit, batteries and elecrtrical supply, avionics equipment, electronic countermeasures, anti-icing and trapped fuel and oil. In other words, it represents the empty mass of the newly manufactured airframe before adding the major systems.

Obviously this weight is not the only factor affecting the recurring flyaway cost of an airframe. Other important factors are the use of advanced materials, the demanded performance levels, the number of partners developing an aircraft, and the number of aircraft to be produced.

Thus, for the F-16, with currently around 3763 aircraft produced or to be produced, the cost per unit weight is fairly low. In contrast, the use of advanced composites as load carrying structure coupled with development being divided amongst three partners from different nations can be seen to increase the cost per unit mass of the EFA to a level even above that of the F-22. Similarly, the empty weight of the F-14, due in part to the variable sweep wing, and the high design speed of the F-15 result in cost per unit weight above the trendline. In general, the increase in cost from 1970 to the present can be attributed to higher demanded performance, the use of advanced materials such as composites, and greater complexity of flight control and weapons delivery systems along with the associated software. In other words, more capable aircraft cost more, as expected.

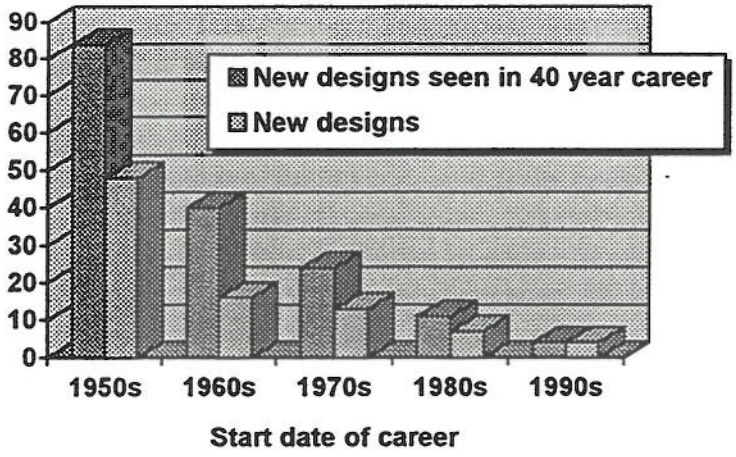

Fig. 10: Designer Career Length vs. No. of New Designs (Kraus, 1995)

When the reductions in expenditure on defense are combined with the increase in cost and complexity of the procured systems, it is not surprising that the number of different types of systems being developed at any given time should decrease drastically. In Figure 10, the number of new aircraft developed in a given decade is compared with the total number likely to be seen by a designer, assuming an average 40 year career (Kraus, 1995). If a designer's career began in the 1950s, he or she was likely to see over 80 new designs. In contrast, a designer beginning his career in the 1960s already had the number of new designs he or she might have participated in reduced to 40, or less than 50%.

Budgetary reductions and their impact on stealth aircraft procurement are discussed by Sweetman (Sweetman, 1994). Despite 15 years of development work, only one wing of 55 F-117As exists, and the planned B-2 bomber procurement has been reduced from originally 132 to 20. Table 1 summarizes these changes.

Aircraft	*1989 (planned)*	*1994 (actual)*
B-2 Stealth Bomber	132	20
F-117A Stealth Fighter	100	55
F-22 ATF	750	440
A-12 (A-6 replacement)	450	cancelled

Table 1: Procurement, planned and actual (Sweetman, 1994), (Taylor, 1989/90)

In order to understand the political, economical and technical debate about advanced technology, it is useful to examine some of the tactical and strategic reasoning behind the procurement of these platforms.

2.3 Tactical and Strategic Considerations

Most of the advanced technologies being considered as a part of this research program were conceived when the military threat was perceived to be

well defined. The cold war face-off in Europe was used as the justification and design driver for increasing performance and low observable characteristics of combat aircraft. For example, for the NATO alliance, the Warsaw Pact was considered the datum threat against which most systems had to perform (Sweetman, 1994). In terms of ground based and airborne threats, SAM sites and the capabilities of the opposing air forces, respectively, were of primary importance for aircraft. The first of these consisted of a highly developed network of different types of missiles, including medium to long range, most of them controlled by radar. Aircraft thus began to be developed with reduced radar cross-section from all aspects. Similarly, the perceived airborne threat was to be countered by increasing the capabilities of combat aircraft, in particular in terms of agility and stealth.

More recently, with the breakdown of the Warsaw Pact, the perceived threat has changed. Instead of facing adversaries which have clearly defined strategies and tactics, it is thought that future opponents will be more unpredictable, less technologically advanced, and more widely dispersed. The catch phrase "Major Regional Conflict", perhaps exemplified by the Gulf War, is often referred to when procurement of advanced technology is discussed. When combined with the previously described budgetary pressures, the changes in the perceived threat have strongly affected the philosophy behind combat aircraft development.

In the past, aircraft were developed along the lines of a specific performance requirement. Targets for turn rates, flight envelope, weapons load, range and mass were frequently required by the customer. Little regard was paid to the maintainability, reliability or life cycle costs of an aircraft. Life cycle costs refers to all of the costs incurred during the life of an aircraft, and include not only the cost of research, development, testing and evaluation and manufacturing, but also of training, maintenance, spares, support, and disposal. (Woodford, 1995) The second part of this cost can make up a significant part of the total, and can be strongly influenced by the type of development targets set at the conceptual design stage. Aircraft development for a specific performance target, for example minimum weight, can often result in program delays and severe cost escalation. This is because the desire to reach the ultimate in performance often bears no relation to the costs invoved in doing so.

In order to avoid such difficulties, the design philosophy has moved from requiring a specified performance or design target to one in which key performance characteristics are specified. The optimum design parameters are not fixed, but can be varied as the design progresses, as long as the overall characteristics are still maintained. For example, the F-22 had no actual minimum aircraft weight specified in its contract (Boatman, 1993). Instead, a series of ten performance characteristics were established, the exact interpretation of which was left to the design teams. They consisted of the following list:

1. radar cross section
2. supercruise
3. acceleration
4. radar contact range
5. C-141 loads
6. reliability
7. maintainability
8. turn performance at 30000 ft
9. range at supersonic speeds
10. range at subsonic speeds

It is interesting to analyze in more detail these requirements, because they explain how future aircraft may be designed to match tactical and strategic requirements rather than performance targets set in stone. The list contains the usual set of design requirements expected of any combat aircraft, i.e. speeds, turn performance, altitude, range and acceleration. The exact figures are not available because they are classified. It is also not surprising that an aircraft designed for low observables should have requirements related to radar cross section. More importantly, the above list attempts to have a direct influence over operational, tactical, strategic and life cycle cost issues. Thus, reliability and maintainability, which would be expected to play a role in reducing life cycle costs, are directly specified as design targets. An interesting requirement is the specification for C-141 loads. This relates to the number of flights using a C-141 transporter needed to support a squadron of F-22s deployed in the field. Finally, the requirement for radar contact range relates directly to aircraft operations, because it defines what type of threat the aircraft is designed to meet.

(Lindsey, 1989) has conducted an investigation into the strategic and tactical implications of introducing stealth technology to a variety of weapons platforms. The overriding justification for such a step is that modern combat depends to a very large degree on an interaction of the forces, using radar, infrared, electro-optical and, to a lesser degree, acoustic means of surveillance, detection, tracking and weapons engagement. Lindsey concludes that low observables, when applied to aircraft, ballistic, cruise and short-range missiles, will

- cause some deterioration in the certainty of detecting a first strike,
- strengthen the certainty of retaliation from submarines,
- complicate active defence against ballistic missiles, and
- increase the probability of success for a surprise attack by aircraft and missiles.

Clearly, low observables are of limited value for strategic purposes. The essence of strategic deterrence is to succesfully convince a potential adversary that a first strike will certainly result in retaliation. Such a picture can be painted by having weapons platforms whose locations are difficult to predict, for example submarines, or which have very short reaction and weapons-on-

target times, such as ballistic missiles. Any application of low observables to these platforms will only minimally enhance their strategic deterrence effect. Submarines are already very difficult to detect, and ballistic missiles rely on easily detectable rocket propulsion for the initial phase of flight. Besides, because of their high flight speeds, it is very difficult to employ any sort of countermeasures against them.

In contrast to ballistic missiles and submarines, the strategic value of combat aircraft is very limited. They are designed for shorter ranges, and need large amounts of support, both in terms of personnel and supplies. Basing them within range of strategic targets may take considerable time and logistical effort. Thus they are better suited for tactical roles.

A number of authors have investigated the tactical utility of aircraft incorporating stealth technology. (Chun, 1991) indicates that aircraft such as the F-117A can be used for long-range strikes against targets of high tactical or even strategic value. Precision strike technology combined with low observables means that fewer aircraft can perform the same role. Indeed, these aircraft can accomplish missions previously completed by other means. However, the trade-off is that these types of aircraft are more expensive to develop. Lindsey (Lindsey, 1989) has found that the consequence of stealth within a tactical environment is to return dominance of the battlefield to air power. It will be less likely that surface ships will be able to defend themselves against air launched attacks. Finally, the importance of passive sensors will grow as the use of active sensors is restricted to a minimum.

2.4 Analysis and Design Methodologies for Advanced Technology

In summary, the issues confronting the conceptual design phase of aircraft development are a mixture of traditional and novel ideas. Trade-off studies have always played an important role in the assessment of new technologies and configuration alternatives. However, as the preceding chapters have illustrated, conventional wisdom is being challenged by a variety of factors, both technical and non-technical. Multi-role requirements are leading to aircraft designs which must compromise between conflicting technical requirements, directly influencing the optimum parameters of the aircraft geometry. A drive towards higher performance and advanced features such as low observables in the face of unpredictable threat environments is increasing aircraft complexity and hence cost. At the same time, reductions in procurement budgets are driving efforts to enhance combat aircraft effectiveness and maintainability and keep total life cycle costs as low as possible.

In such a complicated design environment these conflicting requirements must be considered at as early a stage in the development program as possible. Computerized conceptual design tools have made an enormous contribution to this end in recent years. Examples for military aircraft are described in (Lovell, 1988), (Serghides, 1987), (Kehayas, 1992), and (Kirkpatrick et. al., 1990). These are all based on similar design methodologies and represent relatively simple tools with moderate requirements in terms of computing power. Their disadvantages are that they were designed for a specific class of aircraft and are

thus extremely limited in the scope of applicability. In (Lovell, 1988), a conventional swept-wing combat aircraft with side intakes is modelled. (Serghides, 1987) concentrated on canard-delta configurations, (Kehayas, 1992) developed a version for advanced short take off and vertical landing, while (Kirkpatrick, et. al., 1990) describe a variety of enhancements to existing design synthesis codes to cater for advanced technology. None of the just mentioned design synthesis methodologies can account for a very large variety of aircraft configurations.

(Kirkpatrick et. al., 1990) also describe a civil transport aircraft design optimization code. The application of a variety of optimization techniques to civil transport aircraft design was studied by (Crispin, 1992). Methods developed specifically for complex engineering problems was invetigated by (Gage and Kroo, 1992). Multidisciplinary objective functions for optimization of transport aircraft designs were investigated by (Dovi and Wrenn, 1990) and (Morris and Kroo, 1989). Most of the work in these references emphasizes the optimization process and its organization more than the actual design synthesis process, which as a consequence must be kept fairly simple.

An analysis of the available methodologies in relation to the requirements outlined above has shown the necessity of developing a design synthesis code to cater for advanced generations of combat aircraft. The main feature of this synthesis is the incorporation of low-observables features into a flexible synthesis architecture with sufficient accuracy to study the effect even of minor changes in the design parameters on the optimum aircraft. In summary, the conceptual design should

- incorporate advanced combat aircraft features, such as low observables,
- be numerically efficient through the use of empirical algorithms and prediction methodologies, to allow rapid evaluation of candidate designs,
- possess a flexible design layout for a wide range of configurations, and
- allow for further growth potential and future updates by using a more sophisticated fuselage model and a modular program structure.

The following chapters will set out how the above requirements and objectives were achieved. Chapter 3 describes the development of the baseline aircraft design, including a discussion of design considerations. Chapter 4 presents the design relationships developed by the author, and Chapter 5 will analyze the results and the evaluate the prediction methodologies. A discussion of the results is presented in Chapter 6, and conclusions and recommendations for further work can be found in Chapter 7.

3. DEVELOPMENT OF A BASELINE CONFIGURATION

Before beginning with the detailed coding of the design synthesis, a baseline configuration was defined. The features included in the aircraft were chosen as a result of an extensive literature survey and defined in consultation with the DRA. Common to the original aircraft design synthesis given in (Lovell, 1988) are side mounted intakes, the option of twin or single engines, and a straight-tapered, trapezoidal wing. Additional requirements were the provision of

- Axisymmetric or two-dimensional, vectoring nozzles
- Single or twin, canted fins,
- Single or twin, tandem cockpit, and
- Internal weapons carriage.

Component	Options	Design Requirements for Sizing
Cockpit	–Single or twin tandem	Mil. Standards
Engines	–Twin or single	Thrust scaling factor Nozzle types Separation distance
Fins	–Twin or single –Canted or uncanted	Wing leading edge sweep Cant angle
Combination of flying surfaces	–Wing alone –Wing and horizontal stabilizer –Wing and complete empennage	Align leading and trailing edges Wing and horizontal stabilizer in one plane Intake geometry
Nozzles	–Two-dimensional or axisymmetric	Aspect Ratio (height to width)
Weapons Bay	–Choice of one, two, three or none	Weapons load

Table 2: Summary of Baseline Aircraft Characteristics

As described in the previous section, stealth characteristics were considered to be of prime importance to advanced combat aircraft designs. Therefore, the following features were additionally chosen to best model the geometric design characteristics of such aircraft:

- Alignment in the planform of leading and trailing edges of wing, tailplane and vertical stabilizer, if canted,
- Wing and tailplane in the same horizontal plane

- Canting of the fuselage side to match fin canting,
- Curved intake ducts to shield the engine face, and
- Complex definition of fuselage geometry using splines and ellipses.

Table 2 lists the major aircraft components and summarizes the options which were included in the synthesis code along with the principal geometry descriptors. Figure 11 shows how the options just listed were incorporated into a baseline aircraft layout. It does not represent any particular design, but instead is intended to be representative of the sort of configurations capable of being modelled using this design synthesis.

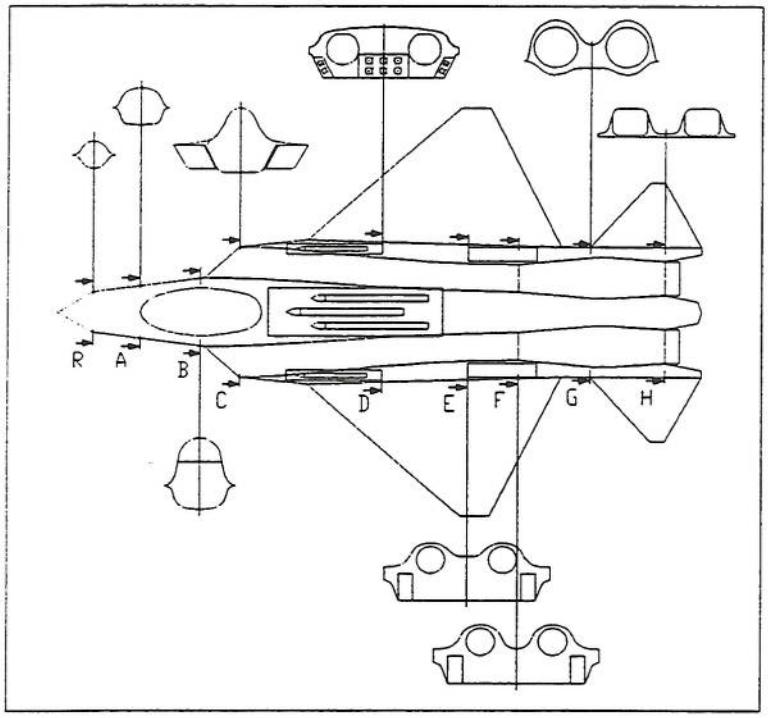

Fig. 11: Baseline Configuration

A detailed description of the reasoning which lead to the above choices being made is given in the sections below.

3.1 Fin Arrangement

In many aircraft design cases, the layout of the vertical tail may require using twin fins. The reasons for such a step are quite varied, and the study of reference material reveals that the conclusions are often far from straightforward, particularly when an attempt is made to address aerodynamics and stability and control issues (Mangold, 1982), (Whitford, 1989).

Aerodynamically, the main argument in favor of twin fins is the fact that one fin will always be in relatively undisturbed flow during sideslip. Also, by

locating the fins in proximity to the horizontal stabilizer, they may act as endplates, increasing its effective aspect ratio. On the other hand, twin fins will have a larger wetted area than an aerodynamically equivalent single fin, increasing the subsonic friction drag. Also, their performance may be degraded by mutual interference effects if insufficient fin lateral separation distance is not provided for. It has been stated that twin fins may guarantee directional stability at high angles of attack, as in the case of the F/A-18. During the design evolution of the F-16, on the other hand, twin fins were found to show unstable characteristics at the same flight conditions due to adverse interference from the forebody vortices (Whitford, 1989).

The apparently contradictory data on twin-fin aerodynamics can be clarified with more straightforward considerations of other design aspects. From a stealth point of view, twin fins are desirable for a number of reasons. First, they will diminish the signature of the aircraft when viewed side-on by reducing the visual cross-section as well as by shielding the infrared radiation of the engine and exhaust. Twin fins can be canted out of the vertical plane and thus reduce the radar cross section both by reflecting incident energy away from the receiver and by eliminating the corner reflector formed by fin and wing on single-fin aircraft. Finally, the canting of the fins will enable the projections of the leading and trailing edges of the fin into the horizontal plane to be aligned with the corresponding edges of the wing.

From a structural point of view, twin fins are less susceptible to flutter because of their reduced dimensions. Also, they can be located further from the engines and thus suffer less from thermal and acoustic stress. On the other hand, overall aircraft mass will increase not only because of the greater mass of twin fins, but also because of the additional structure required to react the fin loads on either side of the engine bay.

P. Mangold (Mangold, 1982) presents a detailed analysis of the aerodynamics of twin-fins as compared with single fins. Throughout the angle of attack range investigated (0° to 70°), twin fins canted outward at 25° generally improved the yawing and rolling moment stability while a single fin has a more constant rudder effectiveness. Within the limits posed by the tail-fin interference, increasing the cant angle seems to improve the lateral characteristics. In general, modifications to the fins produce changes only to the magnitude of the lateral derivative curves, but not to their shape.

The shape and size of the aircraft forebody seems to have a much more significant influence with respect to these derivatives. For example, flattening the nose means that the aircraft will have better restabilization characteristics at high angles of attack but will tend to lose roll stability. This is significant because the rolling moment coefficient due to sideslip is the predominant factor affecting spin departure tendency. Another important conclusion reached by Mangold is that strakes located on the aircraft forebody are an effective way to improve all lateral stability coefficients, including the tendency for yaw departure. Interestingly, it was found that a canard-configured aircraft may prove to be unstable at certain sideslip angles. Frequently, the canard must be

fairly large in order to provide the desired pitch maneuver capability, but a smaller canard would prove to provide better lateral stability.

In view of what has been said above, it is therefore likely that the choice of single or twin fins will depend less upon aerodynamic considerations and more upon structural and stealth features.

As mentioned previously, an important consideration in the design of low-observable aircraft is the requirement to align the leading edge of the wing and the fin leading edge sweep when projected into the horizontal. This is done to minimize the number of spikes of radar energy scattered towards the receiver. In other words, the fin leading edge sweep and cant angles must be chosen to conform to a given sweep of the horizontal projection. On the other hand, the choice of fin sweep may be made for aerodynamic reasons, such as a specific drag requirement. This may lead to conflicting design requirements, as illustrated in the following paragraphs.

Referring to Fig. 13, it can be found that the relationship between fin cant angle (QEF), leading edge sweep (QEFL) and leading edge sweep of the horizontal projection (QEFLH) is

$$\sin(\mathrm{QEF})\cdot\frac{\tan(\mathrm{QEFLH})}{\tan(\mathrm{QEFL})}=1 \qquad (1)$$

The relationship is valid only if QEF is not equal to 0 and if QEFLH is greater than or equal to QEFL. Assuming therefore that QEFLH is fixed, there are two possible ways of finding the other two angles.

The first would be to fix QEFL according to aerodynamic requirements. Usually, it is important that the critical Mach number of the fin should be greater than that of the wing in order to maintain control capability in the critical Mach region. Alternatively, the sweep may be chosen to provide the fin with a subsonic leading edge at the design supersonic Mach number. In this case, the fin leading edge sweep must be greater than $\cos^{-1}\left(1/\mathrm{Ma}\right)$. While this may be aerodynamically correct, the resulting value for the fin cant angle may be unacceptable in terms of the overall radar reflectivity of the aircraft. Hence the other approach. By defining a cant angle to conform to some desired radar cross section, a fin leading edge sweep may be found by fixing QEF and QEFLH. In this case the resulting sweep will be less than that required for supersonic Mach numbers.

The second of these two approaches was chosen for the baseline, in line with the requirement to design aircraft for low-observables. Although the supersonic drag of the vertical tail is not negligible, it can be argued that its magnitude is sufficiently small for it to play only a secondary role in the layout of the vertical fin of a stealthy aircraft. Therefore, designing a fin which is aerodynamically off-optimum is one of the penalties of stealth configured aircraft.

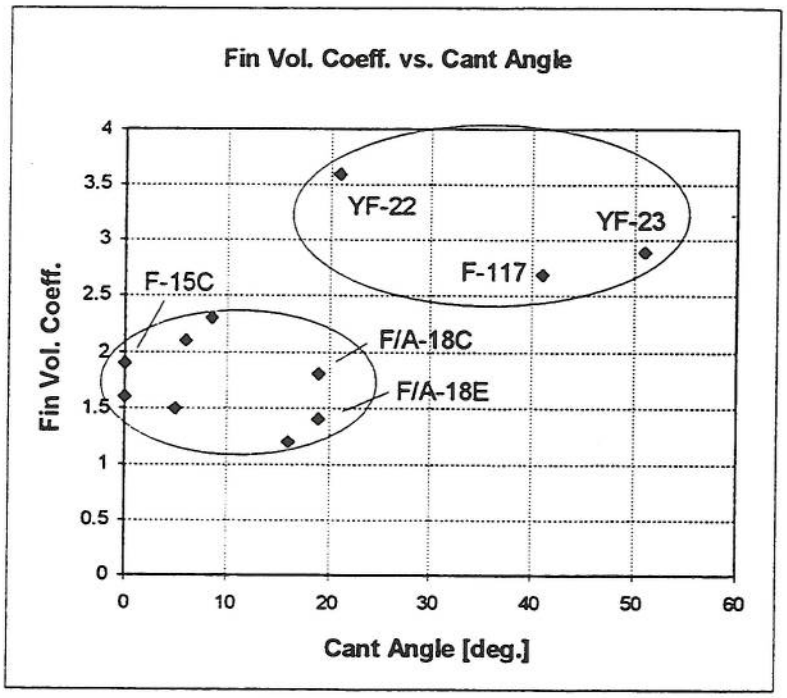

Fig. 12: Volume Coefficient vs. Cant Angle

In Figure 12, a variety of tail volume coefficients, calculated using the methodology suggested by (Lovell, 1988), are plotted against the fin cant angle. All of the sample cases shown are twin fin aircraft, and it is interesting to note that two groups can be distinguished. The YF-22, YF-23 and F-117 were all designed for low-observables, whereas the others were not.

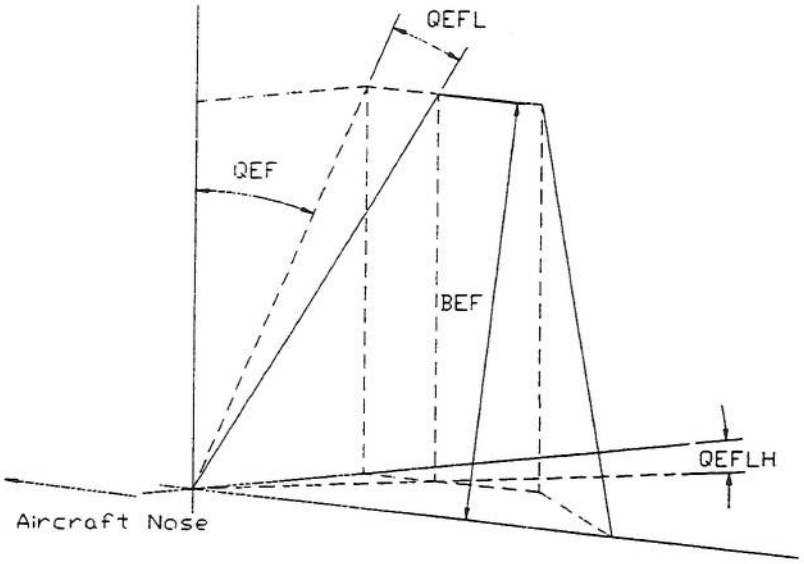

Fig. 13: Geometry of a Canted Fin

As described above, the choice of single or twin fins has important implications for the aerodynamics, stability and control and the structural design. The design synthesis accounts for these effects through use of the fin volume coefficient. It will have a different value for single or twin fins. In order to determine the mass of two fins, the mass of one of the two is calculated from its area and several other geometric parametric parameters, and then doubled. A similar procedure is followed to evaluate the drag.

3.2 Internal Weapons Bay

One of the greatest difficulties to be confronted during the conceptual design of aircraft with internal weapons bays is the estimation of the mass effects. Methods given in the literature for general fuselage cutouts such as doors and windows are generally not applicable because of the large dimensions of the bay in relation to the fuselage. Additionally complicating the issue is the fact that a weapons bay will normally be located in the center fuselage, a highly stressed part of the structure which carries not only the fuselage bending moments but also those of the wing, as well as shear and torsion loads. Moreover, other components which must be fitted near the center fuselage such as the engine intake ducts and the main landing gear compete with the weapons bay for space and load carrying structure to support them.

In combat aircraft, the structural and geometrical complexity of the fuselage generally leads to a layout in which the loads are carried to a large extent by mass booms, as opposed to a stressed skin, monocoque design common in simpler fuselage shapes on transport aircraft. The advantage of such a design is that a weapons bay can be located without too much difficulty in the cavities formed by the main wing box spars. The effect of the additional surrounds on the fuselage mass will not be quite as severe, since the skin itself is not as highly stressed. Also, structural modifications may incur less of a mass penalty if the doors are mounted to frames already designed to carry large loads.

On the other hand, the type of weapons bay to be implemented in a low-observable aircraft may necessitate a significant amount of structure for the launcher mechanism. It is subjected to highly dynamic loading as a result not only of the inertia loads during the launch process itself but also because of the heavy aerodynamic forces experienced when the bay doors are opened into the slipstream. The literature available on the aerodynamics of cavities (Vakili and Gauthier, 1994), (Chen, 1990), (Om, 1986), (Gharib et al, 1985) shows that the oscillations induced by the slipstream can be quite severe. Structural damage may occur if measures are not taken to control the flow in the cavity. Brian Wilson, in his lecture on the Navy Advanced Tactical Fighter (Wilson, 1993), mentioned the fact that the "noise of an open weapons bay at transonic speeds is quite horrendous". Further mass penalties may arise from the doors themselves, because they must be able to open in flight at all maneuvering conditions and can not carry any fuselage structural loads. This results in a strengthened fuselage structure to transmit the loads normally carried through the aircraft skin replaced by the weapons bay cavity.

Internal weapon bays are not very common on conventional combat aircraft. This fact is reflected in the lack of open literature available about such configurations. Despite the sometimes complicated aeroelastic effects during flight, stores, including tanks, have frequently been carried externally because of the simpler design of the supporting structure and ease of installation and maintenance, reducing turnaround time. External stores can also be added at a later stage in an aircraft's lifetime, although that is highly undesirable from an aircraft designer's point of view. Once an aircraft has dropped its external load, it has become relatively clean aerodynamically and is better suited for rapid egress from the combat area, aided by the fact that no excessive structural mass penalty is paid when compared with the essentially useless mass of an empty internal weapons bay.

On the other hand, external weapons create a significant amount of wave and interference drag, significantly degrading the aircraft range and performance. Also, they provide additional radar and visual reflection points, essentially degrading the low observable characteristics of the configuration. This argument is the main driver behind the desire of locating weapons internally.

For the purposes of this research program, it was decided to synthesize a weapons bay configuration which would allow a high degree of flexibility in the choice and arrangement of internal stores. During the optimization process, the size and initial mass of the weapons bay plus stores remains constant. Only the position may be varied by changing the value of two independent coordinates describing the positioning of the bays in the longitudinal and directions. Internally, the arrangement of the weapons may be varied by specifying the number of store points in the vertical, longitudinal and lateral directions. Furthermore, a choice of none, one, two or three bays is possible, as summarized in Table 2. The mass effects are catered for in the methods described in Chapter 4, consisting of mass terms for doors, surrounding structure, roof mass, and launcher mechanism installation mass. Furthermore, the dimensions of the bays are one of the main sizing drivers for the fuselage, significantly affecting its geometry, layout and mass.

3.3 Engine Bay and Intake Diffusers

The synthesis of the engine bay follows closely the approach given in (Lovell, 1988), modified by the author to cater for two-dimensional exhaust nozzles. A detailed description is given in Chapter 4.

The intake diffusers have a complicated, three dimensional geometry which arises mainly from the need to curve them around the internal weapons bay. In addition, flexibility needs to be provided for three different arrangements. The geometry is slightly different for twin- or single-engined aircraft. In addition, there is an option for the weapons bay to be located either below the diffusers or between the diffusers. Finally, the three-dimensional curvature of the intakes is necessary in order to hide the engine face from the intake as much as possible. This will reduce the infrared, acoustic and radar emissions from the aircraft when viewed head-on.

The mass effect of the engines, including installation, is calculated by a set of equations given in (Lovell, 1988). Engine size will also strongly affect the dimensions of the fuselage and hence its mass. The effect of the intake diffusers is included within the fuselage mass estimation methodology.

3.4 Thrust Vectoring Exhaust Nozzles

Vectoring exhaust nozzles are attractive for installation on future combat aircraft for a number of reasons. They are most advantageous in the extremes of the aircraft flight envelope, namely during high speed combat maneuvers as well as in the low speed, high angle of attack range. Another application is in the reduction of take off and landing distances. In any case, the full potential of vectored thrust will only be achieved if it is included in the aircraft design process from the outset, rather than considering it as an addition to an existing airframe.

Vectored thrust works in essentially two ways. The first and most obvious one is the capability of pointing the thrust vector in a direction away from the engine centerline. Thus, the engine/nozzle combination ceases to be an instrument for the provision of simple forward thrust. Instead, it can provide additional lift and sideslip forces as well as pitch and yaw moments. If two engines are used, roll control may additionally be possible. Since the magnitude of the forces and moments is quasi independent of the speed of the aircraft, vectoring can be employed at any point within or even outside of the conventional, aerodynamic flight envelope. Typical examples are the use of vectored thrust to influence the takeoff and landing distances as well as to control the high angle of attack, post-stall flight envelope (Gal-Or, 1994).

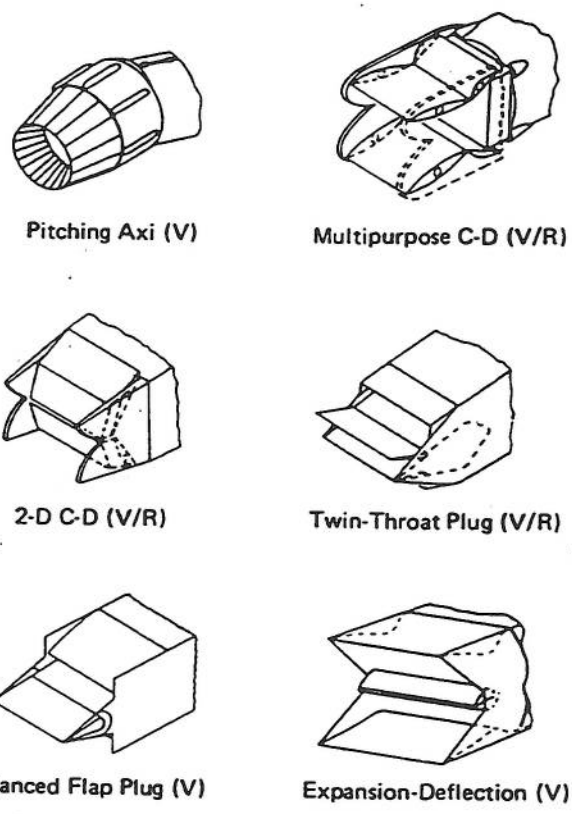

Fig. 14: Thrust vectoring nozzle types (Hiley et. al., 1976)

Vectored thrust can also affect the aerodynamics of the aircraft-nozzle combination by inducing supercirculation. Research into this phenomenon is quite old, and Poisson-Quinton (Poisson, 1956) gives a good summary of the physics of supercirculation. Thus, blowing a jet of air out

of the trailing edge of a body at an angle will influence both the boundary layer, by delaying the separation point, as well as the circulation, but it will not affect the transition from laminar to turbulent flow. Siestrunck states that the resultant force upon an airfoil with a jet flap is a sum of the forces due to Kutta-Joukowski circulation around the whole configuration (airfoil plus jet) on the one hand and the additional momentum of the jet on the other (Siestrunck, 1961). The additional lift is therefore due to the combination of an apparent increase in chord with a change in the camber.

The literature provides a large variety of experimental data and descriptions on different vectoring nozzle concepts, which can be broadly classified into two categories: axisymmetric and two-dimensional. Figure 14 shows some of these nozzle concepts. Axisymmetric vectoring nozzles are an extension of conventional, round nozzles. Thrust vectoring is achieved either by rotating the entire nozzle about a gimbal or by appropriately deflecting a circumferential array of paddles. As the name implies, they are symmetrical about the longitudinal axis.

Two-dimensional nozzles have rectangular cross sections and may take on a number of different shapes. One extremely common type is known as convergent-divergent (CD). As with the axisymmetric CD nozzles, the internal contour consists of a fixed-geometry convergent section followed by a variable divergent part. In some cases, the rear portion of the nozzle is replaced by a single expansion ramp. Such nozzles were developed for use on aircraft with vertical or short take off and landing characteristics, the idea being that the ramp provides extremely efficient and effective vectoring at large angles in one direction only. An interesting side effect of this last nozzle type is that the infrared emissions are also highly directional, thus making them attractive for installation on stealthy aircraft.

Thrust vectoring can provide a number of benefits which must be seen in conjunction with a perceived shift in emphasis away from high energy maneuvering towards rotational-translational agility (Herrick, 1988). In addition to pitch/yaw thrust vectoring, some of the more important features of modern aircraft which lead in this direction are high thrust-to-weight ratios, rapid thrust onset, stall resistant engines and integrated flight controls.

For example, the F-14, F-18, F-16 and F-15 were designed with high turn rates as well as rapid climb and acceleration in mind. In contrast, their cruise efficiency is very low. However, by employing thrust vectoring nozzles from the outset of the design process, the aircraft can be aerodynamically designed for supercruise conditions while retaining very good maneuvering capabilities in the transonic and high subsonic regimes. Consequently, reducing the size of the flying surfaces and controls to reduce drag may also sharply reduce gross weight. Potential benefits for low observable aircraft are the reductions both in visual signature as well as in radar cross section.

Contrary to the somewhat optimistic picture painted above, Kitowski raises a number of important points about the use of thrust vectoring (Kitowski, 1992). The key issue in its implementation appears to be the level of flying qualities expected upon failure of the nozzle vectoring system. Obviously, as in

the case of active controls, a balance must be struck between the desired improvement in performance and the reduction in flying qualities when thrust vectoring is inoperative. If vectoring is flight essential, failure will result in loss of control of the aircraft. Other problems associated with highly agile aircraft are the increased maneuver and gyroscopic forces experienced by the pilot during combat and increased inertia loads on aircraft components because of the higher pitch and yaw rates.

Mace and Nyberg showed how the use of thrust vectoring provided more overall benefits than achievable with flight controls only (Mace and Nyberg, 1992). Because of the trend in development towards multi-role aircraft, advanced technologies should be employed to improve the performance in ground attack roles while not degrading combat maneuverability. In addition to the payoffs mentioned above, the use of thrust vectoring can lead to redundancy in flight controls, helping to increase aircraft survivability. Also, the improvements in mission performance seem to be larger if the external stores present less drag, i.e. if air-to-air missiles are carried rather than air-to-ground. In other words, a low observable configuration configured by necessity with an internal weapons bay would benefit to an even larger extent from such improvements.

The design of vectoring nozzles must take into account the usage of vectoring and its impact upon the durability of the nozzle materials. Not only the increased loads in the vectored position are of importance but also fatigue due to the nozzle vectoring rate and cycle. Cain and Doane reported on a study about the analysis and usage of vectored thrust (Cain and Doane, 1992). By simulating flight usage in an accelerated mission test, they were able to create a database defining the pitch and yaw vectoring rates and cycles. They found that average yaw deflections are close to zero while pitch deflections had a significant pitch up tendency.

The pitch cycles were also highly autocorrelated, whereas yaw cycles tended to be driven by short, independent events. This is thought to be a result of the way pitch and yaw vectoring are used in combat. While the former tends to be employed for longer periods of time, such as for nose pointing or trim, the latter is mainly used for directional control at high angles of attack and is thus very cyclic. Most vectoring was found to occur at rates of around 0.75 Hz. However, fatigue crack rates are increased by chemical reactions in conjunction with vibrations at frequencies below 1.5 Hz (Cain and Doane, 1992). Finally, it was found that there is very little correlation between pitch and yaw vectoring cycles.

The decision whether to use axisymmetric or two-dimensional nozzles depends largely upon the aircraft configuration under consideration. Both types of nozzle can be designed to have similar vectoring characteristics, although two-dimensional ones are generally less efficient because the axisymmetric engine airflow needs to transition to a rectangular duct. Capone has found that round nozzles produce more supercirculation lift than two-dimensional ones but exhibit more drag (Capone, 1976). The reason for this appears to be that two-dimensional nozzles integrate more readily with the

aircraft afterbody. Also, as mentioned, two-dimensional nozzles can be made to have directional infrared and radar cross section characteristics. It appears, therefore, that they are more attractive for installation on stealthy aircraft than axisymmetric nozzles.

The literature provides very little concrete information about the mass effects of using vectoring nozzles compared with conventional ones. (Stevens et. al., 1981) have shown that mass increases may result from using higher expansion ratios, from higher normal forces as a result of vectoring, as well as from an increase in the ratio of width to height because of the corresponding increase in transition section length. This section is necessary in order to change the flowfield from circumferential to rectangular. On the other hand, the reduction in size of the control surfaces now possible with the introduction of thrust vectoring nozzles may well offset this increase.

The design synthesis accounts for the mass and external geometric characteristics of the thrust vectoring nozzles, if present. Mass increments can be specified for the nozzles and transition section, which, if necessary, are scaled following the approach developed in (Lovell, 1988). No additional increments to the fuselage structure are made to account for the effects of thrust vectoring usage on the supporting structure. Geometrically, the nozzle dimensions will have a large effect on the afterbody size and layout, thus affecting the fuselage mass (through wetted area and volume) and the boat tail drag (via the boat tail angle). Further work would be necessary to fully account for the complexities of thrust vectoring installations, including the effects of actuators and associated hydraulics as well as advanced materials on the mass of the aircraft. Furthermore, the current methodology does not take into account stability and control characteristics or thrust loss due to vectoring, both of which are essential for modeling the full impact on aircraft performance.

3.5 General Design Considerations

The main driver for the geometry of the aircraft types under consideration in this research project was the design of a layout which would simultaneously minimize the emissions and/or reflections of electromagnetic (radio, infrared and optical frequencies) and acoustic energy. At the same time, the requirements of the aircraft role were to be met, including the ability to carry a specified weapons load for a given distance whilst meeting performance constraints. The weapons capacity directly determines the size of the internal weapons bay, and the aircraft must in effect be designed around a weapons bay (Wilson, 1993).

In general, the initial layout will involve the definition of threat directions. Once the likelihood of a given system such as radar or heat-seeking missile to be used against the aircraft has been determined, the direction from which this threat is most likely to be employed must be identified. As an example, the front and rear head-on views of the aircraft are extremely common threat directions. This is not only due to the fact that an aircraft attacking a target is most likely to do so in a head-on direction, but also because it is more likely to

be illuminated head-on by surveillance radar or tail-on by airborne missile attack radar.

Once these threat directions have been agreed upon, their relative significance should be assessed. This is necessary in order to determine design priorities, since the aircraft emissions and reflections can generally not be minimized simultaneously for all threat directions. From an analysis of the available literature on stealth design, it was determined that the most likely threat directions needing attention are the head-on, rear and lateral ones. The following general design rules were derived from these requirements:

First, the overall fuselage height should be kept as low as possible. This will particularly reduce the optical signature of an aircraft when viewed from the side or head-on. It can also be said that the aircraft should be as small as possible, for the same reason. Second, the fuselage sides should be tilted away from the vertical. This will tend to scatter incident radiation, in particular the large reflective spikes associated with radar energy, away from the observer. Also, the joining of two surfaces at right angles must be avoided at all costs in order to prevent the creation of corner reflectors.

Second, the engines should be shielded as much as possible, both by burying them as far as possible within the fuselage and by hiding the intakes and exhausts. This can be accomplished by curving the ducts and by choosing a twin-fin arrangement.

Finally, any straight edges such as chines or wing and tailplane leading edges should be oriented in parallel to each other. This is done in order to reduce the number of reflective parts generating distinct spikes of radar energy to as few as possible. Wing and horizontal stabiliser should be located in the same plane. Surfaces should be treated in the same manner: the fuselage sides, as an example, must all reflect incident energy at the same angle.

The fact that the combined wing and fuselage horizontal surfaces may offer a large reflector is not considered to be of extreme importance, because the likelihood that an aircraft will be illuminated by a threat from directly above or directly below is extremely small.

Minimizing the reflections and emissions will be the result of simultaneously juggling a large number of variables. The design of the fuselage for a stealth aircraft and in particular the provision of code for the numerical synthesis must reflect this. Thus, it may appear that some of the fuselage cross sections described in the following chapters are excessively complicated. However, it is felt that only in this way can the desired design flexibility be achieved.

4. Description of the Design Methodology and Tools

In the following chapters, a detailed description of the design synthesis and analysis tools developed for and used in this research project is given. Section 4.1 describes the design synthesis models and algorithms designed, developed and coded in FORTRAN by the author. They represent the bulk of the design work for this research program. This chapter will only describe those mathematical relationships developed, modified or enhanced by the author, whereas the description of the ones retained unmodified from the original work in (Lovell, 1988) is left as a reference.

In Section 4.2, the graphical output tool developed by the author and the numerical optimizer as provided by the DRA are described. Finally, this chapter closes with a description of the complete multivariate optimization code.

4.1 Aircraft Design Synthesis

The aircraft design synthesis for the numerical modelling of a swept wing combat aircraft is described below. It consists of a large number of modules, or subroutines in FORTRAN, containing design relationships to estimate the geometry and mass of the major aircraft components. Furthermore, a set of modules, partially described here, is used to describe the aerodynamic and performance characteristics of the complete aircraft and its components, if applicable. Examples of the latter include the wing, the empennage and the engine.

The synthesis of the geometry follows a modified nose-to-tail approach. This means that fuselage cross-sections are synthesized in order from the front to the rear of the aircraft. Certain reference fuselage stations are synthesized before other, intermediate positions. Fixed items of the geometry are calculated once at the beginning of the synthesis. They include the radome, the cockpit, and the weapons and gun bays. Once these items have been mathematically described, a series of cross sections are generated according to several criteria. Firstly, they must fit around all of the internal components. Secondly, the area at each cross-section must match an area given by the fairing curve, or area distribution. For a description of the fairing curve see (Lovell, 1988). A total of ten reference fuselage stations are defined. Their locations were chosen so as to coincide with major changes in the fuselage shape and to be most representative of the aircraft geometry at those points. Examples include the front of the cockpit, the intake position, the engine face and the front of the engine exhaust nozzle. They are described in more detail in Section 4.1.1.6. Minimum dimensions are derived from the location of and size of the internal components at each cross section.

The general layout of the aircraft geometry has been shown in Chapter 3, Fig. 11 (page 17). A schematic diagram of the synthesis sequence of the fuselage

and the reference stations as well as a more detailed description of their location is given in Fig. 32 (page 77) and Section 4.1.1.7.

4.1.1 Geometry

The geometry of the aircraft is built up of a number of components. Only the geometry of the radome, the cockpit, the intake diffusers and engine, the weapons bay, the empennage and the fuselage cross-sections are described in detail here, because these are the components whose synthesis relationships were newly developed by the author. For a complete description of the remaining components, including the fairing curve and the wing, the reader is referred to (Lovell, 1988).

4.1.1.1 Radome

The diameter of the nose at the position of the radar dish is determined by an antenna diameter, DAR, and an increment, EDAR, to allow for clearances. It is assumed that the cross sectional area varies linearly from the front of the radome to the radar dish with a gradient given by GOF1.

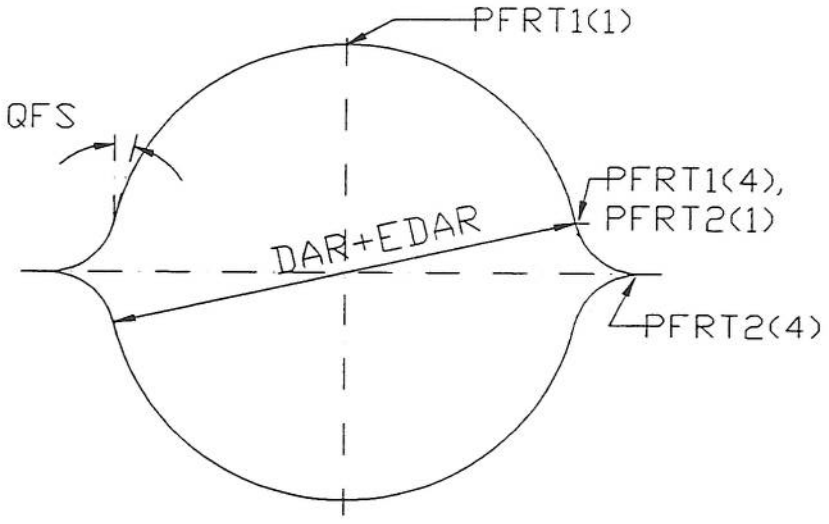

Fig. 15: Fuselage Cross-Section at Radar Dish

Referring to Figure 15, a spline is fitted to the radome such that

$$\begin{aligned} \text{PFRT2}(1,1) &= \frac{\text{DAR}+\text{EDAR}}{2\cdot\cos(\text{QFS})}, \\ \text{PFRT2}(1,2) &= 0, \\ \text{PFRT2}(4,1) &= 0.5\cdot(\text{DAR}+\text{EDAR})\cdot\cos(\text{QFS}), \\ \text{PFRT2}(4,2) &= 0.5\cdot(\text{DAR}+\text{EDAR})\cdot\sin(\text{QFS}), \end{aligned} \tag{2}$$

G1 = 0 , and

G2 = -tan(0.5·π - QFS) ,

using the subroutine BEZFIT to calculate the remaining points of the spline. Subroutine BEZFIT is explained in detail in Appendix C.

Also,

$$\begin{aligned} &PFRT1(1,1) = 0 , \\ &PFRT1(1,2) = 0.5\cdot(DAR + EDAR) , \\ &PFRT1(4,1) = PFRT2(1,1) , \text{ and} \\ &PFRT1(4,2) = PFRT2(1,2) . \end{aligned} \tag{3}$$

G1 and G2 have the same value as in Eq. 2. The perimeter and cross-sectional area of the radome are found using BEZEVAL, described in Appendix C, as well as the relationships

$$PFR = 3.14\cdot(DAR + EDAR)\cdot\frac{1}{1 - 2.0\cdot\frac{QFS}{3.14}} , \text{ and} \tag{4}$$

$$\begin{aligned} OF1 = &\left(1 - 2.0\cdot\frac{QFS}{3.14}\right)\cdot 0.785\cdot(DAR + EDAR)^2 + \\ &+ 0.5\cdot(DAR + EDAR)^2\cdot\sin(QFS)\cdot\cos(QFS) + 4.0\cdot area(PFRT) . \end{aligned} \tag{5}$$

The length, volume and wetted area of the radome are given by

$$\begin{aligned} XFR &= \frac{OF1}{GOF1} , \\ VFR &= \frac{1}{3}GOF1\cdot XFR^2 , \text{ and} \\ WFR &= \frac{2}{3}\cdot PFR\cdot XFR \end{aligned} \tag{6}$$

respectively.

4.1.1.2 Cockpit

The design synthesis of the cockpit follows closely the approach given in (Lovell, 1988), with modifications as proposed by J. Kirk of the Defence Research Agency to allow for the option of single or twin, tandem cockpits. The dimensions and arrangement of components were based upon information obtained from (MIL-STD-1333B, 1987) and (MS33574, 1987) as well as (DEF STAN 00-970). If a one-seat cockpit is chosen, the layout is as given by Lovell. Fig. 16 shows the layout for a two seat arrangement.

Thus,

$$QCFOOT = \sin^{-1}\left[\frac{HC3 \cdot \sin(QCSEAT) + HCSEAT \cdot \cos(QCSEAT)}{HC2}\right], \tag{7}$$

$$HCEYE = HC1 \cdot \cos(QCSEAT) + HC3 \cdot \sin(QCSEAT) + \\ + HCSEAT \cdot \cos(QCSEAT) \quad , \tag{8}$$

$$LCEYE1 = HC1 \cdot \sin(QCSEAT) + HC2 \cdot \cos(QCFOOT) + LCFOOT \ , \tag{9}$$

$$LCFL1 = HC2 \cdot \cos(QCFOOT) + LCFOOT + HC3 \cdot \cos(QCSEAT) - \\ - HCSEAT \cdot \sin(QCSEAT) + \frac{EHCS}{\cos(QCSEAT)} \ , \tag{10}$$

$$HC5 = HCEYE - LCEYE1 \cdot \tan(QCEYE1) \ , \tag{11}$$

$$HCWSC = (HCSEAT + HC1) \cdot \cos(QCSEAT) + HC6 \cdot \sin(QCEYE2) \ , \tag{12}$$

$$LCWSC = LCEYE1 - (HC6 - HC3) \cdot \cos(QCSEAT) \ , \text{ and} \tag{13}$$

$$HC7 = 0.5 \cdot BCH \cdot \tan(QCEYE3) \ . \tag{14}$$

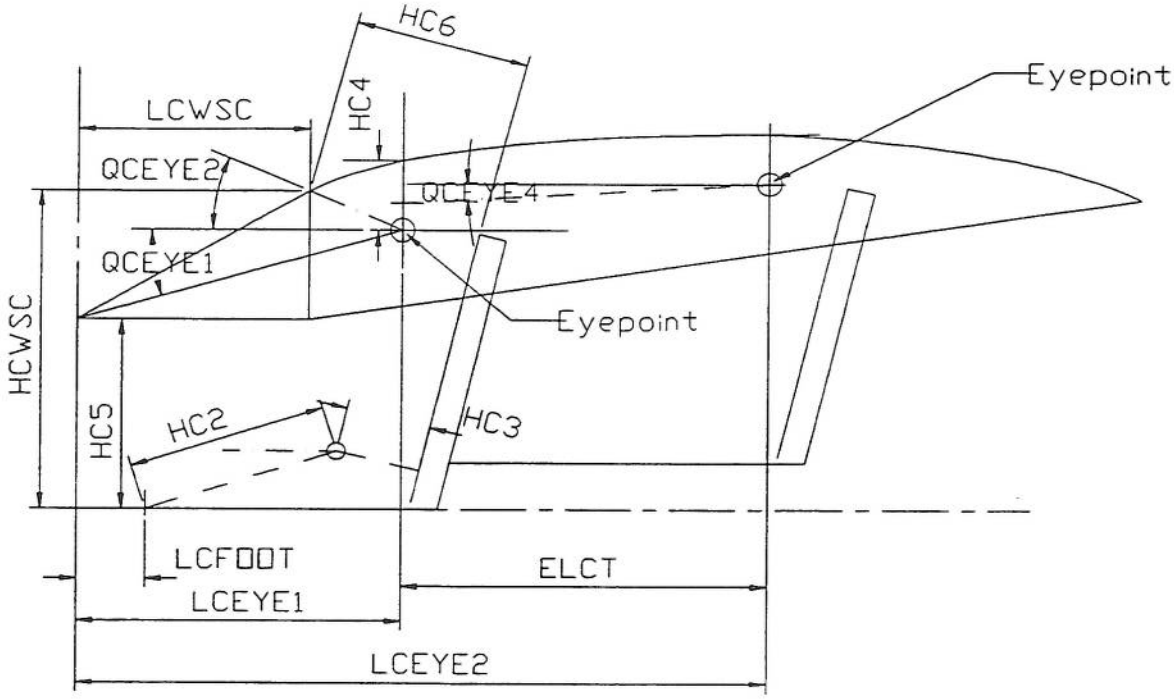

Fig. 16: Cockpit Layout for Twin-Seat Arrangement

The vertical coordinate of the canopy top centreline is described by a cubic, with a front and rear section the size of which depends upon whether a single or two-seat configuration is chosen. The gradient used to define the forward section is obtained from the windscreen inclination angle:

$$QCWSC = \tan^{-1}\left(\frac{HCWSC - HC5}{LCWSC}\right). \tag{15}$$

For a single seat cockpit, LCT=LCFL1, and the following additional relationships apply:

$$HCCANS = HCEYE + HC4 \quad \text{and} \tag{16}$$

$$LCCANS = LCEYE1 - LCWSC\,. \tag{17}$$

The values for LCWSC, HCWSC, QCWSC, LCEYE1, and HCCANS are used to fit the cubic for the front part of the canopy, and stored in the array FZCF. At the rear of the canopy, the vertical coordinate used to define the cubic is calculated from

$$HCCANR = HCEYE - HC7 + (LCCAN - LCEYE1)\cdot\tan(QCCAN)\,, \tag{18}$$

which makes use of QCCAN, the cockpit side inclination angle, and the canopy length, LCCAN, both of which are external variables. The gradient of the canopy top centreline is given by

$$GCCANR = 2 \cdot \frac{ZCCANR - HCCANS}{LCCANS - LCEYE1} \quad . \tag{19}$$

The resulting cubic is stored in the array FZCR. Should a twin-seat cockpit have been chosen, then

$$LCT = LCFL1 + ELCT \quad , \tag{20}$$

$$HCT = HC4 + ELCT \cdot \tan(QCEYE4) \quad , \tag{21}$$

$$LCFL2 = ELCT - HCT \cdot \tan(QCSEAT) \quad , \tag{22}$$

$$LCEYE2 = ELCT + LCEYE1 \tag{23}$$

$$HCCANS = HCEYE + HC4 + HCT \quad , \text{ and} \tag{24}$$

$$LCCANS = LCEYE2 - LCWSC. \tag{25}$$

Using the values calculated above, the front cubic is fitted between the rear of the windscreen and the point at which the canopy is assumed to reach its maximum height, located above the eyepoint of the rear seat. For the aft portion of the canopy cubic,

$$ZCCANR = HCEYE - HC7 + (LCCAN - LCEYE1) \cdot \tan(QCCAN) \text{ and} \tag{26}$$

$$GCCANR = 2 \cdot \frac{ZCCANR - HCCANS}{LCCAN - LCEYE2} \quad . \tag{27}$$

4.1.1.3 Weapons Bay

The synthesis methodology of the weapons bay was designed to allow a great deal of flexibility for the specification of the weapons load while maintaining an overall simple algorithmic structure. An external variable, NWEPB, chooses the number of weapons bays to be synthesized. Thus, if NWEPB=1, a single bay located on the centreline is chosen. If NWEPB=2, two bays outboard of the diffusers are selected. Finally, if NWEPB=3, then both an inner and two outer bays are implemented. Alternatively, NWEPB=0 allows the implementation of no weapons bay.

A group of external variables, NLBI, NBBI, and NHBI control the number of store stations lengthwise, in width, and in height, respectively. Using some clearance factors, LB1K, BB1K and HB1K for the inboard ones and LB2K, BB2K and HB2K for the outboard ones, the bay dimensions are found as

$$\begin{aligned} &LB1BI = NLB1I \cdot LB1I + LB1K, \\ &BB1BI = NBB1I \cdot BB1I + BB1K, \text{ and} \\ &HB1BI = NHB1I \cdot HB1I + HB1K \end{aligned} \tag{28}$$

for the inner bay, and

$$\begin{aligned} &LB2BI = NLB2I \cdot LB2I + LB2K, \\ &BB2BI = NBB2I \cdot BB2I + BB2K, \text{ and} \\ &HB2BI = NHB2I \cdot HB2I + HB2K \end{aligned} \tag{29}$$

for each outer bay. The cross-sectional area of the weapons bay cavities on the fuselage surface are given by

$$\begin{aligned} &OB1BI = BB1BI \cdot LB1BI \text{ and} \\ &OB2BI = BB2BI \cdot LB2BI \end{aligned} \tag{30}$$

for the inner and each outer bay, respectively. The volume of the bays is given by

$$\begin{aligned} &VB1BI = OB1BI \cdot HB1BI \text{ and} \\ &VB2BI = OB2BI \cdot HB2BI \ . \end{aligned} \tag{31}$$

4.1.1.4 Empennage

The initial sizing of the vertical tail is accomplished using the vertical tail volume coefficient, REFSW, but with a slightly different approach as compared to that suggested in (Lovell, 1988). It is given by the following expression:

$$\mathrm{REFSW} = \frac{\mathrm{SEFNV} \cdot \mathrm{LEFCQM}}{0.5 \cdot \mathrm{XWCQM} \cdot \mathrm{DFC}^2}, \tag{32}$$

from which SEFNV, the projection of the fin area into the vertical plane, is derived. SEFNV gives the total area of the fins, that is, in the case of twin fins, the area of one fin is found by halving SEFNV. LEFCQM is obtained from the design variables by subtracting from XEFCQM the position of the mean aerodyamic quarter-chord point, XWCQM. XEFCQM, in turn, is a function of a design variable which gives the position of the fin mean aerodynamic quarter-chord point aft of the nose of the aircraft as a fraction of the fuselage length. This procedure also allows the fin trailing edge to extend beyond the nozzle exit plane. Although Equation 32 uses the equivalent fuselage diameter at Station C (DFC), the link between fin size and fuselage cross sectional area may need further investigation.

The cant angle of the fins is QEF, measured from the vertical plane, and thus the fin area is found from

$$\mathrm{SEFN} = \frac{\mathrm{SEFNV}}{\cos(\mathrm{QEF})}. \tag{33}$$

Similarly, the projection of the fin area into the horizontal plane, SEFNH, is found from

$$\mathrm{SEFNH} = \mathrm{SEFN} \cdot \sin(\mathrm{QEF}). \tag{34}$$

Once a fin volume coefficient has been chosen and the fin areas have been calculated, the rest of the fin dimensions may be determined. Thus, the length of the fin root chord is found from

$$\mathrm{BEFN} = \sqrt{\frac{\mathrm{AEFN} \cdot \mathrm{SEFN}}{\mathrm{NFIN}}} \quad \text{and} \tag{35}$$

$$\mathrm{CEFB} = \frac{2}{1 + \mathrm{UEFN}} \cdot \mathrm{BEFN}, \tag{36}$$

where NFIN is the number of fins. The tip chord and the mean aerodynamic chord of the fin are given by

$$CEFT = CEFB \cdot UEFN \quad \text{and} \tag{37}$$

$$CEFM = \frac{2}{3} \cdot CEFB \cdot \frac{1 + UEFN + UEFN^2}{1 + UEFN}, \tag{38}$$

respectively, and the mean aerodynamic chord vertical location above the root chord is found from

$$ZEFM = \cos(QEF) \cdot BEFN \cdot \frac{CEFB - CEFM}{1 - UEFN}. \tag{39}$$

The mean quarter chord point is located a distance

$$XEFM = BEFN \cdot \frac{CEFB - CEFM}{1 - UEFN} \cdot \tan(QEFL) + 0.25 \cdot CEFM \tag{40}$$

aft of the leading edge of the fin.
The distance of the fin leading edge at the root aft of the nose is given by

$$XEFLB = XWCQM + LEFCQM - XEFM . \tag{41}$$

The volume of the fin is given by

$$VEFF = 0.15 \cdot UEFF \cdot RTEF \cdot CEFB^2 \cdot BEFN \cdot (1 + UEFN + UEFN^2) . \tag{42}$$

For the horizontal stabilizer,

$$SETN = \frac{RETSW \cdot SW \cdot CWMG}{LETCQM} . \tag{43}$$

In a manner similar to LEFCQM, LETCQM is found from a design variable, XETCQM, from which is subtracted XWCQM. No account needs to be taken of the fin contribution to the horizontal stabilizer effectiveness (if canted) because this is catered for by appropriate choice of fin volume coefficient. Furthermore,

$$BETN = \sqrt{SETN \cdot AETN} , \tag{44}$$

$$CETB = 2.0 \cdot \frac{BETN}{AETN \cdot (1 + UETN)} , \tag{45}$$

$$CETT = CETB \cdot UETN \ , \tag{46}$$

$$CETM = \frac{2}{3} \cdot CETB \cdot \frac{1 + UETN + UETN^2}{1 + UETN} \ , \text{ and} \tag{47}$$

$$XETM = \frac{CETB - CETM}{1 - UETN} \cdot 0.5 \cdot BETN \cdot \tan(QETL) + 0.25 \cdot CETM \, . \tag{48}$$

The leading edge of the horizontal stabilizer at the root is located aft of the aircraft nose a distance

$$XETLB = XWCQM + LETCQM - XETM \, . \tag{49}$$

4.1.1.5 Engine Bay and Diffusers

The development of the thrust vectoring module followed closely the engine and nozzle design synthesis given in (Lovell, 1988). The original engine bay specification was retained, with modifications where appropriate to accomodate two-dimensional vectoring nozzles.

The engine geometry when axisymmetrical nozzles are used is defined by Fig. 17 (page 44), and an engine with two-dimensional nozzles is shown in Fig. 19 (page 45). The difference is in the presence of a section for transition from a circular cross-section to a rectangular one if two-dimensional nozzles are being used. A set of external variables define a reference engine in terms of the lengths, diameters and masses of the gas generator, reheat section including refuelling, nozzle and thrust reverser, if fitted. Using a scaling factor, RTP, which is also a design variable, the reference engine is scaled to match the aircraft thrust requirements according to a set of correlations given below.

$$\begin{aligned} LP12 &= LP12R \cdot RTP^{FLP1K} \ , \\ LP22A &= LP22AR \cdot RTP^{FLP2K} \ , \\ LP2A4 &= LP2A4R \ , \\ LP2B3 &= LP2B3R \cdot RTP^{FLP3K} \ \text{and} \\ LP34 &= LP34R \cdot RTP^{FLP4K} \ , \end{aligned} \tag{50}$$

and therefore

$$LP22B = LP22A + LP2A4 - LP3 - LP2B3. \tag{51}$$

If axisymmetric nozzles are used, LP23 is equal to LP22B, otherwise LP23 is equal to LP22B+LP2B3.

The overall engine length is given by

$$LPG = LP12 + LP23 + LP34. \tag{52}$$

At each reference station a diameter is found from the following relationships:

$$\begin{aligned} DP1 &= DP1R \cdot \sqrt{RTP}, \\ DP2 &= DP2R \cdot \sqrt{RTP}, \\ DP3 &= DP3R \cdot \sqrt{RTP} \quad \text{and} \\ DP4 &= DP4R \cdot \sqrt{RTP}. \end{aligned} \tag{53}$$

When two-dimensional nozzles are being used, the reference diameter at station 2B is assumed to be the same as for station 3.

The number of engines is set by an external variable, NENG, and therefore the total nozzle exit area is given by

$$OPN = NENG \cdot \frac{\pi}{4} \cdot RTP \cdot DP4R^2 . \tag{54}$$

If an axisymmetric nozzle has been installed, then the reference engine is assumed to have circular cross sections at all of the reference stations. When two-dimensional nozzles are installed, the transition from a circular to a rectangular cross section is assumed to occur between section 2B and section 3. In order to determine the dimensions at station 4, an aspect ratio is defined:

$$AP4 = \frac{HP4}{BP4} \tag{55}$$

and consequently the height and width may be determined by considering the cross-sectional area defined in equation (54):

$$\begin{aligned} HP4 &= \sqrt{\frac{OPN}{NENG} \cdot AP4} \\ BP4 &= \frac{HP4}{AP4} \end{aligned} \tag{56}$$

A set of vertical and horizontal clearances are applied to the scaled engine defined above. They are defined as the sum of all the gaps between engine and fuselage, including the gap between engines for a twin-engine installation. Together, they form the engine bay, which represents the minimum dimensions of the installed propulsion system. The clearances at each station are found from linear functions of the respective engine diameters. Also, they are constrained to lie within specified minimum and maximum values. Cubic splines are used to fair the joins between the limiting values in order to ensure a smooth variation of the engine clearance with engine size. Thus, the overall clearances on height are found to be

$$\begin{aligned} EHP1 &= FHP1K \cdot DP1 \quad \text{for} \quad EHP1S \le EHP1 \le EHP1H \\ EHP2 &= FHP2K \cdot DP2 \quad \text{for} \quad EHP2S \le EHP2 \le EHP2H \\ EHP3 &= FHP3K \cdot DP3 \quad \text{for} \quad EHP3S \le EHP3 \le EHP3H . \end{aligned} \tag{57}$$

The clearance at station 2B is assumed to be the same as at station 3. On breadth, the clearances are dependent upon the presence of twin or single engines, and may be calculated from

$$\begin{aligned} EBP1 &= \frac{FBP1K \cdot DP1}{NENG} \quad \text{for} \quad EBP1S \le EBP1 \le EBP1H \\ EBP2 &= \frac{FBP2K \cdot DP2}{NENG} \quad \text{for} \quad EBP2S \le EBP2 \le EBP2H \\ EBP3 &= \frac{FBP3K \cdot DP3}{NENG} \quad \text{for} \quad EBP3S \le EBP3 \le EBP3H . \end{aligned} \tag{58}$$

The factors FBPK and the limits EHPS, EHPH, EBPS and EBPH have different values for a twin- and a single-engine installation. Accordingly, the overall clearance on bay width is divided between the number of engines to obtain figures appropriate to a side-by-side installation. There are no clearances at station 4, the nozzle exit plane.

The dimensions of a two-dimensional nozzle at station 3 are found by considering the dimensions at station 4. The width of the nozzles is assumed to remain constant between sections 3 and 4, and therefore the height of the nozzle at station 3 may be found from the area defined by the reference diameters in equation (53):

$$\begin{aligned} BP3 &= BP4 - EBP3 \\ HP3 &= \frac{\frac{\pi}{4} \cdot DP3^2}{BP3} \end{aligned} \tag{59}$$

If axisymmetric nozzles are installed, then the cross sections of the stations of a single engine installation are assumed to be elliptical in shape, with the

major and minor axes fixed by the engine diameter at the respective station plus the clearances. Thus,

$$OP1B = NENG \cdot \frac{\pi}{4} \cdot (DP1 + EHP1) \cdot (DP1 + EBP1) ,$$

$$OP2B = NENG \cdot \frac{\pi}{4} \cdot (DP2 + EHP2) \cdot (DP2 + EBP2) , \text{ and} \qquad (60)$$

$$OP3B = NENG \cdot \frac{\pi}{4} \cdot (DP3 + EHP3) \cdot (DP3 + EBP3) .$$

Should two-dimensional nozzles be installed, the diameter at stations 3 and 4 is replaced by the respective heights and widths of the nozzle, calculated in Equations (56) and (59). In this case, the cross-sectional area at section 3 becomes

$$OP3B = NENG \cdot [(BP3 + EBP3) \cdot (HP3 + EHP3) - 0.21 \cdot EBP3 \cdot EHP3. \qquad (61)$$

This expression was derived by considering the corners of the nozzle to be elliptical in shape, as shown in Fig. 18 (page 44). The cross-sectional area at station 2B is considered to be:

$$OP2BB = NENG \cdot \frac{\pi}{4} \cdot (DP3 + EBP3)(DP3 + EHP3) \qquad (62)$$

and is equal to the cross sectional area of station 3 for the axisymmetric nozzle installation.

For an engine with axisymmetric nozzles, the volume of the engine bay is found using the assumption that the height and width vary linearly between stations 1, 2, 3 and 4. Hence,

$$VP12B = \qquad (63)$$

$$= \frac{LP12}{3} \cdot \left\{ OP1B + OP2B + NENG \cdot \frac{\pi}{8} \cdot \left[\begin{matrix} (DP1 + EHP1) \cdot (DP2 + EBP2) + \\ + (DP2 + EHP2) \cdot (DP1 + EBP1) \end{matrix} \right] \right\}$$

$$VP23B = \qquad (64)$$

$$= \frac{LP23}{3} \cdot \left\{ OP2B + OP3B + NENG \cdot \frac{\pi}{8} \cdot \left[\begin{matrix} (DP2 + EHP2) \cdot (DP3 + EBP3) + \\ + (DP3 + EHP3) \cdot (DP2 + EBP2) \end{matrix} \right] \right\}$$

and

$$VP34B = \frac{LP34}{3}\cdot\left\{OP3B + OPN + NENG\cdot\frac{\pi}{8}\cdot DP4\cdot[2\cdot DP3 + EHP3 + EBP3]\right\}. \tag{65}$$

When two-dimensional nozzles are installed, volume VP12B does not change and VP22BB is set equal to VP23B. However, VP34B is now found from

$$VP34B = 0.5\cdot(OP3B + OP4B)\cdot LP34 \tag{66}$$

and VP2B3B is found with

$$VP2B3B = 0.5\cdot(OP2BB + OP3B)\cdot LP2B3\ . \tag{67}$$

Finally, the total engine bay volume becomes

$$VPB = VP12B + VP23B + VP34B + VP2B3B, \tag{68}$$

with VP2B3B equal to the value computed by equation 67 for two-dimensional nozzles or set to zero if axisymmetric nozzles are used.

For a twin engine installation, the engine spacing, YPCH, is found as the maximum of the distances given by the application of an engine separation factor, FYPCH, to each engine bay station in turn. The minimum value is defined by FYPCH=1.22. Similarly, a maximum engine bay height is found by examining the installed height of each station in turn. This value, HPH, is used to determine the vertical engine position relative to the wing position.

The geometry of the intake diffusers is relatively complex, and makes use of cubic curve fits between predetermined fuselage stations according to the internal component arrangement.. First, a general diffuser cross section is shown in Fig. 20 (page 45). An aspect ratio is defined as

$$AII = \frac{HII}{BII}\ . \tag{69}$$

Referring to the figure, the following variables are defined:

$$HIIB = \frac{HII\cdot\cos(QID1)}{\sin\left(\frac{\pi}{2} - QID1 + QID2\right)} \tag{70}$$

$$BIIB = BII \cdot \cos(QID2) \tag{71}$$

The coordinates of the center of the parallelogram, defined as the intersection of the diagonals, are given as follows:

$$ZIDC = \frac{HIIB + BII \cdot \sin(QID2)}{2} - BII \cdot \sin(QID2) \tag{72}$$

$$YIDC = \frac{BIIB + HIIB \cdot \tan(QID1)}{2} \tag{73}$$

These relationships describe the geometry of the enclosing parallelogram. For a given station, the ratio of the enclosing area to the actual cross-sectional area is given by ROIDX. This value is assumed to vary linearly from the intake plane to a station which is located one engine diameter ahead of the engine face. At this last station, ROIDX is given by the ratio of the area of a square to the area of the inscribed circle. Thus, for the variation of ROIDX with axial distance, we have

$$ROIDX = 1 + \left(\frac{4}{\pi} - 1\right) \cdot \frac{XID}{LIDG - DIE} \tag{74}$$

Similarly, the cross-sectional area as well as the angles giving the inclination of the parallelogram are assumed to vary linearly from the intake to the diffuser exit. Thus,

$$OIX = OII + \frac{OIE - OII}{LIDG - DIE} \cdot XID, \tag{75}$$

$$QIDX1 = QFC3 \cdot \left(1 - \frac{XID}{LIDG - DIE}\right), \text{ and} \tag{76}$$

$$QIDX2 = QFC2 \cdot \left(1 - \frac{XID}{LIDG - DIE}\right) \tag{77}$$

The aspect ratio is similarly assumed to vary linearly with axial distance. At the engine face, it is equal to 1 and thus

$$AIDX = AII \cdot \left(1 - \frac{XID}{LIDG - DIE}\right). \tag{78}$$

Using the values defined above, it is possible to find the dimensions of a given diffuser station. The vertical inboard coordinate is found as

$$HIDBX = \frac{\sqrt{\frac{AIX \cdot OISX}{2}} \cdot \cos(QIX1)}{\sin\left(\frac{\pi}{2} - QIX1 + QIX2\right)}, \text{ with} \tag{79}$$

$$OISX = OIX(XID) \cdot ROIDX(XID) \ . \tag{80}$$

The three-dimensional geometry of the diffusers is modelled as shown in Fig. 21 (page 46). It has been divided into a forward and a rear section, with the latter extending to a station which is located one engine diameter forward of the compressor face. The Y- and Z-coordinates of the center of any given diffuser station are given by the equations

$$\begin{aligned} ZIX &= ZI + FZIA \cdot X^3 + FZIB \cdot X^2 \text{ and} \\ YIX &= YI + FYIA \cdot X^3 + FYIB \cdot X^2 \ . \end{aligned} \tag{81}$$

For the forward section of the diffuser, X is measured rearwards from XII and

$$\begin{aligned} FZIA &= \frac{-2 \cdot (ZI1 - ZII)}{(XI1 - XII)^3} \quad \text{and} \\ FZIB &= \frac{3 \cdot (ZI1 - ZII)}{(XI1 - XII)^2} \ . \end{aligned} \tag{82}$$

Similarly, for the equation giving the Y-coordinate,

$$\begin{aligned} FYIA &= \frac{-2 \cdot (YI1 - YII)}{(XI1 - XII)^3} \quad \text{and} \\ FYIB &= \frac{3 \cdot (YI1 - YII)}{(XI1 - XII)^2} \ . \end{aligned} \tag{83}$$

In order to find the centerline coordinates of the rearward portion of the intake diffuser, the same relationships as in equations 81, 82 and 83 may be

used. This time, however, X is measured from XI1, (YI1-YII) is replaced by (YI2-YI1), (ZI1-ZII) is replaced by (ZI2-ZI1) and (XI1-XII) is replaced by (XI2-XI1).

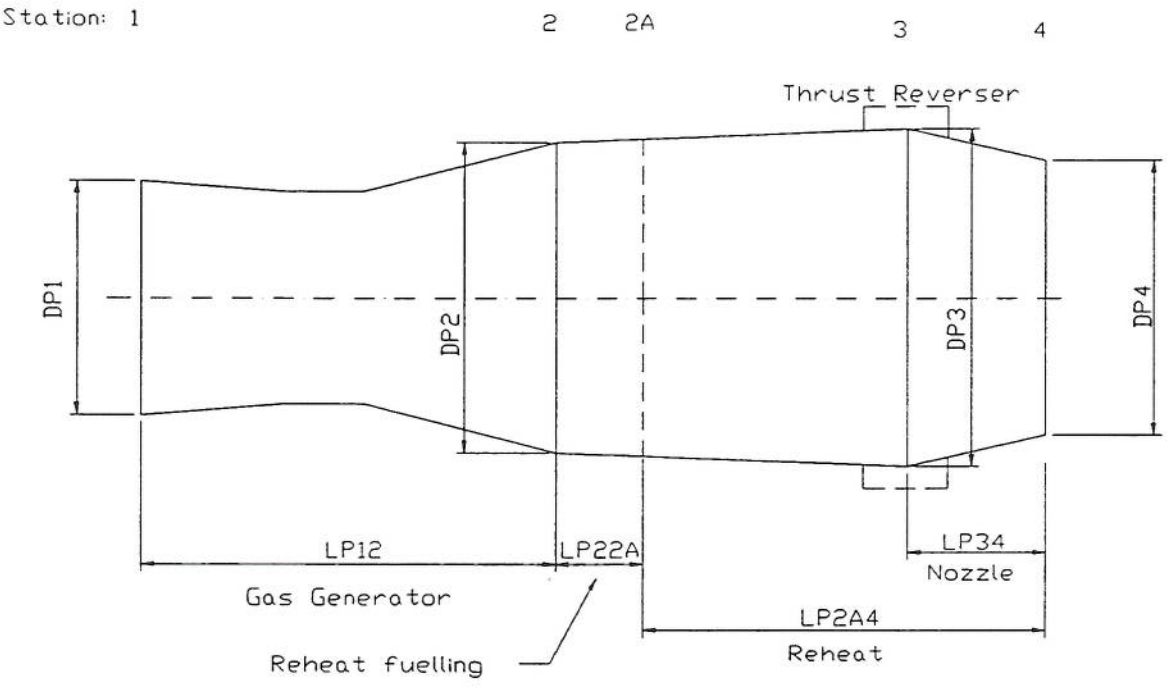

Fig. 17: Engine Bay Geometry, Axisymmetric Nozzles

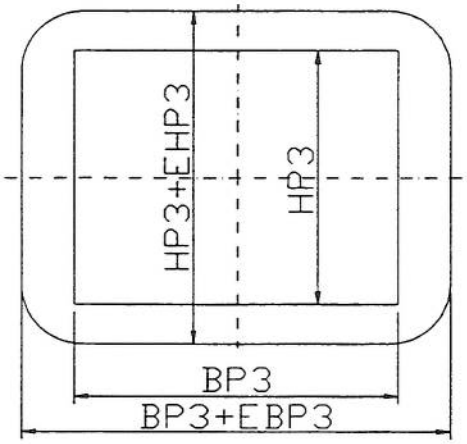

Fig. 18: Two-dimensional Nozzle Cross-Section

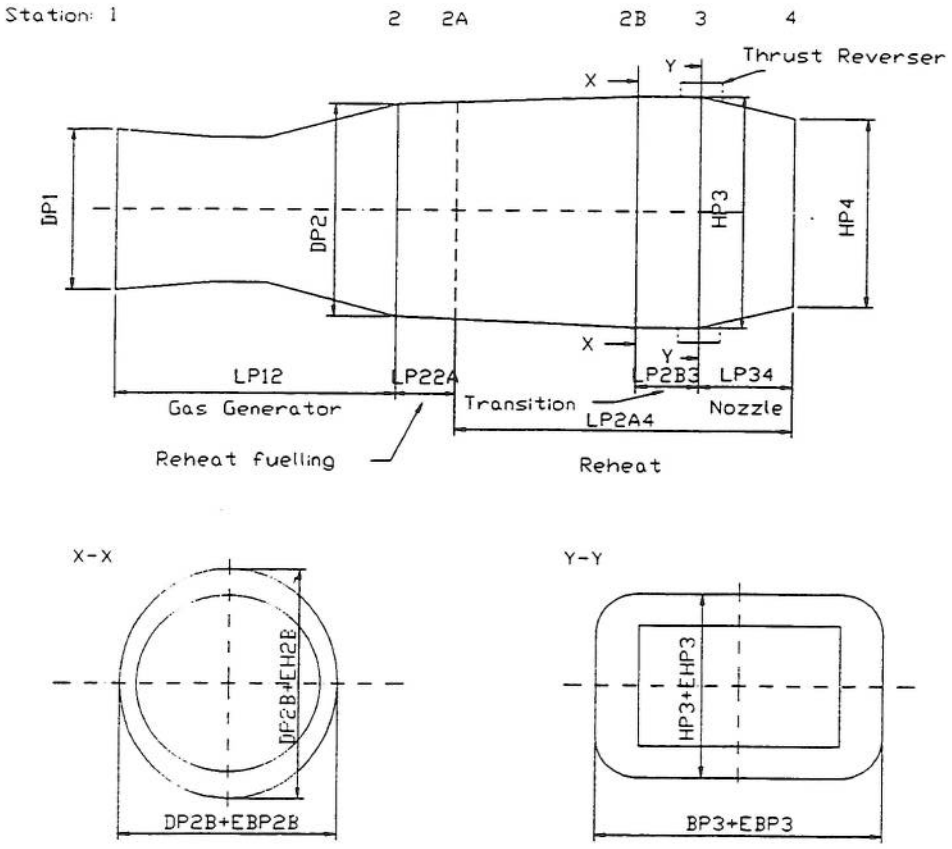

Fig. 19: Engine Geometry with Two-Dimensional Nozzles

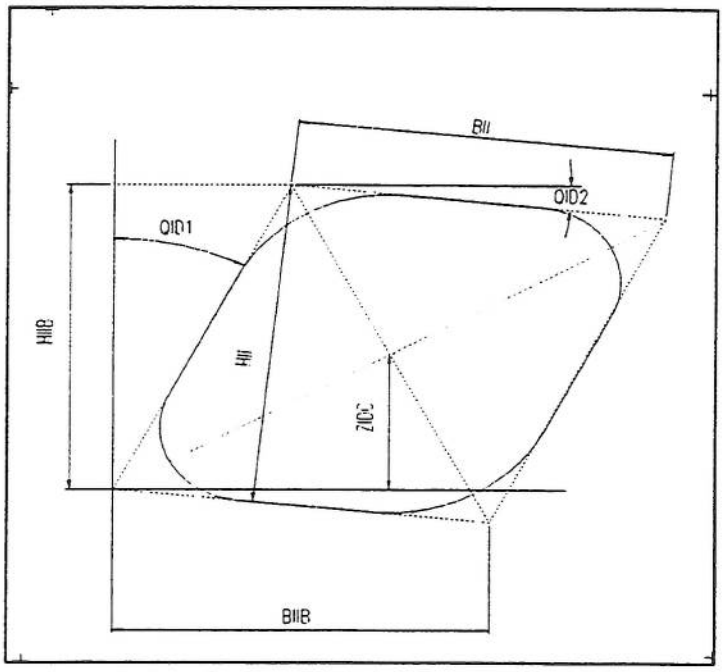

Fig. 20: General Intake Diffuser Cross Section

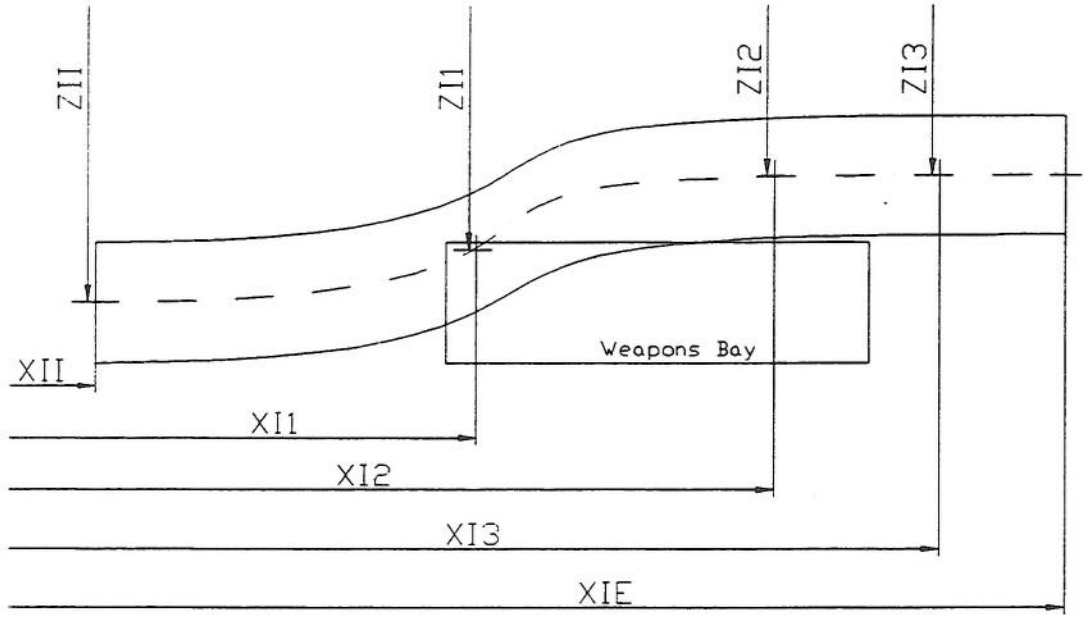

Fig. 21: Modelling of the Intake Diffuser Geometry

4.1.1.6 Fuselage Cross-Sections to Enclose Contents

Now that the major aircraft components have been described, the synthesis of the cross sections required to enclose the fuselage contents is given. The order in which they are described below corresponds to the order in which the modules are arranged within the synthesis code.

Station C is located aft of the pilot's head and contains the rear portion of the cockpit as well as the intake diffusers. The height of the fuselage at station C, HFC, is defined from

$$HFC = H1 - ZB1C + 0.5 \cdot HB1BI \,, \tag{84}$$

where

$$H1 = ZFLOOR + xcubic(XFC - XFA, FZCR, 4) \,. \tag{85}$$

The function xcubic evaluates the cubic whose coefficients are stored in FZCR at the X value XFC-XFA.

The width of the fuselage at the cockpit side is initially set equal to the cockpit width, BCH, and the width at the bottom of the fuselage, BFCB, is constrained to be the greater of BB1BI and BCH, using the blending function. Referring to Fig. 22, two Bezier splines are used to define the top part of the fuselage (above the intakes), while the bottom part is constructed of straight line segments.

In order that the height of the intakes does not exceed the height of the fuselage minus the canopy, HIIB is found to be the lesser of a value defined by the intake aspect ratio AII (Eq. 70) and an expression involving the cockpit. Thus,

$$HIIB = \min(HIIB,\ H2 - ZB1C + 0.5 \cdot HB1BI), \tag{86}$$

with

$$H2 = ZFLOOR + HCEYE - HC7 + \tan(QCCAN) \cdot (XFC - XFB), \tag{87}$$

and using the blend function to ensure a smooth variation in the derivatives.

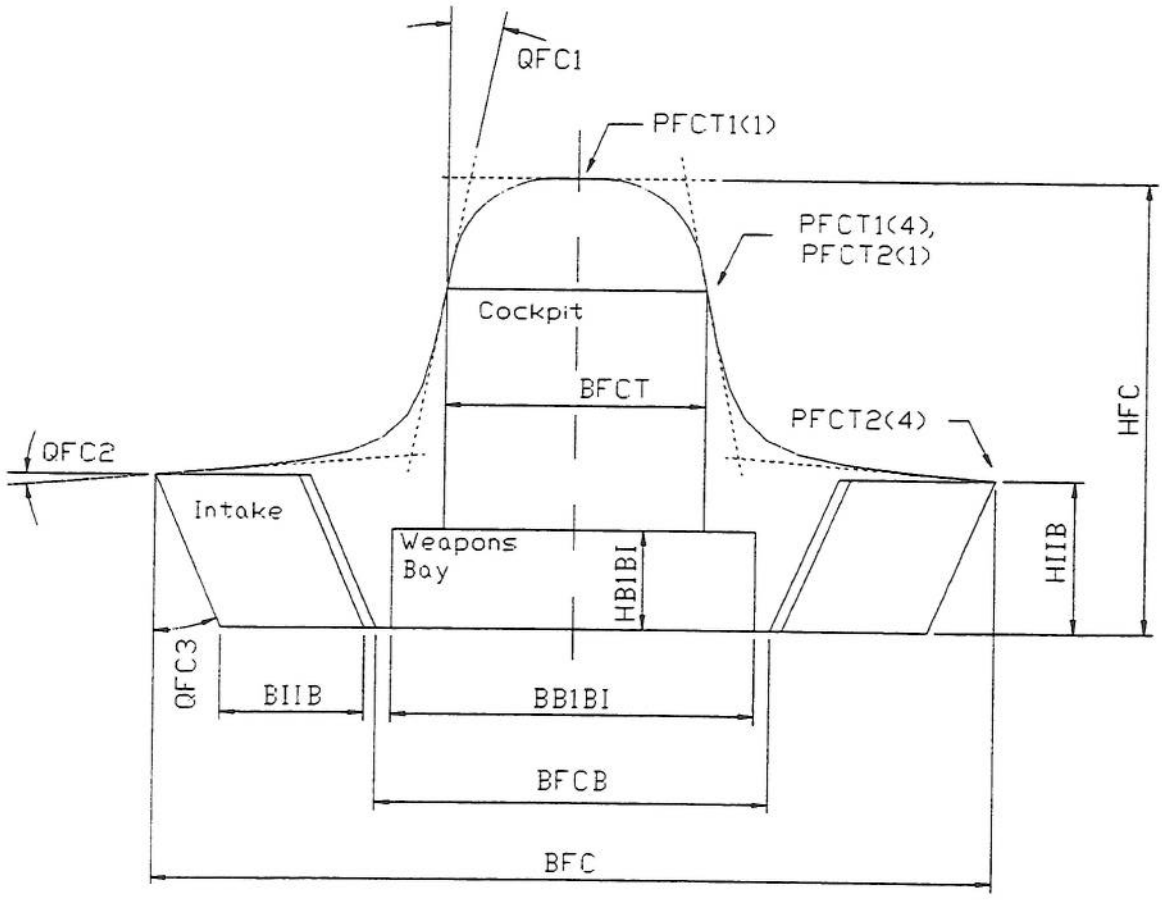

Fig. 22: Cross-Section of Fuselage at Station C

Then, to resize the intakes, if necessary,

$$
\begin{aligned}
HII &= \frac{HIIB \cdot \sin(90°-QID1+QID2)}{\cos(QID1)}, \\
AII &= \frac{2.0 \cdot HII^2}{OII}, \\
BII &= \frac{HII}{AII}, \text{ and} \\
BIIB &= BII \cdot \cos(QID2).
\end{aligned}
\tag{88}
$$

The top spline is defined by

$$
\begin{aligned}
G1 &= 0.0, \\
G2 &= -\frac{1.0}{\tan(QFC1)}, \\
PFCT1(1,1) &= 0.0, \\
PFCT1(1,2) &= ZB1C - 0.5 \cdot HB1BI + HFC, \\
PFCT1(4,1) &= 0.5 \cdot BFCT, \text{ and} \\
PFCT1(4,2) &= H2 \ .
\end{aligned}
\tag{89}
$$

H2 has been defined in Eq. 87. The lower spline is defined by

$$
\begin{aligned}
G1 &= G2, \\
G2 &= -\tan(QID2), \\
PFCT2(1,1) &= PFCT1(4,1), \\
PFCT2(1,2) &= PFCT1(4,2), \\
PFCT2(4,1) &= 0.5 \cdot BFCB + \left[ZW - (ZB1C - 0.5 \cdot HB1BI)\right] \cdot \tan(QFC1) + BIIB \\
PFCT2(4,2) &= ZW.
\end{aligned}
\tag{90}
$$

The cross-sectional areas enclosed by the curves as well as their perimeters are summed and stored in the variables OFCS and PFC, respectively. In addition, the fuselage width at C is given by

$$
BFC = 2 \cdot PFCT2(4,1) \ . \tag{91}
$$

The total cross sectional area required at station C is given by the value previously stored in OFCS and by

$$
\begin{aligned}
OFCS = OFCS &+ 0.5 \cdot (BFCB + BFC - 2.0 \cdot BIIB - 2.0 \cdot BVI) \cdot \\
&\cdot |ZW - ZB1C + 0.5 \cdot HB1BI|.
\end{aligned}
\tag{92}
$$

Also, the total perimeter is given by PFC, using the value from the splines above and with

$$PFC = PFC + BFCB + 2.0 \cdot \left[\frac{HIIB}{\cos(QID1)} + \frac{BIIB}{\cos(QID2)} \right]. \tag{93}$$

A net scaling factor is defined by the ratio of required cross-sectional area to the value calculated in OFCS, using

$$ROFCNS = \frac{OFC - OII - OVI}{OFCS}. \tag{94}$$

The value found is used to scale BFCT, BFCB, and HFC with

$$\begin{aligned} BFCT &= BFCT \cdot \sqrt{ROFCNS}, \\ BFCB &= BFCB \cdot \sqrt{ROFCNS}, \quad \text{and} \\ HFC &= (HFC - RCCAN) \cdot \sqrt{ROFCNS} + RCCAN. \end{aligned} \tag{95}$$

The vertical position of the cockpit floor is adjusted using

$$ZFLOOR = ZB1C - 0.5 \cdot HB1BI + HFC - H1, \tag{96}$$

where H1 has been defined in Eq. 85. Using an iterative procedure, it is possible to find the correct dimensions in order to match the actual to the required cross-sectional area.

Station A is located at the front cockpit bulkhead. Referring to Fig. 23, minimum values for HFA and BFA are found from

$$HFA = ZFLOOR + HC5 - ZFUS \tag{97}$$

$$BFA = 2 \cdot YFA, \tag{98}$$

and they remain fixed throughout the scaling described below.
Also,

$$\begin{aligned} HFAT &= 0.5 \cdot (ZFLOOR + HC5 - ZSA), \\ HFAB &= 0.5 \cdot (ZSA - ZFUS) \\ BFAT &= \text{blend}\left(\frac{OFA}{HFA}, BFR, ABOVE, 0.001\right), \quad \text{and} \\ BFAB &= BFAT. \end{aligned} \tag{99}$$

Using these values, Bezier curves describe the top and bottom parts of the cross-section. For the top part,

$$
\begin{aligned}
&G1 = -\frac{1.0}{\tan(QFA1)}, \\
&G2 = -\tan(QFA2), \\
&PFAT2(1,1) = 0.5 \cdot BFAT, \\
&PFAT2(1,2) = ZSA + HFAT, \\
&PFAT2(4,1) = YFA, \quad \text{and} \\
&PFAT2(4,2) = ZSA.
\end{aligned}
\tag{100}
$$

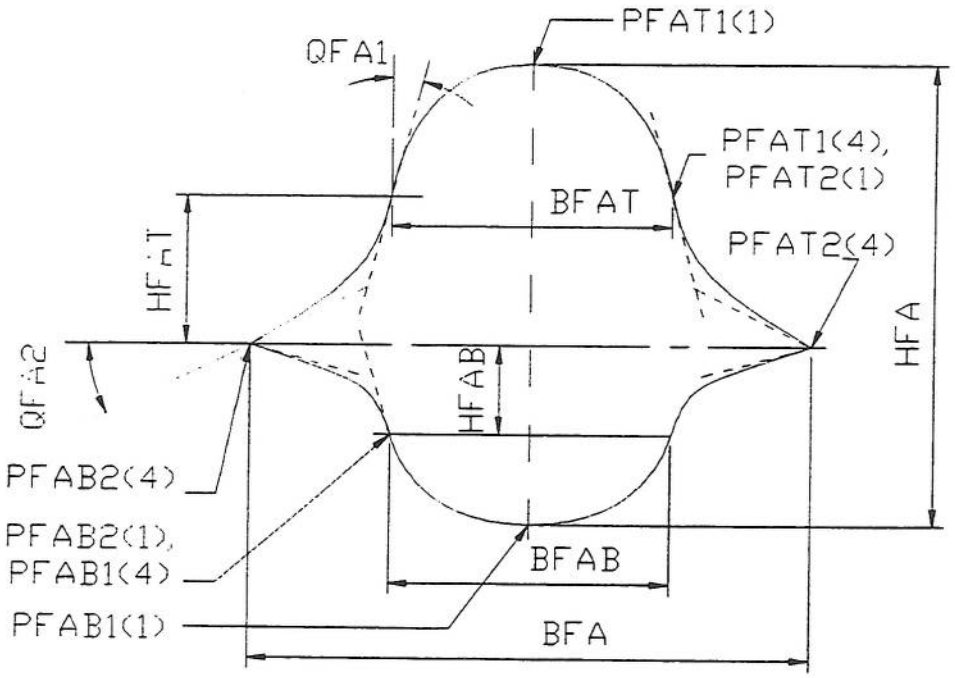

Fig. 23: Cross-Section of Fuselage Station A

For the bottom part,

$$
\begin{aligned}
&G1 = \frac{1}{\tan(QFA1)}, \\
&G2 = \tan(QFA2), \\
&PFAB2(1,1) = 0.5 \cdot BFAB, \\
&PFAB2(1,2) = ZSA - HFAB, \\
&PFAB2(4,1) = YFA, \quad \text{and} \\
&PFAB2(4,2) = ZSA.
\end{aligned}
\tag{101}
$$

Next,

$$
\begin{aligned}
&G2 = -\frac{1}{\tan(QFA1)},\\
&G1 = 0.0,\\
&PFAT1(1,1) = 0.0,\\
&PFAT1(1,2) = ZFLOOR + HC5,\\
&PFAT1(4,1) = PFAT2(1,1), \text{ and}\\
&PFAT1(4,2) = PFAT2(1,2).
\end{aligned}
\tag{102}
$$

Finally,

$$
\begin{aligned}
&G1 = 0.0\\
&G2 = \frac{1}{\tan(QFA1)},\\
&PFAB1(1,1) = 0.0,\\
&PFAB1(1,2) = ZFUS,\\
&PFAB1(4,1) = PFAB2(1,1), \text{ and}\\
&PFAB1(4,2) = PFAB2(1,2).
\end{aligned}
\tag{103}
$$

The above series of equations appears in this order in the synthesis code.

OFAS is the area enclosed by the spline curves just described. It is incremented by terms which account for the internal structure, such that

$$OFAS = OFAS(splines) + HFAB \cdot BFAB + HFAT \cdot BFAT\ . \tag{104}$$

In order to scale the cross section at A to match the fairing curve, a scaling factor is derived from the calculated area, OFAS and the required fairing curve area, OFA:

$$ROFAS = \frac{OFA}{OFAS}. \tag{105}$$

ROFAS is applied to BFAT using

$$BFAT = BFAT \cdot \sqrt{ROFAS} \tag{106}$$

and setting BFAB = BFAT. An iterative procedure is used to find the correct value for BFAT.

Fuselage station B is located at the pilot's eyepoint, the longitudinal position of which is derived from the cockpit geometry. Firstly,

$$BFB = 2 \cdot YSB \,, \tag{107}$$

which defines the width of the fuselage at B in terms of the forebody chine geometry given by YSB. Also, several width and height descriptors are given in a manner similar to station A, these being

$$\begin{aligned} BFBT &= BCH, \\ BFBB &= 0.5 \cdot \frac{BFB}{FFS} \,, \\ HFBT &= ZFLOOR + HCEYE - HC7 - ZSB \,, \text{ and} \\ HFBB &= \frac{ZSB - ZFUS}{2.0} \,. \end{aligned} \tag{108}$$

Figure 24 shows how these variables are defined.

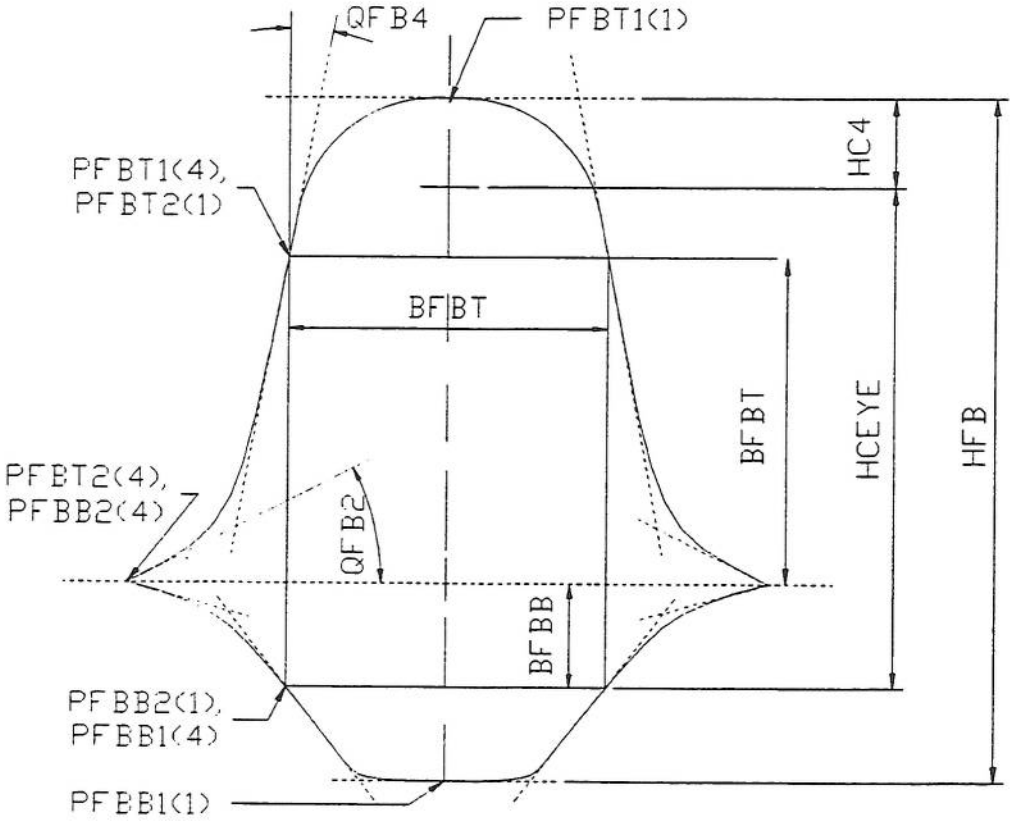

Fig. 24: Fuselage Station B

The spline used at the top of the cross-section to fit the canopy is dependent upon whether a single or a twin seat cockpit has been chosen. In the first case,

$$PFBT1(1,2) = ZFLOOR + HCEYE + HC4 \tag{109}$$

while in the second case

$$PFBT1(1,2) = ZFLOOR + xcubic(XFB - XFA, FZCF, 4)\,. \tag{110}$$

FZCF contains the coefficients of the cubic describing the top front cockpit canopy outline, and the function xcubic() evaluates this cubic at the X-coordinate XFB-XFA. Equations 109 and 110 are based upon the assumption that for a single-seat cockpit the maximum canopy elevation is located above the pilot's eyepoint.

Furthermore, we have

$$\begin{aligned} &G1 = 0.0, \\ &G2 = -\frac{1.0}{\tan(QFB1)}\,, \\ &PFBT1(1,1) = 0.0, \\ &PFBT1(4,1) = 0.5 \cdot BFBT, \text{ and} \\ &PFBT1(4,2) = ZSB + HFBT. \end{aligned} \tag{111}$$

For the rest of the upper spline,

$$\begin{aligned} &G1 = -\frac{1}{\tan(QFB1)}, \\ &G2 = -\tan(QFB2), \\ &PFBT2(1,1) = PFBT1(4,1), \\ &PFBT2(1,2) = PFBT1(4,2), \\ &PFBT2(4,1) = 0.5 \cdot BFB, \text{ and} \\ &PFBT2(4,2) = ZSB. \end{aligned} \tag{112}$$

The lower portion of the fuselage at B has splines defined by the following values:

$$
\begin{aligned}
&G1 = 0.0 \\
&G2 = \frac{1.0}{\tan(QFB1)}\ , \\
&PFBB1(1,1) = 0.0, \\
&PFBB1(1,2) = ZFUS, \\
&PFBB1(4,1) = 0.5 \cdot BFBB, \text{ and} \\
&PFBB1(4,2) = ZSB - HFBB.
\end{aligned}
\tag{113}
$$

$$
\begin{aligned}
&G1 = \frac{1}{\tan(QFB1)}, \\
&G2 = \tan(QFB2), \\
&PFBB2(1,1) = PFBB1(4,1), \\
&PFBB2(1,2) = PFBB1(4,2), \\
&PFBB2(4,1) = 0.5 \cdot BFB, \text{ and} \\
&PFBB2(4,2) = ZSB.
\end{aligned}
\tag{114}
$$

The height of the fuselage at Station B is subsequently calculated to be

$$HFB = PFBT1(1,2) - PFBB1(1,2)\ , \tag{115}$$

and this value remains constant throughout the scaling process described below. A scaling factor is formed using the cross-sectional area enclosed by the splines and the that required at station B, found from the fairing curve, such that

$$ROFBS = \frac{OFB}{OFBS}\ . \tag{116}$$

Using an iterative procedure, the square root of the scaling factor is applied to BFBT, HFBT, and BFBB, until agreement is obtained between the actual and the required cross-sectional areas:

$$
\begin{aligned}
&BFBT = BFBT \cdot \sqrt{ROFBS}\ , \\
&HFBT = \frac{HFBT}{\sqrt{ROFBS}}\ , \text{ and} \\
&BFBB = BFBB \cdot \sqrt{ROFBS}\ .
\end{aligned}
\tag{117}
$$

In order to define the vertical geometry of the fuselage aft of the cockpit, station F needs to be defined before stations D and E. It is located at the face of the engine compressor, which is also engine station number 1. This cross

section additionally contains a part of the wing box as well as the main landing gear bays. The synthesis of station F was fairly complicated because account needed to be taken of the possible different positions of the main gear when retracted as well as the options for positioning the weapons bay, as shown schematically in Figure 25. Also, the vertical position of the engine centreline is determined in this module by relating it to the main gear and weapons bay positions, depending upon the clearances necessary in order to avoid the main gear bay extending below the bottom of the fuselage as defined by the weapons bay.

First, a vertical position of the engine, denoted by ZPCH, is found by relating the geometry to the datum position given in ZDATWB, which is the bottom of the weapons bay, given by

$$ZDATWB = ZB1C - 0.5 \cdot HB1BI. \tag{118}$$

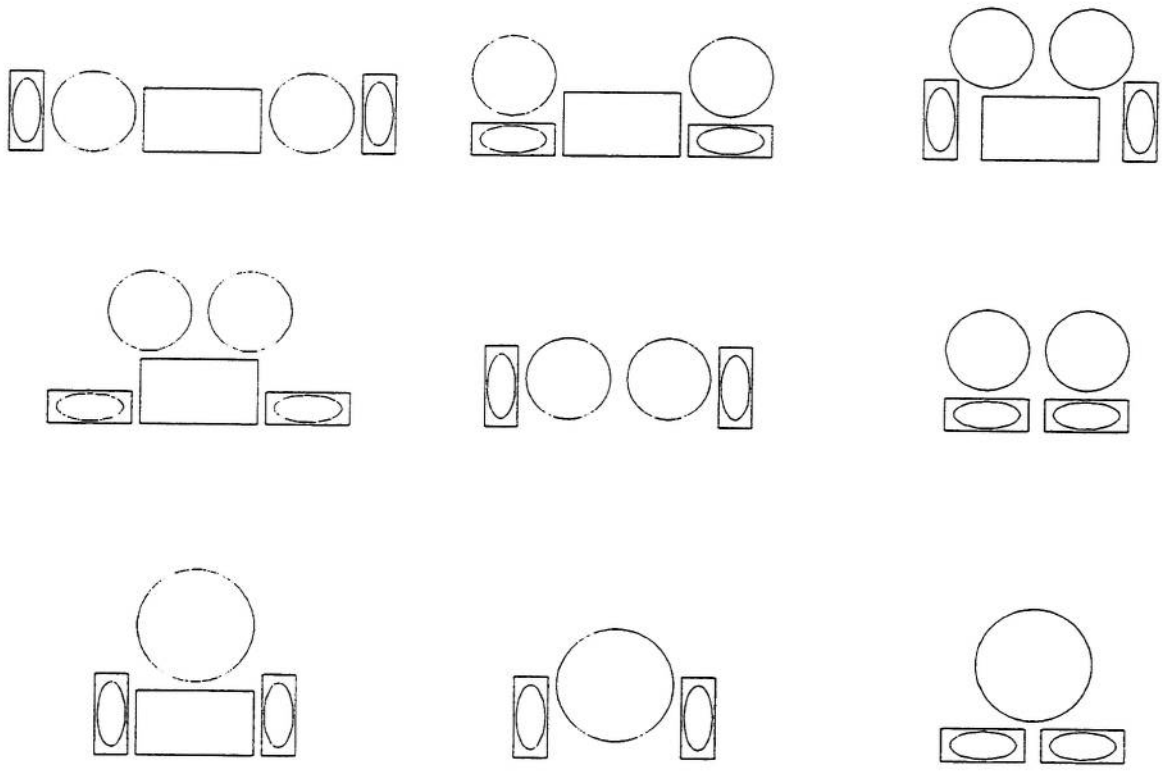

Fig. 25: Options for internal component arrangement at Station F

If the weapons bay is located between the diffusers and the main gear is stowed vertically, the engine is assumed to be located between the main gear bay and the weapons bay, and ZPCH is found under the assumption that

sufficient clearance exists between the fuselage underside and the engine to pass the wing structure around the bay. Thus,

$$ZPCH = ZDATWB + 0.5 \cdot HWBF \cdot FHWBF + 0.5 \cdot (DP1 + EHP1). \quad (119)$$

Alternatively, if the main gear is stowed horizontally, the engine bay is located above the main gear bay, and its width, BUMG, is added to equation 119.

If the weapons bay is located underneath the diffusers, no account needs to be taken of the main gear position for determining ZPCH, so

$$ZPCH = ZDATWB + HB1BI + 0.5 \cdot FHWBF + 0.5 \cdot FHWBF \cdot HWBF + 0.5 \cdot (DP1 + EHP1). \quad (120)$$

In equations 119 and 120 the variable FHWBF denotes a factor on the height of the wing root chord at station F to allow for additional wing carry through structure.

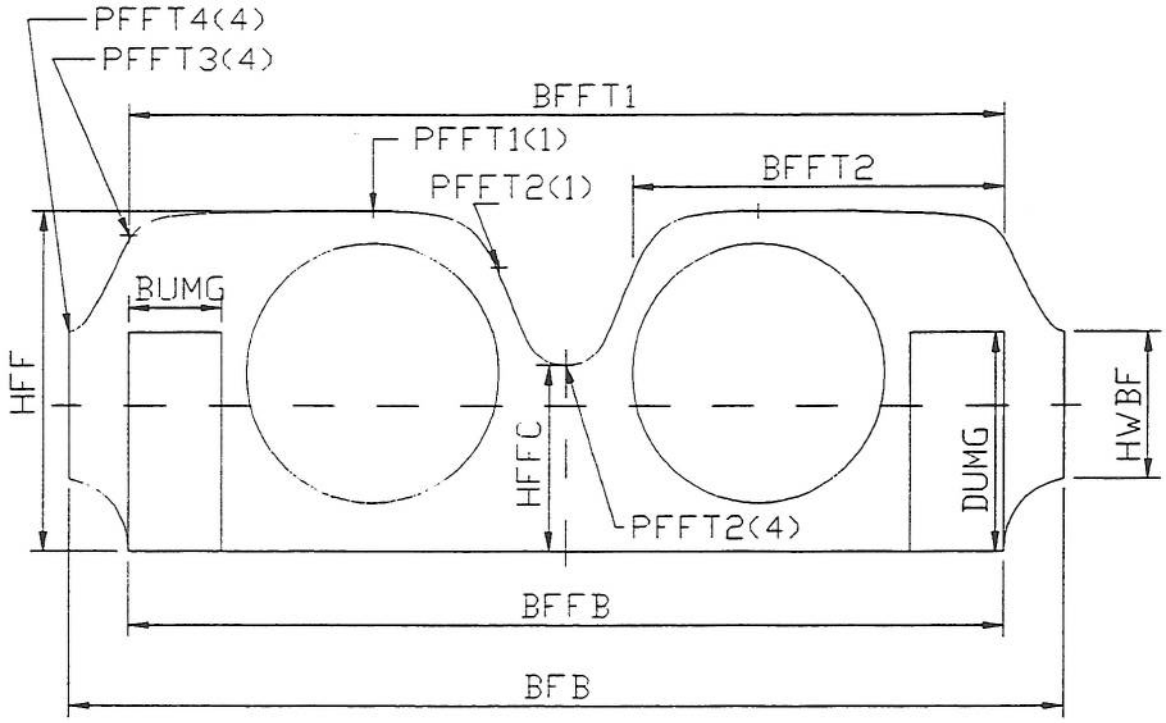

Fig. 26: Twin-engine Geometry for Fuselage Station F

In order to fit the splines in a uniform fashion for all four of the above cases, the following variables are defined. For the twin-engined case, they are defined as in Figure 26.

If the weapons bay is located between the diffusers,

$$\begin{aligned} &BFFT1 = YPCH + DP1 + EBP1, \text{ and} \\ &BFFT2 = DP1 + EBP1. \end{aligned} \tag{121}$$

Additionally, if the main gear is stowed vertically, then

$$\begin{aligned} &BFFB = YPCH + 2.0 \cdot BUMG + DP1 + EBP1, \text{ and} \\ &ZFFTP = \text{blend}\begin{pmatrix} ZPCH + 0.5 \cdot (DP1 + EHP1) + 0.5 \cdot FHWBF \cdot HWBF, \\ ZDATWB + DUMG + HWBF \cdot FHWBF, 0.001, ABOVE \end{pmatrix}. \end{aligned} \tag{122}$$

Otherwise,

$$\begin{aligned} &BFFB = YPCH + \text{blend}(DUMG, DP1 + EBP1, 0.001, ABOVE) \text{ and} \\ &ZFFTP = ZPCH + 0.5 \cdot (DP1 + EHP1) + 0.5 \cdot HWBF \cdot FHWBF. \end{aligned} \tag{123}$$

In these equations, ZFFTP denotes the z-coordinate of the fuselage perimeter located above the centreline of the propulsion bay, while ZFFTC denotes the corresponding z-coordinate at the fuselage centreline. Also, DUMG denotes the diameter of the main wheel bay, including clearances.

If the weapons bay is located underneath the diffusers, then

$$\begin{aligned} &ZFFTP = ZPCH + 0.5 \cdot FHWBF \cdot HWBF + 0.5 \cdot (DP1 + EHP1), \text{ and} \\ &BFFB = \text{blend}(YPCH + DP1 + EBP1, BB1BI, 0.001, ABOVE) + \\ &\quad + 0.5 \cdot HWBF \cdot FHWBF. \end{aligned} \tag{124}$$

Also, if the main gear is stowed vertically, then

$$\begin{aligned} &BFFT1 = YPCH + DP1 + EBP1 + 2.0 \cdot BUMG, \text{ and} \\ &BFFT2 = DP1 + EBP1 + BUMG. \end{aligned} \tag{125}$$

Otherwise,

$$\begin{aligned} &BFFT1 = YPCH + DP1 + EBP1 \text{ and} \\ &BFFT2 = DP1 + EBP1. \end{aligned} \tag{126}$$

The relationship for BFFB in Equation 124 ensures that the fuselage is wide enough to accomodate the greater of the widths obtained from the weapons bay and the propulsion bay. BUMG denotes the width of the main gear bay including clearances.

Some variables are the same for all of the above cases, these being

$$\begin{aligned} &ZFFTC = ZW + 0.5 \cdot FHWBF \cdot HWBF, \\ &HFFC = ZFFTC - ZDATWB, \quad \text{and} \\ &RHHV = \frac{ZFFTC - ZW}{HFFC} \ . \end{aligned} \tag{127}$$

HFFC is the fuselage height at station F at the centreline, while RHHV denotes the ratio of the distance between the wing centreline and the top of the fuselage at the centreline to the fuselage height. The latter value is needed for the definition of the aftbody shape in the case of twin engines being installed.

After the above variables have been defined, spline curves are fitted according to the following relationships. First, a fuselage width is defined using

$$BFF = FFS \cdot \left[BFFB + 2.0 \cdot (ZW - 0.5 \cdot HWBF - ZDATWB) \cdot \tan(QFS) \right]. \tag{128}$$

Then, two temporary variables, Z1 and Z2, are calculated from

$$Z1 = \text{blend} \begin{pmatrix} ZDATWB + Z1W + FHWBF \cdot HWBF, \\ ZW + 0.5 \cdot HWBF, 0.001, ABOVE \end{pmatrix} - (ZW + 0.5 \cdot HWBF) \tag{129}$$

and

$$Z2 = Z1 \cdot \frac{BFF - BFFT1}{BFF - BFFB} \ . \tag{130}$$

In Equation 129, Z1W denotes a variable to account for the main wheel dimensions. It is equal to DUMG if the main gear is stowed vertically, and BUMG if it is stowed horizontally. The variables Z1 and Z2 were created to allow for sufficient structural clearance between the fuselage skin and the top of the main gear bay.

The splines are then calculated in the following order, using definitions

$$\begin{aligned} &G1 = 0.0, \\ &G2 = -\frac{1.0}{\tan(QFF1)}, \\ &PFFT1(1,1) = 0.5 \cdot YPCH, \\ &PFFT1(1,2) = ZFFTP, \\ &PFFT1(4,1) = 0.5 \cdot BFFT1, \\ &PFFT1(4,2) = 0.5 \cdot (ZW + 0.5 \cdot HWBF + Z2 + ZFFTP), \end{aligned} \tag{131}$$

and

$$
\begin{aligned}
&G1 = -\frac{1.0}{\tan(QFF1)},\\
&G2 = -2.0 \cdot \frac{Z1}{BFF - BFFB},\\
&PFFT2(1,1) = PFFT1(4,1),\\
&PFFT2(1,2) = PFFT1(4,2),\\
&PFFT2(4,1) = 0.5 \cdot BFF,\\
&PFFT2(4,2) = ZW + 0.5 \cdot HWBF
\end{aligned}
\tag{132}
$$

for the upper outer section of the cross-section, and

$$
\begin{aligned}
&G1 = 0.0,\\
&G2 = \frac{1.0}{\tan(QFF1)},\\
&PFFT3(1,1) = PFFT1(1,1),\\
&PFFT3(1,2) = PFFT1(1,2),\\
&PFFT3(4,1) = \text{blend}(0.5 \cdot BFFT1 - BFFT2, 0.0, 0.01, \text{ABOVE}),\\
&PFFT3(4,2) = 0.5 \cdot (PFFT1(1,2) + ZFFTC),
\end{aligned}
\tag{133}
$$

as well as

$$
\begin{aligned}
&G1 = \frac{1.0}{\tan(QFF1)},\\
&G2 = 0.0,\\
&PFFT4(1,1) = PFFT3(4,1),\\
&PFFT4(1,2) = PFFT3(4,2),\\
&PFFT4(4,1) = 0.0, \text{ and}\\
&PFFT4(4,2) = ZFFTC
\end{aligned}
\tag{134}
$$

for the upper centre section. As the scaling to match the fairing curve progresses, ZFFTC (Equations 133 and 134) is modified in order to maintain the correct fuselage shape:

$$ZFFTC = \max(ZFFTC, ZZ1), \tag{135}$$

with

$$ZZ1 = PFFT3(4,2) - \frac{PFFT3(4,1)}{\tan(QFF1)}. \tag{136}$$

For the lower section (underneath the wing centreline), a spline is defined by

$$
\begin{aligned}
&G1 = \frac{1.0}{\tan(QFF1)}, \\
&G2 = 0.0, \\
&PFFB1(1,1) = 0.5 \cdot BFFB, \\
&PFFB1(1,2) = ZDATWB, \\
&PFFB1(4,1) = 0.5 \cdot BFF, \text{ and} \\
&PFFB1(4,2) = ZW - 0.5 \cdot HWBF.
\end{aligned}
\tag{137}
$$

After the areas enclosed by the splines and their perimeters have been found and stored in OFFS and PFF, respectively, any additional sections of the cross-sectional area are found, using

$$
\begin{aligned}
OFFS = OFFS + 2.0 \cdot \left[PFFB1(4,1) - PFFB1(1,1)\right] \cdot 0.5 \cdot HWBF + \\
+ BFFB \cdot (ZW - ZDATWB)
\end{aligned}
\tag{138}
$$

and

$$PFF = PFF + 2.0 \cdot HWBF + BFFB. \tag{139}$$

A scaling factor is defined using the actual and required cross-sectional areas,

$$ROFFS = \frac{OFF}{OFFS} \ . \tag{140}$$

ROFFS is applied to ZFFTP, BFFT1, and BFFB using

$$
\begin{aligned}
&ZFFTP = ZFFTP \cdot \sqrt{ROFFS}, \\
&BFFT1 = BFFT1 \cdot \sqrt{ROFFS}, \text{ and} \\
&BFFB = BFFB \cdot \sqrt{ROFFS}.
\end{aligned}
\tag{141}
$$

BFFT2 is recalculated using

$$BFFT2 = BFFT1 - YPCH. \tag{142}$$

The curve fitting is repeated until the actual cross-sectional area corresponds to that required by the fairing curve. HFF is found as the greater of HFFC and ZFFTP-ZDATWB.

Station D is located at the front of the outer weapons bays, and is shown in Fig. 27.

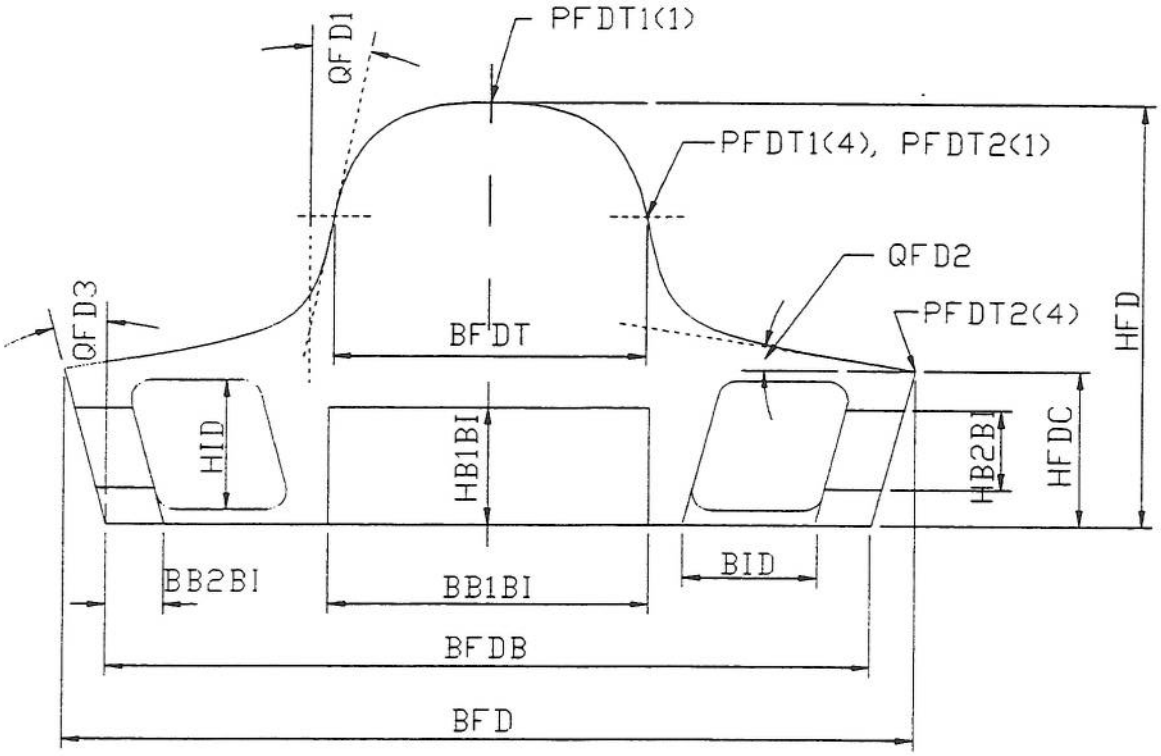

Fig. 27: Fuselage Station D

The height at the centreline is defined using a curve fit between stations C and F, and remains constant during the iteration to match the minimum required area to the fairing curve.

The width at the bottom of the fuselage is given as

$$BFDB = 2.0 \cdot YID + BID + 2.0 \cdot BB2BI , \tag{143}$$

where YID is the y-coordinate of the diffusers at station D and BID is the corresponding diffuser width.

Also,

$$HFDC = ZW + 0.5 \cdot HWBD - ZB1C + 0.5 \cdot HB1BI \tag{144}$$

$$BFD = BFDB + 2.0 \cdot HFDC \cdot \tan(QFD3), \text{ and,}$$

in order to ensure a viable fuselage shape aft of Station C,

$$BFDT = BFCT \tag{145}$$

where HWBD is the height of the wing box at the fuselage side at D, so that finally the height of the fuselage at D is

$$HFD = ZFD - ZB1C + 0.5 \cdot HB1BI \,. \tag{146}$$

ZFD is the z-coordinate of the fuselage spine at station D, found from the curve fit mentioned above.

Once again a series of Bezier fits are defined using

$$\begin{aligned} &G1 = 0.0, \\ &G2 = -\frac{1.0}{\tan(QFD1)}, \\ &PFDT1(1,1) = 0.0, \\ &PFDT1(1,2) = ZB1C - 0.5 \cdot HB1BI + HFD, \\ &PFDT1(4,1) = 0.5 \cdot BFDT, \text{ and} \\ &PFDT1(4,2) = ZB1C - 0.5 \cdot HB1BI + HFDT \end{aligned} \tag{147}$$

for the upper spline, and

$$\begin{aligned} &G1 = -\frac{1.0}{\tan(QFD1)}, \\ &G2 = -\tan(QFD2), \\ &PFDT2(1,1) = PFDT1(4,1), \\ &PFDT2(1,2) = PFDT1(4,2), \\ &PFDT2(4,1) = 0.5 \cdot BFD, \text{ and} \\ &PFDT2(4,2) = ZB1C - 0.5 \cdot HB1BI + HFDC. \end{aligned} \tag{148}$$

Finally,

$$HFDT = 0.7 \cdot (BFD - BFDT) \cdot \tan(QFD2) + HFDC \,.$$

The rest of the cross-sectional area is found using OFDS from the splines in Equations 147 and 148 and the folowing expression:

$$OFDS = OFDS + 0.5 \cdot (BFD + BFDB) \cdot HFDC + BFDT \cdot (HFDT - HFDC) \tag{149}$$

The rest of the perimeter is similarly found, using

$$PFD = PFD + BFDB + 2.0 \cdot \frac{HFDC}{\cos(QFD3)} \,. \tag{150}$$

The scaling factor, ROFDS, is found from

$$\text{ROFDS} = \frac{\text{OFD}}{\text{OFDS}}. \tag{151}$$

The square root of the scaling factor is applied as follows:

$$\begin{aligned} \text{BFDT} &= \text{BFDT} \cdot \sqrt{\text{ROFDS}}, \\ \text{BFDB} &= \text{BFDB} \cdot \sqrt{\text{ROFDS}}, \end{aligned} \tag{152}$$

and BFD is recalculated using the expression in Equation 144.

Station E is located at the front of the main gear bay, and its minimum dimensions depend, as for station F, upon the way the main gear is stowed.

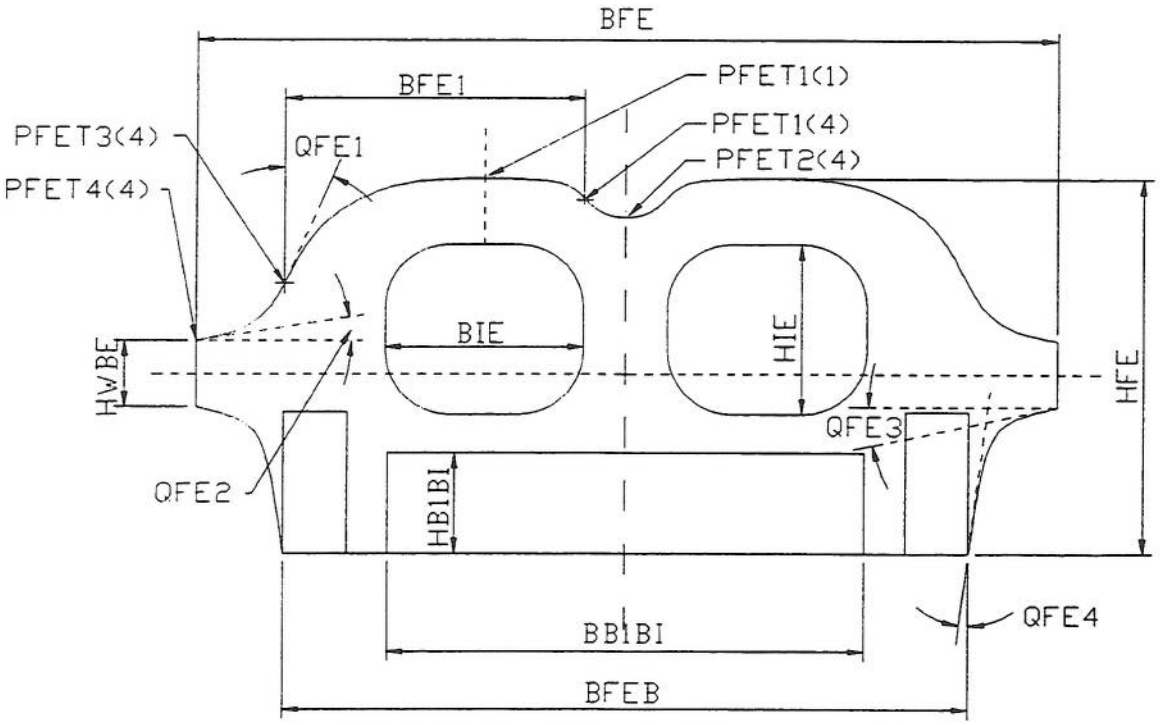

Fig. 28: Fuselage Station E

If the wheel is retracted vertically, then

$$\text{BFE1} = \text{BIE} + \text{BUMW} \cdot \text{FBUMW}, \tag{153}$$

where BIE is the width of the diffuser at station E, and

$$\text{BFEB} = \text{YIE} + \text{BIE} + 2.0 \cdot \text{BUMW} \cdot \text{FBUMW}, \tag{154}$$

where YIE is the y-coordinate of the diffuser centreline at station E.

Also,

$$ZFEBP = \text{blend}\begin{pmatrix} ZB1C - 0.5 \cdot HB1BI, \\ ZIXE - 0.5 \cdot HIE - 0.5 \cdot HWBE, 0.001, BELOW \end{pmatrix}, \quad (155)$$

which denotes the Z-coordinate of the fuselage underneath the intake diffuser.

If, on the other hand, the main wheel is stowed horizontally, then

$$\begin{aligned} BFE1 &= \text{blend}(BIE, DUMW \cdot FDUMW, 0.001, ABOVE), \\ BFEB &= 2.0 \cdot (YIE - 0.5 \cdot BIE + BFE1), \text{ and} \\ ZFEBP &= \text{blend}\begin{pmatrix} ZB1C - 0.5 \cdot HB1BI, \\ ZIE - 0.5 \cdot HIE - 0.5HWBE - BUMW \cdot FBUMW, \\ 0.001, BELOW \end{pmatrix}. \end{aligned} \quad (156)$$

In this equation, ZIE denotes the z-coordinate of the diffuser centreline at station E. In order to maintain a realistic fuselage shape, BFEB is set to be the larger of BFDB and the value found in Eq. 156. Furthermore,

$$\begin{aligned} HFEC &= ZW - ZFEBP, \\ HFE &= ZFE - (ZB1C - 0.5 \cdot HB1BI), \text{ and} \\ HFET &= \text{blend}\begin{pmatrix} ZFETC - ZFETB, \\ ZIE + 0.5 \cdot HIE + 0.5 \cdot HWBE - ZFEBP, 0.001, ABOVE \end{pmatrix}. \end{aligned} \quad (157)$$

The procedure to fit the area at station E to the value required by the fairing curve begins by fixing ZFETC, the z-coordinate of the fuselage spine at station E based upon the curve fit between C and F and then fitting Bezier splines defined by the following:

$$\begin{aligned} G1 &= 0.0, \\ G2 &= -\frac{1.0}{\tan(QFE1)}, \\ PFET1(1,1) &= YIE, \\ PFET1(1,2) &= ZFEBP + HFET, \\ PFET1(4,1) &= 0.5 \cdot BFE1 + PFET1(1,1), \text{ and} \\ PFET1(4,2) &= ZFEBP + 0.5 \cdot (HFET + HFEC + 0.5 \cdot HWBE). \end{aligned} \quad (158)$$

Now, a fuselage width for station E can be defined as

$$BFE = FFS \cdot \text{blend}\begin{pmatrix} BFEB + 2.0 \cdot \tan(QFE4) \cdot HFEC, 2.0 \cdot PFET1(4,1) + \\ +2.0 \cdot \tan(QFE1) \cdot (PFET1(4,2) - ZW + 0.5 \cdot HWBE), \\ 0.001, ABOVE \end{pmatrix}. \quad (159)$$

Next,

$$\begin{aligned} G1 &= -\frac{1.0}{\tan(QFE1)}, \\ G2 &= -\tan(QFE2), \\ PFET2(1,1) &= PFET1(4,1), \\ PFET2(1,2) &= PFET1(4,2), \\ PFET2(4,1) &= 0.5 \cdot BFE, \text{ and} \\ PFET2(4,2) &= ZW + 0.5 \cdot HWBE. \end{aligned} \quad (160)$$

$$\begin{aligned} PFET3(1,1) &= PFET1(1,1), \\ PFET3(1,2) &= PFET1(1,2), \\ PFET3(4,1) &= PFET1(4,1) - BFE1, \\ PFET3(4,2) &= 0.5 \cdot (ZFETC + PFET1(1,2)), \\ G1 &= 0.0. \end{aligned} \quad (161)$$

In order to obtain a practical fuselage shape at E, for this spline, if PFET3(4,2) is less than ZFETC, then

$$G2 = -\frac{1.0}{\tan(QFE1)}, \quad (162)$$

else

$$G2 = \frac{1.0}{\tan(QFE1)}. \quad (163)$$

Finally, for the top part of fuselage station E, G1 is equal to G2 from Eq. 162or 163, and

$$
\begin{aligned}
&G2 = 0.0,\\
&PFET4(1,1) = PFET3(4,1),\\
&PFET4(1,2) = PFET3(4,2),\\
&PFET4(4,1) = 0.0, \text{ and}\\
&PFET4(4,2) = ZFETC.
\end{aligned}
\tag{164}
$$

The bottom part of the fuselage cross-section at E contains one Bezier spline defined by

$$
\begin{aligned}
&G1 = \frac{1.0}{\tan(QFE4)},\\
&G2 = \tan(QFE3),\\
&PFEB1(1,1) = 0.5 \cdot BFEB,\\
&PFEB1(1,2) = ZW - HFEC,\\
&PFEB1(4,1) = 0.5 \cdot BFE, \text{ and}\\
&PFEB1(4,2) = ZW - 0.5 \cdot HWBE,
\end{aligned}
\tag{165}
$$

and, if $ZFEBP < ZB1C - 0.5 \cdot HB1BI$, then the following is defined:

$$
\begin{aligned}
&PFEB2(1,1) = PFEB1(1,1) - BFE1,\\
&PFEB2(1,2) = PFEB1(1,2),\\
&PFEB2(4,1) = 0.5 \cdot BB1BI, \text{ and}\\
&PFEB2(4,2) = ZB1C - 0.5 \cdot HB1BI.
\end{aligned}
\tag{166}
$$

The rest of the points are not defined using the Bezier fitting routine, but are defined by

$$
\begin{aligned}
&PFEB2(2,1) = PFEB2(1,1),\\
&PFEB2(2,2) = PFEB2(4,2),\\
&PFEB2(3,1) = PFEB2(4,1), \text{ and}\\
&PFEB2(3,2) = PFEB2(4,2).
\end{aligned}
\tag{167}
$$

Following the evaluation of the cross-sectional area enclosed by these splines, a scaling factor is defined using

$$
ROFES = \frac{OFE}{OFES},
\tag{168}
$$

where OFE is the required area obtained from the fairing curve and OFES is the minimum area calculated from the splines. Using an iterative procedure, BFEB is adjusted until the desired cross-sectional area is achieved:

$$BFEB = BFEB \cdot \sqrt{ROFES}. \tag{169}$$

Fuselage station G is located at the engine bay station 2, which corresponds to the rear of the gas generator. The geometry depends upon whether a single or twin engine layout is chosen. For the single engine case,

$$\begin{aligned} &BFG1 = DP2 + EBP2, \\ &HFG = DP2 + EHP2, \\ &HFG1 = ZPCH + 0.5 \cdot HFG - ZW, \\ &HFG2 = HFG - HFG1, \text{ and} \\ &BFG = BFG1 + 2.0 \cdot \text{blend}(HFG1, HFG2, 0.001, ABOVE) \cdot \tan(QFG1). \end{aligned} \tag{170}$$

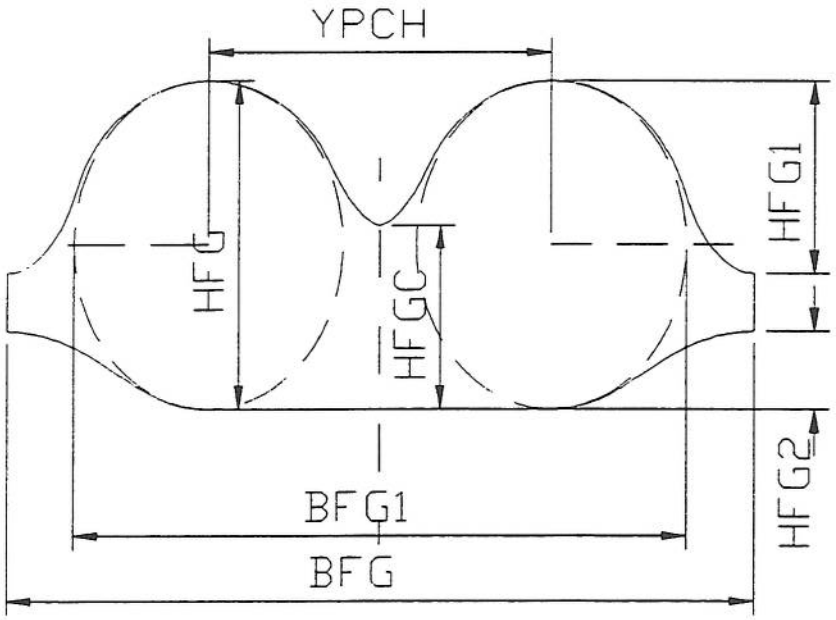

Fig. 29: Fuselage Station G for Twin-Engine Case

In this case, an elliptic fit has been used for the fuselage contour, so the controlling parameters are found as follows:

$$
\begin{aligned}
&PFGT1(1,1) = 0.0,\\
&PFGT1(1,2) = ZW + 0.5 \cdot HWBG,\\
&PFGT1(2,1) = 0.5 \cdot BFG,\\
&PFGT1(2,2) = ZPCH + 0.5 \cdot HFG - ZW - 0.5 \cdot HWBG,\\
&PFGT1(3,1) = 1.0, \text{ and}\\
&PFGT1(3,2) = NN,
\end{aligned}
\tag{171}
$$

where NN is an exponent as described in Appendix D, the value of which depends upon FFS, the fuselage chine factor. If FFS is greater than 1.0, then NN=-1.5, else NN=0.0.

Furthermore,

$$
\begin{aligned}
&PFGB1(1,1) = 0.0,\\
&PFGB1(1,2) = ZW - 0.5 \cdot HWBG,\\
&PFGB1(2,1) = 0.5 \cdot BFG,\\
&PFGB1(2,2) = \text{blend}\begin{pmatrix} ZW - 0.5 \cdot HWBG - ZPCH + 0.5 \cdot HFG, \\ 0.0, 0.001, \text{ABOVE} \end{pmatrix},\\
&PFGB1(3,1) = 1.0, \text{ and}\\
&PFGB1(3,2) = NN.
\end{aligned}
\tag{172}
$$

After the area enclosed by the superellipse has been evaluated, a scaling factor is defined using

$$
ROFGS = \frac{OFG}{OFGS}\ , \tag{173}
$$

where OFG is the cross-sectional area required by the fairing curve and OFGS is the minimum area as calculated from the elliptical curve fit defined above. The scaling is accomplished with an iterative procedure using

$$
\begin{aligned}
&HFG = HFG \cdot \sqrt{ROFGS} \quad \text{and}\\
&BFG1 = BFG1 \cdot \sqrt{ROFGS}.
\end{aligned}
\tag{174}
$$

If twin engines are chosen, a slightly more complicated shape results, as shown in Fig. 29. Thus, BFG2, HFG, HFG1, HFG2, BFG1, and BFG are defined as in Equation 170. There are now three elliptical fits, the one defined by Equation 175 being the outboard fit at the top of the fuselage section:

$$
\begin{aligned}
&PFGT1(1,1) = 0.5 \cdot YPCH,\\
&PFGT1(1,2) = ZW + 0.5 \cdot HWBG,\\
&PFGT1(2,1) = 0.5 \cdot (BFG - YPCH),\\
&PFGT1(2,2) = ZPCH + 0.5 \cdot HFG - ZW - 0.5 \cdot HWBG,\\
&PFGT1(3,1) = 1.5, \text{ and}\\
&PFGT1(3,2) = NN.
\end{aligned}
\tag{175}
$$

Furthermore, for the top inboard section

$$
\begin{aligned}
&PFGT2(1,1) = PFGT1(1,1),\\
&PFGT2(1,2) = ZW + RHHV \cdot HFGC,\\
&PFGT2(2,1) = 0.5 \cdot YPCH,\\
&PFGT2(2,2) = ZPCH + 0.5 \cdot HFG - PFGT2(1,2),\\
&PFGT2(3,1) = 1.0, \text{ and}\\
&PFGT2(3,2) = NN,
\end{aligned}
\tag{176}
$$

In this equation, RHHV and HFGC are given by

$$RHHV = 1 - YPCH \cdot (0.662 \cdot YPCH + 0.0144) \text{ and} \tag{177}$$

$$HFGC = HFFC \cdot \left(1 - \frac{XF(29) - XF(26)}{LT - XF(26)}\right). \tag{178}$$

XF(26) and XF(29) are the fuselage stations corresponding to engine bay stations 2 and 3, respectively. LT is the total length of the aircraft, as defined in Section 4.1.1.7 below.For the bottom section of station G, a flat underside is assumed at the centre, with the outer elliptic fit similar to the one for a single-engine case. Thus,

$$
\begin{aligned}
&PFGB1(1,1) = 0.5 \cdot YPCH,\\
&PFGB1(1,2) = ZW - 0.5 \cdot HWBG,\\
&PFGB1(2,1) = 0.5 \cdot (BFG - YPCH),\\
&PFGB1(2,2) = \text{blend}(Z1, Z2, 0.01, \text{ABOVE}),\\
&PFGB1(3,1) = 1.0, \text{ and}\\
&PFGB1(3,2) = NN,
\end{aligned}
\tag{179}
$$

with

$$Z1 = ZW - 0.5 \cdot HWBG - ZPCH + 0.5 \cdot HFG$$
and
$$Z2 = HFGC \cdot (1.0 - RHHV). \qquad (180)$$

The scaling factor is the same as in Eq. 173.
and the scaling is accomplished via iteration by applying the square root of ROFGS in turn to

$$HFG = HFG \cdot \sqrt{ROFGS},$$
$$HFGC = HFGC \cdot \sqrt{ROFGS}, \text{ and} \qquad (181)$$
$$BFG2 = BFG2 \cdot \sqrt{ROFGS}.$$

Fuselage station H is located at engine station 3, which is also the entrance to the nozzle. Therefore, its shape depends not only on whether one or two engines are present, but also upon the type of exhaust nozzle chosen, two-dimensional or axisymmetric. Figure shows the geometry at Station H for a two-dimensional nozzle.

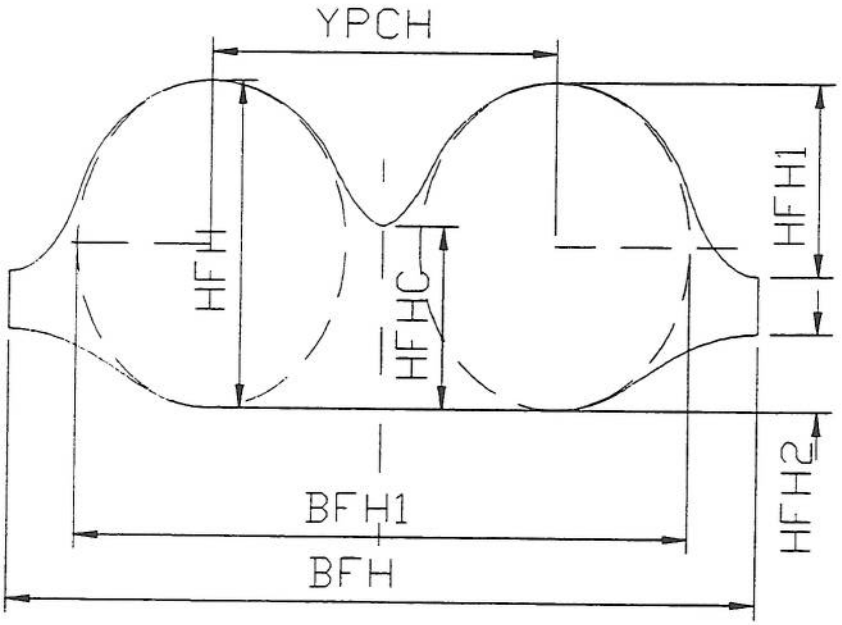

Fig. 30: Station H for Axisymmetric Nozzles

The curve fits are again elliptical in form. To begin with, a value for NN is defined using the same criteria as for station G. Then, for axisymmetric nozzles and a single engine, several reference width and height values are calculated:

$$
\begin{aligned}
&BFH1 = DP3 + EBP3,\\
&HFH = DP3 + EHP3,\\
&HFH1 = ZPCH + 0.5 \cdot HFH - ZW,\\
&HFH2 = HFH - HFH1, \text{ and}\\
&BFH = BFH1 + 2.0 \cdot \text{blend}(HFH1, HFH2, 0.001, \text{ABOVE}) \cdot \tan(QFH1).
\end{aligned}
\tag{182}
$$

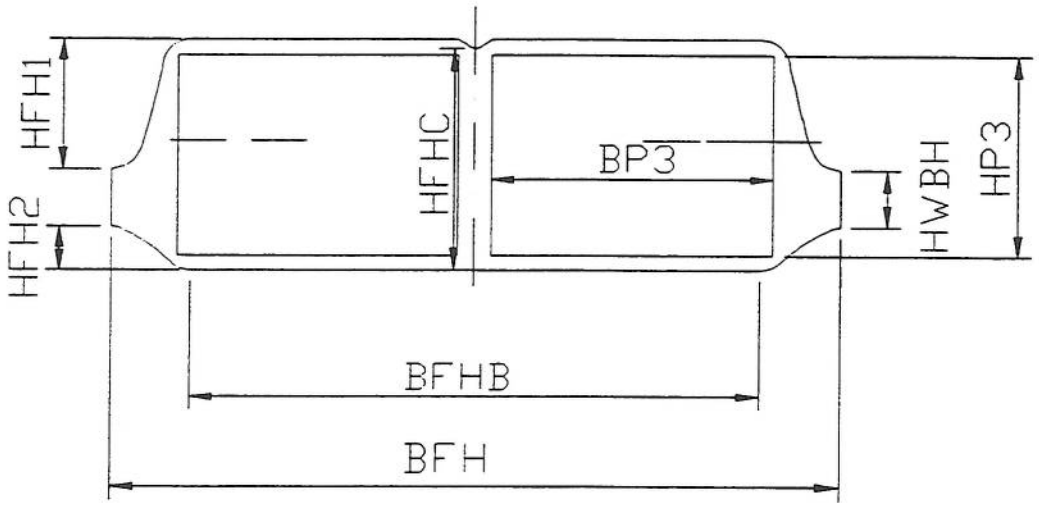

Fig. 31: Station H for Rectangular Nozzles

The elliptical curve fits are made to the upper and lower section. For the top part,

$$
\begin{aligned}
&PFHT1(1,1) = 0.0,\\
&PFHT1(1,2) = ZW + 0.5 \cdot HWBH,\\
&PFHT1(2,1) = 0.5 \cdot BFH,\\
&PFHT1(2,2) = ZPCH + 0.5 \cdot HFH - ZW - 0.5 \cdot HWBH,\\
&PFHT1(3,1) = 1.0, \text{ and}\\
&PFHT1(3,2) = NN.
\end{aligned}
\tag{183}
$$

For the lower section,

$$
\begin{aligned}
&\text{PFHB1}(1,1) = 0.0,\\
&\text{PFHB1}(1,2) = \text{ZW} - 0.5 \cdot \text{HWBH},\\
&\text{PFHB1}(2,1) = 0.5 \cdot \text{BFH},\\
&\text{PFHB1}(2,2) = \text{blend}\begin{pmatrix}\text{ZW} - 0.5 \cdot \text{HWBH} - \text{ZPCH} + 0.5 \cdot \text{HFH},\\ 0.0, 0.001, \text{ABOVE}\end{pmatrix},\\
&\text{PFHB1}(3,1) = 1.0, \quad \text{and}\\
&\text{PFHB1}(3,2) = \text{NN}.
\end{aligned}
\tag{184}
$$

For the scaling factor,

$$
\text{ROFHS} = \frac{\text{OFH}}{\text{OFHS}}\,, \tag{185}
$$

and it is applied in turn to HFH and BFH1 such that

$$
\begin{aligned}
&\text{HFH} = \text{HFH}\sqrt{\text{ROFHS}}\\
&\text{and}\\
&\text{BFH1} = \text{BFH1}\sqrt{\text{ROFHS}}.
\end{aligned}
\tag{186}
$$

For a twin-engined aircraft with axisymmetric nozzles,

$$
\begin{aligned}
&\text{BFH2} = \text{DP3} + \text{EBP3},\\
&\text{HFH} = \text{DP3} + \text{EHP3},\\
&\text{HFH1} = \text{ZPCH} + 0.5 \cdot \text{HFH} - \text{ZW},\\
&\text{HFH2} = \text{HFH} - \text{HFH1},\\
&\text{BFH1} = \text{YPCH} + \text{BFH2}, \quad \text{and}\\
&\text{BFH} = \text{BFH1} + 2.0 \cdot \text{blend}(\text{HFH1}, \text{HFH2}, 0.001, \text{ABOVE}) \cdot \tan(\text{QFH1}).
\end{aligned}
\tag{187}
$$

Then,

$$
\begin{aligned}
&\text{PFHT1}(1,1) = 0.5 \cdot \text{YPCH},\\
&\text{PFHT1}(1,2) = \text{ZW} + 0.5 \cdot \text{HWBH},\\
&\text{PFHT1}(2,1) = 0.5 \cdot (\text{BFH} - \text{YPCH}),\\
&\text{PFHT1}(2,2) = \text{ZPCH} + 0.5 \cdot \text{HFH} - \text{ZW} - 0.5 \cdot \text{HWBH},\\
&\text{PFHT1}(3,1) = 1.5, \quad \text{and}\\
&\text{PFHT1}(3,2) = \text{NN}
\end{aligned}
\tag{188}
$$

as well as, for the outer bottom section,

$$
\begin{aligned}
&PFHB1(1,1) = 0.5 \cdot YPCH,\\
&PFHB1(1,2) = ZW - 0.5 \cdot HWBH,\\
&PFHB1(2,1) = 0.5 \cdot (BFH - YPCH),\\
&PFHB1(2,2) = \text{blend}(Z1, Z2, 0.001, \text{ABOVE}),\\
&PFHB1(3,1) = 1.0 \text{ and}\\
&PFHB1(3,2) = NN,
\end{aligned}
\tag{189}
$$

with

$$
\begin{aligned}
&Z1 = ZW - 0.5 \cdot HWBH - ZPCH + 0.5 \cdot HFH\\
&\text{and}\\
&Z2 = HFHC \cdot (1.0 - RHHV).
\end{aligned}
\tag{190}
$$

For the top outer section,

$$
\begin{aligned}
&PFHT2(1,1) = PFHT1(1,1),\\
&PFHT2(1,2) = PFHB1(1,2) - PFHB1(2,2) + HFH \cdot RHHV,\\
&PFHT2(2,1) = 0.5 \cdot YPCH,\\
&PFHT2(2,2) = ZPCH + 0.5 \cdot HFH - PFHT2(1,2),\\
&PFHT2(3,1) = 1.0, \text{ and}\\
&PFHT2(3,2) = NN
\end{aligned}
\tag{191}
$$

A scaling factor is defined using Eq. 185 and is applied to

$$
\begin{aligned}
&HFH = HFH\sqrt{ROFHS},\\
&HFHC = HFHC\sqrt{ROFHS}, \text{ and}\\
&BFH2 = BFH2\sqrt{ROFHS}.
\end{aligned}
\tag{192}
$$

In the case of one engine with rectangular (two-dimensional) nozzles,

$$
\begin{aligned}
&BFH1 = BP3 + EBP3,\\
&HFH = HP3 + EHP3,\\
&HFH1 = ZPCH + 0.5 \cdot HFH - ZW,\\
&HFH2 = HFH - HFH1, \text{ and}\\
&BFH = BFH1 + 2.0 \cdot \text{blend}(HFH1, HFH2, 0.001, \text{ABOVE}) \cdot \tan(QFH1).
\end{aligned}
\tag{193}
$$

Then, superellipses are fit to the upper and lower sections defined by

$$
\begin{aligned}
&PFHT1(1,1) = 0.5 \cdot BFH1,\\
&PFHT1(1,2) = ZW + 0.5 \cdot HWBH,\\
&PFHT1(2,1) = 0.5 \cdot BFH,\\
&PFHT1(2,2) = ZPCH + 0.5 \cdot HFH - ZW - 0.5 \cdot HWBH,\\
&PFHT1(3,1) = 1.0, \quad \text{and}\\
&PFHT1(3,2) = NN
\end{aligned}
\tag{194}
$$

for the upper section and

$$
\begin{aligned}
&PFHB1(1,1) = 0.5 \cdot BFH1,\\
&PFHB1(1,2) = ZW - 0.5 \cdot HWBH,\\
&PFHB1(2,1) = 0.5 \cdot BFH,\\
&PFHB1(2,2) = \text{blend}\begin{pmatrix} ZW - 0.5 \cdot HWBH - ZPCH + 0.5 \cdot HFH, \\ 0.0, 0.001, \text{ABOVE} \end{pmatrix},\\
&PFHB1(3,1) = 1.0, \quad \text{and}\\
&PFHB1(3,2) = NN
\end{aligned}
\tag{195}
$$

for the lower section.
The scaling factor is defined as in Eq. 185 and it is applied to

$$
\begin{aligned}
&HFH = HFH\sqrt{ROFHS}\\
&\text{and}\\
&BFH1 = BFH1\sqrt{ROFHS}.
\end{aligned}
\tag{196}
$$

Similary, for a twin-engined aircraft with axisymmetric nozzles,

$$
\begin{aligned}
&BFH2 = BP3 + EBP3,\\
&HFH = HP3 + EHP3,\\
&HFH1 = ZPCH + 0.5 \cdot HFH - ZW - 0.5 \cdot HWBH,\\
&HFH2 = HFH - HFH1 - HWBH,\\
&BFH1 = YPCH + BFH2, \quad \text{and}\\
&BFH = BFH1 + 2.0 \cdot \text{blend}(HFH1, HFH2, 0.001, \text{ABOVE}) \cdot \tan(QFH1).
\end{aligned}
\tag{197}
$$

Then, for the outer upper curve fit,

$$
\begin{aligned}
&PFHT1(1,1) = 0.5 \cdot (YPCH + BFH2),\\
&PFHT1(1,2) = ZW + 0.5 \cdot HWBH,\\
&PFHT1(2,1) = 0.5 \cdot (BFH - YPCH - BFH2),\\
&PFHT1(2,2) = ZPCH + 0.5 \cdot HFH - ZW - 0.5 \cdot HWBH,\\
&PFHT1(3,1) = 1.5, \text{ and}\\
&PFHT1(3,2) = NN
\end{aligned}
\tag{198}
$$

Then, the lower section is given by

$$
\begin{aligned}
&PFHB1(1,1) = PFHT1(1,1),\\
&PFHB1(1,2) = ZW - 0.5 \cdot HWBH,\\
&PFHB1(2,1) = 0.5 \cdot (BFH - YPCH - BFH2),\\
&PFHB1(2,2) = \text{blend}(Z1, Z2, 0.001, \text{ABOVE}),\\
&PFHB1(3,1) = 1.0, \text{ and}\\
&PFHB1(3,2) = NN,
\end{aligned}
\tag{199}
$$

with Z1 and Z2 calculated using Equation 190. For the upper inboard curve fit,

$$Z1 = \max (0.5\text{-}(YPCH - BP3), 0.0)$$

to ensure the correct fit of the ellipse given by

$$
\begin{aligned}
&PFHT2(1,1) = PFHT1(1,1) - BFH2,\\
&PFHT2(1,2) = ZW + RHHV \cdot HFHC,\\
&PFHT2(2,1) = PFHT1(2,1)\\
&PFHT2(2,2) = ZPCH + 0.5 \cdot HFH - PFHT2(1,2),\\
&PFHT2(3,1) = 1.0, \text{ and}\\
&PFHT2(3,2) = NN.
\end{aligned}
\tag{200}
$$

The scaling factor is defined as in Eq. 185, and is applied as in Equation 192.

4.1.1.7 The Entire Aircraft

After having defined the geometry and layout of the major aircraft components as well as the cross-sections of several fuselage reference stations, there remain a number of relationships to be defined which will ensure the correct packaging of the items presented above. Firstly, the longitudinal positioning of the fuselage stations will be described.

The total aircraft length is determined from the nozzle exit position and the location of the trailing edge of either the tailplane or the fin, whichever is the greater. Thus, the trailing edge of the empennage at the body side is allowed to extend beyond the rear of the aircraft fuselage, such that

$$LT = \max(XEFLB+CEFB, XETLB+CETB, XFN). \tag{201}$$

However, this length can only be determined after the empennage has been sized, which in turn depends upon the size of fuselage station C described in the previous section. For this purpose, an equivalent diameter is defined such that

$$DFC = 2 \cdot \sqrt{\frac{OFC}{\pi}}. \tag{202}$$

DFC is used to size the fin.

The aircraft length up to the nozzle exit plane, XFN, is divided into 9 reference stations, the geometry of which has been defined above. Their location is given schematically in Fig. 32. For the purpose of integrating the fuselage perimeter to obtain the surface area of the fuselage, the intervals between the reference stations have been divided into a number of intermediate stations, 38 in total. This subdivision will now be described.

The length of the radome, XFR, was given in Equation 6. It is divided into two equally spaced sections of length $\frac{XFR}{2}$. Behind the radome, a radar avionics bay of length LAR as well as the front part of a general avionics bay of length LAX1 are located, so that station A is located at a distance

$$XFA = XFR + LAR + LAX1 \tag{203}$$

from the aircraft nose. The distance between radome and front cockpit bulkhead has been divided into 5 equally spaced sections.

The axial location of station B is determined from the position of the pilot's eyepoint, so

$$XFB = XFA + LCEYE1. \tag{204}$$

The intakes are positioned aft of the pilot's head, and so XFC is equal to XII and

$$XII = XFB + (HC4 + HCEYE)\cdot\tan(QCSEAT). \quad (205)$$

The description of the boundary layer diverter is the same as given by Lovell. Because of the presence of the intakes at XFC, a jump in the cross-sectional area distribution occurs, a discontinuity which is dealt with by defining two fuselage stations at the same longitudinal location (Lovell, 1988).

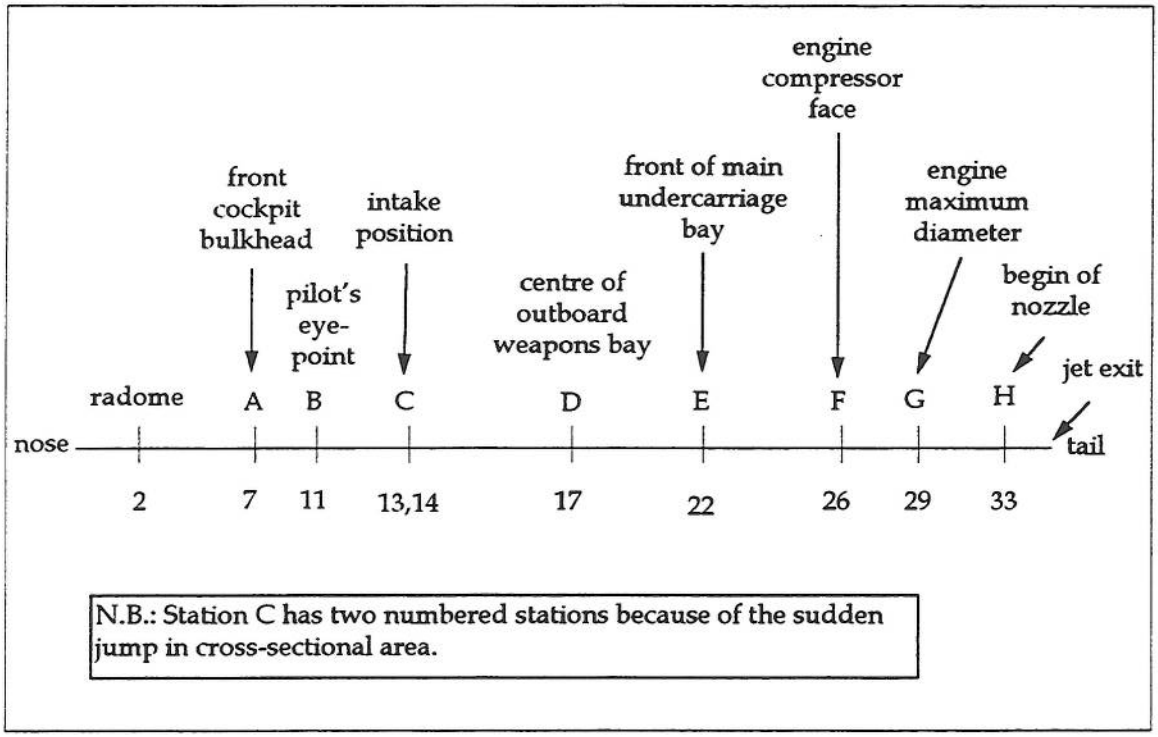

Fig. 32: Fuselage Station Location

A minimum cockpit floor height is defined by relating it to the pilot's forward vision requirement. Thus,

$$ZFLOOR = XFA\cdot\tan(QCEYE1) - HC5, \quad (206)$$

assuming that the nose is not drooped to aid in achieving this requirement.

After defining the forward fuselage in the manner described above, station C can now be sized, followed by the definition of the front fuselage

chine, assumed to proceed laterally along the nose from the radome to the intake position. Thus,

$$XSI = XII \quad \text{and}$$
$$ZSI = ZW \tag{207}$$

At the intermediate positions (stations A and B as well as the radome), the z-coordinates of the chine are found to be

$$ZSA = (XFA - XFR) \cdot \frac{ZSI}{XSI - XFR} \quad \text{and} \tag{208}$$

$$ZSB = (XFB - XFR) \frac{ZSI}{XSI - XFR}. \tag{209}$$

Also, the y-coordinates of the chine are found from

$$YSI = 0.5 \cdot BFC \tag{210}$$

and hence

$$YSA = YFR + (XFA - XFR) \cdot \frac{YSI - YFR}{XSI - XFR} \quad \text{and} \tag{211}$$

$$YSB = YFR + (XFB - XFR) \cdot \frac{YSI - YFR}{XSI - XFR}. \tag{212}$$

Fuselage station D has been described above, and its location is set by using the independent variable XB2C, which is the x-coordinate of the outer weapons bay centre of gravity. Therefore,

$$XFD = XB2C. \tag{213}$$

The fuselage stations coincident with the propulsion bay are defined as given in (Lovell, 1988):

$$XFF = XFN - LPG,$$
$$XFG = XFF + LP12, \quad \text{and} \tag{214}$$

XFH = XFF + LP12 + LP23 .

The engine spacing for a twin engined layout is found by obtaining from the design variables a factor on the diameter of the engines, YFPCH, which is applied to the minimum dimensions of the engine bay as follows:

$$Z1 = FYPCH\cdot(DP1+EBP1),$$
$$Z2 = FYPCH\cdot(DP2+EBP2), \tag{215}$$

$$Z3 = FYPCH\cdot(DP3+EBP3), \text{ and} \tag{216}$$
$$Z4 = FYPCH\cdot(DP4).$$

If two-dimensional nozzles are being used, then

$$Z3 = FYPCH\cdot(BP3+EBP3) \text{ and}$$
$$Z4 = FYPCH\cdot BP4. \tag{217}$$

The minimum separation distance, YPCH, is found from the maximum of Z1, Z2, Z3, and Z4. FYPCH is also constrained to be at least 1.122, as described in (Lovell, 1988).

The contour of the lower front fuselage between the weapons bay and the radome is found by fitting a Bezier spline between station B and the radome, defined as follows. First, a temporary variable to subdivide the distance between the radome and Station B is found:

$$X1 = \frac{XFB - XFR}{3} \tag{218}$$

This is followed by the definition of the forward and rearward spline endpoints:

$$\begin{aligned} &ZFUS(1,1) = XFR, \\ &ZFUS(1,2) = ZSR - 0.5\cdot(DAR + EDAR), \\ &ZFUS(4,1) = XFB, \text{ and} \\ &ZFUS(4,2) = ZB1C - 0.5\cdot HB1BI. \end{aligned} \tag{219}$$

The intermediate points are found from the following relationships, which were designed to safeguard the shape of the front fuselage:

$$
\begin{aligned}
&ZFUS(2,1) = ZFUS(1,1) + X1, \\
&ZFUS(2,2) = \frac{ZFUS(1,2)}{ZFUS(1,1)} \cdot X1, \\
&ZFUS(3,1) = ZFUS(4,1) - X1, \text{ and} \\
&ZFUS(3,2) = ZFUS(4,2).
\end{aligned}
\tag{220}
$$

Having defined the layout of the front fuselage, stations A and B are now synthesized, followed by the definition of the net wing as described by (Lovell, 1988) and the determination of the fuel mass in the net wing. This mass is used to find an initial landing reference mass for the sizing of the gear and the definition of station E, which is positioned at the front of the main gear bay. If the main gear is retracted forward, then

$$XUMB = XWCQM + RLUPCW \cdot CWMA + ELUP - LUMB. \tag{221}$$

Otherwise,

$$XUMB = XWCQM + RLUPCW \cdot CWMA - ELUP. \tag{222}$$

Consequently, XFE=XUMB.

Having now defined all of the axial positions of the fuselage stations, the intake duct geometry is defined using the relationships in Section 4.1.1.5, followed by the synthesis of the fuselage cross-sections D through H. The contour of the fuselage spine between C and F is described using a conic-cubic curve fit whose coefficients are stored in the array FZFCF.

Next, the fuselage wetted area and volume are found by integrating along the x-axis the perimeters and cross-sectional areas found during the sizing of the stations. The volume integration follows the method given by (Lovell, 1988), as does the volume accounting and mass estimation, with slight modifications outlined in the following sections.

4.1.2 Mass Estimation and Fuselage Sizing

The following sections describe the mass estimation methodology used for this work. First, an overview of the algorithms developed by (Lovell, 1988) is given, followed by a section detailing the enhancements to the weapons bay mass estimation developed by the author. More detailed information about the general mass estimation methods, including the mathematical relationships, may be found in (Lovell, 1988).

4.1.2.1 Aircraft Mass and Fuel Available

A large part of the mass estimation methodologies for the type of aircraft under consideration in this research were retained from the original design synthesis. They consist of a combination of algorithms developed at the DRA and, in the case of the wing and fuselage structure, British Aerospace (Lovell, 1988).

For each major component of the aircraft, the mass is estimated separately based upon its geometric characteristics and, in some cases, by a correlation with the aircraft mass. Thus, the landing gear dimensions and mass are found by a correlation with an aircraft reference mass upon landing. The major fuselage dimensions of width, height and length are used in conjunction with the volume and wetted area to find the fuselage mass, which is divided into three major components: two contributions from the skin and the internal structure, and one consisting of the fuselage fixed equipment, such as air, hydraulic and electrical systems. For the wing, component mass estimates are found for the wing box, the leading and trailing edge structure, flaps, spoilers and ailerons, and miscellaneous attachments, fairings and paint. For the empennage, a much simpler correlation with the major geometric parameters half-chord sweep, aspect, taper and thickness to chord ratios is used.

The fuel available in the synthesized aircraft is included in the mass estimation by considering the volume available for fuel once the internal components have been sized and accounted for. Fuel in the wing is located in a fuel tank within the wing box structure. A fraction of the fin volume is also available for fuel carriage. Volume fractions are used to account for the fact that not all of the residual volume in the fuselage is available for fuel.

It becomes clear from the relationships just described that the mass and dimensions of some of the items just described will depend upon the geometry of others. As the initial size is not known a priori, some form of iterative loop is necessary to size the aircraft. The procedure used is a sizing based upon the aircraft take-off mass, with an initial guess used for a first estimate of the size and mass of the geometry dependent components.

4.1.2.2 Weapons Bay

The enhancements of Lovell's mass estimation methods undertaken by the author in order to account for the presence of a weapons bay are detailed in this section. Two methods were available for this calculation, the first having been

developed from work done by (Burt and Phillips, 1952) and the second being provided by the DRA.

The first method consists of an estimation of the effect on the aircraft of four parts: the mass of the doors, the mass of the surroundings, including the landings and hinges of the doors, the mass of the weapons bay roof and, finally, the mass of the launcher. The last item is currently an external variable, while the method for predicting the mass of the first three is presented in the following paragraphs.

The mass of the doors is given by the equation

$$MBBID = PNDKG \cdot FMBBI1 \cdot OBBI^{FMBBI2} \cdot VD^{FMBBI3} \tag{223}$$

where OBBI is the area of the weapons bay door in sq. ft., VD is the design dive speed in knots, and PNDKG is a conversion factor from pounds into kilograms. Factors FMBBI1=0.03644, FMBBI2=0.91863, and FMBBI3=0.78258. This relationship was derived from a curve fit to the chart in Burt and Phillips, using a program for nonlinear regression obtained from (Press et al, 1989) and modified for the multi-variate case. The results of this analysis are shown in Figure 33. If the doors open into the fuselage, then they will be lighter than if they open into the airstream, but the hinges and mountings will be heavier, the net effect being a reduction in the door mass of 95%.

The mass of the surroundings is given by an equation relating the weapons bay width and length, shown in Equation 224, to the average mass per sq. ft. of the fuselage shell skin-stringer combination, shown in Equation 226.

$$FMBI = OBBI + LBBI + 5.0 \cdot BBBI \tag{224}$$

The additional mass has contributions from several terms. The first allows for the redistribution of the direct loads. According to Burt and Phillips, the effects of using longerons instead of the original skin approximately cancel each other out, so that the weight of the replacement material is the same as that of the uncut shell.

The second term caters for the redistribution of shear loads, now being carried by extra plating and frames fore and aft of the cutout. In the case of a weapons bay, it is assumed that the roof takes the larger share of the shear loads, and thus this term is replaced by the relationship shown in Figure 34, relating the weapons bay area in sq. ft. to the roof weight. The graph was approximated using the equation

$$MBBIR = PNDKG \cdot FMBBI4 \cdot OBBI^{FMBBI5}. \tag{225}$$

where MBBIR is the weight of the roof in kg, PNDKG is again a conversion factor, and OBBI is the area of the weapons bay door in sq.ft. In this equation, FMBBI4=2.00508 and FMBBI5=1.05409.

The last term in Equation 224 caters for the material for the landings. In summary, then, the weight of the material for surrounds excluding the term for the shear loads is given by MFXAVG·FMBI, where MFXAVG is the average weight of the skin stringer combination per m^2. The cutout is assumed to be rectangular, and the weight of the surrounding material is then in kg. The average skin weight is derived from the relationship given by (Lovell, 1988) based upon the British Aerospace method by dividing the mass of the fuselage shell by the wetted area of the fuselage:

$$MFXAVG = FMF2\left[0.07232(VD-180)^{0.9} + \frac{0.0000002602 \cdot XFN \cdot ULTN \cdot TPGD^{0.8}}{BFCDH + HFCDH} + 3.7\right] \quad (226).$$

In this equation, FMF2 is a materials factor and ULTN is the ultimate load factor.

In addition to the material needed to carry the fuselage loads around the weapons bay, reinforcements will be needed to carry the missile including its launcher and redistribute the loads into the fuselage structure. While it could be assumed that the missiles will be mounted to existing frames, resulting in only a very small increment in weight, Burt and Phillips suggest using an increment of 30 lb. per 1000 lb. of missile weight. However, they warn that this increment is very approximate and may be significantly in error for loads greater than 10,000 lb. Such loads are unlikely to be carried on the type of aircraft under consideration in this research program. Thus the given increment was adopted.

In summary, the mass effect of the weapons bay is given by

$$EMFBI = MBBID + MBBIR + MFXAVG \cdot FMBI + 0.03 \cdot (MBI + MLI), \quad (227)$$

where MBI and MLI are, respectively, the masses of the internal stores and of the launchers.

The method available from the DRA for estimating the mass effects of a weapons bay is similar to the method of Burt and Phillips in the sense that the mas increment is broken down into contributions from the door, the door mechanism, the weapons support structure, and the fuselage cutout, but the expression for calculating the total door mass includes a function of AMMX, the maximum airframe Mach number.

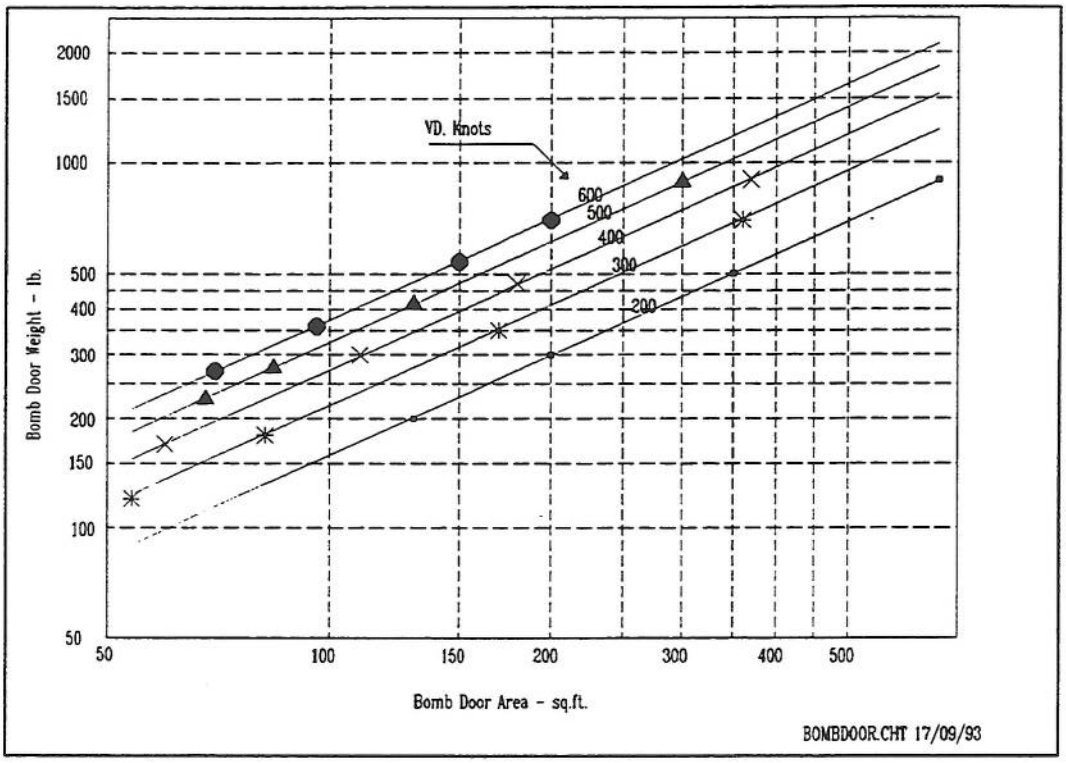

Fig. 33: Bomb Door Weight vs. Area

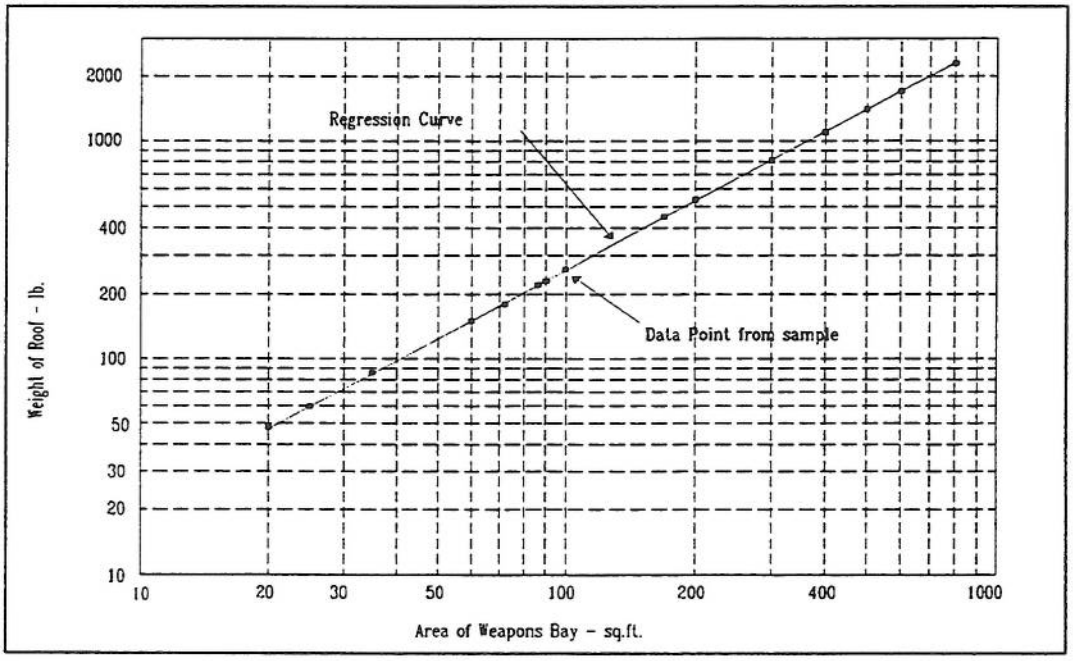

Fig. 34: Weight of the Bomb Bay Roof

4.1.3 Aerodynamics

4.1.3.1 Drag Estimation

The estimation of drag is described in detail in (Lovell, 1988). It consists of three elements: the subsonic zero lift drag, the transonic and supersonic zero lift drag, and the drag due to lift. The drag curve as a function of Mach number is estimated separately for the major components of the aircraft, these being wing, fuselage and tailplane. Allowances are made for items such as landing gear, cockpit canopy, external stores and gun ports. The drag components are then added, assuming linear theory, with additional factors for interference between components and for losses from surface irregularities and control surface gaps and leaks.

The subsonic friction drag estimation forms the basic drag for all Mach regions, including the transonic and supersonic. The estimation method, which is valid for Mach numbers of less than 0.8, assumes a fully turbulent boundary layer and is derived from Prandtl's skin friction drag formula for flat plates. It is modified using two form factors, one to cater for the Reynolds number variation across the lateral dimensions of the body and the other to account for the thickness of the body compared with a flat plate. An additional factor is used to calculate the effect of the skin roughness height on the friction coefficient. Having found the drag values for the wing, fuselage, empennage, boundary layer diverter, intake spillage, external stores and landing gear, if extended, the individual values are referenced to the gross wing area before being summed to find the total friction drag. Interference amongst aircraft parts (such as between wing and fuselage) as well as increments due to the presence of gaps and fairings between flight control surfaces are factored on to the basic drag values defined above, using empirically derived constants.

The method requires the definition of drag values at several reference Mach numbers through which a curve fit is undertaken to obtain the variation of drag with the rest of the Mach regime under consideration. First, for each major component such as wing, fuselage and tailplane, the wave drag at Mach numbers of 1.0 and 1.3 is estimated. Thereafter, the component drag values are summed to give the total configuration drag at these Mach numbers. Next, a drag divergence Mach number is defined for the point at which the drag increment above the basic value at M=0.8 is 0.002 and where the gradient of the wave drag with respect to the Mach number equals 0.1. Finally, the wave drag above Mach=1.3 is assumed to remain constant. Using the values thus defined in combination with an estimation of the gradient of the drag curve at M=1.0, a cubic variation is assumed between the drag divergence Mach number and M=1.0. From M=1.0 to M=1.3, an empirically derived formula is given.

The drag due to lift is assumed to have a parabolic shape. The curve is defined by three parameters: two factors, K1 and K2, which govern the shape of the parabola, and a critical lift coefficient, CLC, which determines the point of transition between the two regions of the drag polar. The transition region is

determined by fitting a cubic to the values of the drag polar at points slightly above and below the critical lift coefficient.

The factor K1 was derived empirically from a series of curve fits to aerodynamic data, as described by (Lovell, 1988). It is estimated separately for subsonic ($0.8 \leq M$) and supersonic ($M \geq 1.20$) Mach numbers. In the subsonic regime, K1 is dependent upon the quarter-chord sweep of the wing, the aspect ratio and taper ratio of the gross wing as well as the wing thickness-to-chord ratio. In the supersonic regime, K1 depends upon the trailing and leading edge sweep angles, the Mach number, the taper ratio and aspect ratio of the gross wing, the mid-chord sweep, the geometric mean chord and the distance between the mean quarter-chord point of the tail and the mean quarter-chord point of the wing. The factor K2, in the form of an increment on K1, and the critical lift coefficient as a function of Mach number are provided to the synthesis code in tabular form and are valid only for the class of aircraft for which they were determined.

4.1.3.2 Lift Estimation

The estimation of aircraft lift is divided into two parts: the estimation of the variation with Mach number of the slope of the lift curve as a function of angle of attack at zero lift, and the prediction of maximum lift. Whereas the former is calculated using methods developed by Lovell, the latter is provided to the design synthesis in tabular form as external constants versus Mach number. According to (Lovell, 1988), the original proposal of using DATCOM methods for the prediction of maximum usable lift was discarded after a correlation and comparison with data from real combat aircraft. It was found that the maximum lift was dependent upon too many factors outside the scope of the design synthesis.

The estimation of the lift curve slope is based on the assumption that it is linear in the angle of attack range in which aircraft performance will be evaluated. For the purposes of this investigation, this premise was retained, since the investigation of maneuverability, specifically at high angles of attack in the non-linear part of the lift curve, was not a requirement. In (Lovell, 1988), the lift curve slope is calculated for the zero-lift condition as a function of Mach number, separately in the subsonic, transonic and supersonic regimes. In order to ensure a match between the three areas, the subsonic and supersonic lift curve slopes are used to determine a cubic fit for estimation of the lift in the transonic regime. Initially, a critical Mach number is defined for the point at which the wing leading edge becomes supersonic. The values of the lift curve slope at this Mach number and at $M=0.8$ as well as the respective gradients at these points are used to fit the abovementioned cubic, using Skrobanski's method of conic-cubic interpolation (Skrobanski, 1985).

The subsonic lift gradient, at Mach numbers less than 0.8, is estimated by first calculating the gradient for the airfoil section using a DATCOM method (DATCOM, 1960), and then calculating the aircraft lift curve slope using a formula given by Lovell. For the supersonic regime above the critical Mach number, linear theory is used.

4.1.4 Mission and Performance Analysis

Using the abovementioned aerodynamic relationships in conjunction with the mass of fuel available aboard the aircraft, an analysis of the design sortie is carried out. Different combinations of Mach number, altitude, range or time may be specified for up to ten mission legs, each one representing either cruise or combat. During the analysis, checks are made to ensure that enough fuel and/or thrust are available to fly the specified leg. If not, the leg is flown under the assumption that there is enough fuel or thrust available. This procedure ensures the mathematical continuity of the constraints required for optimization purposes. Using the results of the mission analysis, a residual fuel figure is calculated at the end of the mission. This number can be positive or negative, indicating either excess or insufficient fuel, respectively, to fly the mission.

Up to fifteen performance constraints can be specified, either individually or as a combination of sustained turn rate, attained turn rate, ride quality, acceleration and maximum Mach number at different altitudes and/or Mach numbers. Additionally, take off and landing conditions are checked. These constraints are used in conjunction with the residual fuel figure to size the aircraft when the synthesis is linked with an optimization routine.

4.2 Analysis and Optimization Tools

In addition to the synthesis package just described, two additional tools were used for analysis and optimization purposes. The first is a graphical output program, developed by the author. Its main feature is that it makes use of a three-dimensional representation of the geometrical results of the synthesis. In order to obtain sized aircraft and to study trends of optimum designs for given changes in design requirements, a numerical optimization tool provided by the DRA was used.

The graphical output and the optimization package are described in the following sections.

4.2.1 Graphical Output using Splines

As described in Chapter 4.1, extensive use has been made of parametric spline representations for the description of the aircraft geometry. They have several advantages. Not only are they flexible enough to cover a wide variety of shapes, but also sufficiently robust to be independent of singularities which often create problems with more explicit representations of the spline curve. Also, it is possible to represent the defining coefficients in matrix form, which facilitates internal storage as well as curve transformation, rotation and scaling as well as changing from one spline representation to another.

The following paragraphs describe some of the applications of splines used in the development of a graphics package and the method for producing the output to UNIRAS graphics routines.

4.2.1.1 Surface Modeling

Partly in order to facilitate the generation of graphical output, a surface model using Bezier splines was incorporated into the design synthesis code at the outset of the program development. By extending the initial two-dimensional model to three dimensions, it was possible to obtain a description of the entire aircraft surface as well as a fairly simple method of generating the necessary descriptive parameters.

The underlying principle is the representation of the aircraft surface in terms of a three-dimensional surface, described by parametric cubic splines as shown in (Foley et al, 1990). The general surface representation can be given in matrix form as

$$X(s,t) = S \cdot M \cdot G \cdot M^T \cdot T^T \tag{228}$$

where $S = \begin{bmatrix} s^3 & s^2 & s & 1 \end{bmatrix}$ and $T = \begin{bmatrix} t^3 & t^2 & t & 1 \end{bmatrix}$ are the parameter vectors, G is some geometry matrix containing the points in three coordinates which define the surface, and M is a basis matrix relating the parameter vectors with the geometry matrices. Furthermore, $s = [0,1]$ and $t = [0,1]$ for each patch.

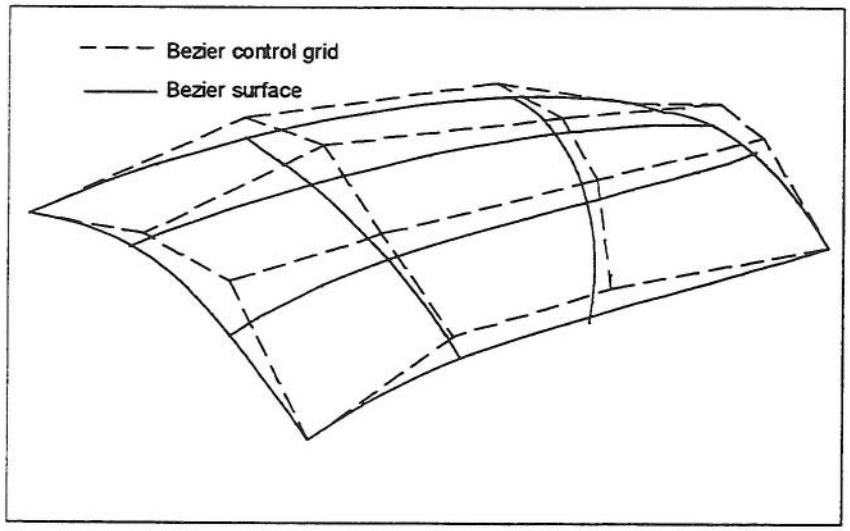

Fig. 35: Bezier patch geometry

In the case of the Bezier representation used for this work, G consists of 4x4 control points, therefore M is a 4x4 matrix, although representations using more than 16 points are also possible. Figure 35 shows how the sixteen Bezier control points define the surface: there are four corner points and 12 intermediate points. The creation of this geometry matrix for the aircraft graphics model is described in Section 4.2.2.3 below.

Another spline representation used in this work is the Catmull-Rom spline. It has the advantage of being capable of interpolating exactly its control

points. The mathematical representation is similar to the one used for the Bezier surface, and is given by

$$\mathbf{X}(t) = \frac{1}{2} \cdot \mathbf{T} \cdot \mathbf{M} \cdot \mathbf{G} \ . \tag{229}$$

Once again, T is the parameter vector, with the parameter t defined in the interval [0,1] for each segment, M is the basis matrix, and G is the geometry vector containing the control points. As can be seen from figure 36, each set of n points will define n-3 segments, and for each segment j, the corresponding geometry vector G_j is given by

$$\mathbf{G}_j = \begin{bmatrix} \mathbf{p}_j \\ \mathbf{p}_{j+1} \\ \mathbf{p}_{j+2} \\ \mathbf{p}_{j+3} \end{bmatrix}, \text{ with } \mathbf{X}_j(t) = \frac{1}{2} \cdot \mathbf{T} \cdot \mathbf{M} \cdot \mathbf{G}_j \ . \tag{230}$$

The basis matrix M is derived by taking into account the tangent to the curve at each control point, obtained as an average between the two adjacent control points.

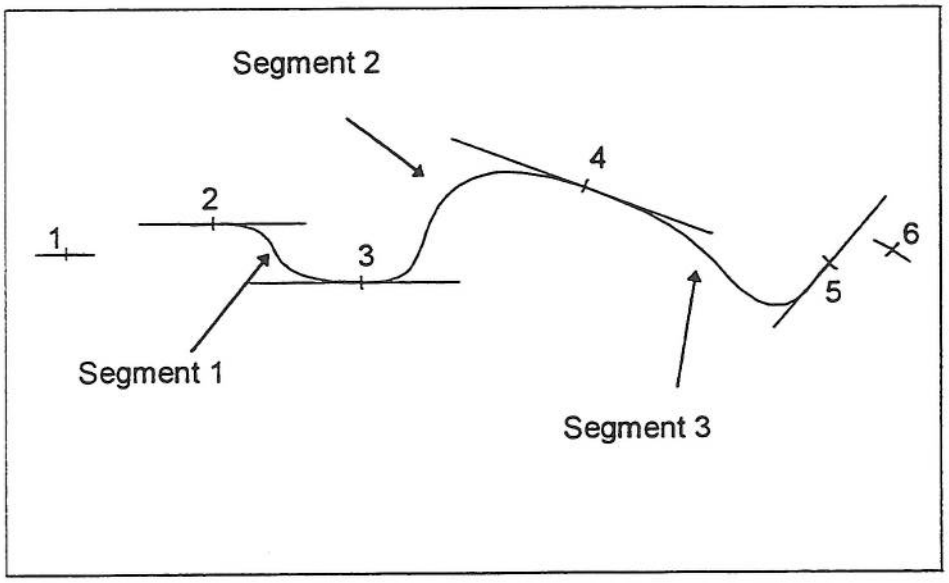

Fig. 36: Catmull-Rom spline geometry

Bezier splines possess the convex-hull property, which states that a given curve will not lie outside of a polygon defined by its control points. This makes them attractive for aircraft surface modelling, because it means that a cubic spline will be free of spurious inflections and bulges often associated with other

cubic curves. On the other hand, a larger number of control points is needed, making the generation of the spline more difficult than a simple interpolation of previously defined geometric points.

Catmull-Rom splines do not posess the convex-hull property, but their use is far simpler than Bezier splines. They are attractive when it is necessary to exactly interpolate all of the control points using a robust curve fitting method, and they were used extensively in this work.

4.2.1.2 Transformation of Spline Representations

Each form of spline representation has its advantages and disadvantages, and these differences sometimes make it necessary to be able to transform a spline from one representation to another. This can be done so long as the basis matrices are of a similar form. In the case of the spline representations used in this work, the Catmull-Rom spline was used to interpolate fuselage geometry points not previously used to fit a Bezier spline. Having generated the Catmull-Rom splines, they are transformed to the Bezier representation. This is because the patches described in Section 4.2.1.1 required the surface to be bounded by Bezier splines.

The procedure to transform one spline representation into another can be derived by considering two arbitrary representations,

$$\mathbf{X}_1 = \mathbf{T}_1 \cdot \mathbf{M}_1 \cdot \mathbf{G}_1 \text{ and } \mathbf{X}_2 = \mathbf{T}_2 \cdot \mathbf{M}_2 \cdot \mathbf{G}_2 \,, \tag{231}$$

and requiring equality between X_1 and X_2 . If representation 1 is to be transformed into representation 2, then another way of stating the problem is to find the geometry matrix G_2 for the given basis matrix M_2 such that $X_2 = X_1$. This results in the equation $\mathbf{G}_2 = \mathbf{M}_2^{-1} \cdot \mathbf{M}_1 \cdot \mathbf{G}_1$. It can be seen that in order to transform from a given spline representation to a target spline representation, it is necessary to compute the inverse of the target basis matrix.

4.2.1.3 Surface Model Generation

The methodology for generating the surface model is demonstrated in Figure 37 using the canopy as an example. In this side view it can be seen how use is made of the known geometry to obtain the unknowns.

Surface patches are obtained by dividing the aircraft into components. Each component is then modelled using rows of Bezier patches extending longitudinally along the aircraft beginning from the point nearest to the nose. For example, the canopy shown below is modelled using three patches. In the vertical plane, most fuselage stations are defined using Bezier splines, thus defining four control points on the forward and aft boundary of each patch.

The upper and lower boundaries are defined by first fitting a Catmull-Rom spline to the known geometry points at the fuselage stations of the component. Two additional points are needed for this type of spline, as described in Section 4.2.1.1, and they can be chosen such that a smooth fit is

obtained. By transforming the thus defined Catmull-Rom splines into Bezier form, it is possible to generate four further control points for each patch.

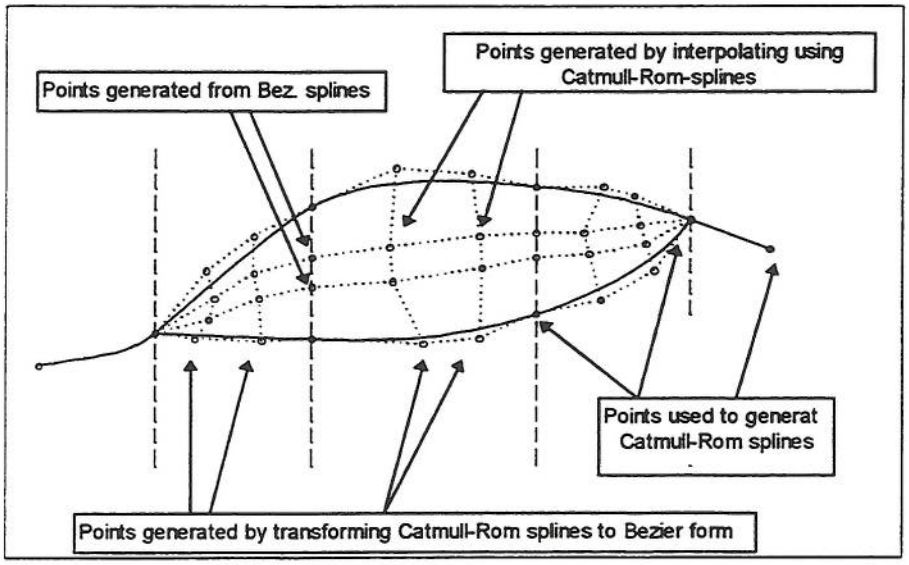

Fig. 37: Surface model generation

Finally, the control points of the Bezier splines generated during the aircraft synthesis process are themselves interpolated using Catmull-Rom splines. However, in this case the splines are not transformed into Bezier form, but are instead found by evaluating the fitted spline at a specified interval between the control points.

4.2.1.4 Generation of Polygons for UNIRAS

The UNIRAS graphics package (UNIRAS, 1992) contains several routines to plot three-dimensional objects, based upon algorithms for the rendering of polygons. Thus, in order to obtain a three-dimensional image of an object, a list of polygons describing its surface must be created by the user. The following section describes how this was done using the spline surfaces described in the previous two sections.

First, a list of points to be rendered by the graphics package must be generated by evaluating the Bezier patch at a given number of points. If a given patch is divided into (n-1)×(n-1) subpatches, it will be defined by n×n points. The method for evaluating the Bezier patch is given in (Foley et al, 1990). Thereafter, the list of n×n points must be transformed into a second list which is arranged such that four consecutive points describe one rectangle or triangle. In the latter case, the fourth point will be identical to the first one. All points must be arranged in either clockwise or counterclockwise order around the polygon.

Consider the patch shown in Figure 38.

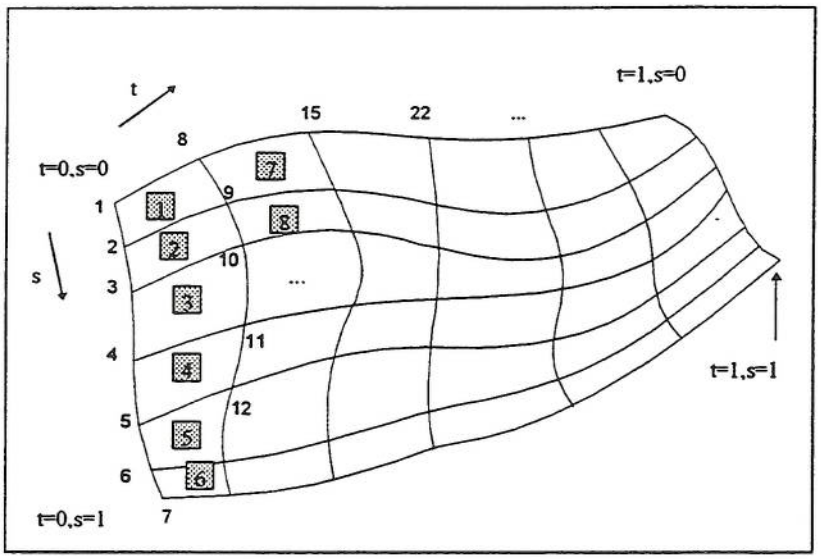

Fig. 38: Bezier Patch Setup for List Generation

For subpatch 1, the correct order of points in the polygon list L is $L_i = \mathbf{p}_1$, $L_{i+1} = \mathbf{p}_2$, $L_{i+2} = \mathbf{p}_9$ and $L_{i+3} = \mathbf{p}_8$. By introducing two counters, *cs* and *ct*, and the number of points in the s-direction and the t-direction, *ns* and *nt*, the generation of the UNIRAS list can be summarized in the algorithm shown below:

```
...
cs ← 1
ct ← 0
count i from 1 to ns · nt
    plist(i_p) ← tlist(i + ct)
    plist(i_p + 1) ← tlist(i + ct + 1)
    plist(i_p + 2) ← tlist(i + ct + ns + 2)
    plist(i_p + 3) ← tlist(i + ct + ns + 1)
     / rem /  update counters:
    i_p ← i_p + 4
    cs ← cs + 1
    if cs = ns + 1 then
        cs ← 1
        ct ← ct + 1
    end of if - block
end of loop to count i
...
```

Fig. 39: List generation algorithm

A sample picture generated with the help of this graphics program is shown in Figure 40.

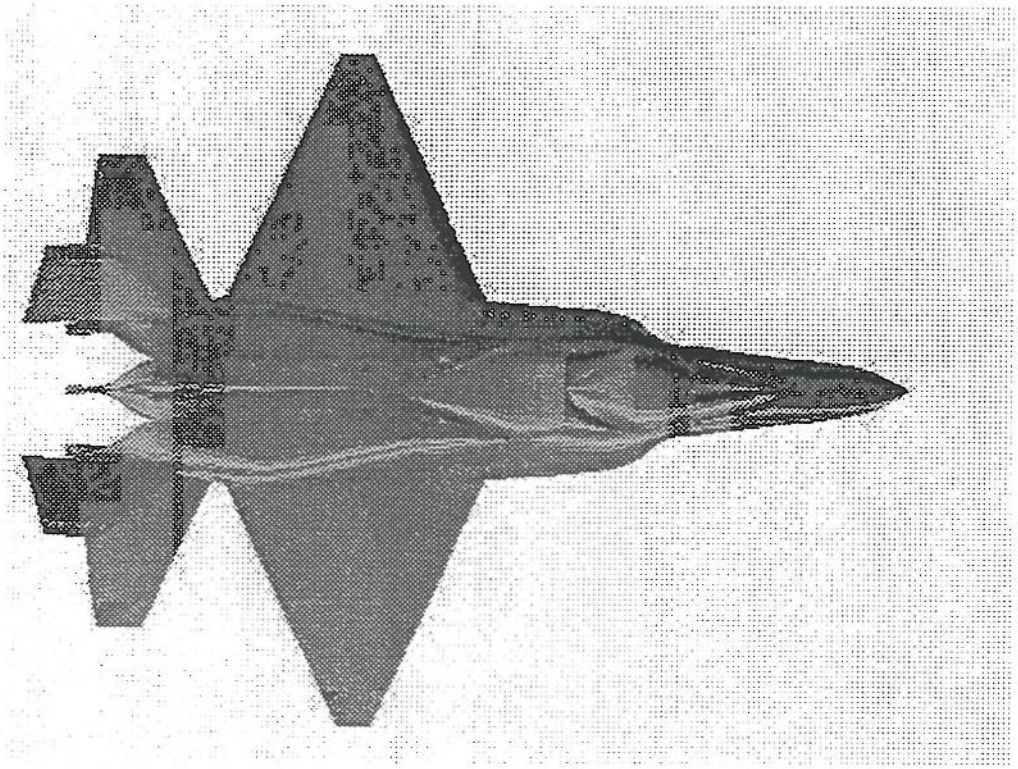

Fig. 40: Sample Graphics Output

4.2.2 Numerical Optimizer

RQPMIN, a numerical optimization package (Skrobanski, 1994), was provided by the DRA for the purposes of this research program.

RQPMIN is a gradient based methodology for solving nonlinear constrained minimization problems of the form

$$\text{minimize } f(x) \ . \tag{232}$$

f(x) is called the objective function, where x is a vector $x=[x_1,x_2,x_3,\ldots,x_n]$ containing n problem variables. At the solution to the problem, each of the variables must satisfy the condition $x_{iL} \le x_i \le x_{iU}$ $(i=1,\ldots,n)$, where the x_{iL} and x_{iU} are lower and upper bounds, or side constraints, on the variables. These bounds can be specified in an *RQPMIN* input file.

Furthermore, a series of problem functions or constraints must be satisfied, such that

$$\left.\begin{array}{l} c_i(x)=0 \\ \text{or} \\ c_i(x)\le 0 \\ \text{or} \\ a_i \le c_i(x) \le b_i \end{array}\right\} \ (i=1,\ldots,m) \ . \tag{233}$$

In this set of conditions, the functions $c_i(x)$ are the constraint functions and the a_i and b_i are constants specified as input to the minimization problem. Constraints can be classified either as active or inactive according to a set of criteria given in (Skrobanski, 1994).

The above formulation of the minization problem is well known and frequently used to set up optimization algorithms (Gill, et. al., 1981), but different methods may be used to achieve this aim. *RQPMIN* makes use of a gradient-based penalty function method. Briefly, the penalty function method consists in adding to the objective function a penalty term whose magnitude is determined by considering the effect of active constraints, as described in (Skrobanski, 1994). By using such a procedure *RQPMIN* is able to determine values for the objective function even when the constraints are violated, and the magnitude with which the constraints influence the penalty function will provide an indication about the search direction to be taken to minimize the problem.

RQPMIN has several important features which make it appropriate for the type of problem under consideration in this research. It is fast, i.e. it converges quadratically, when it is reasonably close to the minimum. One of the reasons for this is the concept of perifeasibility introduced by Skrobanski. Essentially, *RQPMIN* can consider certain points (which may violate the constraints by a specified maximum tolerance) to be perifeasible. As the minimum is

approached, the constraints automatically become satisfied. Therefore, *RQPMIN* can make rapid progress when it is far from the minimum because it does not needlessly spend time satisfying the constraints exactly. Also, *RQPMIN* is well suited to continuous problem formulations such as this aircraft design case. Finally, it has the ability to calculate derivative information using finite differences.

There are three main drawbacks to *RQPMIN*. First, it requires smooth functions with smooth derivative information. Any discontinuity may cause it to fail. This requirement also means that, in the absence of explicit derivative information, this must be provided using finite differences. They take many function evaluations to compute, and the accuracy of computation can strongly influence the result of the optimization. Finally, *RQPMIN* can not be considered a global minimization procedure because it can search only a limited portion of the function definition space and because it has no method for distinguishing a local minimum from a global minimum.

4.3 Linking the Design Synthesis with the Optimizer

4.3.1 Multivariate Optimization Package Structure

The elements of the design synthesis, namely geometry description, mass and aerodynamics estimation, and point performance and mission analysis were arranged to provide an efficient and logical flow of information. Each functional subgroup was coded as a separate module. This made testing and evaluation of each new section of code as it was added easier as well as providing a structured layout for the program.

Figure 43 shows how the synthesis code was structured. Upon entry, during the first call to the design synthesis, the input data file is read and a number of fixed items are calculated. These remain constant throughout the optimization and thus need only to be calculated once. This includes the gun geometry, the weapons bay geometry, the radome and the cockpit. Similarly, at the final call to the design synthesis, a number of output quantities are calculated and written to a file, including the graphical output information as well as the design data of the final solution. The remaining subroutines are evaluated at every call to the synthesis, and represent all of the items dependent upon the problem variables.

After finding the size of the engine bay and the intake duct, the fairing curve is set up according to the input variables, followed by the geometry of the wing independent of the fuselage. After the empennage has been sized, it is possible to find the length of the fuselage as described in Chapter 4.1. Using the initial guess for the take-off mass a first estimate for the size of the fuselage is found. The calculated mass is used as the new estimate for the fuselage size, and this process is repeated until the two values (estimated and calculated) differ by no more than a pre-determined accuracy, currently set for 0.005 kg. Although such a low number may seem inordinately accurate for a value which may be of the order of 10000 to 30000 kg, termination of internal iteration loops

with high precision is deemed essential in avoiding problems with the optimization algorithm (Gill et al, 1981).

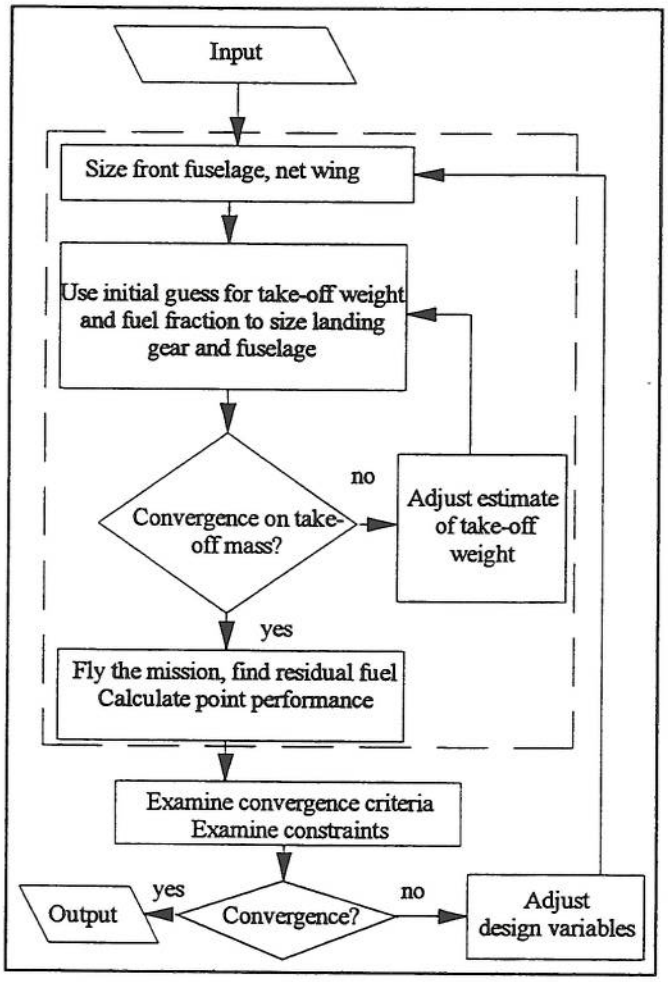

Fig. 41: Optimization Flow Chart

Once a size and mass for the fuselage and indeed for the entire aircraft are known, the aerodynamic, point performance and mission analysis are carried out, at which point the synthesis terminates and returns control of the program to the optimization routine. This program logic flow is shown in Figure 41. As currently structured, the sizing of the fuselage cross-sections using iterative loops may duplicate the effect of some of the constraints.

Whilst the design synthesis program was being developed, care was taken to account for the requirements of *RQPMIN*. In order to reduce computation time, the synthesis modules were divided into repeating and non-repeating calculations, as explained above and shown in Figure 43. Also, smooth functional relationships were used throughout to avoid discontinuities in the first and second derivatives. A blending function was used where these could not be avoided. Furthermore, the use of internal iterative loops was kept to a minimum, as shown in the functional decomposition of the design synthesis

and optimization package in Figure 42. Lines to the right of the diagonal indicate the flow of information from a given module forward to another one, whereas lines to the left indicate feedback loops. The most important of these is the connection between the constraint evaluation and the beginning of the synthesis, but a further feedback loop can be seen from the mass estimation to the geometry synthesis module. In the synthesis code, this represents the iteration on take-off mass to size the fuselage.

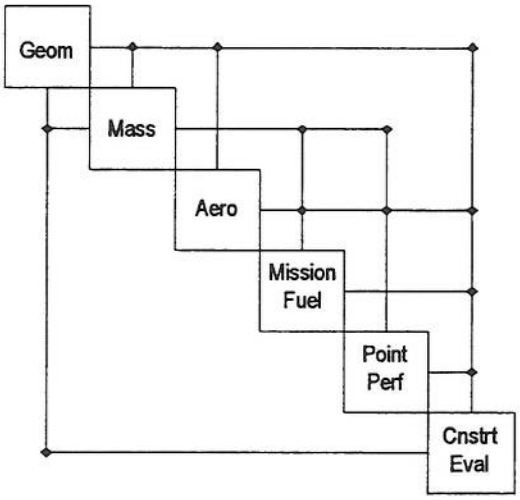

Fig. 42: Optimization Structure

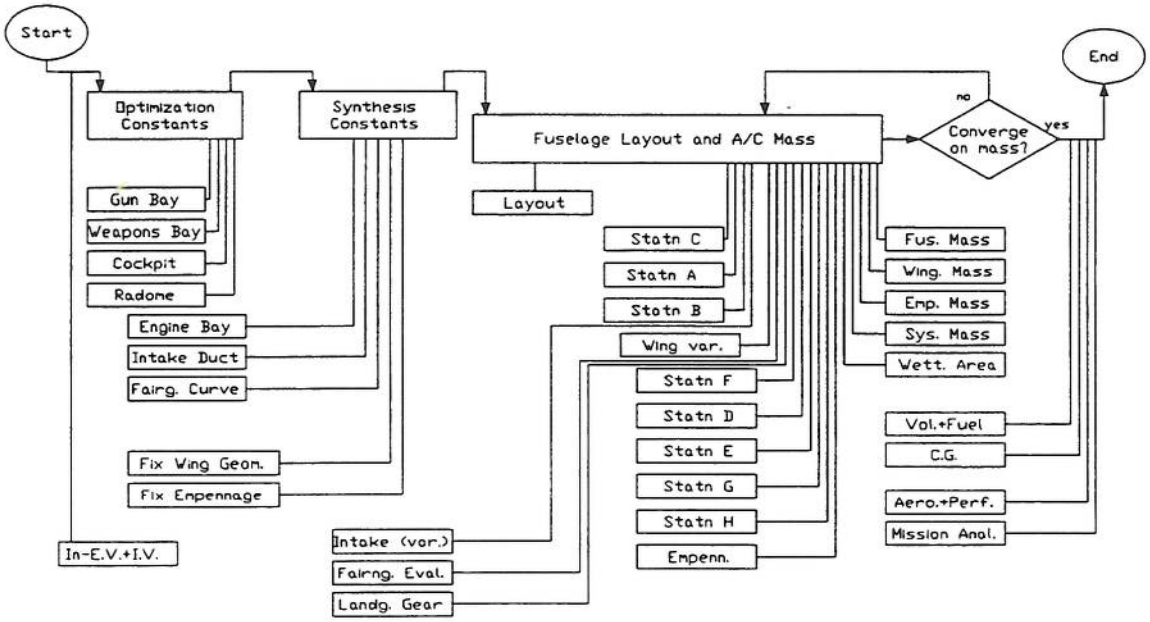

Fig. 43 Design Synthesis Program Structure

4.3.2 Description of Design Variables and Constraints

A comprehensive list of variables is given in the Table 3.

No.	*Description*
1	Engine Scale Factor
2	Wing Area [m²]
3	Wing quarter chord sweep [°]
4	Wing Thickness to Chord Ratio
5	Wing Taper Ratio
6	Wing Aspect Ratio
7	Wing Front Spar Position as a fraction of the chord
8	Wing Rear Spar position as a fraction of the chord
9	Span of the trailing edge flaps as a fraction of the wing span
10	Span of the wing net fuel box as a fraction of the wing span
11	Fuselage length from nose to nozzle exit [m]
12	Fairing curve RLTMFN
13	Fairing curve RLTFFN
14	Fairing curve RLTCFN
15	Fairing curve RLTAFN
16	Wing quarter chord position aft of nose as a fraction of the fuselage length
17	Fairing OT6N
18	Fuel volume fraction of forward fuselage
19	Fuel volume fraction in center fuselage
20	Fuel volume fraction in rear fuselage
21	Fin quarter chord position aft of nose as a fraction of the fuselage length
22	Tail quarter chord position aft of nose as a fraction of the fuselage length
23	Weapons bay (inboard) c.g. position in x-axis (as a frac. of fus. length)
24	Weapons bay (outboard) c.g. position in x-axis (as a frac. of fus. length)
25	Weapons bay (inboard) c.g. position in z-axis (as a frac. of fus. length)
26	Weapons bay (outboard) c.g. position in z-axis (as a frac. of fus. length)
27	Engine separation distance, factor on diameter on twin engine installation

Table 3: Independent Variables

Constraint functions were developed which take into account the peculiarities of stealth configured aircraft, along with other constraints to ensure the correct relationship of the aircraft components to one another and to the aerodynamics and performance calculations. The constraints are listed in Table 4, and a brief description is given here.

Constraint 1 ensures that the wing and tailplane are separated by a specified minimum amount. Constraint 2 is an aerodynamic restriction on the wing geometry, designed to prevent unacceptable pitch-up behaviour close to the stall point, and is a commonly used rule of thumb for wing design. Constraints 3 through 10 ensure that sufficient cross-sectional area is available from the fairing curve to fit all of the internal components, i.e. that the minimum required at a given station is less than or equal to the cross-sectional

area obtained from the fairing curve. Constraints 11 and 12 relate the shape of the rear fuselage to the aerodynamic requirement for attached flow. Therefore, the boattail angle is required to be both positive (i.e. converging fuselage sides, constraint 11) and less than a given maximum (constraint 12). Figure 44 demonstrates how the boattail angle is defined for axisymmetric cross-sections.

Constraints 14 through 16 are designed to ensure that the minimum length of the fuselage is great enough to contain all of the internal components, whilst constraints 17 through 19 perform a similar function for the volume. Constraint 20 ensures that the geometry of the aircraft at the rear of the fuselage (driven by the engine) matches the geometry given by the fairing curve. Constraints 21 through 24 check that the aircraft centre of gravity is located within the limits on mean aerodynamic chord set by the user as input. Constraint 25 ensures that the diffuser is long enough to avoid excessive curvature and hence unacceptable flow conditions. Constraint 26 controls the shape of the fairing curve at the rear of the aircraft.

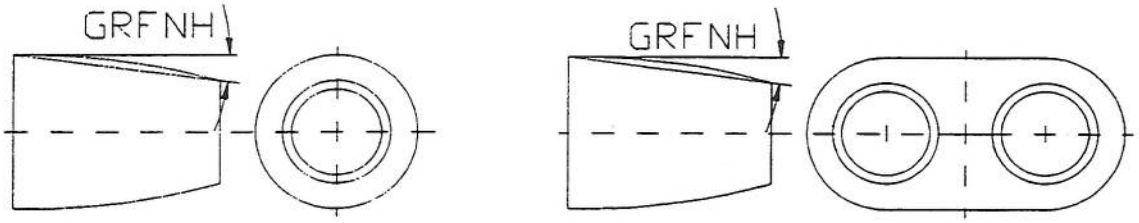

Fig. 44: Boattail Angle for Single- and Twin-engine Configurations

In order to allow the synthesis of stealthy configurations, costraints 27 and 28 control the shielding of the engine face and the alignment of the wing leading and trailing edges, respectively. Constraint 29 ensures the correct sizing of the aircraft for the mission requirement, i.e. there must be no residual fuel after the mission has been completed. Aerodynamic and aeroelastic effects of the external carriage of stores are covered by constraint 30, which is a function of the wing geometry and structure. Aerodynamic limitations are further covered by constraints 32 through 34, whilst constraint 31 ensures the availability of sufficient take-off distance. With constraint 35, the aircraft can be optimized in such a manner as to burn all of the fuel in the exposed section of the wing before reaching the combat legs of the mission. Constraints 37 through 39 ensure that the internal weapons bays do not overlap any of the other internal components. Constraint 40 ensures that the tailplane and fin are, in fact, attached to the aircraft, whilst constraints 41 and 42 allow maximum aircraft width and length to be specified. This may be useful if the optimum aircraft is required to fit within given shelters or hangars. Constraints 43 and 44 were included to ensure the correct order of the fuselage stations. Finally,

constraint 45 was included to allow a minimum leading edge sweep of the wing to be specified. This can be used to control the radar signature of the leading edge of the wing or to ensure a minimum sweep for aerodynamic reasons.

Constraints 50 through 65 can be used for point performance calculations, and are described in detail in (Lovell, 1988).

No	*Definition*	*Equation*	*Type*[1]
1	Separation distance between wing T.E. and tailplane L.E. at body side	LWTTL-LWTTLS≥0	IC
2	Restriction on combinations of wing aspect ratio and wing sweep	$3.2 - AW[\tan(QW4)]^{0.8} \geq 0$	IC
3	Excess underfloor cross-sectional area at station A	OFA-OFAS≥0	IC
4	Excess fuselage cross-sectional area at station B	OFB-OFBS≥0	IC
5	Excess fuselage cross-sectional area at station C	OFC-OFCS≥0	IC
6	Excess fuselage cross-sectional area at station D	OFD-OFDS≥0	IC
7	Excess fuselage cross-sectional area at station E	OFE-OFES≥0	IC
8	Excess fuselage cross-sectional area at station F	OFF-OFFS≥0	IC
9	Excess fuselage cross-sectional area at station G	OFG-OFGS≥0	IC
10	Excess fuselage cross-sectional area at station H	OFH-OFHS≥0	IC
11	Limitation on upper value of boattail angle	GRFNH-GRFXH≥0	IC
12	Positive boattail angle	GRFN≥0	IC
13	Separation between intake lip and wing	LIIWL-LIIWLS≥0	IC
14	Lower limit on fuselage length set by gun	XFN-XFR-LAR-LGC-LUMB-LPG≥0	IC
15	Lower limit on fuselage length set by nose undercarriage bay	XFN-XFR-LAR-LUNB-LUMB-LPG≥0	IC
16	Lower limit on fuselage length set by inboard weapons bay	XFN - XFR - LAR - LB1BI - LUMB - LPG≥ 0	IC
17	Limitation on minimum diffuser length for duct area increase	LIDG-LIDS≥0	IC
18	Volume in front fuselage for avionics, air systems and fuel	VFI-VAR-VUNB1-VGC1-VCKPT≥0	IC
19	Volume in rear fuselage for fuel	VFT-VPB≥0	IC

[1] IC: denotes an inequality constraint of the form $c(x) \geq 0$. EC: denotes an equality constraint of the form $c(x) = 0$. Note that the inequality constraints have been formulated exactly opposite to the form required for *RQPMIN*, which can be easily changed by swapping the sign of the constraint function.

20	Difference between the increment in cross-sectional area at nozzle from the i.v. and that derived from the intake and engine bay geometry	FOT6N-OT6N=0	EC
21	Distance of aircraft c.g. aft of forward c.g. limit (empty aircraft)	XTECG-XWCQM+RLTCL·CWMA≥0	IC
22	Distance of aircraft c.g. aft of forward c.g. limit (full aircraft)	XTTCG-XWCQM+RLTCL·CWMA≥0	IC
23	Distance of aircraft c.g. forward of aft c.g. limit (empty aircraft)	XWCQM-RLTCA·CWMA-XTECG≥0	IC
24	Distance of aircraft c.g. forward of aft c.g. limit (full aircraft)	XWCQM-RLTCA·CWMA-XTTCG≥0	IC
25	Limitation on minimum diffuser length for duct curvature	LIDG-XVE+XVI-DP1≥0	IC
26	Limitation to negative curvature in cubic area distribution for rear fuselage	-OTA3K≥0	IC
27	Distance between duct centreline at intake and engine centerline at compressor face	EDIIE - EDIIES ≥ 0	IC
28	Equal but opposite angles for leading and trailing edges of wing	QWL+QWT=0	EC
29	Mass of fuel remaining in aircraft when sortie has been flown	MTGF-FSUM-MTTF-MTLF=0	EC
30	Acceptable store release disturbance on wing	FDBH-RTW·cos(QW4)² ≥ 0	IC
31	Unused distance of the total allowed for take-off ground roll	LTTH-TOG≥0	IC
32	Stall margin during landing approach	$\frac{VTLH}{VSTAPP} - 1.3 \geq 0$	IC
33	Amount by which take-off wing loading exceeds specified min. value	FMTSW-FMTSWL≥0	IC
34	Amount by which specified max. take-off wing loading exceeds actual	FMTSWL-FMTSW≥0	IC
35	Mass of fuel burnt in sortie before combat, in excess of that in wing	FSUM-MWBEF≥0	IC
36	Separation distance between front of outboard weapons bays and intake lip	XB2C-0.5·LB2BI-XFC-LBI2S≥0	IC
37	Sep. distance between rear of outboard weapons bay and front of main gear bay	XFE-XB2C-0.5·LB2BI≥0	IC
38	Sep. distance between rear of inboard weapons bay and engine compressor face	XFF-XB1C-0.5·LB1BI-LBI1PS≥0	IC
39	Separation distance between front of inboard weapons bay and rear of cockpit	XB1C-0.5·LB1BI-XFB-LCFL≥0	IC
40	Constraint for empennage beyond nozzle	max(FCEFB*CEFB, FCETB*CETB) - (LT - XFN)≥0	IC

41	Maximum aircraft length	LTH - LT ≥ 0	IC
42	Maximum aircraft width	BWH - BW ≥ 0	IC
43	Ensure that XFD is less than XFE	XFE-XFD≥0	IC
44	Ensure that XFE is less than XFF	XFF-XFE≥0	IC
45	Minimum l.e. sweep of the wing	QWL-QWLS≥0	IC
50 51 52 ... 65	(performance constraints as per Lovell ... ...)		

Table 4: Constraint Function Definition

5. Analysis of the Design Methodologies

The development process of the design synthesis and optimization was organized to allow a continual testing and evaluation of each new module. The first step consisted of an evaluation and comparison with experimental data of the aerodynamic estimation methodologies, described in Section 5.1. In Section 5.2, the procedures used to test the design synthesis and optimization code are described. Two test cases were run to check the accuracy and validity of the synthesis methodology. Furthermore, tests and analyses were conducted to ensure the correct functioning of the synthesis in conjunction with the optimization routine.

5.1 Validation of the Aerodynamic Estimation Methodologies

Figures 45a through 45c show the types of experimental configurations found in the open literature and used as validation for the aerodynamic estimation methods.

To compare the model configurations with the calculation methodologies, the geometry of each model was obtained as accurately as possible, using either the experimental data given by the references or by extracting the relevant dimensions from the figures. This was used as input to the equations given in (Lovell, 1988). For the estimation of the lift-dependent drag, the parameters CLC and DK2 (Lovell, 1988) are supplied as a table versus Mach number, using a standard set of values supplied by (Kirk, 1993). This input data was used to calculate the zero-lift and lift-dependent drag as well as the lift curve slope as a function of Mach number.

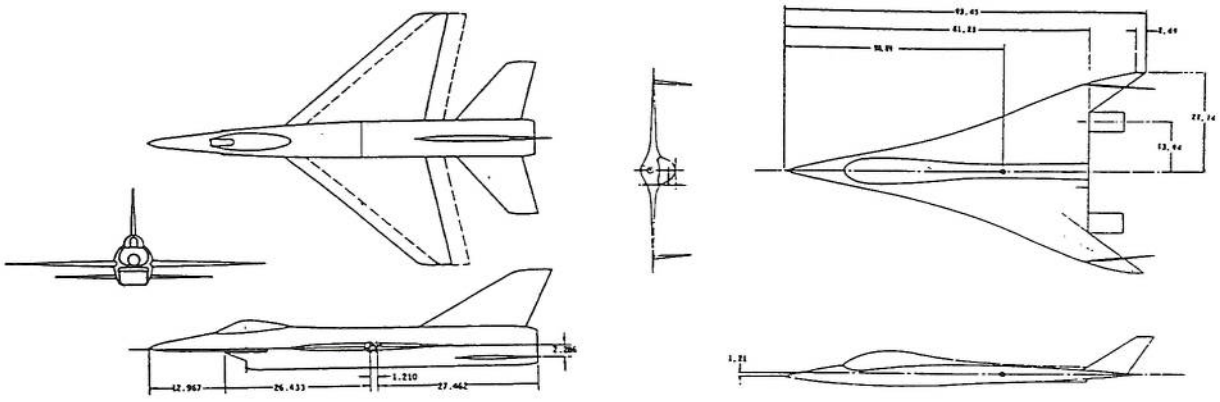

Fig. 45a: NASA TM X-3078 (left), (Dollyhigh, 1974)
and NASA TM 78764 (right), (Dollyhigh, 1979)

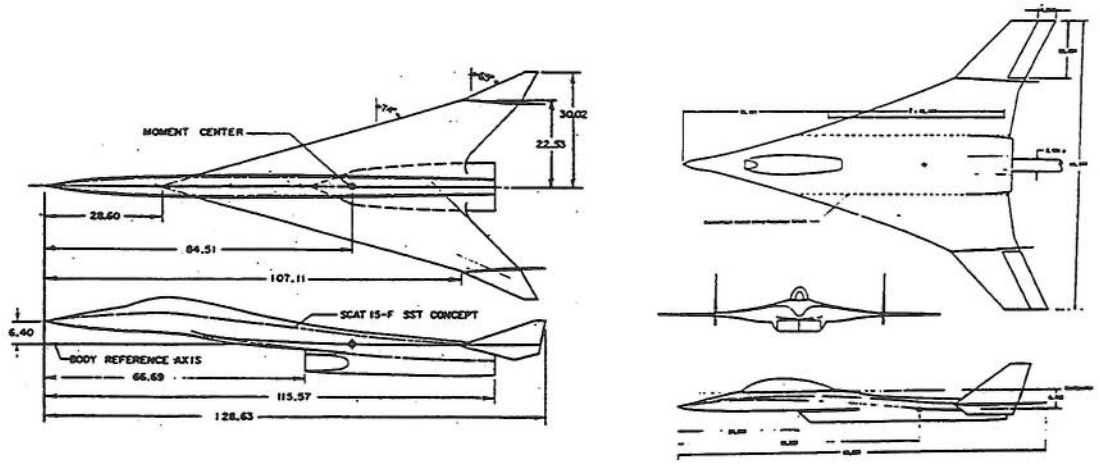

Fig. 45b: NASA TM X-3530 (left), (Morris, 1977)
and NASA TM X-3559 (right), (Shrout, 1977)

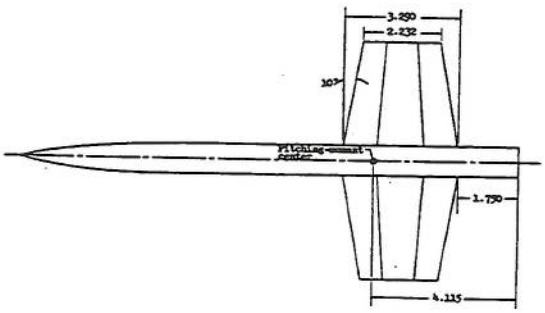

Fig. 45c: NASA TN D-2236 (Hicks and Hopkins, 1974)

Figure 46 shows how for eight different configurations the friction drag at Ma 0.8, calculated using Lovell's method, compares with experimental results. Very good agreement exists between the values calculated without interference and the experiment because of the lack of excrescences, gaps, fairings and control surfaces on the models which otherwise would lead to an increase in drag. Moreover, the good agreement holds true regardless of the type of configuration, suggesting that Lovell's methodology could be retained unaltered.

In order to investigate the accuracy of the wing drag due to lift, the geometric parameters of the wing upon which the drag due to lift depends were extracted from the drawings of the models. The drag polars for the selected configurations were then calculated and compared with the experimental results. This is shown in Figures 47, 48, 49 and 50. The most important conclusion from the comparisons is that, in general, the calculation matches the experiment at moderate lifting conditions and at Mach numbers in the transonic regime. At subsonic speeds, the drag due to lift is underestimated, while the opposite occurs at supersonic Mach numbers. Since combat aircraft will tend to perform most maneuvering, including combat, around the transonic regime, these results are encouraging. Furthermore, most of the mission and performance calculations in this design synthesis were developed for low to moderate angles of attack. However, they also indicate the necessity of refining the induced drag estimation, possibly by adding the interference effects of the wing/fuselage junction and other components.

Figures 51a and 51b show the results of a comparison between the slope of lift curve with respect to angle of attack as a function of Mach number for four configurations. The calculation was done for the wing alone, as this is the only method currently implemented within the design synthesis code. It can be seen that the estimation method is not very accurate. The errors are seen to be both in the magnitude and shape of the curve, indicating that the method should be applied with caution to the design synthesis.

Meaningful results for the estimation and comparison of the wave drag with respect to Mach number were not obtained using the method of comparison as above. This was due mainly to the lack of experimental data necessary to perform the comparison with calculated values. However, since the estimation of this drag component is based on the DATCOM method (DATCOM, 1960), its applicability was assumed as given.

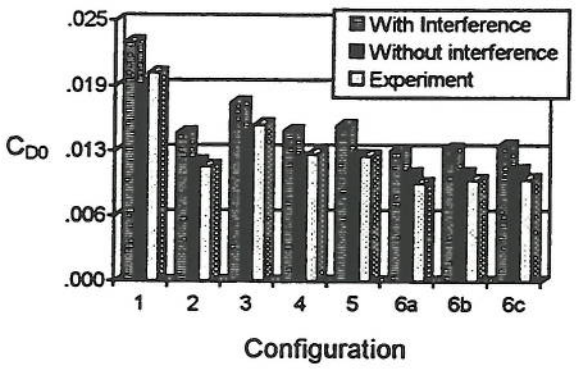

Fig. 46: Comparison of experimental with estimated C_{D0}

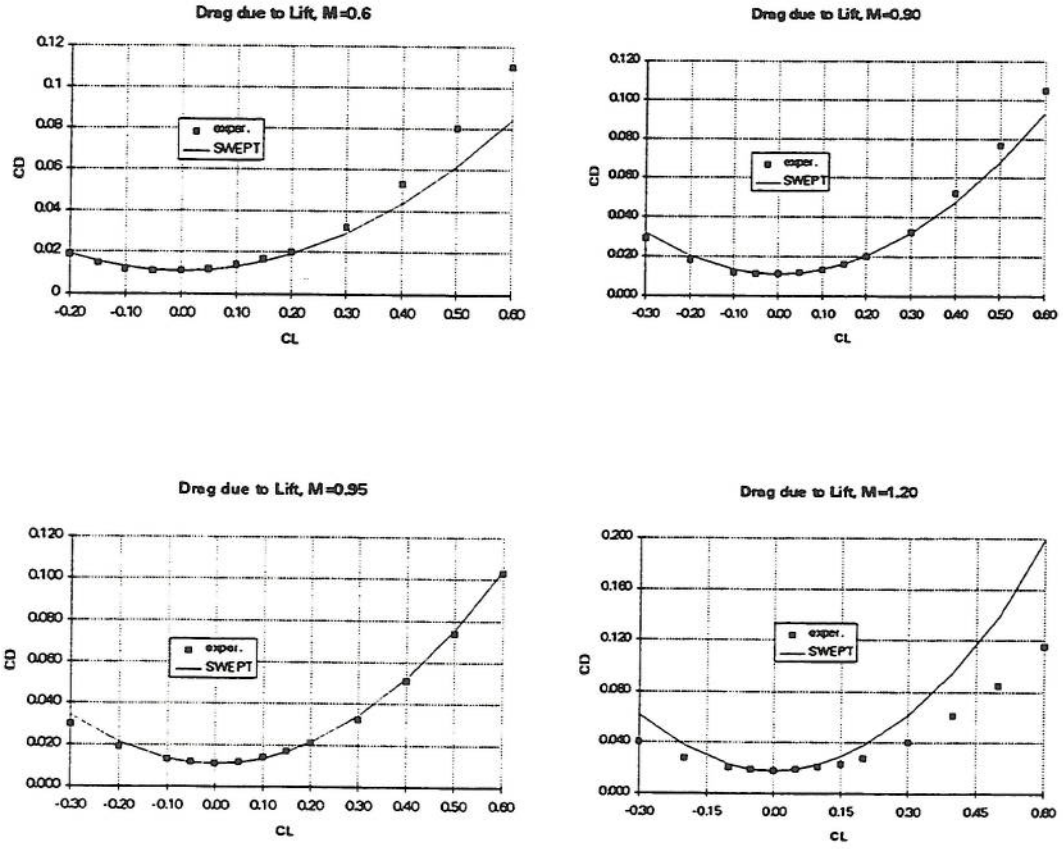

Fig. 47: Drag due to lift, NASA TM 78764

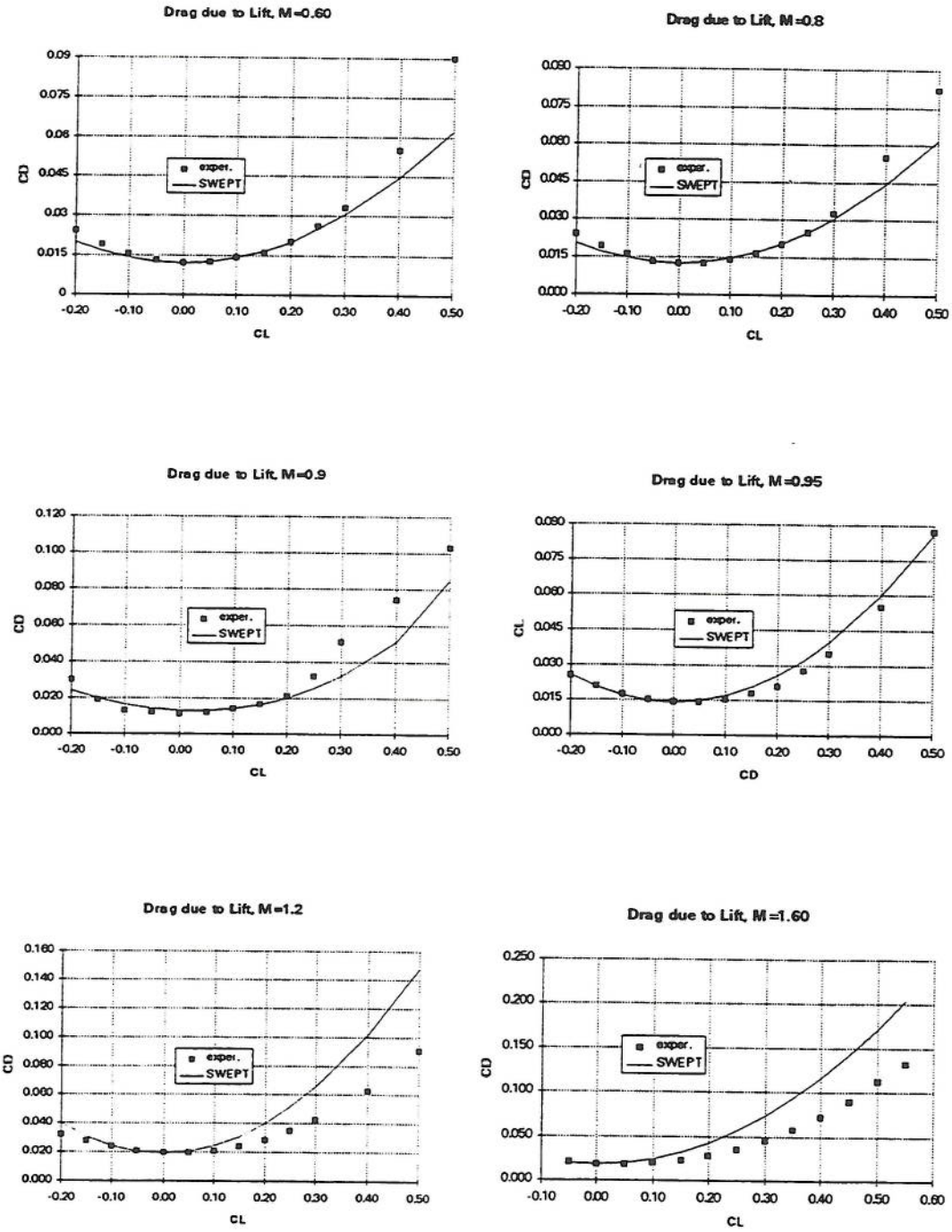

Fig. 48: Drag due to Lift, NASA TM X-3559

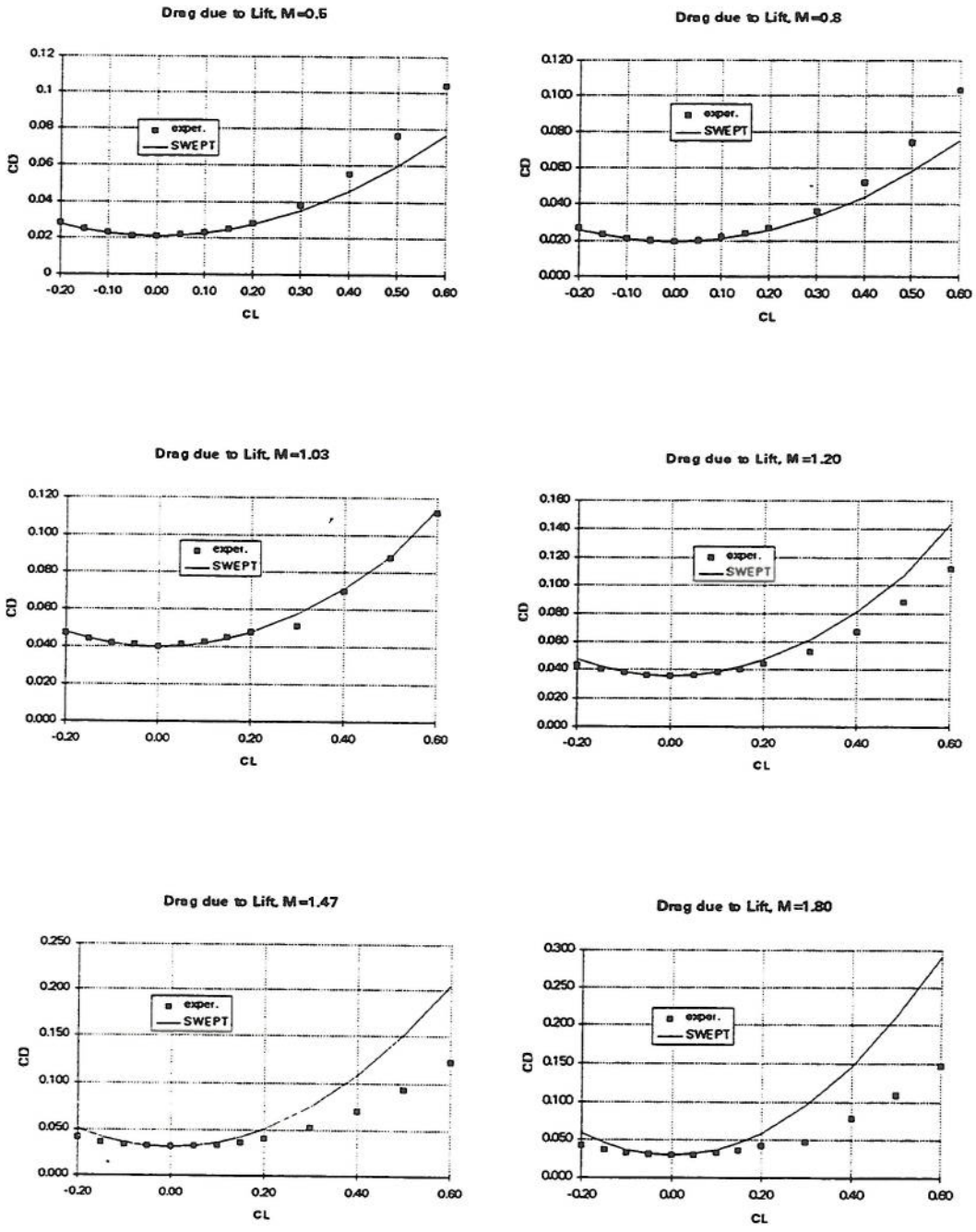

Fig. 49: Drag due to lift, NASA TM X-3078

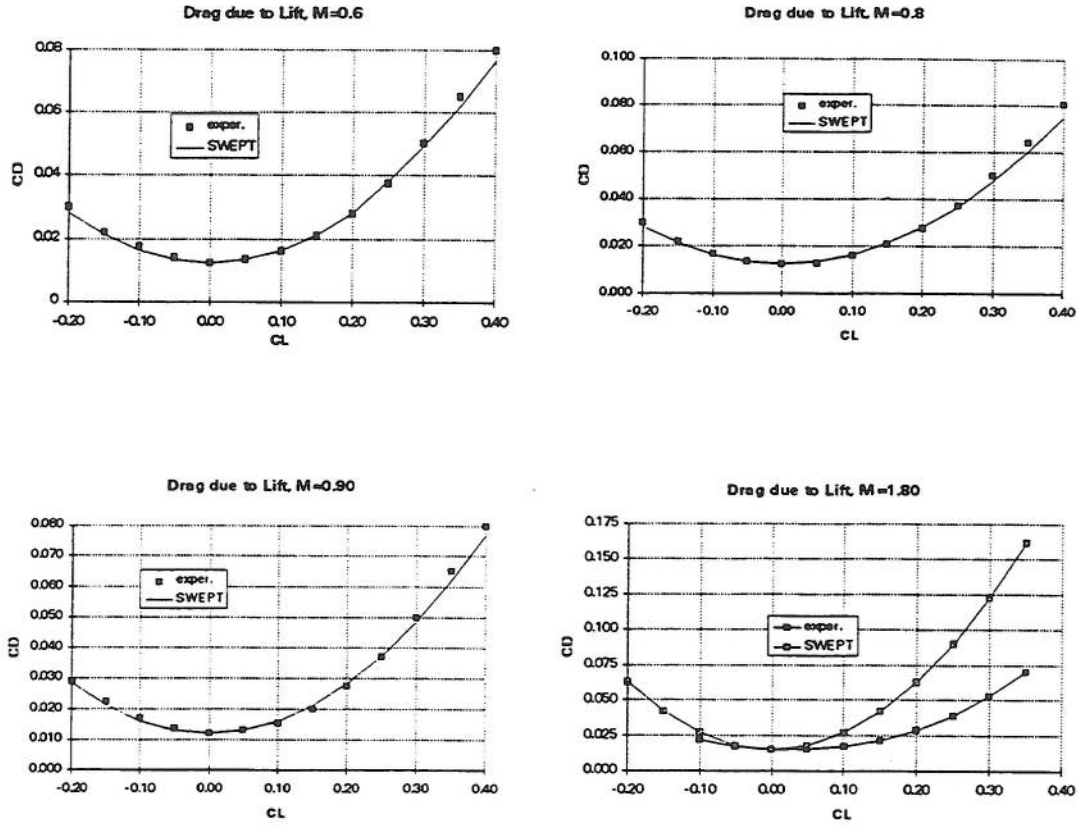

Fig. 50: Drag due to lift, NASA TM X-3530

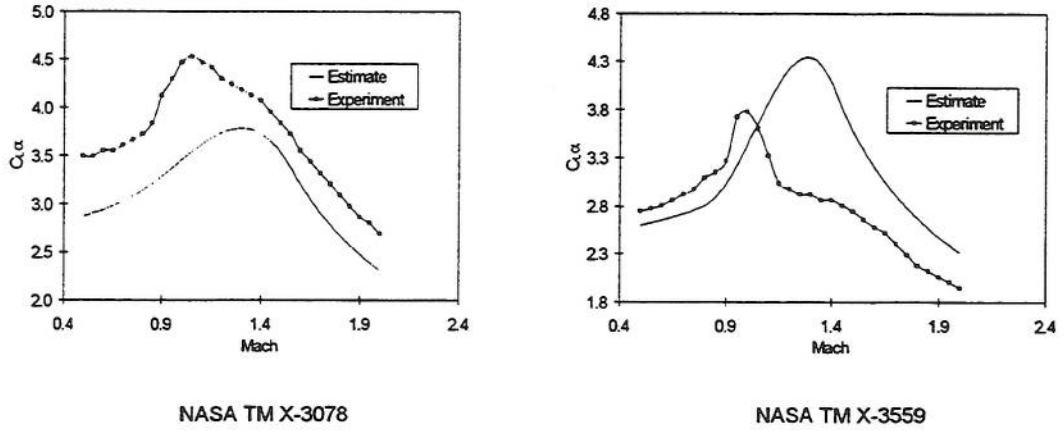

Fig. 51a: Lift curve slope

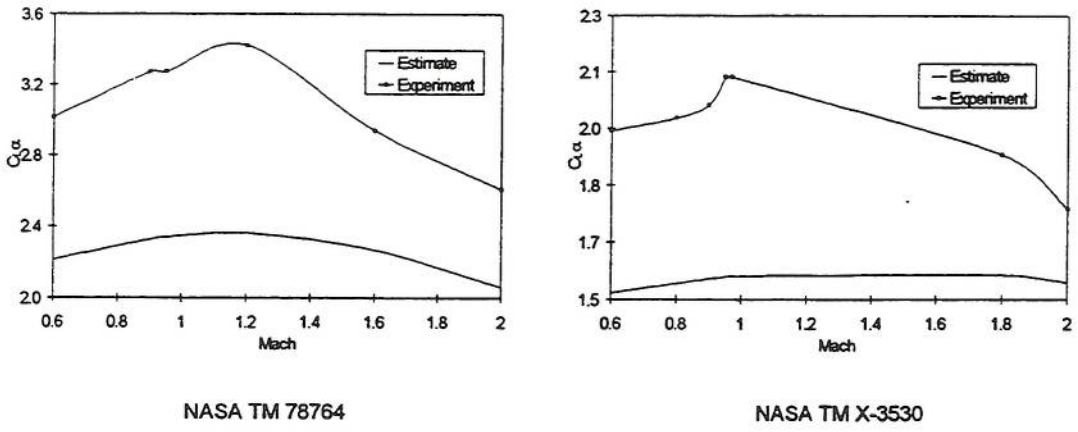

NASA TM 78764

NASA TM X-3530

Fig. 51b: Lift curve slope

5.2 Synthesis Code Development and Testing

The development of the design synthesis code was conducted in several stages. First, modules were tested for completeness and functionality as they were integrated into the design synthesis. A series of test cases were examined to ensure that all of the configuration options described in Chapter 4 were interacting correctly with the synthesis geometry. Finally, the program was extensively tested and debugged in conjunction with the numerical optimizer *RQPMIN*, Version 3.0. The way this was done is described in the following paragraphs.

Succesful optimization trials will depend on a number of factors. Besides the initial parameters required by *RQPMIN*, the shape of the objective function is very important. It must be both smooth and continuous. For the purposes of this research, it is sufficient to guarantee smoothness by ensuring that the derivatives of the objective function and the constraints with respect to the optimization variables have no sudden changes in value. Similarly, continuity of the objective and constraint functions means that there should be no region within the validity of the optimization variables which is undefined. Furthermore, inaccurate definition of internal iteration loops such as that for the take off mass described in Chapter 4 may lead to oscillations in the objective function. Some of the consequences of not meeting these conditions are described in (Gill et al, 1981). They can include failure to converge to an optimum and convergence to an incorrect optimum.

Most of the obvious cases within the synthesis code were dealt with during the program development. For example, appropriate use was made of the *BLEND* subroutine (Lovell, 1988) to ensure continuous function and first derivative values, as described in Chapter 4. But other cases were discovered only after an extensive analysis of the convergence history of the optimization variables, constraint and objective functions and the variables involved in their calculation.

Figure 52 shows how a convergence history was used to discover function definition errors in the calculation of the boat tail angle constraint. GRFN is a constraint which ensures that the boat tail angle remains positive. During the initial optimization trials, it was found that this constraint was oscillating between an upper and lower bound. By plotting the convergence history of this constraint and the parameters used in its calculation, it was possible to isolate and correct the cause of the oscillation.

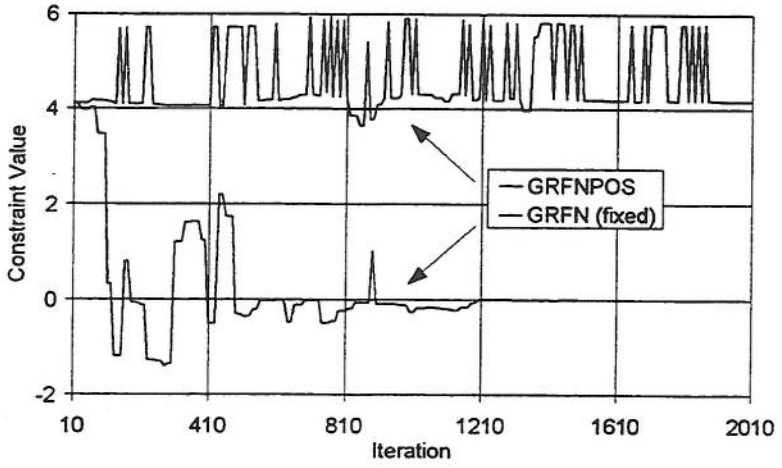

Fig. 52: Convergence history for boat tail angle examination

5.2.1 Example Optimization Trials

The design synthesis and optimization package was tested using two sample cases, a combat air patrol and a ground attack mission. Both were designed for low observables, with internal weapons carriage. Table 5 presents the point performance requirements used to size the two aircraft. The configuration is a twin-engine aircraft with conventional, aft-mounted taiplane and a single fin.

Type	*Flight Condition (50% fuel)*	*Requirement*
Acceleration	10000m, max thrust, Ma 0.8	70s
Maximum Mach	sea level, max thrust	Ma 1.1
Maximum Mach	10000m, max thrust	Ma 1.6
SEP	10000m, max thrust, Ma 0.9	100 m/s
Sustained Turn	10000m, max thrust, Ma 0.9	7 deg/s
Sustained Turn	1000m, max thrust, Ma 0.8	16 deg/s
Attained Turn	10000m, max thrust, Ma 0.9	10 deg/s

Table 5: Baseline Performance Constraints

5.2.1.1 *Combat Air Patrol*

Table 6 and Figure 53 describe the combat air patrol mission used to test the design synthesis and optimization package. It has an outbound and inbound cruise leg flown at Ma 0.7 and 10000m for a distance of 325 km. The outbound leg is followed by a 45 minute loiter at 9000m and Ma 0.6. Combat legs are flown at 9000m and Ma 1.3 and 1000m and Ma 0.8, respectively. The total armament carried consists of two AMRAAMs and two ASRAAMS, as well as a gun with 400 rounds of amunition.

Leg	*Description*
Outbound cruise	325 km, 10000m, Ma 0.7
Loiter	45 min, 9000m, Ma 0.6
Combat turns	9000m, Ma 1.3, fire ASRAAMs
Combat turns	1000m, Ma 0.8, fire AMRAAMs
Inbound cruise	325 km, 10000m, Ma 0.7

Table 6: Combat Air Patrol Baseline Mission Description

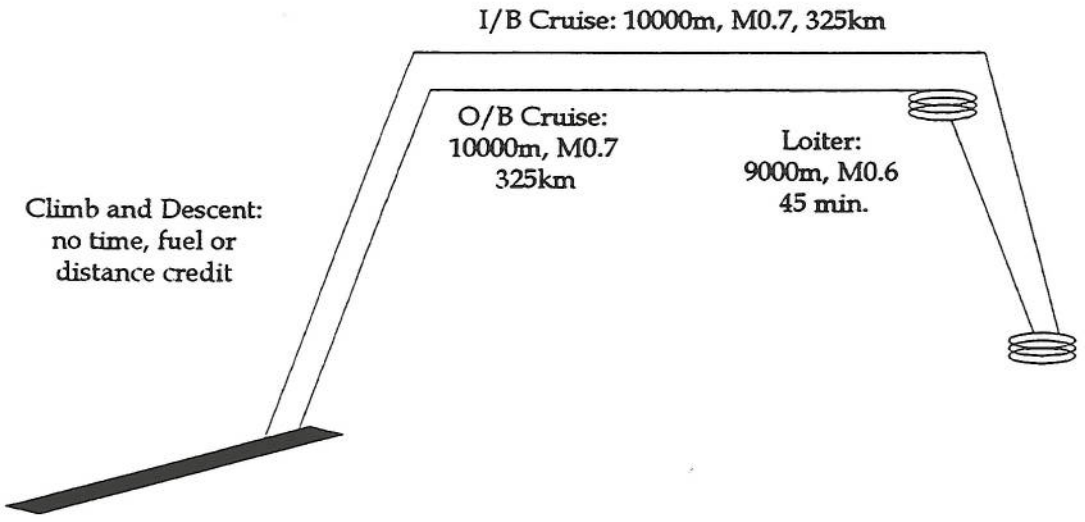

Fig. 53: Baseline Combat Air Patrol Mission

Table 7 compares some of the initial design parameters with the optimized aircraft parameters.

Parameter	*Initial Value*	*Optimized Value*
Thrust Scale Factor	1.36	1.17
Wing Area [m²]	35.81	32.32
Wing 1/4 Chord Sweep [°]	30	29.47
Wing Aspect Ratio	2.2	3.86
T/W at Take Off	1.3	0.955
W/S at Take Off [kg/m²]	411.8	431.6
Empty Mass [kg]	10739	9539
Take Off Mass [kg]	14748	13950
Fuel Fraction	0.225	0.267

Table 7: Combat Air Patrol Aircraft Major Parameters

Figure 54 shows how the area and perimeter distribution of the combat air patrol aircraft were optimized. PFX refers to the perimeter at a given fuselage station, OFX gives the cross-sectional area distribution, whilst the suffixes INIT and OPT refer to initial and optimum, respectively. From the shape of the perimeter distribution (PFXINIT and PFXOPT), it can be seen how the wetted area was reduced by a general smoothing and reduction in value. This results in a lower fuselage mass and hence total aircraft mass, as seen in Table 7. Furthermore, the observed reduction will also serve to reduce the aircraft drag, which is reflected in the fact that the sweep angle of the wing has been reduced slightly.

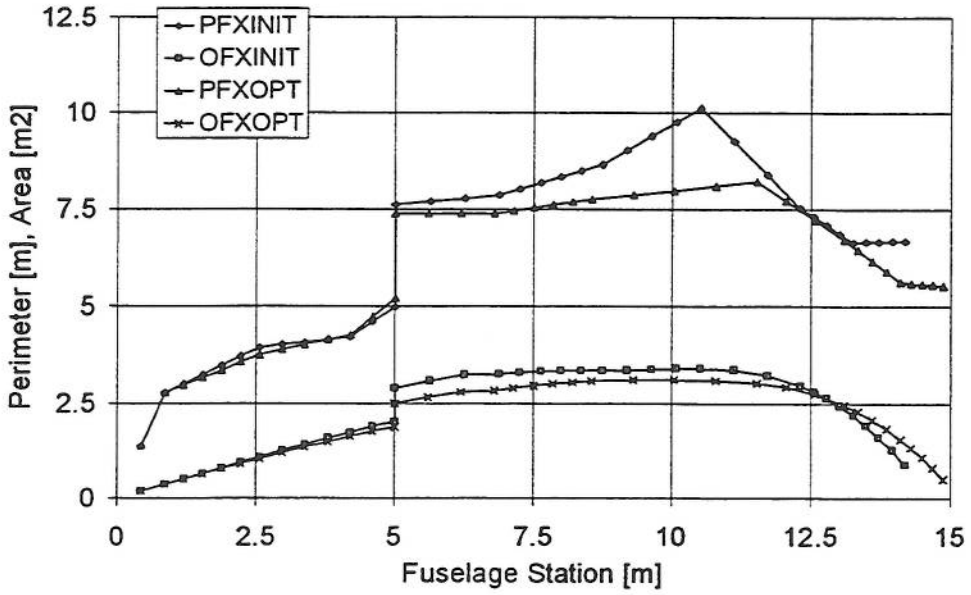

Fig. 54: Initial and Optimum Area and Perimeter Distribution, CAP

In a similar fashion, the cross sectional area distribution was slightly reduced in magnitude. Furthermore, it can be seen how the fuselage length was increased slightly, with a shift in the area distribution towards the rear of the aircraft. This will lead to a reduction in wave drag as the gradient of the area distribution is reduced at the front of the aircraft.

5.2.1.2 *Ground Attack*

Table 8 and Figure 55 describe the ground attack mission used to further test the design synthesis. It has an outbound and inbound cruise leg of 350 km, flown at 10000m and Ma 0.7. This is followed by a low-level dash outbound of 50 km, flown at 70m and Ma 0.8. Combat turns are flown at the same altitude and Mach number, with weapons drop. This is followed by an inbound low-level dash with the same parameters as the outbound one. The total armament carried is the same as for the combat air patrol aircraft, with the AMRAAMs being replaced by bombs.

Leg	*Description*
Outbound cruise	350 km, 10000m, Ma 0.7
Low level dash outbound	50 km, 70m, Ma 0.8
Combat turns	70m, Ma 0.8, drop weapons
Low level dash inbound	50 km, 70m, Ma 0.8
Inbound cruise	350 km, 10000m, Ma 0.7

Table 8: Ground Attack Baseline Mission Description

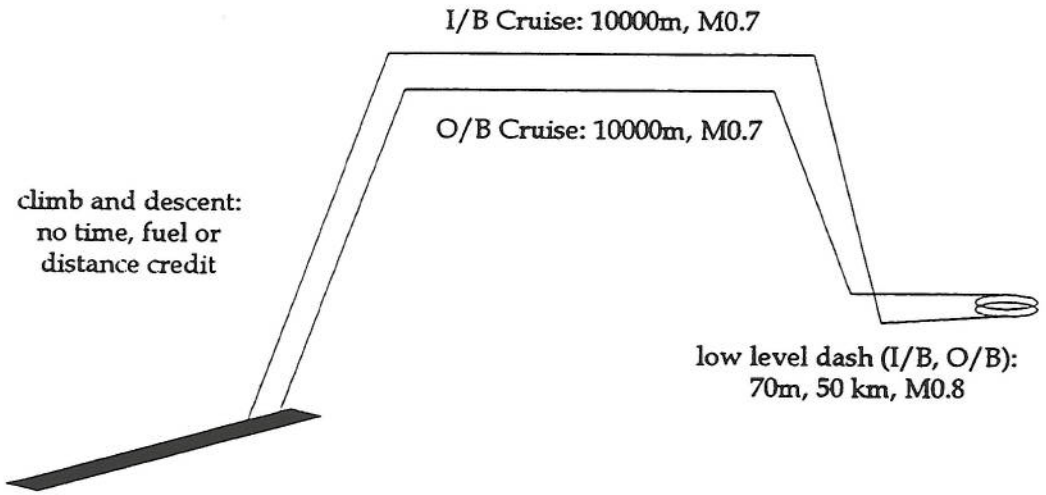

Fig. 55: Baseline Ground Attack Mission

Table 9 shows how the initial values for the ground attack aircraft compare with the optimized ones. Due to the relatively undemanding mission, flown entirely without afterburner, the aircraft has a very low fuel fraction of just over 18%. This has a similarly positive effect on the take off mass of only 11037 kg. A relatively low weapons load also contributes to the small aircraft size. Nevertheless, the thrust to weight ratio at take off is fairly high, a result of the fairly demanding point performance calculations, which include supersonic Mach numbers and high sustained turn rates.

Parameter	*Initial Value*	*Optimized Value*
Thrust Scale Factor	1.4	0.8
Wing Area [m²]	35.81	27.92
Wing 1/4 Chord Sweep [°]	35	34.4
Wing Aspect Ratio	3.0	3.59
T/W at Take Off	1.095	1.037
W/S at Take Off [kg/m²]	509.8	395.3
Empty Mass [kg]	12537	8330
Take Off Mass [kg]	18358	11037
Fuel Fraction	0.276	0.183

Table 9: Ground Attack Aircraft Major Parameters

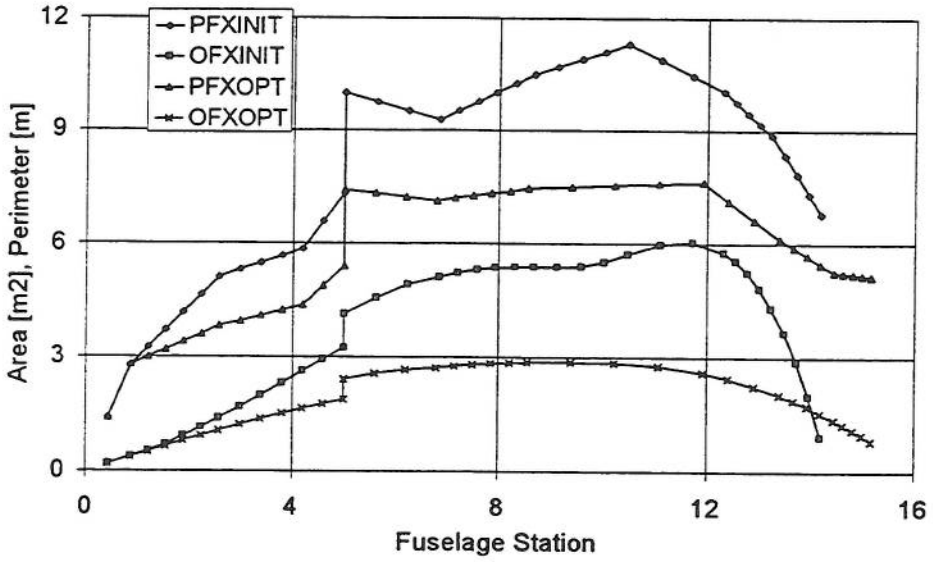

Fig. 56: Initial and Optimum Area and Perimeter Distribution, A-G

Figure 56 shows how the cross-sectional area (OFX) and perimeter (PFX) distribution for the ground attack aircraft were optimized. The shape of the two curves is smoother for the optimum aircraft, and the magnitude has been

reduced considerably. More so than with the combat air patrol aircraft this leads to a significant reduction in drag and mass due to the reduced wetted area and volume of the fuselage.

5.2.2 Comparison with Existing Aircraft

The two test cases described above were compared with data available from the literature to check the validity of the design synthesis relationships. In Figure 57, the mass breakdown for the optimum aircraft were compared with two configurations obtained from (O'Neill et al, 1994) designed for low observability. Aircraft AG1 and CAP are the ground attack and combat air patrol configurations, respectively, described above. The other two configurations are optimized for low agility and moderate low-observables technology (aircraft B-Lo) and for low agility and very low observables technology (aircraft C-Lo).

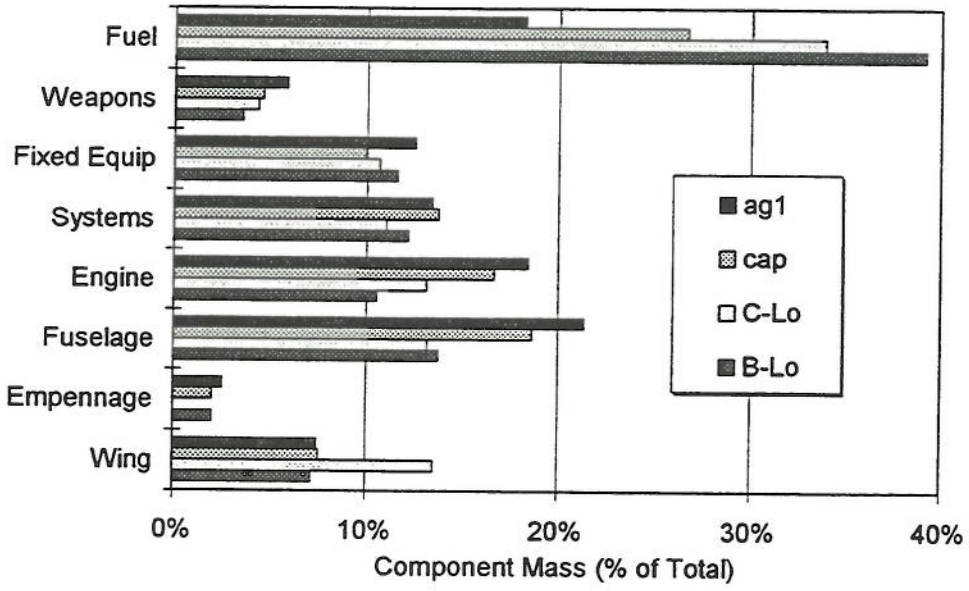

Fig. 57: Mass Breakdown Comparison

The aircraft from (O'Neill et al, 1994) have a very high fuel fraction due to the mission requirement of two minutes at full afterburner for warm up before take off. For the test aircraft, the reduced contribution of the fuel to the take off mass is reflected mainly by increases in the fractions for engine and fuselage. Configuration C-Lo is a flying wing with a correpsondingly high mass fraction for that component. It is interesting to note that the contributions from the systems, fixed equipment, wing and weapons are similar for all four aircraft, with the only major variations to be seen in the fuselage, fuel and engine. These last three items are heavily dependent on the mission and point performance,

particularly with respect to the fuel requirement and engine size, which will directly influence the size of the fuselage.

Using (O'Neill et al, 1994) for comparison with the test cases presented in this work has one major disadvantage. The configurations B-Lo and C-Lo in Figure 57 do not represent real aircraft. Instead, they are the result of design trade-off studies. Although it can be said with reasonable confidence that the organization carrying out the investigations had access to a much larger database than that used for this work, a certain amount of caution must still be applied when interpreting the results.

A better way of comparing the test cases is by using a database of real aircraft and attempting to model them using this design synthesis. However, while attempting to find aircraft representative of the type modelled in this work, it soon became apparent that such a comparison would be virtually impossible for a number of reasons. The first problem is inherent in the methodology used to model the synthesized aircraft. As described in Chapter 4, this work makes extensive use of empirical aircraft design data and highly simplified geometric models of the components. Thus the results can only be viewed as an initial approximation to the real aircraft. Nevertheless, with design data from real aircraft, the model could be calibrated for more accurate results.

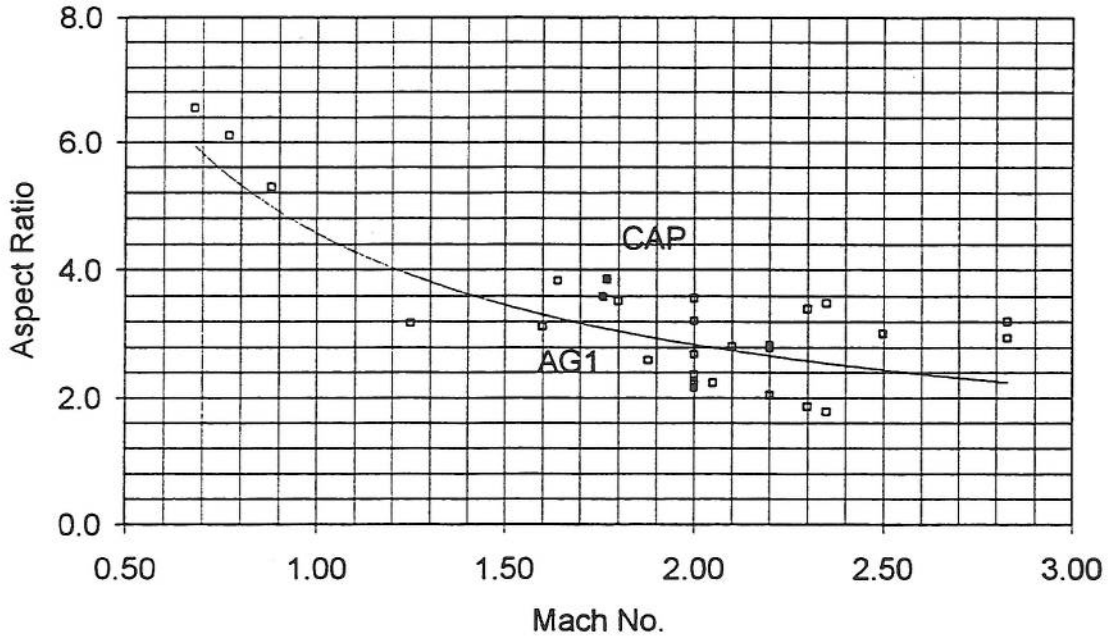

Fig. 58: Aspect Ratio vs. Mach Number Comparison

This leads to the second difficulty. In order for comparisons with actual aircraft to be realistic, it is necessary to have as much information as possible about the design parameters and requirements, in particular the point

performance and mission profile, because these are the main design drivers for the optimization routine. Yet for reasons of commercial or military confidentiality such information is rarely readily available, and indeed none was found which would have been of use for this work. Furthermore, it is usually not the intention to use design synthesis tools such as the one described in this report to establish the absolute optimum aircraft for a given set of requirements. Instead, it can be used much more effectively to study the relative effects of modifications to the design requirements.

Because of the lack of design data available in the open literature, it was decided to use correlations of major aircraft design parameters and to compare these with the test cases. Such correlations are often used to establish initial values for the aircraft geometry when starting a new design from scratch. The correlations used here are from (Woodford, 1995), modified by the author to match the requirements of this work. The database was compiled mainly from (Taylor, 1995), and includes trainers as well as combat aircraft.

Figure 58 shows a correlation of wing aspect ratio vs. quoted maximum Mach number for a variety of actual combat aircraft designs. It can be seen that the two test cases, CAP (combat air patrol) and AG1 (ground attack) are both located very close to the average.

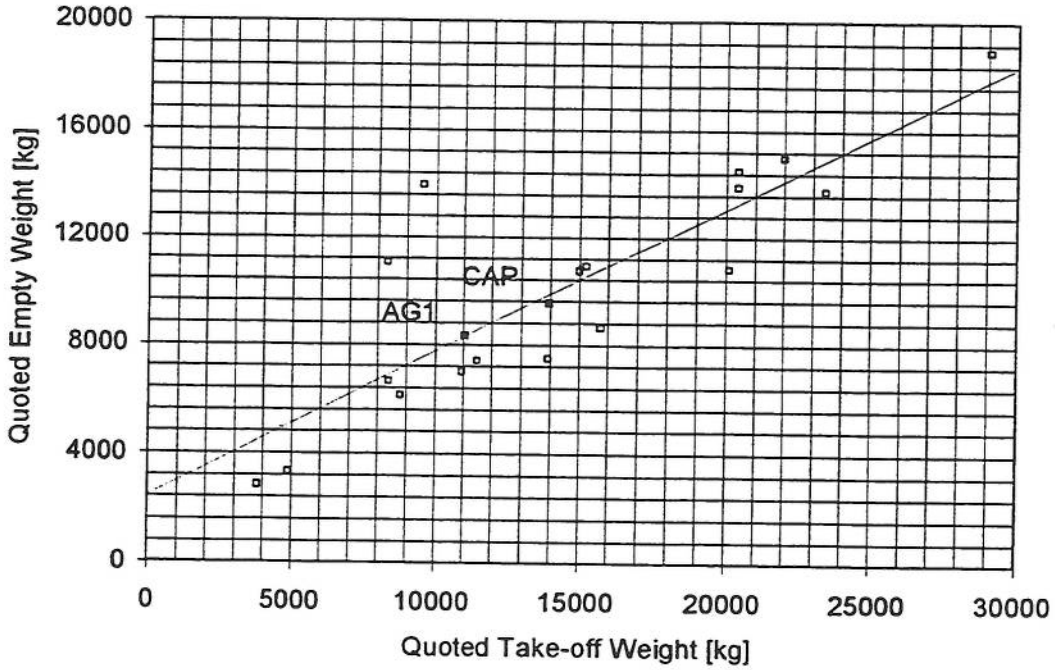

Fig. 59: Correlation of Empty vs. Take-Off Mass

An even better fit is obtained when comparing the quoted empty weight with the quoted take off weight. This correlation is shown in Figure 59, which shows that, as take off mass increases, the fraction of this which is empty mass

decreases. The two aircraft lie almost exactly on the trend line. CAP, being the heavier of the two test cases, also has a lower empty mass fraction than AG1. A look at Tables 7 and 9 shows that the empty mass fractions can be worked out to be 0.68 and 0.75 for the combat air patrol and ground attack aircraft, respectively.

In Figure 60, the aircraft overall length is plotted against take off mass. Although the correlation is shown as a curve, a straight line fit may have been just as valid. As can be seen, the combat air patrol aircraft is almost exactly on the trend line, whereas the ground attack aircraft lies slightly above and to the left. The reason for this is the slightly greater length of the ground attack aircraft despite having a lower take off mass than the combat air patrol one. This was caused by active fuselage length constraints, which ensure that all of the internal components such as intake diffusers, weapons bay and engine bay fit into the fuselage. In this example, the weapons bay was being constrained in the forward position by the rear of the cockpit, and in the rearward position by the engine compartment and main landing gear.

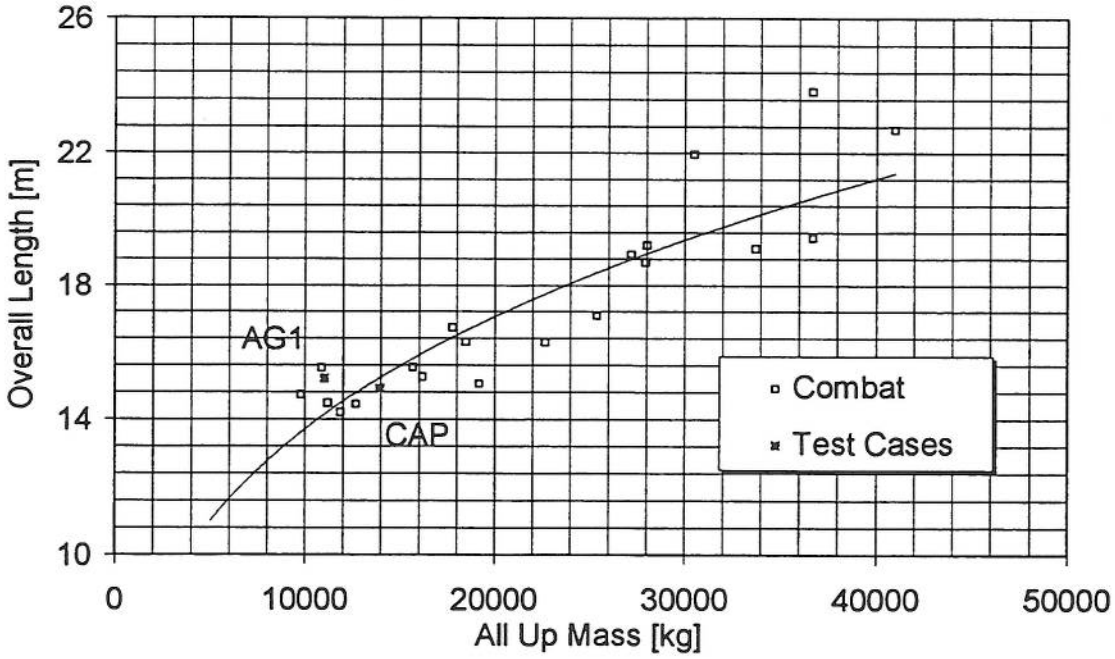

Fig. 60: Aircraft Length Correlated Against Take-Off Weight

5.2.3 Trend Studies

5.2.3.1 Variation of Combat Radius

As described in Chapter 2, design synthesis codes are frequently used to conduct trade studies, sometimes also known as answeres to "what-if" questions. In Figure 61, the combat radius for a mission similar to the one shown in Section 5.2.1.1 was varied to study the effect on the objective function, in this case the empty mass, or MTE. Also shown for comparison purposes is the maximum take-off weight, or MTOW. Each one of the data points in Figure 61 represents a fully optimized and sized configuration, which meets all of the performance constraints and completes the mission with zero residual fuel.

The results usually expected from such a parametric study would be an increase in aircraft mass as the combat radius is increased. This is because the increase in cruise range would cause an increase in the amount of fuel necessary to accomplish the mission. In order to retain the aircraft performance characteristics, the geometry of the wing would be expected to change slightly, usually reflected in an increase in wing area and hence mass. This can be seen in Figure 62, where the wing area is seen to increase with increasing combat radius. What is not so clear from Figure 61 is why the trend is not smooth, particularly at a combat radius of 575 km, where a sudden drop in the aircraft mass is observed.

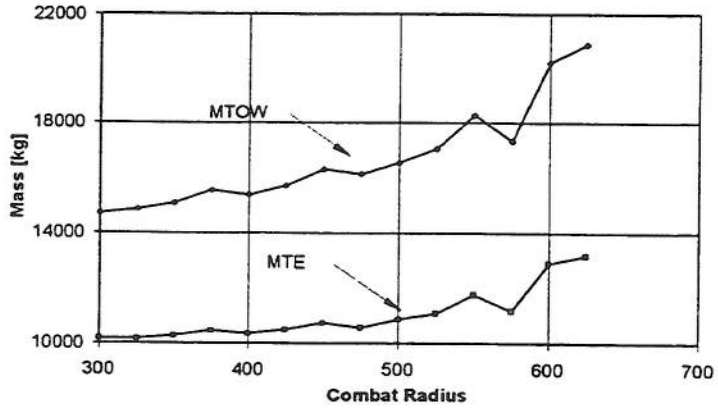

Fig. 61: Mass versus Combat Radius

Figure 62 again provides a clue. The wing area, which is, incidentally, a design optimization variable, appears to increase rather smoothly, despite inflections similar to those in Figure 61. Yet the sweep angle is behaving in an almost entirely random fashion. What is happening is that, as the combat radius is incresed, the wing is being optimized to the planform resulting in

minimum drag and mass. During this process, the values of the wing parameters are being traded off one against the other. For example, as the sweep angle increaes, so does the thickness to chord ratio, in order to keep the wing mass at as low a value as possible.

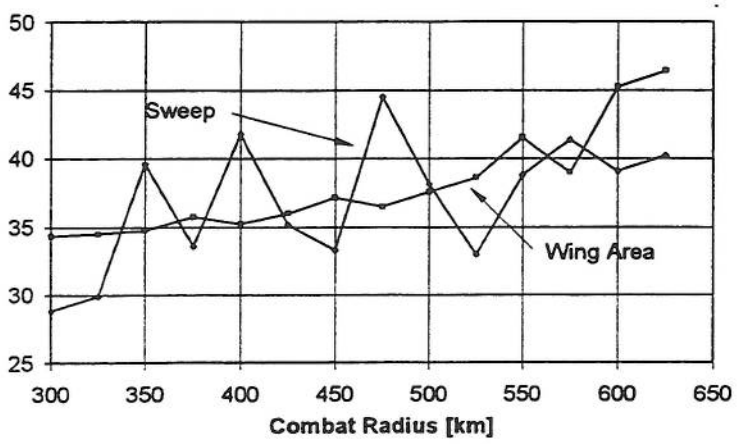

Fig. 62: Wing Area [m²] and Sweep [°] versus Combat Radius

From Figure 62 it is also clear that the wing area is following the mass trend seen in Figure 61, an observation which is borne out by the tabulation of correlation coefficients in Table 12 (page 125). To produce these numbers, the series of optimized results seen in the Figures of this section along with others not shown here were correlated against each other to determine if a realtionship existed between any given pairs. Thus, it can be seen that a perfect correlation exists between the wing area and the empty mass, indicating that, as wing area is increased, a corresponding increase in empty mass takes place.

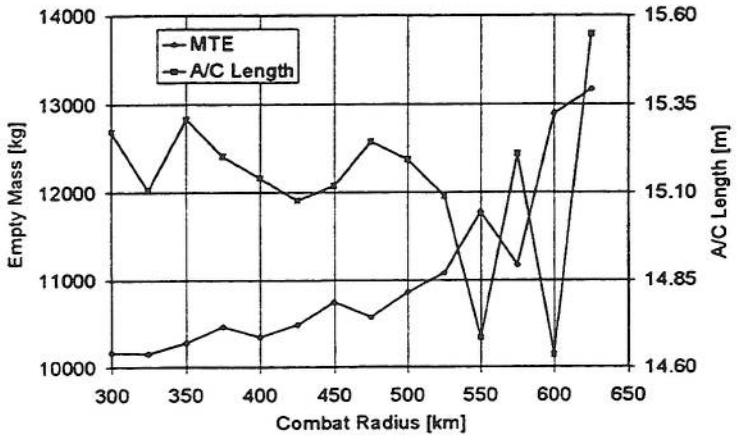

Fig. 63: Aircraft Length versus Combat Radius

Another interesting result observed in Table 12 is the close correlation between the fuselage mass and the aircraft empty mass, in particular the internal structure mass. An examination of the mass estimation methodology used in this design synthesis (Lovell, 1988) indicates that the main contributors to the fuselage shell and internal masses are the wetted area and volume, respectively. Other factors, but of a lower order of magnitude, are the fuselage length and the fuselage maximum width and height. The internal structural mass is further modified by the length of the wing chord at the body side, which itself is dependent upon the fuselage width.

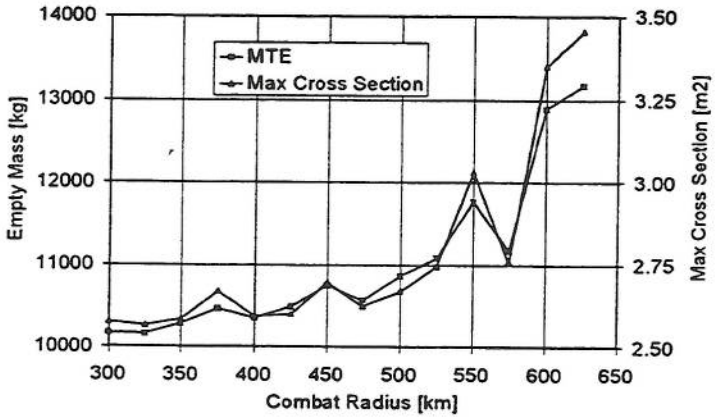

Fig. 64: Maximum Cross Sectional Area versus Combat Radius

In order to determine the effect of these parameters on the fuselage mass, several plots with respect to the combat radius were produced. Figure 63 shows the variation of the aircraft length with increasing combat radius. The correlation with the empty mass is fairly poor, with a coefficient of –0.23. Figure 64, on the other hand, shows a very good agreement between the empty mass series and the maximum cross-sectional area, obtained from the fairing curve. The correlation coefficient between these two series, from Table 12, is equal to 0.99. Thus, it can be concluded that the cross-sectional area plays a more significant role in the fuselage and hence empty mass than the fuselage length. This observation is supported by the fact that the fuselage length varies only between a minimum of 14.635 and a maximum of 15.549, a range of 0.914, or 6.2% of the minimum value. This compares with a range of variation for the maximum cross section of 0.891, from 2.564 to 3.455 (See Table 10). In this case, it represents a more than 34% increase over the lower value.

One of the reasons why the cross sectional area plays such a more significant role in the calculation of the empty mass is that it has a very strong influence on the volume and wetted area. This conclusion is reached when examining Table 12 once again, which shows that the fuselage volume and wetted area correlate with the cross sectional area with coefficients of 0.99 and 0.95, respectively. Wetted area and volume are plotted against combat radius in

Figure 66. Furthermore, the fuselage maximum width and height, plotted in Figure 65, correlate very well with the cross-sectional area, the empty mass, and even, to a slightly lesser extent, the wing area and mass.

	A/C Length	Max Cross Section
Mean	15.130	2.779
Standard Deviation	0.233	0.290
Range	0.914	0.891
Minimum	14.635	2.564
Maximum	15.549	3.455

Table 10: Aircraft length and cross section statistics

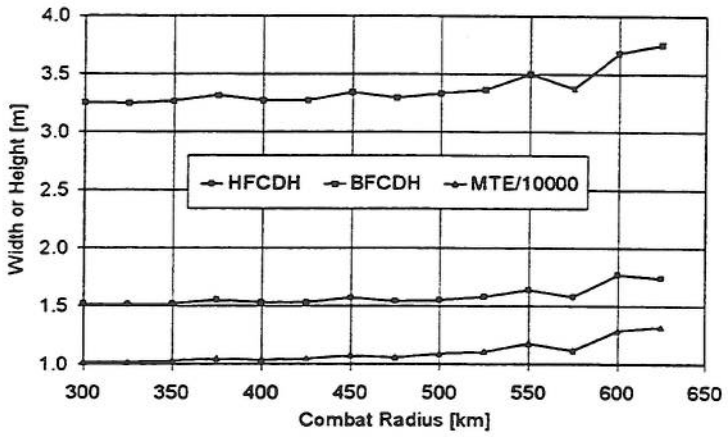

Fig. 65: Maximum Fuselage Width (BFCDH) and Height (HFCDH) versus Combat Radius

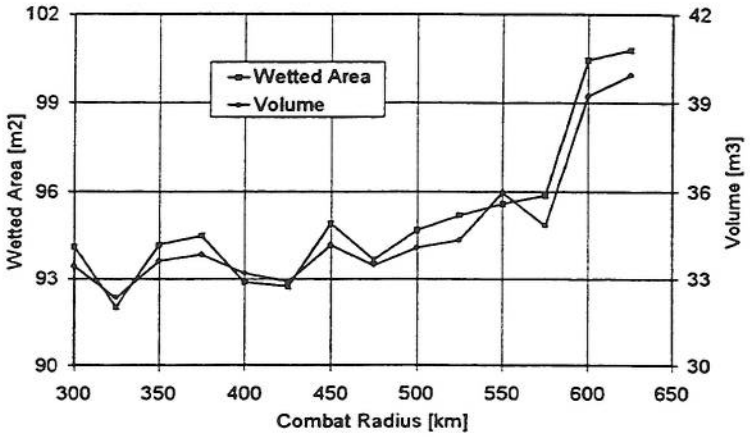

Fig. 66: Wetted Area and Volume versus Combat Radius

The observed correlations can be explained as follows. The fuselage maximum width and height are largely a result of the fuselage maximum cross-sectional area, given by the fairing curve (Lovell, 1988), which in turn is driven by design optimization variables. These three items have the greatest influence upon the fuselage mass. Furthermore, as the aircraft mass increases, there is a corresponding increase in wing area and mass. However, Table 12 shows a distinct lack of correlation between the wing parameters thickness to chord and aspect ratio. Although not shown here, the sweep angle shows a similarly weak correlation. This would indicate that the wing area, which is a design optimization variable, is being sized to match the increase in fuselage mass caused by the cross-sectional area, in other words an attempt to maintain the wing loading such that the point performance constraints are met.

Table 11 shows how the data from the trials supports this conclusion. The combat wing loading was calculated using the combat reference mass in the left column and a mass assuming 50% of the internal fuel unused. The first of these two cases uses a mass calculated by the design synthesis in the original mass estimation version (Lovell, 1988). The combat reference mass consists of the maximum take off mass reduced by the mass of the external stores and by the mass of the fuel in the exposed section of the wing. Fuel in the wing will vary according to the size of the wing and the span of the wing box containing fuel, which is an independent variable. This accounts for the wider spread in wing loading values observed in the left column of Table 11. Here, the wing loading has a mean value of 376.8 kg/m^2, with a range of ±19.75 kg/m^2, with a standard deviation of 10.5. The confidence level for the 95th percentile is ±5.5 kg/m^2.

Of more significance for the point performance calculations is the aircraft mass state in which 50% of the internal fuel has been used. This is the value used for this trial series, and it can be specified as an input variable separately for each constraint. In the right hand column of Table 11, this fuel mass state was used to calculate the wing loading. As can be seen, the calculated values varied from 369.9 kg/m^2 to 375.4 kg/m^2, with a confidence level (95th precentile) of 0.7 kg/m^2 and a standard deviation of 1.3 kg/m^2. These results indicate quite clearly that the requirement to meet a given set of point performance constraints at a given fuel mass state has resulted in optimum aircraft which are very similar in terms of wing loading.

	W/S [kg/m^2] (Combat Reference)	W/S [kg/m^2] (50% Fuel)
Mean	376.8	373.5
Standard Deviation	10.5	1.3
Range	39.5	5.5
Minimum	365.0	369.9
Maximum	404.5	375.4
Confidence Level (95%)	5.5	0.7

Table 11: Combat Wing Loading Descriptive Statistics

	Empty Mass	Mass Wing	Mass Fus. Struct	Mass Fus. Shell	Wing Area	T/C	Aspect Ratio	A/C Length	Max Cross Section	Fus. Vol	Fus. Wetted Area	Fus. Height	Fus. Width
Empty Mass	1.00												
Mass Wing	0.98	1.00											
Fuse Struct	0.99	0.97	1.00										
Fuse Shell	0.96	0.92	0.97	1.00									
Wing Area	1.00	0.99	0.99	0.95	1.00								
T/C	-0.39	-0.37	-0.42	-0.29	-0.39	1.00							
Aspect R	-0.30	-0.19	-0.32	-0.21	-0.31	0.58	1.00						
A/C Length	-0.23	-0.24	-0.27	-0.12	-0.25	0.28	0.17	1.00					
M. Cross Sec.	0.99	0.96	0.98	0.96	0.98	-0.41	-0.35	-0.22	1.00				
Volume	0.98	0.95	0.98	0.99	0.97	-0.33	-0.26	-0.16	0.99	1.00			
Wetted Area	0.95	0.92	0.96	1.00	0.94	-0.28	-0.21	-0.10	0.95	0.98	1.00		
Fus. Height	0.98	0.95	0.99	0.96	0.98	-0.37	-0.32	-0.32	0.99	0.98	0.96	1.00	
Fus. Width	0.99	0.96	0.99	0.96	0.99	-0.39	-0.33	-0.20	1.00	0.99	0.96	0.99	1.00

Table 12: Correlation Coefficients for Trend Example

5.2.3.2 *Example of Low-Observables Impact on Optimum Aircraft*

The following section demonstrates the capability of this design synthesis to examine variations in aircraft configuration related specifically to low observables requirements. Two of the more significant factors affecting such characteristics are the nozzle shape and size. As described in Chapter 4, the design synthesis makes use of an option to switch between rectangular and two-dimensional nozzles. It has been examined in Chapter 3 that the nozzle shape can contribute significantly to the afterbody nozzle/airframe integration and hence the aerodynamics. Furthermore, in terms of low observables, rectangular nozzles can be used to directionally tailor the infrared signature to a desired shape. Also, the nozzle aspect ratio, here defined as height divided by width (see Chapter 4), can be used to influence the radar signature. This is because for a given nozzle exit area a lower aspect ratio will reduce the fuselage height, which is consistent with low-observables requirements. It should be noted that the effect of two-dimensional nozzles on aircraft performance is not modelled by the design synthesis. Instead, any such effects must be included in the engine model, obtained in tabular form from an external input file. Such a data set was not available for the results shown here.

The following example illustrates how the effect of a reduction in nozzle aspect ratio on the optimum aircraft can be shown using the design synthesis. Table 13 details the ground attack mission used, and Table 14 shows the point performance sizing constraints. The configuration under investigation here is a twin-engine aircraft with conventional tailplane and internal weapons carriage. The armament consists of two ASRAAMS and two 250kg bombs as well as a gun with 400 rounds of ammunition.

Leg	*Description*
Outbound cruise	600 km, 10000m, Ma 0.7
Low level dash outbound	100 km, 70m, Ma 0.8
Combat turns	70m, Ma 0.8, drop weapons
Low level dash inbound	100 km, 70m, Ma 0.8
Inbound cruise	600 km, 10000m, Ma 0.7

Table 13: Ground Attack Baseline Mission Description for Low-Observables

Type	*Flight Condition*	*Requirement*
Acceleration	10000m, Ma 0.8, max thrust, 50% fuel	60s
Maximum Mach	sea level, max thrust, 50% fuel	Ma 1.1
Maximum Mach	10000m, max thrust, 50% fuel	Ma 1.6
SEP	10000m, max thrust, Ma 0.9, 50% fuel	100 m/s
Sustained Turn	10000m, max thrust, Ma 0.9, 50% fuel	7 deg/s
Sustained Turn	1000m, max thrust, Ma 0.8, 50% fuel	16 deg/s
Attained Turn	10000m, max thrust, Ma 0.9, 50% fuel	10 deg/s
Ride Quality	1000m, max thrust, Ma 0.8, 50% fuel	5 s^{-1}

Table 14: Ground Attack Baseline Performance Constraints for Low-Observables

Figure 67a shows how the maximum take off mass increases in response to a decrease in the nozzle aspect ratio (height divided by width) from 0.75 to 0.55. Also evident is the corresponding increase in wing area, in order to maintain the wing loading for combat conditions. This result is not surprising when the effect on the aircraft afterbody of a wider nozzle is considered. A lower nozzle aspect ratio would be expected to produce a greater perimeter requirement for a given cross-sectional area. This is because the increased nozzle width (for a twin-engine installation) will cause an increase in the engine separation distance to maintain the necessary structural clearance.

These conclusions are supported by Fig. 68, in which a clearly increasing perimeter and engine separation distance with decreasing nozzle aspect ratio are shown. Above a nozzle aspect ratio of 0.65, the rate of increase in the optimum parameters shown in Figs. 67a and 68 appears to get larger, indicating that now the engine separation distance is playing a much more significant role in the afterbody changes than in the other cases. Figures 67b and 67c are interesting because the trends in quarter chord sweep, taper ratio and wing loading are not as obvious as the increase in mass observed in Figure 67a, similar to the results in Section 5.2.3.1. However, the values are consistently within very close values of the mean, indicating that the aircraft is

effectively being designed for the same sweep, wing loading and taper ratio in all five cases.

Figure 69 shows how the constraints drive the design under investigation here. They were plotted by normalizing each constraint to its requirement. The ones satisfied exactly, in this case the acceleration (Accel), specific excess power (SEP), sustained turn rate at 10000m (STR1) and attained turn rate (ATR) are therefore at 100, whereas the other constraints exceed the requirement by varying amounts. Figure 69 is representative of all five cases; all of the designs were driven by the same constraints, and the ones exceeding their requirements did so by the same amounts.

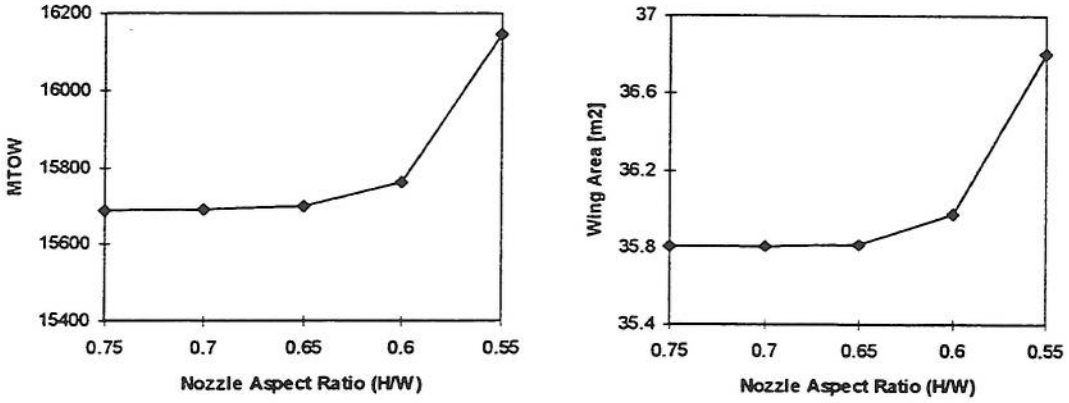

Fig. 67a: Optimum Parameter Variation with Nozzle Shape

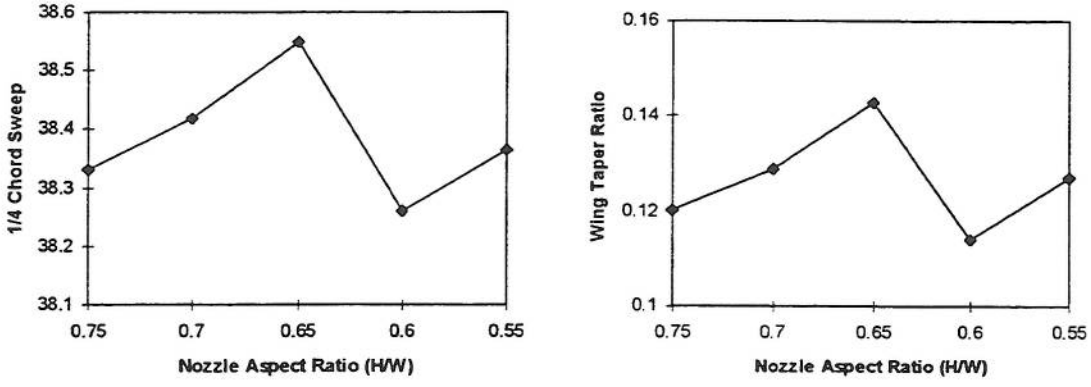

Fig. 67b: Optimum Parameter Variation with Nozzle Shape (cont.)

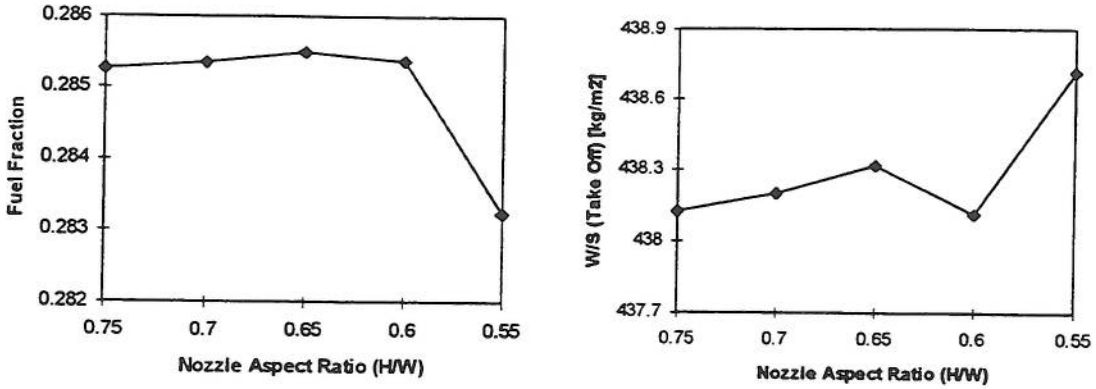

Fig. 67c: Optimum Parameter Variation with Nozzle Shape (cont)

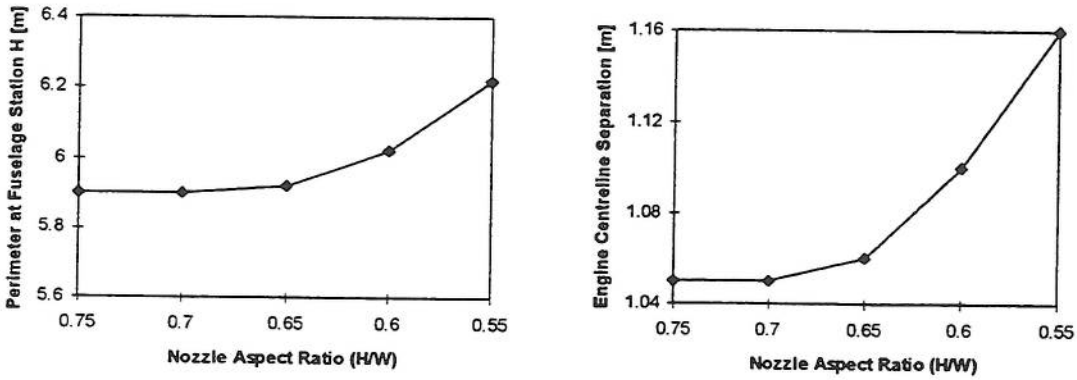

Fig. 68: Aft Fuselage Parameters

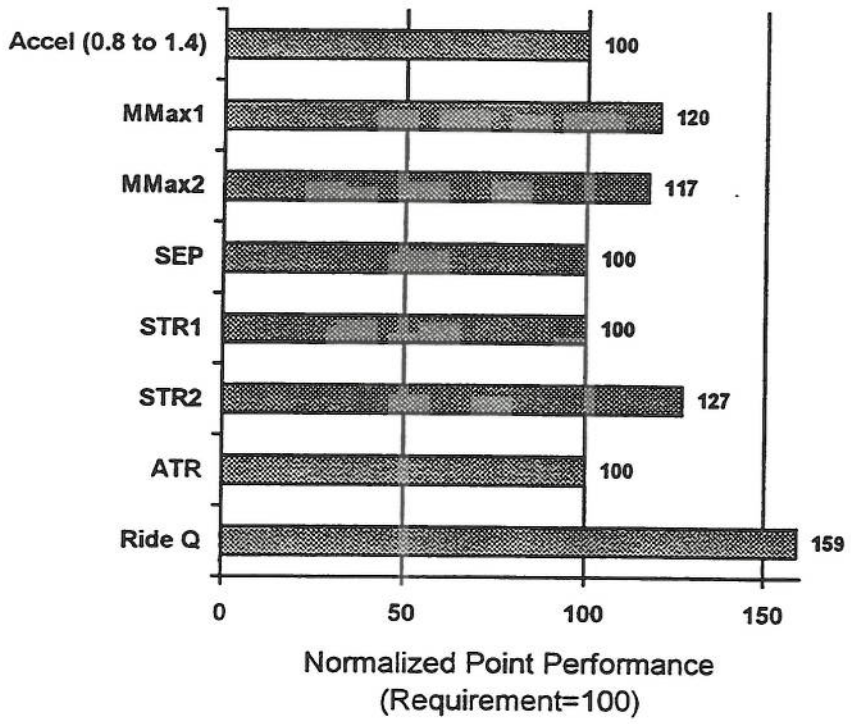

Fig. 69: Optimum Aircraft Point Performance Constraints (Low Observables)

6. DISCUSSION

The work described and analyzed in Chapters 2, 3, 4, and 5 was the result of an intensive three-year investigation into the modelling of advanced combat aircraft design features. A literature survey was conducted, concentrating on the aerodynamic and mass estimation methods, aircraft design synthesis and optimization methodologies, and advanced geometric features related mostly to low observables. Considerable reference material was found relating to the aerodynamics of advanced configurations, allowing good comparisons with the prediction methods to be made. Mass estimation data or methodologies were very difficult to find, and almost entirely related to civil transport aircraft. A search of references relating to aircraft design synthesis and optimization revealed a distinct lack of methodologies for military aircraft, in particular those that would be flexible enough to allow for the design of a large variety of configurations whilst ensuring sufficient modelling accuracy and computational efficiency. The work presented in this report fills this gap, and a review of the progress as well as a discussion of the results obtained is presented in the following sections.

6.1 Baseline Aircraft and Synthesis Development

Development of the synthesis methodology began after the initial literature search and once the geometric features of the baseline aircraft had been defined. New algorithms were developed for the cockpit, radome, weapons bay, engine bay and intake geometry. The method for synthesizing the fuselage geometry was also redesigned. For all of the major internal aircraft components, detailed mathematical relationships for the geometry are complemented by methodologies for estimating their effect on mass and center of gravity. In particular the intake geometry is fairly complex, requiring the evaluation of several cubic segments to find the correct layout whilst ensuring that no interference with other components takes place. However, this procedure also allows a very flexible layout of the diffuser. The weapons bay has three different internal arrangements. The number, dimensions and mass of the weapons carried internally can be specified by the user via external design constants. Two methodologies for the estimation of the mass effects were developed and succesfully incorporated into the code. Options for modelling thrust vectoring nozzles were included for the synthesis of the engine geometry. The model allows the external shape as well as the mass effects of the nozzle to be controlled by the user, whilst the size is linked to the engine size using the engine scale factor. The geometry of the cockpit accurately models the major geometric parameters necessary for the inclusion of a second seat in tandem with the first one, and the radome geometry was developed on the assumption of a low-observable fuselage shape.

The synthesis of the aircraft incorporates a high degree of flexibility and is sufficiently accurate for conceptual design optimization. Different

configuration options can be examined by appropriate choice of external input variables, and the effects on the aircraft layout, mass and aerodynamics are calculated by the design synthesis. The following table summarizes them.

Configuration Option	*Effects on Mass and Aerodynamics*
Nozzle type: axisymmetric or two-dimensional	Affects aircraft length, width, volume and wetted area and hence mass, no special mass factors included. Mass of nozzles given as external input.
Combination of flying surfaces	Affects mass and drag, no special mass factors included, canting of fins has no mass effect
Cockpit, single or twin?	Affects aircraft length and height, mass of cockpit controlled by external variables
Internal weapons bay	Affects fuselage layout and dimensions, special mass factors for effect on structure are included
Radome	Mass effect given by external variables, affects drag and fuselage mass via the wetted area
Intakes	Affects length and width of fuselage, spillage drag calculated by synthesis, intake losses included with engine data
Blended fuselage cross-section (chine or diamond shape)	Increases aircraft width used in mass formula, increases wetted area and volume

Table 15: Configuration Option Effects on Aircraft

Geometrical accuracy and layout flexibility was maximized by the use of splines to model the fuselage cross-sectional shapes. In the parametric representation (Chapter 4.2.2), they are both robust and simple to define. Furthermore, their use has facilitated the development of graphical output as well as the calculation of accurate values for fuselage wetted area and volume. Not all of the benefits of parametric splines will be fully utilized by this design synthesis. The accurate surface model is not used for radar cross section or aerodynamic analyses, because the codes to do this are too complex and computationally time consuming for this type of synthesis. Also, fully utilizing the inherent flexibility of splines would mean introducing into the design synthesis further variables, in addition to the large amount already reauired as input. Thus, a compromise was reached between the possibilities available through the use of splines and the requirement for numerical simplicity, but the option for enhancing the design synthesis methodology remains.

The features described above and those summarized in Table 15 are consistent with requirements for advanced technology. Low observables features dictate the use of internal weapons carriage, a two-dimensional nozzle, canted fins, and curved intake ducts, mainly to reduce radar cross section.

Parametric splines allow the creation of surfaces with a double curvature as well as cross sections with diamond or chine shapes. Corner reflectors can be avoided when using this design synthesis by canting the fins and by blending the fuselage and the flying surfaces. Wing, empennage and fin leading and trailing edges can be aligned by using constraints in conjunction with the numerical optimizer. Options are also available to link the leading edge sweep of the wing with that of the fin and tailplane.

It can be seen from the discussion of the baseline aircraft in Chapter 3 that many of the features of aircraft designed for low observables are consistent also with improved aerodynamic characteristics. For example, a smooth, blended shape and the internal carriage of weapons both reduce radar reflectivity and drag. Chine shaped forebodies may be beneficial at high angles of attack. Twin fins reduce the visual and radar signatures and also may provide stability and control benefits at high angles of attack. On the other hand, the requirement for curved intake ducts and rectangular nozzles both may lead to a deterioration in engine performance.

During the development of the synthesis code, care was taken to ensure maximum program portability, modularity and ease of maintenance. This was achieved by firstly structuring the design synthesis process into functional units which were then coded as subroutines. The code containing the sections of the original methodology developed by Lovell and retained for this work were either linked as subroutines or incorporated into the new code. Variables were given names according to the convention proposed in (Lovell, 1988). The result of this approach was that continual testing of the software was conducted as each module was added to the main program. Also, the modular structure allows for ease of maintenance and future growth.

6.2 Evaluation of the Methodologies

A detailed investigation of the aerodynamic estimation methodologies, obtained from (Lovell, 1988), was carried out, using data obtained from the open literature, as described in Chapter 5.1. The motivation for this work was the desire to determine their scope, applicability and validity to the types of aircraft under consideration in this research program. To ensure a good comparison, five different reports were found with aerodynamic wind-tunnel data for different configurations at different Mach numbers. Some of the configurations have blended fuselage-wing shapes, while others are similar to more conventional combat aircraft designs (see Chapter 5).

Generally, it was found that good agreement exists between the methodology used for this synthesis and the data in the experimental studies. The best correlation was found for the subsonic friction drag, the estimation of which agreed very well with the experiments. The drag polars were found to be accurate in the high subsonic regime, i.e. Mach greater than 0.7 and less than 1.0, and at low to moderate values of C_L. For the other Mach regions, the drag due to lift was either underestimated (at low Mach numbers) or overestimated (at high Mach numbers). At higher values of the lift coefficient the error becomes more pronounced. This result indicates that the methodology is

suitable for the flight regimes most likely to be encountered during combat conditions, i.e. high subsonic or low supersonic. Furthermore, since the use of this design synthesis is restricted to low to moderate angles of attack, it is safe to rely upon this method until a more accurate overall estimation methodology may become available.

Insufficient data was available for a full analysis of the wave drag estimation methodology. However, the existing one can be considered applicable to this design synthesis for a variety of reasons. Firstly, it is based upon a well established and much used handbook method (DATCOM, 1975). It does not depend on details of the fuselage geometry, but merely requires the estimation of the location and size of the maximum fuselage cross-sectional area and the fuselage length as well as some major wing and empennage geometric parameters. These are all readily available from the design synthesis. Since the fuselage can be assumed to be a slender body, then the wave drag will be independent of the detailed shape and dependent only on the area distribution. A slender body is guaranteed by the smooth area distribution given by the fairing curve. Furthermore, the requirements of low observable aircraft dictate a fuselage skin designed with a smooth surface, without gaps, excrescences or excessive fairings. Similar considerations apply to the wing and empennage. Thus, it can be seen how the requirements of slender body theory match well with considerations of reduced electromagnetic reflectivity and radar cross section. Nevertheless, it is recommended that further work be carried out to study the effects of non-circular fuselage shapes on wave drag.

The greatest obstacle to evaluating the mass estimation methodologies for the fuselage was the lack of data and methods available in the open literature. A closer examination of the method given in (Lovell, 1988) and used in the design synthesis indicates some of the doubts about its applicability. The fuselage mass is calculated with two main terms, one for the skin and one for the internal structure. The two elements depend strongly upon the wetted area and volume, respectively, of the fuselage. Other important parameters are the fuselage length and the maximum fuselage height and width. Wetted area, volume and length are all accurately available from the design synthesis, as are width and height. However, caution must be exercised in their determination from the fuselage shape.

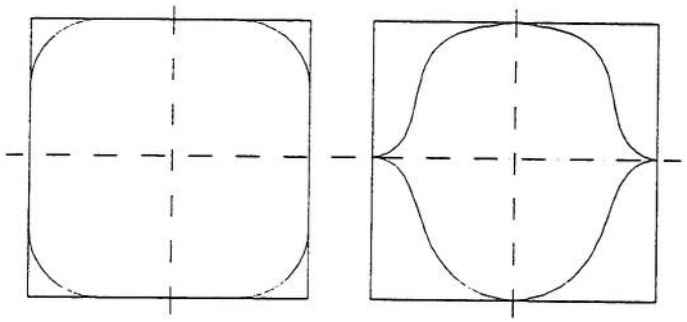

Fig. 70: Effect of Chine Shape on Fuselage Width and Height

Figure 70 demonstrates the effect of chine shapes on the fuselage width and height. The boxes enclosing the cross sections symbolize the width and height values used within the mass formulae. It can be seen that, for the conventional shape on the left, the box has the same width and height as the fuselage section and closely corresponds to the section itself. Conversely, the box around the chine shape on the right is much larger than the cross section itself. This would indicate that the fuselage mass contribution from these dimensions will be overestimated for chine-shaped fuselages. On the other hand, the chine shape has a lower cross-sectional area for the same width and height, leading to a reduction in volume and hence mass. The results in Chapter 5 have shown that the volume and wetted area are significant contributors to the mass. Further work is recommended to quantify and determine the relative importance of the contributions to fuselage mass of width, height, wetted area and volume.

6.3 Results

Results were obtained from the design synthesis in conjunction with the optimizer to demonstrate the correct functioning of the complete multidisciplinary optimization code, presented in Chapter 5. When compared with data obtained from the open literature, the two test cases, combat air patrol and ground attack, can be seen to fit well within the trend of actual combat aircraft designs. Mass breakdowns of the test aircraft were compared with results obtained from (O'Neill et al, 1994). Good agreement can be seen to exist between the industry study and the test cases. Although the aircraft in (O'Neill et al, 1994) have a higher fuel fraction and hence a slightly different mass breakdown, this was attributed to differing mission requirements.

A set of aircraft optimized for empty mass were obtained in order to prove the usefulness of the synthesis for trend studies. For the first case, it was found that the optimum mass of the aircraft increases as the combat radius is increased. Despite a lack of clear trends for some of the optimum parameters, a close examination of the relationships between the variables found that the aircraft in the trial series were being consistently being optimized for the point performance constraints. These were calculated using a wing loading derived assuming 50% of the internal fuel used. As the combat radius was increased, the aircraft size was increasing as well, whilst maintaining constant the wing loading at the point performance conditions.

In the second case, the use of the design synthesis to investigate the effect of low observables features on the optimum aircraft was demonstrated. For a given misison and point performance requirement, the nozzle shape was varied in such a manner as to increase the width whilst reducing the height. Furthermore, a slightly more balanced set of point performance constraints was used to drive the optimization. The results again indicate convergence to optimum points consistent with a design driven by the point performance constraints and mission requirement.

7. CONCLUSIONS

A numerical synthesis methodology for the conceptual design optimization of combat aircraft was developed. It consists of a set of algorithms and mathematical relationships to describe the geometry, mass, aerodynamic and performance characteristics of conceptual aircraft. The main features of the types of aircraft under consideration in this study are design for low observables, side mounted intakes and a straight-tapered, trapezoidal wing planform. Further options are available to synthesize the geometry of the empennage, landing gear and flying surfaces. The aircraft is capable of carrying a mix of weapons both externally and internally.

An analysis of the open literature relating to such aircraft types along with the results obtained from the design synthesis and optimization code indicate the following conclusions:

- The increasing complexity of the combat aircraft design task, from an engineering, political and economic point of view, justifies the inclusion at as early a stage as possible of any advanced features likely to affect the outcome of the design.

- Many of these advanced features of combat aircraft, such as fuselage shape and external or internal weapons arrangement, can be deemed appropriate for inclusion in the design both for aerodynamic/performance reasons as well as from a low observables standpoint.

- Low observables can be modelled for the aircraft conceptual design phase by the addition of fairly simple geometric features.

- These models allow sufficient design accuracy to investigate the impact of minor design changes on the objective function.

- Within certain limits and as long as no more suitable methodologies are available, conventional aerodynamic estimation methodologies may with reasonable confidence be applied to the class of unconventional designs under consideration in this research program,.

Further work will be required to

- determine the effects of unconventional shapes on the mass of the aircraft, and

- fully quantify the influence of unconventional fuselage shapes on the aerodynamic characteristics.

The design synthesis was developed in a modular fashion and opens completely new areas of research into conceptual design optimization of aircraft configured for low observables, including but not limited to

- trade-off studies into the effects of low-observables on the optimum aircraft conceptual design,
- the enhancement of the synthesis options to include alternative intake and flying surface arrangements, e.g. canard,
- investigation into the effects of low-observables on operational requirements, and
- the inclusion of additional objective function options to quantify measures of low observables, such as radar signature, and other parameters such as life cycle cost.

8. REFERENCES

Blanchard, B.S. (1992) *Logistics Engineering and Management.* Prentice Hall International, Inc.

Boatman, J. (1993) "Striving to shape the F-22 force". Jane's Defence Weekly. October 23, 1993, 29-30.

Brown, A.C. (1993) "Fundamentals of Low Radar Cross-Sectional Aircraft Design". Journal of Aircraft, vol. 30, no. 3, 289-290.

Burns, B.R.A. (1982) Advanced Aerodynamic Design for Future Combat Aircraft. ICAS-82-1.1.2. In: *Proceedings of the 13th Congress of the ICAS*, Seattle, WA, Aug. 22-27, 1982, vol. 1, 23-33.

Burt, M.E.; Phillips, J. (1952) Prediction of Fuselage and Hull Structure Weight. RAE Report Structures 122.

Cain, A.B. and P.M. Doane (1992) A Methodology for the Analysis and Modelling of Thrust Vectoring Usage. AIAA-92-0389.

Capone, F.J. (1976) Effects of Nozzle Exit Location and Shape on Propulsion-Induced Aerodynamic Characteristics Due to Vectoring Twin Nozzles at Mach Numbers from 0.4 to 1.2. NASA TM X-3313.

Capone, F.J., Smerecniak, P., Spetnagel, D. and Thayer, E. (1992) Comparative Investigation of Multiplane Thrust Vectoring Nozzles. AIAA 92-3263, In: *AIAA/ASME/SAE/ASEE 28th Joint Propulsion Conference and Exhibit*, July 6-8, 1992, Nashville, TN.

Capone. F.J. (1981) Aeropropulsive Characteristics of Twin Nonaxisymmetric Vectoring Nozzles Installed with Forward-Swept and Aft-Swept Wings. NASA TP-1778.

Chen, D. (1990) Stores Separation Characteristics from a Generic Bay at Transonic Speeds. AIAA-90-1415, In: *AIAA 16th Aerodynamic Ground Testing Conference*, June 18-20, 1990, Seattle, WA.

Chun, C.K.S. (1991) The Lockheed F-117A. P-7746-RGS, Rand Corporation, Santa Monica, CA.

Cramer, E.J., Frank, P.D., Shubin, G.R., Dennis, jr., J.E. and Lewis, R.M. (1992) On Alternative Problem Formulations for Multidisciplinary Design Optimization. AIAA-92-4752-CP. In: *Proceedings of the 4th AIAA/USAF/NASA/OAI Symposium on Multidisciplinary Analysis and Optimization*, Sept. 21-23, 1992, Cleveland, OH.

Crispin, Y. (1992) Aircraft Conceptual Optimization Using Simulated Evolution. AIAA-94-0092.

DATCOM (1975) *USAF Stability and Control Data DATCOM.* McDonnel Douglas Corporation, Douglas Aircraft Division.

Dollyhigh, S.M. (1974) Subsonic and Supersonic Longitudinal Stability and Control Characteristics of an Aft Tail Fighter Configuration with Cambered

and Uncambered Wings and Uncambered Fuselage. NASA TM X-3078.

Dollyhigh, S.M. (1979) Experimental Aerodynamic Characteristics at Mach Numbers from 0.60 to 2.70 of Two Supersonic Cruise Fighter Configurations. NASA TM 78764.

Dovi, A.R.; Wrenn, G.A. (1990) Aircraft Design for Mission Performance Using Nonlinear Multiobjective Optimization Methods. NASA CR 4328.

Economist (1996) "American monsters, European minnows". The Economist, vol 338, no. 7948, 69-72.

Foley, J.D., van Dam, A., Feiner, S.K. and Hughes J.F. (1990) *Computer Graphics Principles and Practice.* Addison-Wesley Publising Company.

Foley, T.M. (1995) "Finding a job in aerospace". Aerospace America. March 1995, 35-41.

Fuhs, A.E. (1982) *The No-See-Um Book: Radar Cross Section Lectures.* American Institute of Aeronautics and Astronautics, New York.

Fulgham, D.A. (1993) "Signature Reduction Key to A-10 Survival". Aviation Week and Space Technology, June 7, 1993, 135-136.

Gage, P. and Kroo, I. (1992) Development of a Quasi-Procedural Method for Use in Aircraft Configuration Optimization. In: *Proceedings of the 4th AIAA/USAF/NASA/OAI Symposium on Multidisiplinary Analysis and Optimization.* Sept. 21-23, 1992, Cleveland, OH. AIAA 92-4693.

Gal-Or, B. (1994) "Fundamentals and Similarity Transformations of Vectored Aircraft". Journal of Aircraft, vol. 31, no. 1, 181-187.

Gharib, M., Roshko, A. and Sarchia, V. (1985) Effect of Flow Oscillations on Cavity Drag and a Technique for their Control. JPL-PUB-85-72, Jet Propulsion Lab, Pasadena, CA.

Gill, P.E., Murray, W. and Wright, M.H. (1981) *Practical Optimization.* Academic Press, London.

Herrick, P.W. (1988) Air Combat Payoffs of Vectoring/Reversing Exhaust Nozzles. AIAA 88-3239, In: *AIAA/ASME/SAE/ASEE 24th Joint Propulsion Conference,* July 11-13, 1988, Boston, Massachusetts.

Hicks, R.E. and Hopkins, E.J. (1964) Effects of Spanwise Variation of Leading Edge Sweep on the Lift, Drag, and Pitching Moment of a Wing-Body Combination at Mach Numbers from 0.7 to 2.94. NASA TN D-2236.

Hiley, P.E.; Wallace, H.W.; Booz, D.E. (1976) "Nonaxisymmetric Nozzles Installed in Advanced Fighter Aircraft". Journal of Aircraft, Vol. 13, No. 12, 1000-1006.

Hinz, W.W. and Miller, E.H. (1979) Propulsion Integration of a Supersonic Cruise Strike Fighter. AIAA-79-0100.

Hooper, R.S. (1977) Technology Development to Meet the Military Require-ments. In: *Fighter Aircraft Design,* AGARD Conference Proceedings No. 241.

Howe, D. (1991) Introduction to the basic technology of stealth aircraft. Part 1: Basic considerations and aircraft self-emitted signals (passive considerations). (ASME/90-GT-116) In: *Transactions of ASME. Journal of engineering for gas turbines and power*, Vol. 113, No. 1. New York : American Society of Mechanical Engineers.

Howe, D. (1991) Introduction to the basic technology of stealth aircraft. Part 2: Illumination by the enemy (active considerations). (ASME/90-GT-117) In: *Transactions of ASME. Journal of engineering for gas turbines and power*, Vol. 113, No. 1. New York : American Society of Mechanical Engineers.

I.M.F. (1994) *Government Finance Statistics Yearbook.* International Monetary Fund

Kehayas, N. (1992) *ASTOVL Combat Aircraft Design Synthesis and Optimization.* PhD Thesis, Cranfield Institute of Technology.

Kirk, J. (1993) Personal Communications.

Kirkpatrick, D.L.I. and Smith, J.S. (1990) Multidisiplinary Optimisation in Aircraft Design. ICAS-90-2.3.1. In: *Proceedings of the ICAS.* 434-441.

Kitowski, J.V. (1992) Fighter Airframe/Propulsion Integration - A General Dynamics Perspective. AIAA-92-3332.

Kraus, W. (1995) Zukünftige Gestaltung des Vorentwurfs bei DASA LM (Future Structure of Conceptual Design at DASA LM). In: *Proceedings of the DGLR Workshop Entwicklungswerkzeuge im Vorentwurf (Tools for Aircraft Design).* Hamburg, Germany, November 11, 1995.

Lindsey, G. (1989) The Tactical and Strategic Significance of Stealth Technology. Centre Québecois de relations interanationales.

Lovell, D.A. (1988) The Application of Multivariate Optimization to Combat Aircraft Design. RAE TR 88003.

Mace, J. and Nyberg, G. (1992) Fighter Airframe/Propulsion Integration - A McDonnell Douglas Aircraft Perspective. AIAA-92-3333.

Mangold, P. (1982) Some Aerodynamic/Flight Mechanic Aspects for the Design of Future Combat Aircraft. ICAS-82-1.1.3. In: *Proceedings of the 13th Congress of the ICAS*, Seattle, WA, vol. 1, 34-43.

Morris, O.A. (1977) Subsonic and Supersonic Characteristics of a Supersonic Cruise Fighter Model With a Twisted and Cambered Wing With 74° Sweep. NASA TM X-3530.

Morris, S.J.; Kroo, I.L. (1989) Aircraft Design Optimization with Multidisciplinary Performance Criteria. In: *Proceedings of the AIAA/ASME/ASCE/AHS/ASC 30th Structural Dynamics and Materials Conference,* Part 2, 909-919.

O'Neill, P.; Nyberg, G.; de Turk, R.; Seal, D.W.; Grethlein, C.E. (1994) Impact of Agility Requirements on Configuration Synthesis. NASA CR 4627.

Om, D. (1986) Navier Stokes Simulation for Flow Past and Open Cavity. AIAA-86-2628.

Poisson-Quinton, Ph. (1956) Einige physikalische Betrachtungen über das Ausblasen an Tragflügeln. In: *Jahrbuch der Wissenschaftlichen Gesellschaft für Luftfahrt e.V.* 1956, 29-51.

Press, W.H.; Flannery, B.P.; Teukosky, S.A. et. al. (1989) *Numerical Recipes: The Art of Scinetific Computing (FORTRAN version).* Cambridge University Press.

Raymer, D.P. (1991) Post-Stall Maneuver and the Classic Turn Rate Plot. AIAA 91-3170.

Ruck, G.T., Barrick, D.E., Stuart, W.D. and Krichbaum, C.K. (1970) *Radar Cross Section Handbook* Plenum Press, New York.

Serghides, V.C. (1987) *Design Synthesis for Canard-Delta Combat Aircraft.* PhD Thesis, Cranfield Institute of Technology.

Shrout, B.L. (1977) Aerodynamic Characteristics at Mach Numbers from 0.6 to 2.16 of a Supersonic Cruise Fighter Configuration with a Design Mach Number of 1.8. NASA TM X-3559.

Siestrunck, R. (1961) General Theory of the Jet Flap in Two-Dimensional Flow. In: G.V. Lachmann, ed. *Boundary Layer and Flow Control, its Principles and Applications.* vol. 1, 342-364.

Skrobanski, J.J. (1994) *RQPMIN Version 3.0 The Constrained Optimization Program User Guide.* The MVA Consultancy.

Stevens, H.L., Thayer E.B. and Fullerton J.F. (1981) Development of the Multi-Function 2-D/C-D Nozzle. AIAA-81-1491.

Sweetman, B. (1994) "The Future of Airborne Stealth". International Defense Review. vol 27, 30-40.

Taylor, J.W.R. (ed) (1989/90) *Jane's All the World's Aircraft.* Jane's Information Group Ltd, London.

Taylor, J.W.R. (ed) (1994/95) *Jane's All the World's Aircraft.* Jane's Information Group Ltd, London.

UNIRAS (1992). UNIRAS FGL/3D RENDER user guide & reference manual. - Version 6.3a.

Vakili, A.D. and Gauthier, C. (1994) "Control of Cavity Flow by Upstream Mass-Injection". Journal of Aircraft, vol. 31, no. 1, 169-174.

Whitford, R. (1987) Design for Air Combat. Jane's Information Group, Ltd.

Wilson, B. (1993) Lecture Notes on F20 and NATF. Lecture held at Cranfield Institute of Technology on May 21, 1993.

Woodford, S. (1995) Personal communications.

Appendix A: Sample Input and Output Files

A.1. Input File

```
* this input file is for rqpmin v. 3.0
VARIABLES
 1 1    1.0     1.1000      0.35       3.0  : Engine Scale Factor
 2 1   10.0     37.000       5.0      100.0  : Wing Area
 3 1   10.0     44.000       0.0       60.0  : Wing 1/4 chrd Sweep
 4 1    0.1     0.0636      0.02       0.10  : Wing T/C Ratio
 5 1    0.1     0.300       0.25       0.99  : Wing Taper Ratio
 6 1    1.0     3.000       1.5        10.0   : Wing Aspect Ratio
 7 1    1.0     0.150       0.05       0.30 : Wing F.Spar/chord
 8 1    1.0     0.600       0.50       0.80 : Wing R.Spar/chord
 9 1    1.0     0.650       0.0        1.0  : Span T/E Flaps
10 1    1.0     0.9676      0.0        1.0  : Span W. Net F. Box
11 1    1.0    14.189      -5.0       50.0  : Fuselage Length
12 1    0.1     0.5500      0.0        1.0  : Fairing:  RLTMFN
13 1    0.1     0.4000      0.0        0.5  : Fairing:  RLTFFN
14 1    0.1     0.2000      0.0        0.99 : Fairing:  RLTCFN
15 1    0.1     0.8900      0.5        0.99 : Fairing:  RLTAFN
16 1    0.1     0.6000      0.0        1.0  : Wing 1/4 pos RXWCQM
17 1    1.0     0.1418     -5.0        5.0  : Fairing:  OT6NVAR
18 1    1.0     0.5780      0.0        0.8 : Fuel Frac. Frt. Fus
19 1    1.0     0.1694      0.0        0.9 : Fuel Frac. Ctr. Fus
20 1    1.0     0.0000      0.0        0.8 : Fuel Frac. Rer. Fus
21 0    1.0     0.8608      0.800    1.00 : Rat Fin Mmt Arm/Wng
22 0    1.0     0.9522      0.800    1.00 : Rat Emp Mmt Arm/Wng
23 1    0.1     0.54000     0.3        0.7 : W.Bay 1 cg X-coord
24 1    0.1     0.54000     0.3        0.7  : W.Bay 2 cg X-coord
25 0    0.1     0.0000     -0.05       0.15 : W.Bay 1 cg Z-coord
26 0    0.1     0.0000     -0.05       0.15 : W.Bay 2 cg Z-coord
27 0    1.0     1.122       1.122      3.00 : Eng. Separation - Y
*28 0    1.0     1.0        0.90       1.10 : Eng. Pos. z-coord.
FUNCTIONS
1   -1    0   0.01    : Wing and Tail Separation
2   -1    0   0.001   : Combinations of AR and Sweep
3   -1    0   0.01    : Excess Area at A
4   -1    0   0.01    : Excess Area at B
5   -1    0   0.01    : Excess Area at C
6   -1    0   0.01    : Excess Area at D
7   -1    0   0.01    : Excess Area at E
8   -1    0   0.01    : Excess Area at F
9   -1    0   0.01    : Excess Area at G
10  -1    0   0.01    : Excess Area at H
11  -1    0   0.01    : Upper value for boattail
*12  -1    0   0.01   : Boattail angle positive
13  -1    0   0.01     : Intake and wing separation
14  -1    0   0.01     : Fuselage length - gun
15  -1    0   0.01     : Fuselage length - nose u.c.
16  -1    0   0.01     : Fuselage length - weapons bay
17  -1    0   0.01     : Minimum diffuser length - area
*18  -1    0    10.0    : Volume in front fuselage
19  -1    0   0.01     : Volume in rear fuselage - fuel
20   1    0   0.01    : Nozzle cross-sectional area incr.
21  -1    0   0.01   : A/C c.g. - fwd lim - empty
22  -1    0   0.01   : A/C c.g. - fwd lim - full
23  -1    0   0.01   : A/C c.g. - rear lim - empty
24  -1    0   0.01   : A/C c.g. - rear lim - full
25  -1    0   0.01     : Minimum diffuser length - curv.
26  -1    0   0.0001   : Fairing curve negative curvature
*27  -1    0   0.01     :  Duct centerline separation
*28   1    0   0.01     :  Wing leading and trailing edge
29   1    0   1.0     : Excess fuel after sortie
*30  -1    0   0.001   : Store release disturbance
31  -1    0   1.0     : Unused take-off distance
32  -1    0   0.1   : Stall margin - landing approach
33  -1    0  0.01   : Take-off wing loading - min.
*34  -1    0   0.01   : Take-off wing loading - max.
*35  -1    0   1.0   : Fuel burnt before combat
36  -1    0   0.01     : Sep. dist. wbay intake
37  -1    0   0.01     : Sep. dist. wbay main gear
38  -1    0   0.01     : Sep. dist. wbay compressor
39  -1    0   0.01     : Sep. dist. wbay cockpit
*40  -1    0   0.01     : Constraint for empennage beyond nozzle
*41  -1    0   0.01     : Max Aircraft length
*42  -1    0   0.01     :  Max aircraft width
*43  -1    0   0.01     :  XFD<XFE
```

```
*44  -1    0   0.01    :  XFE=XFF
45   -1    0   0.01    :  Minimum Leading Edge Sweep
50   -1    0   0.01    :  Acceleration for Mach Increment
51   -1    0   0.01    :  Max Mach
52   -1    0   0.01    :  Max Mach
53   -1    0   0.5     :  SEP
54   -1    0   0.05    :  STR
55   -1    0   0.05    :  STR
56   -1    0   0.05    :  ATR
57   -1    0   0.01    :  Ride Quality
75    0    0   1.0   2  : Objective function (MTE)
CONTROLS
CENTRAL DIFFERENCES
IREP = 0
VARYV
VARYU
RTOL = 0.5
RPMAX = 5.0
NFEMAX = 30000
NIMAX = 5000
SUBTOL = 1.0e-06
XTOLU = 0.5e-05
XTOLV = 0.5e-05
RUN
testtitle
   0   100   10
citen2.dat   frankrqp.pic
      0.95      0.95      0.95      0.05      0.05      0.15      0.15      50.0       0.0       0.00
       0.0       8.0      0.30      0.90      15.0      30.0
         4         0         0
         3
         1
       1.4       0.3      45.0       0.0      2.00      0.06      0.95       0.5   0.11156       1.3
    0.7812    0.2422      0.20
       3.5       0.3      40.0      0.30      0.03      0.95  0.004356     1.549    0.3433      0.20
     400.0       2.0      12.0  16000.0      0.30  0.000015      15.0      1.05      1.00     670.0
     800.0      50.0      1.07       1.0       1.0       0.8       0.2       0.5       0.5       0.0
      0.03     -0.07
      0.65      0.06    0.4200       0.7     200.0       1.0     700.0     500.0      20.0      25.0
         1
     0.745     0.694      0.33     0.254      0.70     0.222     0.627      15.0      15.0      45.0
       5.0      25.0       0.3       0.0      15.0       3.5       0.4       1.1       1.8       1.3
     180.0      90.0
         1         1
     0.400    0.0468    0.0064    0.0068     -42.0       6.0       4.0     756.0    0.5293      0.74
 0.0000108 0.0000329 0.0000196     0.107     0.419     0.318     0.152       1.1       1.5       1.1
       1.5 0.0000045      0.31      0.10      0.25      0.85
     160.0       2.0       0.1      80.0      0.15       0.1
     0.011     -15.9      0.75     500.0       0.5    0.0267     29.90       0.6    0.0293      22.9
    0.0759
      0.65      0.56      0.84      0.57      0.43      0.66      0.42      0.41      0.66      0.35
      0.35      0.53       0.2      0.05      0.09       0.2      0.05      0.09
         1         0
       1.4       6.0       2.0      20.0       9.0     0.014       2.0       0.2
      1.85       0.6      0.15       0.0       0.4     1.000       0.0       0.0
        15
       0.0     0.300     0.700     1.900       0.2     0.300     0.680     1.800
       0.4     0.300     0.660     1.600       0.6     0.410     0.640     1.400
       0.7     0.560     0.630     1.300       0.8     0.820     0.620     1.230
      0.90     1.030     0.600     1.160       1.0     1.010     0.580     1.110
      1.10     0.800     0.550     1.060       1.2     0.420     0.510     1.010
       1.3     0.150     0.400     0.970       1.4     0.000     0.000     0.920
       1.6       0.0       0.0      0.84       1.8       0.0       0.0      0.77
       2.0       0.0       0.0      0.70
       0.0       0.0       0.0       0.0       0.0       1.0       1.0
        15
       0.0     0.000    0.0000     0.000       0.0       0.6     0.000    0.0000     0.000       0.0
       0.8     0.000    0.0000     0.000       0.0      0.85     0.000    0.0000     0.000       0.0
       0.9     0.000    0.0000     0.000       0.0      0.94     0.000    0.0000     0.000       0.0
      0.98     0.000    0.0000     0.000       0.0       1.0     0.000    0.0000     0.000       0.0
      1.02     0.000    0.0000     0.000       0.0      1.05     0.000    0.0000     0.000       0.0
       1.1     0.000    0.0000     0.000       0.0       1.2     0.000    0.0000     0.000       0.0
       1.4     0.000    0.0000     0.000       0.0       1.6     0.000    0.0000     0.000       0.0
       2.0     0.000    0.0000     0.000       0.0
         3         1
         0
         1         2         1
      3.55     0.175     0.175       0.1       0.1       0.2     500.0      50.0
         1         1         1
      3.00     0.127     0.127      0.05       0.1      0.10     100.0      25.0
    0.0364     0.919     0.783     2.005     1.054
         2         1
   70000.0       5.0      70.0       0.4       0.1       1.6       0.4       1.4       0.8       0.0
       0.7      0.75       0.9       0.8      0.55     750.0     250.0     100.0    0.3693       0.5
       0.5       0.5      0.94    0.6517     0.125
CITEN2.DAT
         6         0         0         0         0         0         6      10.0      20.0      0.05
```

3	4					
1	0.7	10000.0	600.0	1.0		
1	0.9	70.0	100.0	1.0		
3	0.8	70.0	1.0	5.0		
3	0.8	70.0	2.0	5.0		
1	0.9	70.0	100.0	1.0		
1	0.7	10000.0	600.0	1.0		
8	300.0	600.0	70.0	9.0	0.08	0.6
1	6	0.8	10000.0	10.0	60.0	0.5
1	5	1.1	0.0	10.0	1.1	0.5
1	5	1.6	10000.0	10.0	1.6	0.5
1	3	0.9	10000.0	10.0	100.0	0.5
1	2	0.9	10000.0	10.0	7.0	0.5
1	2	0.8	1000.0	10.0	16.0	0.5
1	4	0.9	10000.0	10.0	10.0	0.5
1	8	0.8	1000.0	10.0	5.0	0.5
264.6	308.6	1212.5	800000.0	4.496	0.0	1.0

Program RQPMIN Version 3.0 (Sun Edition) Wed Mar 6 14:17:50 1996 Page 1

ANALYSIS OF INPUT FILE DATA AND CONTROL PARAMETERS

File specifications

Input file: aglr2.dat
Results file: aglr2.18
Final values file:
Report file:
Graphics dump file:

Variable data

Number of variables = 27

Index	Status	Scale	Starting value	Lower bound	Upper bound	User title
1	1	0.1000000E+01	0.1300400E+01	0.3500000E+00	0.3000000E+01	Engine Scale Factor
2	1	0.1000000E+02	0.3700000E+02	0.5000000E+01	0.1000000E+03	Wing Area
3	1	0.1000000E+02	0.4400000E+02	0.0000000E+00	0.6000000E+02	Wing 1/4 chrd Sweep
4	1	0.1000000E+00	0.6360000E-01	0.2000000E-01	0.1000000E+00	Wing T/C Ratio
5	1	0.1000000E+00	0.1000000E+00	0.5000000E-01	0.9900000E+00	Wing Taper Ratio
6	1	0.1000000E+01	0.3005000E+01	0.1500000E+01	0.1000000E+02	Wing Aspect Ratio
7	1	0.1000000E+01	0.1500000E+00	0.5000000E-01	0.3000000E+00	Wing F.Spar/chord
8	1	0.1000000E+01	0.6000000E+00	0.5000000E+00	0.8000000E+00	Wing R.Spar/chord
9	1	0.1000000E+01	0.6500000E+00	0.0000000E+00	0.1000000E+01	Span T/E Flaps
10	1	0.1000000E+01	0.9676000E+00	0.0000000E+00	0.1000000E+01	Span W. Net F. Box
11	1	0.1000000E+01	0.1418900E+02	0.5000000E+01	0.5000000E+02	Fuselage Length
12	1	0.1000000E+00	0.5500000E+00	0.0000000E+00	0.1000000E+01	Fairing: RLTMFN
13	1	0.1000000E+00	0.4000000E+00	0.0000000E+00	0.5000000E+00	Fairing: RLTFFN
14	1	0.1000000E+00	0.2000000E+00	0.0000000E+00	0.9900000E+00	Fairing: RLTCFN
15	1	0.1000000E+00	0.8900000E+00	0.5000000E+00	0.9900000E+00	Fairing: RLTAFN
16	1	0.1000000E+00	0.6000000E+00	0.0000000E+00	0.1000000E+01	Wing 1/4 pos RXWCQM
17	1	0.1000000E+01	0.1418000E+00	-0.5000000E+01	0.5000000E+01	Fairing: OT6NVAR
18	1	0.1000000E+01	0.5780000E+00	0.0000000E+00	0.8000000E+00	Fuel Frac. Frt. Fus
19	1	0.1000000E+01	0.1694000E+00	0.0000000E+00	0.9000000E+00	Fuel Frac. Ctr. Fus
20	1	0.1000000E+01	0.0000000E+00	0.0000000E+00	0.8000000E+00	Fuel Frac. Rer. Fus
21	0	0.1000000E+01	0.8608000E+00	0.8000000E+00	0.1000000E+01	Rat Fin Mmt Arm/Wng
22	0	0.1000000E+01	0.9522000E+00	0.8000000E+00	0.1000000E+01	Rat Emp Mmt Arm/Wng
23	1	0.1000000E+00	0.5400000E+00	0.3000000E+00	0.7000000E+00	W.Bay 1 cg X-coord
24	1	0.1000000E+00	0.5400000E+00	0.3000000E+00	0.7000000E+00	W.Bay 2 cg X-coord
25	0	0.1000000E+00	0.0000000E+00	-0.5000000E-01	0.1500000E+00	W.Bay 1 cg Z-coord
26	0	0.1000000E+00	0.0000000E+00	-0.5000000E-01	0.1500000E+00	W.Bay 2 cg Z-coord
27	0	0.1000000E+01	0.1122000E+01	0.1122000E+01	0.3000000E+01	Eng. Separation - Y

Problem function data

Number of constraints = 41

Index	Status	Type	Violation tolerance	Lower bound	Upper bound	User title
1	-1	0	0.1000000E-01			Wing and Tail Separation
2	-1	0	0.1000000E-02			Combinations of AR and Sweep
3	-1	0	0.1000000E-01			Excess Area at A
4	-1	0	0.1000000E-01			Excess Area at B
5	-1	0	0.1000000E-01			Excess Area at C
6	-1	0	0.1000000E-01			Excess Area at D
7	-1	0	0.1000000E-01			Excess Area at E
8	-1	0	0.1000000E-01			Excess Area at F
9	-1	0	0.1000000E-01			Excess Area at G
10	-1	0	0.1000000E-01			Excess Area at H
11	-1	0	0.1000000E-01			Upper value for boattail
13	-1	0	0.1000000E-01			Intake and wing separation
14	-1	0	0.1000000E-01			Fuselage length - gun
15	-1	0	0.1000000E-01			Fuselage length - nose u.c.
16	-1	0	0.1000000E-01			Fuselage length - weapons bay
17	-1	0	0.1000000E-01			Minimum diffuser length - area
19	-1	0	0.1000000E-01			Volume in rear fuselage - fuel
20	1	0	0.1000000E-01			Nozzle cross-sectional area incr.
21	-1	0	0.1000000E-01			A/C c.g. - fwd lim - empty
22	-1	0	0.1000000E-01			A/C c.g. - fwd lim - full
23	-1	0	0.1000000E-01			A/C c.g. - rear lim - empty
24	-1	0	0.1000000E-01			A/C c.g. - rear lim - full
25	-1	0	0.1000000E-01			Minimum diffuser length - curv.
26	-1	0	0.1000000E-03			Fairing curve negative curvature
29	1	0	0.1000000E+01			Excess fuel after sortie
31	-1	0	0.1000000E+01			Unused take-off distance
32	-1	0	0.1000000E+00			Stall margin - landing approach
33	-1	0	0.1000000E-01			Take-off wing loading - min.
36	-1	0	0.1000000E-01			Sep. dist. wbay intake
37	-1	0	0.1000000E-01			Sep. dist. wbay main gear
38	-1	0	0.1000000E-01			Sep. dist. wbay compressor
39	-1	0	0.1000000E-01			Sep. dist. wbay cockpit
45	-1	0	0.1000000E-01			Minimum Leading Edge Sweep
50	-1	0	0.1000000E-01			Acceleration for Mach Increment
51	-1	0	0.1000000E-01			Max Mach
52	-1	0	0.1000000E-01			Max Mach
53	-1	0	0.5000000E+00			SEP
54	-1	0	0.5000000E-01			STR
55	-1	0	0.5000000E-01			STR
56	-1	0	0.5000000E-01			ATR
57	-1	0	0.1000000E-01			Ride Quality
75	0	0	0.1000000E+01			Objective function (MTE)

Objective is function 75 Problem number = 2

Logical control parameters

CENTRAL DIFFERENCES	= T	DEBUG USERD	= F	FIX RHMAX	= F
FORWARD DIFFERENCES	= F	LIST	= F	MONITOR	= F
NOCHEAT	= F	NOFAST	= F	NOFREEC	= F
NOPAUSE	= F	NOPROJECT	= F	NOQUASI	= F
NOSHRINK	= F	TIMID	= F	VARYU	= T
VARYV	= T				

Integer control parameters

FILTER =	0	ICHEAT =	1	ICONV =	1	ICUBIC =	0	IGRAPH =	0	IREP =	0
IRESET =	0	MFEMAX =	30000	MINMAX =	5000	NSETC =	4	NSETCF =	8	NSETV =	4
NSETVF =	8	NSMAX =	20	OFREQ =	0	OFROM =	0	PAGEL =	51		

Real control parameters

BDTOL =	0.1000000E+00	BFSTOL =	0.1000000E-05	CTOL =	0.1000000E-02	DIFTOL =	0.5000000E-03
GTOL =	0.1000000E-01	LMTOL =	0.1000000E+00	MTOL =	0.5000000E+00	MU =	0.1000000E-03
OMEGA =	0.1000000E+00	OMEGAR =	0.1000000E+00	QNTOL =	0.1000000E-05	QNTOLU =	0.1000000E-05
QRTOL =	0.1000000E+02	QTOL =	0.1000000E+00	RHMAX =	0.5000000E+01	RTOL =	0.5000000E+00
STOL =	0.1000000E+01	SUBTOL =	0.1000000E-05	UDEC =	0.5000000E+00	UINC =	0.2000000E+01
UMAX =	0.1000000E+00	UMIN =	0.1000000E-05	VDEC =	0.5000000E+00	VINC =	0.2000000E+01
VMAX =	0.1000000E+00	VMINC =	0.1000000E-05	VMINF =	0.1000000E-02	XTOLGL =	0.1000000E-05
XTOLU =	0.5000000E-05	XTOLV =	0.5000000E-05	ZETAG =	0.1000000E-05	ZETAP =	0.1000000E-05
ZFACTG =	0.9999000E+00	ZFACTP =	0.9999000E+00				

End of input data

Machine epsilon = 0.1192093E-06

```
**********  Stealth Combat Aircraft MVO Version 2.0 / NOV 1994  **********
**********  Dipl.-Ing. Frank Siegers  -  Cranfield University   **********
-------------------------------------------------------------------------

      Begin of user information  -  STARTING POINT

NO AREA RULING   -
SINGLE COCKPIT, THREE INTERNAL WEAPONS BAYS, IN- AND OUTBOARD
TWO ENGINES- FIXED INTAKES, LOCATED AT COCKPIT SIDE
VERTICAL AND HORIZONTAL TAILS -  SINGLE FIN
MAIN GEAR: LEG STOWED REARWARD - WHEEL STOWED VERTICALLY
OBJECTIVE FUNCTION IS EMPTY MASS

         Summary of design data
    Take-off mass:           18523.43 [kg]
    Fuel mass fraction:          0.278
    Wing mass loading at T/O:  500.633 [kg/m2]
    Thrust loading at T/O:       1.002
    Datum sea-level thrust:   182056.000 [N]

       GEOMETRY
-------------------------------------------------------------------------------------------
    FUSELAGE STATION DATA
 FUSELAGE SECTION  ,|   A    |   B    |   C    |   D    |   E    |   F    |   G    |   H
 STATION [m]        |  2.57  |  4.21  |  5.02  |  6.86  |  8.69  | 10.57  | 12.33  | 13.28
 X-SECT AREA [m^2]  |  1.37  |  2.62  |  4.06  |  5.04  |  5.31  |  5.68  |  5.69  |  4.15
 MIN. X-SECT AREA   |  1.29  |  2.47  |  2.44  |  4.00  |  5.23  |  4.48  |  2.09  |  2.07
 WIDTH [m]          |  1.49  |  2.18  |  3.35  |  3.15  |  3.39  |  4.49  |  3.84  |  3.23
 HEIGHT [m]         |  1.71  |  2.35  |  2.01  |  2.05  |  2.05  |  1.77  |  2.35  |  1.21
 BOATTAIL ANGLE (GRFN):      22.313 | MAXIMUM:   22.314 | RANGE: 0.0 TO   25.000
-------------------------------------------------------------------------------------------
    FAIRING CURVE DATA
 AIRCRAFT LENGTH [m]   15.79
 FUSELAGE WETAREA     112.71
 FUSELAGE VOLUME       53.13
   X1     1.112 |  X2     3.802 |  X3     8.196|  X4   ,  9.395 |  X5    13.662 |  XFN   14.189
  OTM     4.597 | OTF3K  -0.179 | OTF4K   0.014| OTA3K ,  0.421 | OTA4K  -0.128
-------------------------------------------------------------------------------------------
    DIFFUSER GEOMETRY
 LENGTH [m]          :   5.55
 INTAKE AREA         :   0.71
 DIAMETER AT ENGINE  :   0.80
 DIVERTER AREA       :   0.11
 INTAKE SIDE CANT    :  20.00
-------------------------------------------------------------------------------------------
    WING GEOMETRY
 SPAN     10.54| ROOT C    6.38| TIP C     0.64| AREA     37.00| A.RATIO  3.005| T.RATIO 0.1000
 LE SWP   51.07| TE SWP    8.47| 1/4C SW  44.00| T/C RAT 0.0636| MAC       4.29| BTANK    10.31
-------------------------------------------------------------------------------------------
```

EMPENNAGE GEOMETRY

HOR. STABILIZER :	NET SPN	5.22	ROOT C	2.30	TIP C	0.69	AREA	7.79	A.RATIO	3.500	T.RATIO	0.3000	
	LE SWP	51.07	TE SWP	31.91	1/2C SW	42.93	T/C RAT	0.0300	MAC	1.64	VOL RTO	0.3000	
VERT STABILIZER :	NET SPN	4.08	ROOT C	4.48	TIP C	1.34	AREA/FIN	11.89	A.RATIO	1.400	T.RATIO	0.300	
	LE SWP	45.00	TE SWP	12.99	1/2C SW	31.61	T/C RAT	0.0600	MAC	3.20	VOL RTO	2.000	

ENGINE BAY GEOMETRY (PER ENG.)

SECTION DATA	STN 1	STN 2	STN 3	STN 4		
WIDTH [m] :	1.03	1.03	1.14	1.09		
HEIGHT [m] :	1.36	1.27	0.85	0.60		
X-SECT. AREA :	1.09	1.02	0.96	0.65		
BAY DATA	TOTAL	BAY 1-2	BAY 2-2A	BY 2A-2B	TRANSIT.	NOZZLE
LENGTH [m] :	3.62	1.76	0.46	0.49	0.00	0.91
VOLUME :	6.47	3.73	1.26	----	0.00	1.47

ENGINE CENTERLINE SEPARATION [m] : 1.27

LANDING GEAR GEOMETRY [m]

MAIN GEAR LEG LENGTH :	1.52	NOSE GEAR LEG LENGTH :	1.12
MAIN GEAR WHEEL DIAMETER :	0.92	NOSE GEAR WHEEL DIAMETER :	0.62
MAIN GEAR WHEEL WIDTH :	0.27	NOSE GEAR WHEEL WIDTH :	0.15

INTERNAL WEAPONS BAY DIMENSIONS [m]

VENTRAL BAY WIDTH :	0.45	VENTRAL BAY LENGTH :	3.65	VENTRAL BAY HEIGHT :	0.38
OUTBOARD BAY WIDTH :	0.23	OUTBOARD BAY LENGTH :	3.05	OUTBOARD BAY HEIGHT :	0.23

MASS BREAKDOWN

FUSELAGE :	3531.1	[SHELL	1394.8	INTERNAL	1416.4	WIND SCREEN	36.2	CANOPY	53.4		
		AIR BRAKE	27.8	INTAKE RAMP	0.0	MISCELLAN.	205.0				
		WBAY DOORS	83.2	WBAY ROOF	87.9	WBAY MISC	481.3				
WING :	1219.9	[BOX	938.9	LEADG EDGE	60.8	TRAIL EDGE	89.4	FLAPS + TRK	61.4		
		AILERONS	8.4	SPOILERS	0.0	R.A.M.	0.0	MISCELLAN.	54.5		
EMPENNAGE:	701.7	[TAIL	306.5	FIN(S)	395.2						
ENGINE :	3124.1	[GAS GENER.	1923.6	REHEAT+NOZ	593.4	THRUST REV.	260.1	INSTALLATN.	347.1		
SYSTEMS :	2536.2	[MAIN UC	670.4	NOSE UC	103.4	UC HYDRAUL.	107.5	AIR SYSTEM	185.5		
		CONTROLS	559.5	ELECTRIC	518.9	FUEL SYSTEM	390.9				
FIXED EQ :	1390.0	[COCKPIT	180.0	GUN	160.0	RADAR	200.0	AVIONICS	700.0		
		PYLONS	0.0	RESIDUAL FUL	50.0	INTL LAUNCH.	100.0				
PAYLOAD :	870.0	[CREW	90.0	AMMO	80.0	TANKS	0.0	STORE 1	0.0		
		STORE 2	0.0	WBAY STRS OB	200.0	WBAY STRS IB	500.0				
FUEL :	5150.4	[FRONT FUS.	700.3	CENTER FUS.	2924.1	REAR FUS.	0.0	WING BOX	1115.8		
		FIN	410.2	EXTERNAL	0.0						
		[UTIL FRONT	0.5780	UTIL CENTER	0.1694	UTIL REAR	0.0000	UTIL WBOX	0.9000		
		UTIL FIN	0.5000								
TOTAL :	18523.4	[EMPTY	12453.1	COMBAT	16527.6	LANDING	15223.2				

CENTER OF GRAVITY CALCULATION

COMPONENT	CG-POS	MOMENT ,
FUSELAGE STRUCTURE	8.46	26502.33
WING EXCLUDING FUEL	8.93	10890.57
WEAPONS BAY (INBOARD)	0.00	0.00
WEAPONS BAY (OUTBOARD)	0.00	0.00
EMPENNAGE - FIN	12.53	4953.57
EMPENNAGE - TAILPLANE	13.67	4121.35
AVIONICS - RADAR	1.22	244.44
AVIONICS - FORWARD BAY	2.07	1450.53
AVIONICS - REARWARD BAY	5.02	0.00
GUN - AMMUNITION	5.02	401.73
GUN	2.57	411.55
AIR SYSTEM EXCL. DISTRIB.	5.02	698.81
COCKPIT AND CREW	3.50	945.22
NOSE UNDERCARRIAGE	2.29	236.72
MAIN UNDERCARRIAGE	8.94	5995.53
ELECTRICAL SYSTEM	10.57	3290.63
ENGINE - GAS GENERATOR	11.45	22027.44
ENGINE - REHEAT + NOZZLE	13.26	7868.43
ENGINE - THRUST REVERSER	13.73	3571.64
ENGINE - INSTALLATION	12.38	4297.21
FUEL IN FRONT FUSELAGE	4.02	2813.39
FUEL IN CENTER FUSELAGE	7.80	22795.34
FUEL IN REAR FUSELAGE	11.29	0.00
FUEL IN EXPOSED WING	9.70	10819.38
FUEL IN FIN	12.53	5140.62
INTERNAL STORES INBOARD	0.00	0.00
INTERNAL STORES OUTBOARD	0.00	0.00

X	PFX	OFX
0.44	1.39	0.18
0.87	2.78	0.37
1.21	3.27	0.52
1.55	3.76	0.70
1.89	4.25	0.91
2.23	4.74	1.13
2.57	5.23	1.37
2.98	5.40	1.67
3.39	5.57	1.98
3.80	5.74	2.30
4.21	5.91	2.62
4.61	6.67	2.93
5.02	7.44	3.23
5.02	10.01	4.06
5.63	9.69	4.48
6.25	9.38	4.85
6.86	9.06	5.04
7.22	9.19	5.16
7.59	9.32	5.25

FORWARD CG LIMIT	8.38
CG WITH FULL TANKS, INTERNAL STORES	8.13
CG WITH EMPTY TANKS, NO INTERNAL STORES	8.66
AFT CG LIMIT	8.91

7.96	9.45	5.30
8.33	9.58	5.31
8.69	9.71	5.31
9.16	10.13	5.31
9.63	10.56	5.33
10.10	10.98	5.48
10.57	11.40	5.68
11.16	10.95	5.92
11.75	10.50	5.97
12.33	10.05	5.69
12.57	9.82	5.45
12.80	9.58	5.12
13.04	9.35	4.69
13.28	9.11	4.15
13.50	8.52	3.52
13.73	7.94	2.76
13.96	7.35	1.88
14.19	6.76	0.86
15.79	0.00	0.00

1 SORTIE PERFORMANCE

STAGE	:	1	2	3	4	5	6
STAGE TYPE	:	CRUISE R	CRUISE R	COMBAT T	COMBAT T	CRUISE R	CRUISE R
HEIGHT M	:	10000.	70.	70.	70.	70.	10000.
MACH	:	0.700	0.900	0.800	0.800	0.900	0.700
END MASS	:	16254.2	15533.7	14912.2	14475.9	13760.0	12154.8
RANGE KM	:	600.0	100.0	9.7	19.4	100.0	600.0
TIME SEC	:	2861.6	326.8	35.6	71.2	326.8	2861.6
LOAD FACTOR	:	1.000	1.000	5.000	5.000	1.000	1.000
MID-MASS CL	:	0.4875	0.0729	0.4303	0.4196	0.0648	0.3671
ALPHA	:	8.738	1.206	7.419	7.235	1.071	6.580
CD TOTAL	:	0.05543	0.02071	0.04598	0.04468	0.02054	0.04051
CD VORTEX	:	0.03517	0.00087	0.02739	0.02605	0.00068	0.01994
CD0 CLEAN	:	0.01810	0.01626	0.01628	0.01628	0.01626	0.01810
CD0 STORES	:	0.00000	0.00000	0.00000	0.00000	0.00000	0.00000
CD SPILL	:	0.00004	0.00146	0.00019	0.00023	0.00147	0.00035
CD BASE	:	0.00212	0.00212	0.00212	0.00212	0.00212	0.00212
THROTTLE PC	:	3.10	2.24	3.29	3.23	2.23	2.50
THRUST N	:	31313.	99240.	135142.	132177.	98737.	24610.
FUEL KG/S	:	0.7021	2.2051	3.4130	3.3218	2.1908	0.5330
AIR KG/S	:	58.695	181.563	211.081	208.464	181.106	51.618
FUEL USED	:	2009.1	720.6	121.4	236.4	715.9	1525.2

FUEL FOR : TAKE-OFF 260.1, RESERVES AND LANDING 257.5, UNUSED -695.85

COMBAT THRUST/WT = 1.6595 EXCESS SEP = 345.79 M/S

POINT PERFORMANCE

NO.	TYPE	LEG	%FUEL	POTENTIAL	REQUIRED	HEIGHT	MACH	THROTTLE	CL-START	ALPHA	CDTOT	CD0GROSS	CDV
ACCELERATION REQUIRED FROM M = 0.800 TO M = 1.400													
1	ACCEL	1	50.0	1.069E+02	6.000E+01	10000.	0.80	10.00	0.11163	1.74540	0.07979	0.07795	0.00184
2	M MAX	1	50.0	1.128E+00	1.100E+00	0.	1.13	10.00	0.04540	0.69563	0.07825	0.07781	0.00044
3	M MAX	1	50.0	1.598E+00	1.600E+00	10000.	1.60	10.00	0.08556	1.52757	0.07877	0.07725	0.00152
4	S E P	1	50.0	1.042E+02	1.000E+02	10000.	0.90	10.00	0.28044	4.63547	0.03086	0.01770	0.01164
5	S T R	1	50.0	5.975E+00	7.000E+00	10000.	0.90	10.00	0.81118	13.40763	0.13425	0.01770	0.11503
6	S T R	1	50.0	1.751E+01	1.600E+01	1000.	0.80	10.00	0.83857	14.45780	0.14091	0.01630	0.12295
7	A T R	1	50.0	8.800E+00	1.000E+01	10000.	0.90	10.00	1.16000	19.17398	0.27677	0.01770	0.25755
8	RIDEQ	1	50.0	2.307E+00	5.000E+00	1000.	0.80	10.00	0.10495	1.80948	0.01958	0.01630	0.00163

TAKE-OFF GROUND ROLL M 511. 600. (TOTAL TOD 722. AIR TO 15M 211.)

LANDING APPROACH SPEED M/S 77.3 70.0 (CLMAX FOR LANDING = 1.488)

STARTING POINT

Variables

Index	Status	Counter	Lower bound	Value	Upper bound	Derivative of Lagrangian	User title
1	dependent	-1	0.3500000E+00	0.1300400E+01	0.3000000E+01	0.2980232E-07	Engine Scale Factor
2	independent	-1	0.5000000E+01	0.3700000E+02	0.1000000E+03	0.3417182E+04	Wing Area
3	dependent	-1	0.0000000E+00	0.4400000E+02	0.6000000E+02	0.0000000E+00	Wing 1/4 chrd Sweep
4	independent	-1	0.2000000E-01	0.6360000E-01	0.1000000E+00	-0.7584866E+02	Wing T/C Ratio
5	independent	-1	0.5000000E-01	0.1000000E+00	0.9900000E+00	-0.8767950E+01	Wing Taper Ratio
6	dependent	-1	0.1500000E+01	0.3005000E+01	0.1000000E+02	0.1117587E-07	Wing Aspect Ratio
7	independent	-1	0.5000000E-01	0.1500000E+00	0.3000000E+00	0.6264589E+02	Wing F.Spar/chord
8	independent	-1	0.5000000E+00	0.6000000E+00	0.8000000E+00	-0.1417361E+03	Wing R.Spar/chord
9	independent	-1	0.0000000E+00	0.6500000E+00	0.1000000E+01	-0.7624345E+01	Span T/E Flaps
10	independent	-1	0.0000000E+00	0.9676000E+00	0.1000000E+01	0.3160878E+01	Span W. Net F. Box
11	independent	-1	0.5000000E+01	0.1418900E+02	0.5000000E+02	0.1959270E+02	Fuselage Length
12	independent	-1	0.0000000E+00	0.5500000E+00	0.1000000E+01	-0.8751831E+00	Fairing: RLTMFN
13	dependent	-1	0.0000000E+00	0.4000000E+00	0.5000000E+00	-0.5960464E-07	Fairing: RLTFFN
14	independent	-1	0.0000000E+00	0.2000000E+00	0.9900000E+00	-0.3009534E+01	Fairing: RLTCFN
15	dependent	-1	0.5000000E+00	0.8900000E+00	0.9900000E+00	-0.2607703E-07	Fairing: RLTAFN
16	dependent	-1	0.0000000E+00	0.6000000E+00	0.1000000E+01	0.1490116E-07	Wing 1/4 pos RXWCQM
17	dependent	-1	-0.5000000E+01	0.1418000E+00	0.5000000E+01	0.4842877E-07	Fairing: OT6NVAR
18	independent	-1	0.0000000E+00	0.5780000E+00	0.8000000E+00	-0.6976895E+01	Fuel Frac. Frt. Fus
19	dependent	-1	0.0000000E+00	0.1694000E+00	0.9000000E+00	0.0000000E+00	Fuel Frac. Ctr. Fus
20	dependent	-1	0.0000000E+00	0.0000000E+00	0.8000000E+00	0.0000000E+00	Fuel Frac. Rer. Fus
21	not optimized		0.8000000E+00	0.8608000E+00	0.1000000E+01		Rat Fin Mmt Arm/Wng
22	not optimized		0.8000000E+00	0.9522000E+00	0.1000000E+01		Rat Emp Mmt Arm/Wng
23	dependent	-1	0.3000000E+00	0.5400000E+00	0.7000000E+00	0.0000000E+00	W.Bay 1 cg X-coord
24	independent	-1	0.3000000E+00	0.5400000E+00	0.7000000E+00	-0.1270433E+02	W.Bay 2 cg X-coord
25	not optimized		-0.5000000E-01	0.0000000E+00	0.1500000E+00		W.Bay 1 cg Z-coord
26	not optimized		-0.5000000E-01	0.0000000E+00	0.1500000E+00		W.Bay 2 cg Z-coord
27	not optimized		0.1122000E+01	0.1122000E+01	0.3000000E+01		Eng. Separation - Y

Functions

Index	Status	Counter	Lower bound	Value	Upper bound	Lagrange multiplier	Norm of gradient	User title
1	inactive single	0		-0.1366764E+01	0.0			Wing and Tail Separation
2	inactive single	0		-0.2777712E+00	0.0			AR and Sweep
3	inactive single	0		-0.7573962E-01	0.0			Excess Area at A
4	inactive single	0		-0.1419458E+00	0.0			Excess Area at B
5	inactive single	0		-0.1616433E+01	0.0			Excess Area at C
6	inactive single	0		-0.1040570E+01	0.0			Excess Area at D
7	inactive single	0		-0.7862902E-01	0.0			Excess Area at E
8	inactive single	0		-0.1200676E+01	0.0			Excess Area at F
9	inactive single	0		-0.3602033E+01	0.0			Excess Area at G
10	inactive single	0		-0.2082032E+01	0.0			Excess Area at H
11	inactive single	0		-0.2686337E+01	0.0			Upper value for boattail
13	inactive single	0		-0.1621538E+01	0.0			Intake and wing separation
14	inactive single	0		-0.5017685E+01	0.0			Fuselage len - gun
15	inactive single	0		-0.5584636E+01	0.0			Fuselage len - nose u.c.
16	inactive single	0		-0.3367685E+01	0.0			Fuselage len - weapons bay
17	inactive single	0		-0.1500453E+01	0.0			Min diffuser length - area
18	inactive single	0		-0.1110804E+02	0.0			Vol in rear fus. - fuel
20	equality			0.4505725E+00	0.0	-0.1157382E-01	0.1038842E+01	Nozzle area incr
21	inactive single	0		-0.2773410E+00	0.0			A/C c.g. - fwd lim - empty
22	single inequality	1		0.2533167E+00	0.0	0.7669245E-03	0.1991641E+01	A/C c.g. - fwd lim - full
23	inactive single	0		-0.1518545E+00	0.0			A/C c.g. -rear lim - empty
24	inactive single	0		-0.6825123E+00	0.0			A/C c.g. - rear lim - full
25	inactive single	0		-0.3131220E+01	0.0			Min diff length - curv.
26	single inequality	1		0.4205999E+00	0.0	-0.6246059E-02	0.1009367E+01	Fair curve negcurvature
29	equality			-0.6958453E+03	0.0	0.9384679E+00	0.1278527E+05	Excess fuel after sortie
31	inactive single	0		-0.8932715E+02	0.0			Unused take-off distance
32	single inequality	1		0.1226711E+00	0.0	-0.9572895E-01	0.1005865E+01	Stall - landing approach
33	inactive single	0		-0.2006333E+03	0.0			Take-off wing load - min.
36	inactive single	0		-0.6154823E+00	0.0			Sep. dist. wbay intake
37	single inequality	1		0.4944649E+00	0.0	-0.2265234E-02	0.2010141E+01	Sep. dist. wbay main gear
38	inactive single	0		-0.1082815E+01	0.0			Sep. dist. wbay compressor
39	single inequality	1		0.2281934E+00	0.0	0.2233912E-04	0.1518260E+01	Sep. dist. wbay cockpit
45	inactive single	0		-0.2106945E+02	0.0			Minimum Leading Edge Sweep
50	single inequality	1		0.4688315E+02	0.0	0.2167851E-02	0.4620396E+03	Accel for Mach Increment
51	inactive single	0		-0.2833474E-01	0.0			Max Mach
52	inactive single	0		0.1789927E-02	0.0			Max Mach
53	inactive single	0		-0.4206276E+01	0.0			SEP
54	single inequality	1		0.1025275E+01	0.0	0.1551774E+00	0.7162215E+01	STR
55	inactive single	0		-0.1506943E+01	0.0			STR
56	single inequality	1		0.1200397E+01	0.0	-0.2013646E+01	0.9799249E+01	ATR
57	inactive single	0		-0.2693295E+01	0.0			Ride Quality
75	objective			0.1245308E+05			0.7511226E+04	Objective function (MTE)

Begin of user information - FINAL POINT

Summary of design data

Take-off mass:	16148.35 [kg]
Fuel mass fraction:	0.283
Wing mass loading at T/O:	438.718 [kg/m2]
Thrust loading at T/O:	0.944
Datum sea-level thrust:	149505.359 [N]

GEOMETRY

FUSELAGE STATION DATA

FUSELAGE SECTION ,	A	B	C	D	E	F	G	H
STATION [m]	2.57	4.21	5.02	6.80	8.57	11.56	13.20	14.18
X-SECT AREA [m^2]	1.04	1.61	2.55	2.92	3.25	3.47	2.79	1.75
MIN. X-SECT AREA	0.87	1.34	2.19	2.63	3.25	3.36	1.89	1.75
WIDTH [m]	1.17	1.56	2.51	2.82	2.92	3.57	2.84	2.44
HEIGHT [m]	1.02	1.65	1.31	1.35	1.35	1.35	1.53	0.78

BOATTAIL ANGLE (GREEN): 1.076 | MAXIMUM: 9.508 | RANGE: 0.0 TO 25.000

FAIRING CURVE DATA

AIRCRAFT LENGTH [m]	15.90										
FUSELAGE WETAREA	93.85										
FUSELAGE VOLUME	34.42										
X1	1.112	X2	3.689	X3	11.510	X4	12.010	X5	13.917	XFN	15.011
OTM	2.883	OTF3K	-0.027	OTF4K	0.000	OTA3K	-0.623	OTA4K	0.119		

DIFFUSER GEOMETRY

LENGTH [m]	:	6.54
INTAKE AREA	:	0.59
DIAMETER AT ENGINE	:	0.72
DIVERTER AREA	:	0.10
INTAKE SIDE CANT	:	20.00

WING GEOMETRY

SPAN	11.92	ROOT C	5.48	TIP C	0.70	AREA	36.81	A.RATIO	3.858	T.RATIO	0.1270
LE SWP	44.78	TE SWP	10.72	1/4C SW	38.36	T/C RAT	0.0628	MAC	3.71	BTANK	9.95

EMPENNAGE GEOMETRY

HOR. STABILIZER :	NET SPN	4.52	ROOT C	1.99	TIP C	0.60	AREA	5.84	A.RATIO	3.500	T.RATIO 0.3000
	LE SWP	44.78	TE SWP	20.65	1/2C SW	34.40	T/C RAT	0.0300	MAC	1.42	VOL RTO 0.3000
VERT STABILIZER :	NET SPN	2.93	ROOT C	3.22	TIP C	0.97	AREA/FIN	6.15	A.RATIO	1.400	T.RATIO 0.300
	LE SWP	45.00	TE SWP	12.99	1/2C SW	31.61	T/C RAT	0.0600	MAC	2.30	VOL RTO 2.000

ENGINE BAY GEOMETRY (PER ENG.)

SECTION DATA	STN 1	STN 2	STN 3	STN 4
WIDTH [m]	0.94	0.95	1.03	0.99
HEIGHT [m]	1.28	1.19	0.78	0.54
X-SECT. AREA	0.95	0.88	0.80	0.54

BAY DATA	TOTAL	BAY 1-2	BAY 2-2A	BY 2A-2B	TRANSIT.	NOZZLE
LENGTH [m]	3.45	1.64	0.41	0.57	0.00	0.83
VOLUME	5.77	3.00	1.66	----	0.00	1.11

ENGINE CENTERLINE SEPARATION [m] : 1.16

LANDING GEAR GEOMETRY [m]

MAIN GEAR LEG LENGTH	1.41	NOSE GEAR LEG LENGTH	1.04
MAIN GEAR WHEEL DIAMETER	0.85	NOSE GEAR WHEEL DIAMETER	0.58
MAIN GEAR WHEEL WIDTH	0.25	NOSE GEAR WHEEL WIDTH	0.15

INTERNAL WEAPONS BAY DIMENSIONS [m]

VENTRAL BAY WIDTH	0.45	VENTRAL BAY LENGTH	3.65	VENTRAL BAY HEIGHT	0.38
OUTBOARD BAY WIDTH	0.23	OUTBOARD BAY LENGTH	3.05	OUTBOARD BAY HEIGHT	0.23

MASS BREAKDOWN

FUSELAGE	2783.9	SHELL	1149.9	INTERNAL	962.6	WIND SCREEN	36.2	CANOPY	53.4		
		AIR BRAKE	27.8	INTAKE RAMP	0.0	MISCELLAN.	156.1				
		WBAY DOORS	83.2	WBAY ROOF	87.9	WBAY MISC	481.7				
WING	1325.8	BOX	1166.1	LEADG EDGE	24.6	TRAIL EDGE	45.7	FLAPS + TRK	10.5		
		AILERONS	11.0	SPOILERS	0.0	R.A.M.	0.0	MISCELLAN.	59.6		
EMPENNAGE	370.8	TAIL	208.3	FIN(S)	162.5						
ENGINE	2622.6	GAS GENER.	1595.7	REHEAT+NOZ	521.9	THRUST REV.	213.6	INSTALLATN.	291.4		
SYSTEMS	2211.6	MAIN UC	575.5	NOSE UC	90.4	UC HYDRAUL.	93.7	AIR SYSTEM	159.4		
		CONTROLS	489.9	ELECTRIC	455.5	FUEL SYSTEM	347.1				
FIXED EQ	1390.0	COCKPIT	180.0	GUN	160.0	RADAR	200.0	AVIONICS	700.0		
		PYLONS	0.0	RESIDUAL FUL	50.0	INTL LAUNCH.	100.0				
PAYLOAD	870.0	CREW	90.0	AMMO	80.0	TANKS	0.0	STORE 1	0.0		
		STORE 2	0.0	WBAY STRS OB	200.0	WBAY STRS IB	500.0				
FUEL	4573.7	FRONT FUS.	54.2	CENTER FUS.	2356.0	REAR FUS.	32.2	WING BOX	1978.6		
		FIN	152.7	EXTERNAL	0.0						
		UTIL FRONT	0.1637	UTIL CENTER	0.2065	UTIL REAR	0.0134	UTIL WBOX	0.9000		
		UTIL FIN	0.5000								
TOTAL	16148.3	EMPTY	10654.6	COMBAT	13289.7	LANDING	13194.1				

CENTER OF GRAVITY CALCULATION

COMPONENT	CG-POS	MOMENT ,
FUSELAGE STRUCTURE	8.75	20869.62
WING EXCLUDING FUEL	8.78	11640.71
WEAPONS BAY (INBOARD)	0.00	0.00
WEAPONS BAY (OUTBOARD)	0.00	0.00
EMPENNAGE - FIN	13.15	2137.25
EMPENNAGE - TAILPLANE	14.43	3006.52
AVIONICS - RADAR	1.22	244.44

FORWARD CG LIMIT	8.34
CG WITH FULL TANKS, INTERNAL STORES	8.34
CG WITH EMPTY TANKS, NO INTERNAL STORES	8.71
AFT CG LIMIT	8.71

AVIONICS - FORWARD BAY	:	2.07	1450.53 |
AVIONICS - REARWARD BAY	:	5.02	0.00 |
GUN - AMMUNITION	:	5.02	401.73 |
GUN	:	2.57	411.55 |
AIR SYSTEM EXCL. DISTRIB.	:	5.02	600.41 |
COCKPIT AND CREW	:	3.50	945.22 |
NOSE UNDERCARRIAGE	:	2.24	202.39 |
MAIN UNDERCARRIAGE	:	8.82	5076.68 |
ELECTRICAL SYSTEM	:	11.56	3158.50 |
ENGINE - GAS GENERATOR	:	12.38	19751.50 |
ENGINE - REHEAT + NOZZLE	:	14.10	7360.46 |
ENGINE - THRUST REVERSER	:	14.60	3117.69 |
ENGINE - INSTALLATION	:	13.28	3871.04 |
FUEL IN FRONT FUSELAGE	:	4.02	217.89 |
FUEL IN CENTER FUSELAGE	:	8.29	19530.99 |
FUEL IN REAR FUSELAGE	:	12.25	394.37 |
FUEL IN EXPOSED WING	:	9.22	18244.87 |
FUEL IN FIN	:	13.15	2007.62 |
INTERNAL STORES INBOARD	:	0.00	0.00 |
INTERNAL STORES OUTBOARD	:	0.00	0.00 |

X	PFX	OFX
0.44	1.39	0.18
0.87	2.78	0.37
1.21	2.98	0.51
1.55	3.17	0.65
1.89	3.36	0.78
2.23	3.55	0.91
2.57	3.74	1.04
2.98	3.84	1.19
3.39	3.94	1.34
3.80	4.04	1.48
4.21	4.15	1.61
4.61	4.57	1.74
5.02	5.00	1.86
5.02	7.33	2.55
5.61	7.35	2.72
6.20	7.37	2.87
6.80	7.39	2.92
7.15	7.47	2.99
7.51	7.55	3.06
7.86	7.63	3.13
8.22	7.71	3.19
8.57	7.79	3.25
9.32	8.08	3.34
10.06	8.37	3.41
10.81	8.66	3.46
11.56	8.95	3.47
12.10	8.37	3.46
12.65	7.80	3.25

13.20	7.22	2.79
13.44	6.97	2.54
13.69	6.72	2.27
13.94	6.47	2.01
14.18	6.22	1.75
14.39	6.20	1.54
14.60	6.17	1.36
14.80	6.15	1.20
15.01	6.13	1.07
15.90	0.00	0.00

1 SORTIE PERFORMANCE

STAGE :	1	2	3	4	5	6
STAGE TYPE :	CRUISE R	CRUISE R	COMBAT T	COMBAT T	CRUISE R	CRUISE R
HEIGHT M :	10000.	70.	70.	70.	70.	10000.
MACH :	0.700	0.900	0.800	0.800	0.900	0.700
END MASS :	14479.2	13862.2	13272.6	12897.3	12283.2	11023.3
RANGE KM :	600.0	100.0	9.7	19.4	100.0	600.0
TIME SEC :	2861.6	326.8	35.6	71.2	326.8	2861.6
LOAD FACTOR:	1.000	1.000	5.000	5.000	1.000	1.000
MID-MASS CL:	0.4363	0.0656	0.3880	0.3784	0.0583	0.3342
ALPHA :	6.687	0.899	5.649	5.509	0.799	5.123
CD TOTAL :	0.04001	0.01804	0.03397	0.03316	0.01793	0.03119
CD VORTEX :	0.02191	0.00055	0.01733	0.01649	0.00044	0.01286
CD0 CLEAN :	0.01604	0.01442	0.01443	0.01443	0.01442	0.01604
CD0 STORES :	0.00000	0.00000	0.00000	0.00000	0.00000	0.00000
CD SPILL :	0.00013	0.00114	0.00028	0.00031	0.00115	0.00036
CD BASE :	0.00193	0.00193	0.00193	0.00193	0.00193	0.00193
THROTTLE PC:	2.82	2.33	3.05	3.00	2.32	2.38
THRUST N :	23069.	84223.	101707.	99878.	83907.	19159.
FUEL KG/S :	0.5087	1.8882	2.5191	2.4636	1.8792	0.4123
AIR KG/S :	45.438	151.570	165.129	163.502	151.284	41.244
FUEL USED :	1455.6	617.0	89.6	175.3	614.1	1179.9

FUEL FOR : TAKE-OFF 213.6, RESERVES AND LANDING 228.7, UNUSED 0.00

COMBAT THRUST/WT = 1.5337 EXCESS SEP = 337.12 M/S

0 POINT PERFORMANCE

NO.	TYPE	LEG	%FUEL	POTENTIAL	REQUIRED	HEIGHT	MACH	THROTTLE	CL-START	ALPHA	CDTOT	CD0GROSS	CDV
ACCELERATION REQUIRED FROM M = 0.800 TO M = 1.400													
1	ACCEL	1	50.0	6.000E+01	6.000E+01	10000.	0.80	10.00	0.09847	1.38264	0.04595	0.04483	0.00112
2	M MAX	1	50.0	1.325E+00	1.100E+00	0.	1.33	10.00	0.02915	0.37903	0.04548	0.04393	0.00010
3	M MAX	1	50.0	1.881E+00	1.600E+00	10000.	1.88	10.00	0.05438	1.24110	0.04388	0.04341	0.00048
4	S E P	1	50.0	1.000E+02	1.000E+02	10000.	0.90	10.00	0.24502	3.35622	0.02407	0.01569	0.00691
5	S T R	1	50.0	6.989E+00	7.000E+00	10000.	0.90	10.00	0.82996	11.36872	0.11198	0.01603	0.09449
6	S T R	1	50.0	2.025E+01	1.600E+01	1000.	0.80	10.00	0.85999	12.51945	0.11757	0.01445	0.10154
7	A T R	1	50.0	9.975E+00	1.000E+01	10000.	0.90	10.00	1.16000	15.88960	0.21759	0.01569	0.20043
8	RIDEQ	1	50.0	3.127E+00	5.000E+00	1000.	0.80	10.00	0.09169	1.33482	0.01699	0.01445	0.00097

0TAKE-OFF GROUND ROLL M 439. 600. (TOTAL TOD 640. AIR TO 15M 201.)

LANDING APPROACH SPEED M/S 70.9 70.0 (CLMAX FOR LANDING = 1.610)

End of iteration number 114

CONVERGENCE DETECTED [Code B] after 8390 calls to user routine

Variables

Index	Status	Counter	Lower bound	Value	Upper bound	Derivative of Lagrangian	User title
1	dependent	-1	0.3500000E+00	0.1067895E+01	0.3000000E+01	-0.7450581E-07	Engine Scale Factor
2	independent	-1	0.5000000E+01	0.3680802E+02	0.1000000E+03	0.7708766E+03	Wing Area
3	independent	-1	0.0000000E+00	0.3836365E+02	0.6000000E+02	-0.9500384E+02	Wing 1/4 chrd Sweep
4	dependent	-1	0.2000000E-01	0.6278772E-01	0.1000000E+00	0.2980232E-07	Wing T/C Ratio
5	independent	-1	0.5000000E-01	0.1270488E+00	0.9900000E+00	0.6753618E+02	Wing Taper Ratio
6	independent	-1	0.1500000E+01	0.3858015E+01	0.1000000E+02	-0.1354854E+02	Wing Aspect Ratio
7	held at lower bound	0	0.5000000E-01	0.5000000E-01	0.3000000E+00	0.4520992E+02	Wing F.Spar/chord
8	independent	0	0.5000000E+00	0.7705865E+00	0.8000000E+00	-0.7182084E+01	Wing R.Spar/chord
9	independent	-1	0.0000000E+00	0.5363613E+00	0.1000000E+01	-0.4264474E+00	Span T/E Flaps
10	independent	-1	0.0000000E+00	0.7912887E+00	0.1000000E+01	-0.3646231E+01	Span W. Net F. Box
11	independent	-1	0.5000000E+01	0.1501070E+02	0.5000000E+02	0.3335492E+03	Fuselage Length
12	dependent	-1	0.0000000E+00	0.7524151E+00	0.1000000E+01	0.1490116E-07	Fairing: RLTMFN
13	independent	-1	0.0000000E+00	0.2647422E+00	0.5000000E+00	0.9282855E+03	Fairing: RLTFFN
14	independent	-1	0.0000000E+00	0.1427612E+00	0.9900000E+00	-0.8274095E+02	Fairing: RLTCFN
15	independent	-1	0.5000000E+00	0.6355440E+00	0.9900000E+00	0.9347856E+02	Fairing: RLTAFN
16	dependent	-1	0.0000000E+00	0.5629937E+00	0.1000000E+01	0.3699097E-07	Wing 1/4 pos RXWCQM
17	dependent	-1	-0.5000000E+01	0.4864594E+00	0.5000000E+01	-0.8568168E-07	Fairing: OT6NVAR
18	independent	0	0.0000000E+00	0.1637482E+00	0.8000000E+00	0.1511398E+01	Fuel Frac. Frt. Fus
19	dependent	-1	0.0000000E+00	0.2065043E+00	0.9000000E+00	0.1192093E-06	Fuel Frac. Ctr. Fus
20	dependent	4	0.0000000E+00	0.1335260E-01	0.8000000E+00	0.2235174E-07	Fuel Frac. Rer. Fus
21	not optimized		0.8000000E+00	0.8608000E+00	0.1000000E+01		Rat Fin Mmt Arm/Wng
22	not optimized		0.8000000E+00	0.9522000E+00	0.1000000E+01		Rat Emp Mmt Arm/Wng
23	dependent	-1	0.3000000E+00	0.5256419E+00	0.7000000E+00	0.1164153E-09	W.Bay 1 cg X-coord
24	dependent	-1	0.3000000E+00	0.4694369E+00	0.7000000E+00	0.4470348E-07	W.Bay 2 cg X-coord
25	not optimized		-0.5000000E-01	0.0000000E+00	0.1500000E+00		W.Bay 1 cg Z-coord
26	not optimized		-0.5000000E-01	0.0000000E+00	0.1500000E+00		W.Bay 2 cg Z-coord
27	not optimized		0.1122000E+01	0.1122000E+01	0.3000000E+01		Eng. Separation - Y

Functions

Index	Status	Counter	Lower bound	Value	Upper bound	Lagrange multiplier	Norm of gradient	User title
1	inactive single	1		-0.2864028E+01	0.0			Wing and Tail Separation
2	inactive single	2		-0.7152557E-06	0.0			Combina. of AR and Sweep
3	inactive single	1		-0.1718572E+00	0.0			Excess Area at A
4	inactive single	0		-0.2774315E+00	0.0			Excess Area at B
5	inactive single	0		-0.3682978E+00	0.0			Excess Area at C
6	inactive single	0		-0.2908182E+00	0.0			Excess Area at D
7	inactive single	3		0.4560947E-03	0.0			Excess Area at E

8	inactive single	0	-0.1054237E+00	0.0			Excess Area at F
9	inactive single	0	-0.9008241E+00	0.0			Excess Area at G
10	single inequality	1	-0.1072884E-05	0.0	0.2482924E+00	0.9292945E+00	Excess Area at H
11	inactive single	0	-0.1549192E+02	0.0			Upper value for boattail
13	inactive single	1	-0.1054593E+01	0.0			Intake/wing separation
14	inactive single	0	-0.6150093E+01	0.0			Fuselage length - gun
15	inactive single	0	-0.6818956E+01	0.0			Fus length - nose u.c.
16	inactive single	0	-0.4500093E+01	0.0			Fus length - weapons bay
17	inactive single	0	-0.2868307E+01	0.0			Min diff. length - area
19	inactive single	0	-0.3014096E+01	0.0			Vol in rear fus - fuel
20	equality		0.2086163E-06	0.0	-0.2336863E+00	0.1098805E+01	Nozzle area incr.
21	inactive single	0	-0.3707606E+00	0.0			A/C c.g.-fwd lim - empty
22	single inequality	4	-0.5960464E-06	0.0	-0.7852474E-03	0.1436429E+01	A/C c.g.-fwd lim - full
23	inactive single	5	0.1134872E-03	0.0			A/C c.g.-rearlim - empty
24	inactive single	0	-0.3706465E+00	0.0			A/C c.g.-rear lim - full
25	inactive single	0	-0.4346115E+01	0.0			Min diffus len - curv.
26	inactive single	3	-0.6233867E+00	0.0			Fair curve neg curvature
29	equality		-0.2259301E-02	0.0	-0.1714279E+01	0.3206439E+04	Excess fuel after sortie
31	inactive single	0	-0.1609819E+03	0.0			Unused take-off distance
32	inactive single	3	0.1729679E-01	0.0			Stall - landing approach
33	inactive single	0	-0.1387182E+03	0.0			T/O wing loading - min.
36	single inequality	4	0.0000000E+00	0.0	0.7925154E-01	0.1573617E+01	Sep. dist. wbay intake
37	single inequality	4	0.0000000E+00	0.0	0.7887141E-01	0.2127513E+01	Sep. dist. wbay main u/c
38	inactive single	0	-0.1842802E+01	0.0			Sep dist wbay compressor
39	single inequality	1	0.1192093E-06	0.0	0.3166548E-02	0.1591751E+01	Sep. dist. wbay cockpit
45	inactive single	0	-0.1477916E+02	0.0			Min Leading Edge Sweep
50	single inequality	1	0.9918213E-04	0.0	0.2825360E+01	0.1186311E+03	Accel for Mach Increment
51	inactive single	0	-0.2254409E+00	0.0			Max Mach
52	inactive single	0	-0.2813153E+00	0.0			Max Mach
53	single inequality	2	0.1525879E-04	0.0	0.1717327E+00	0.1228483E+03	SEP
54	inactive single	5	0.1058626E-01	0.0			STR
55	inactive single	0	-0.4250341E+01	0.0			STR
56	inactive single	5	0.2499199E-01	0.0			ATR
57	inactive single	0	-0.1873025E+01	0.0			Ride Quality
75	objective		0.1065460E+05			0.5425251E+04	Objective function (MTE)

Convergence criteria

FDATUM =	0.1899760E+01	LDATUM =	0.1899760E+01	GDATUM =	0.1700002E-11
VNORMX =	0.1411690E+00	VNORM =	0.1250000E-01	XTOLV =	0.5000000E-05
GLNORM =	0.9282855E+03	XTOLGL =	0.1000000E-05	RTOL =	0.5000000E-05
UNORMX =	0.1772915E-05	UNORM =	0.1772915E-05	XTOLU =	0.5000000E-05
CNORM =	0.9918213E-02	CMAXV =	0.1000000E-01		

Appendix B: User Guide for the Design Synthesis

This appendix describes the use of the aircraft design synthesis and optimization package along with the graphical user output. It contains instructions on compiling, linking and running the code, the formats of the input and output files and how to use them.

B.1. Getting Started

The design synthesis code was developed on a Sun workstation running the Unix operating system. Written mostly in standard FORTRAN 77, the program can be easily ported to a different platform and recompiled. The only limitations are imposed by the optimizer *RQPMIN*, which contains specific files for three different operating systems: Unix (on Sun workstations), MS-DOS (on PCs) and VAX/VMS.

The following files are needed to get started on the Unix (Sun) version:

File Name	*Description*
`stealth.f`	Contains the design synthesis relationships
`outvar.f`	Contains the interface with *RQPMIN* and output routines for trend and variable analysis.
`rqpmin30.for`	Contains the optimization routines of the method of *RQPMIN*
`sun30.for`	Contains the subroutines specific to the implementation of *RQPMIN* on Sun workstations
`engfile`	The input file containing the engine performance data as a function of Mach number, throttle setting and altitude. It must be specified in the design synthesis input file.
`inputfile`	An input file containing the problem and function data, *RQPMIN* control variables, and the external design constants. See Appendix A for an example.
`varfile`	A text file used to plot a convergence history of design synthesis parameters. The name is specified in the input file.
`trend.out`	A text file used to store user-specified output parameters for trend analysis purposes. This file must exist before program execution begins, but can be empty to begin with.

Table 16: Files to get started.

To get started, the above files must all be located in the same directory. The following procedure for compilation and linking is valid for Sun workstations, but applies in principle to all other operating systems.

First, compile the design synthesis `stealth.f` into an object file named `stealth.o` using the following command:

```
f77 -g -C -c stealth.f
```

`f77` is the Sun FORTRAN compiler. The option `-c` forces it to produce only an object file with the name `stealth.o`. The options `-g` and `-C` force the creation of debugging information, and are not strictly required but recommended for program development. Similar commands are used to compile the *RQPMIN* files `rqpmin30.for` and `sun30.for`, resulting in the object files `rqpmin30.o` and `sun30.o`. The object files are linked with the interface to *RQPMIN*, `outvar.f`, using the following command:

```
f77 -g -C stealth.o rqpmin30.o sun30.o -o stealth outvar.f
```

In this case, the option `-o stealth` instructs the compiler to produce an executable output file named `stealth`.

The design synthesis is invoked by typing `stealth` at the command prompt. The program then asks the user for the name of five different files. Only the in- and output files are required by the program, the other three being optional. The user manual for *RQPMIN* provides more information on the use of the optimizer (Skrobanski, 1994).

B.2. Format of the Input File

The input file contains four sections.

The first section begins with the *RQPMIN* keyword `VARIABLES`, followed by a list of the design variables, the format of which can be found in the *RQPMIN* User's Guide (Skrobanski, 1994). For each variable a switch is used to indicate whether it is to be held constant or remain free for modification by *RQPMIN*. The next section, which begins with the *RQPMIN* keyword `FUNCTIONS`, contains a list of the constraint functions along with their violation tolerances and type (i.e. inequality, equality or double inequality). Constraints may be switched on or off by means of an asterisk in the input line, as described in (Skrobanski, 1994). The third section begins with the *RQPMIN* keyword `CONTROLS`, and contains *RQPMIN* control variables, as described in the User's Guide (Skrobanski, 1994). The following table shows some of the recommended values for *RQPMIN* control variables:

Variable Name	*Suggested Value*
RTOL	0.5
RPMAX	5.0
NFEMAX	30000
NIMAX	5000
SUBTOL	$1.0 \cdot 10^{-6}$
XTOLU	$5.0 \cdot 10^{-6}$
XTOLV	$5.0 \cdot 10^{-6}$

Table 17: Suggested Values for *RQPMIN* Control Variables

Also recommended for inclusion in the input file are the control keywords VARYV and VARYU, a description of which is given in (Skrobanski, 1994).

The section that follows the *RQPMIN* controls contains the values of the external design constants, which control the shape, layout and size of the aircraft as well as the aerodynamic and mass estimation methodologies. Its use follows the format of the sample file shown in Appendix A. The following list is a representation of the order in which the constants appear in the input file, and should be read in conjunction with the sample input file given in Appendix A.

```
 title (1 line of 80 characters maximum)
 IAR     IWB     NOUT
 ENGNAM PICNAM
{ the following block contains the wing geometry variables }
 FMWB    FMWL    FMWT    FCWLHT FCWLFT FCWTFT FCWTHL EQWFH  LWFK    FBWS
 AWS     AWA     FBWA    UWBEF  BWH    QWLS
 NWP     NWFK    NWS
{ the following block contains the empennage geometry variables }
 ITAIL
 { this next block is read if a fin is to be synthesized }
 NFIN
 AEFN    UEFN    QEFL    QEF     REFFC  RTEF    FMEF    UEFF    MEF1K   MEF2K
 MEF3K   MEF4K   FCEFB
 { this next block is read if the horizontal tail is to be synthesized }
 AETN    UETN    QETL    RETSW  RTET    FMET    MET1K   MET2K   MET3K   FCETB
{ the following block contains general design constants }
 VD      AMMX    ULTN    MTTI   RMTTF   HTR     QFS     FFS     FBFCB   MTPR
 RFUL    MTOUF   FMF1    FMF2   SFAB    RXFICG  RXFTCG  LIIWLS  LBI2IS  LBI1PS
 RLTCL   RLTCA
{ the following block contains radome design constants }
 DAR     EDAR    GOF1    LAR    MAR     LAX1    MAX     RAX     LTH     GRFNH
{ the following block contains cockpit design information }
 ICKPT
 HC1     HC2     HC3     HC4    HC6     HCSEAT  LCFOOT  QCEYE1  QCEYE2  QCEYE3
 QCEYE4  QCSEAT  EHCS    ELCT   QCCAN   LCCAN   RCCAN   BCH     WCCAN   WCWSC
 MCI     MCP
{ the following block contains landing gear design constants }
 IUML    IUMW
 RMTLIF  FMUMK   FMUNK   FMUHK  MUMK    MUNK    MUHK    LULG1K  LULG2K  RLUNM
 FBUMWK  FDUMWK  FDUNWK  BUMWK  DUMWK   DUNWK   BUNW    FDUMW   FBUMW   FDUNW
 FBUNW   FVUMLK  VUMLBK  RLUPCW ELUP    RLUR
{ gun design constants }
 MGC     LGC     OGM     MGA    VGA     FOGMK
{ systems design variables }
 FMSAK   MSAK    FMSA    RSA    FVSA    FMSEK   MSEK    FMSE    FMSCK   MSCK
 FMSFK
```

```
{ engine bay clearances and intake diffuser design constants }
  FHP1K   EHP1S   EHP1H   FBP1K   EBP1S   EBP1H   FHP2K   EHP2S   EHP2H   FBP2K
  EBP2S   EBP2H   FHP3K   EHP3S   EHP3H   FBP3K   EBP3S   EBP3H
  IP      IRAMP
  ROIEI   FLIDK   AII     QID1    QID2    FBVIK   FLVK    FXII
{ aerodynamic design data }
  FQWTI   CLDES   FMD1    FMD2    RCDK    RCDVK   FDCLL   RCLTL
  NMA
  AERO(4,nma)     { array containing aerodynamic data:  Mach   (K1-K2)   CLCRIT   CLMAX }
{ external tanks, stores and pylons }
  MB1     MB2     MXP     MXT     MXTF    TSDQF   PYLDQF
  NMD
  STORES(5,nmd)   { array with drag data for stores as follows:
                    Mach   D/Q (store1)   D/Q (store2)   D/Q (pylons)   D/Q (tanks)  }
{ internal weapons bays and stores design constants }
  NWEPB   IMBI
  { this variable is read if internal weapons bays are to be synthesized }
  NTE
  { this block is read if a ventral weapons bay is present }
  NLB1I   NBB1I   NHB1I
  LB1I    BB1I    HB1I    LB1K    BB1K    HB1K    MB1I    ML1I
  { this block is read if outboard weapons bays are to be synthesized }
  NLB2I   NBB2I   NHB2I
  LB2I    BB2I    HB2I    LB2K    BB2K    HB2K    MB2I    ML2I
  { internal weapons bay mass estimation design constants }
  FMBBI1  FMBBI2  FMBBI3  FMBBI4  FMBBI5
{ reference engine design constants }
  NENG    INOZ
  TPGD1   MPFD1   MPAD1   OPJD1   MPFS1   LP12R   LP22AR  LP2A4R  LP34R   LP2B3R
  DP1R    DP2R    DP3R    DP4R    AP4     MPBR    MPRR    MPTR    FLP1K   FLP2K
  FLP3K   FLP4K   FMPBK   FMPRK   FMPIK
{ sortie requirement details }
  NSTOT   NSVHM1  NSVHM2  NSDS1   NSDS2   NSDT    NSUAM   FPST    STTIM   RRESF
  NSDS1I  NSDS2I
  KSS     SSDAT(4,nstot)    { array containing sortie requirements }
{ point performance requirement details}
  NPP     FMTSWL  LTTH    VTLH    GTCPH   FDBH    DMINC
  KPP1    KPP2    PPDAT(4,npp) - { array containing point performance details }  PPDAT15
{ costing and objective function coefficients }
  CSTR    CEQP    CAVC    CENG0   CENG1   CF1     CF2
```

B.3. Interpreting the Output Files

Upon completion of a run, the synthesis code in conjunction with the optimizer produces several output files. The most important one is the *RQPMIN* output file, which in this case is also used for the synthesis output. A sample is given in Appendix A. In addition to the *RQPMIN* problem information, the file contains a detailed listing of the aircraft geometry,

arranged in an easy to read format. The location of the information is largely self-explanatory and will not be described in detail here.

Several more output files are produced by the design synthesis. Table 18 lists these along with a short description of their contents.

File name	*Contents*
`trend.out`	User-defined parameters for quickly plotting trends of optimum parameters
`statna, statnb ... statnh`	Plots of the perimeters of the fuselage reference stations A through H, showing the extent of the cross-section scaling. These were included to aid development of the synthesis code.
`radome`	Plot of the cross-section at the rear of the radome
`graphics.pic`	Data for use by the graphical output program, generated only at the final point in an optimization run. The name of the output file is specified in the user input file.
`varfile`	See Table 16

Table 18: Synthesis Output Files

In order to use the ouput file `trend.out` the user must edit the file `outvar.f`, specifically the subroutine `fnlout`, and include in the `write` statement the required parameters. Similarly, the subroutine `outvar` can be edited by the user to include any parameters in the `write` statement for which a convergence plot is required. An example of how a convergence plot was used during program development is shown in Chapter 5. The files `trend.out` and *`varfile`* are created to allow easy portability to standard data analysis packages such as plotting programs or spreadsheets. Data is arranged in tabular form within these files in order to achieve this.

Appendix C: BEZIER SPLINES

This appendix describes the methodology used to fit Bezier splines to the fuselage cross-sections defined in Chapter 4. The relationships presented below were derived from a representation of Bezier splines given by (Foley et al, 1990).

Firstly, an array was defined as given in Table 19 which contains the four Bezier control points.

Point	x-coordinate	z-coordinate
1	SPL(1,1)	SPL(1,2)
2	SPL(2,1)	SPL(2,2)
3	SPL(3,1)	SPL(3,2)
4	SPL(4,1)	SPL(4,2)

Table 19: Definition of Array for Bezier Spline

Figure 71 shows how the points defined in Table 19 are calculated. Points 2 and 3 generally are located separately, but for ease of computation, it was decided to collocate them.

In the design synthesis code, two routines are defined: one to fit the Bezier spline given points 1 and 4 as well as the gradients of the lines joining 1 with 2 and 4 with 3, stored in G1 and G2, respectively, and another routine to evaluate the area enclosed between the reference axes and the Bezier curve. The latter routine differentiates between the area located above or below the curve, depending upon whether the Bezier is located below or above the x-axis.

More specifically, the subroutine BEZFIT obtains as paramers the array SPL as well as the gradients G1 and G2, and calculates the intermediate control points 2 and 3 from the following set of equations.

First, a check is made to prevent division by zero:

$$\text{DELTA}=G1 - G2 \tag{234}$$

If DELTA is not equal to zero, then

$$XX1 = \frac{Y2 - Y1 + G1 \cdot X1 - G2 \cdot X2}{\text{DELTA}} \tag{235}$$

and

$$YY1 = G1 \cdot (XX1 - X1) + Y1, \tag{236}$$

where X1 is equivalent to SPL(1,1), Y1 is equivalent to SPL(1,2), X2 is equivalent to SPL(4,1) and Y2 is equivalent to SPL(4,2). If DELTA is equal to zero, then

$$XX1 = \frac{X2 - X1}{2.0}$$

and

$$YY1 = \frac{Y2 - Y1}{2.0} \quad . \tag{237}$$

The values stored in XX1 and YY1 correspond to the x and y coordinates, respectively, of points 2 and 3.

In order to evaluate the area underneath the Bezier curve, the interval from X1 to X2 is divided into n equally spaced steps of size Δ:

$$\Delta = \frac{1.0}{n} \quad . \tag{238}$$

A series of function evaluations is made for each of the n steps using the Bezier polynomial defined in Equation 239:

$$X(t) = (1-t)^3 \cdot X_1 + 3t(1-t)^2 \cdot X_2 + 3t^2(1-t) \cdot X_3 + t^3 \cdot X_4 \quad . \tag{239}$$

Variable t is a value between 0 and 1 found by multiplying the ith step of the Bezier evaluation with Δ:

$$t = i \cdot \Delta \, . \tag{240}$$

Equation 239 can be evaluated for the y-coordinate by substituting X_1 through X_4 with Y_1 through Y_4. In this case, X_1 corresponds to SPL(1,1), X_4 corresponds to SPL(4,1), and so on. The area and perimeter calculations are performed using a simple trapezoidal integration scheme, as shown schematically in Figure 71, where dA is the increment in area.

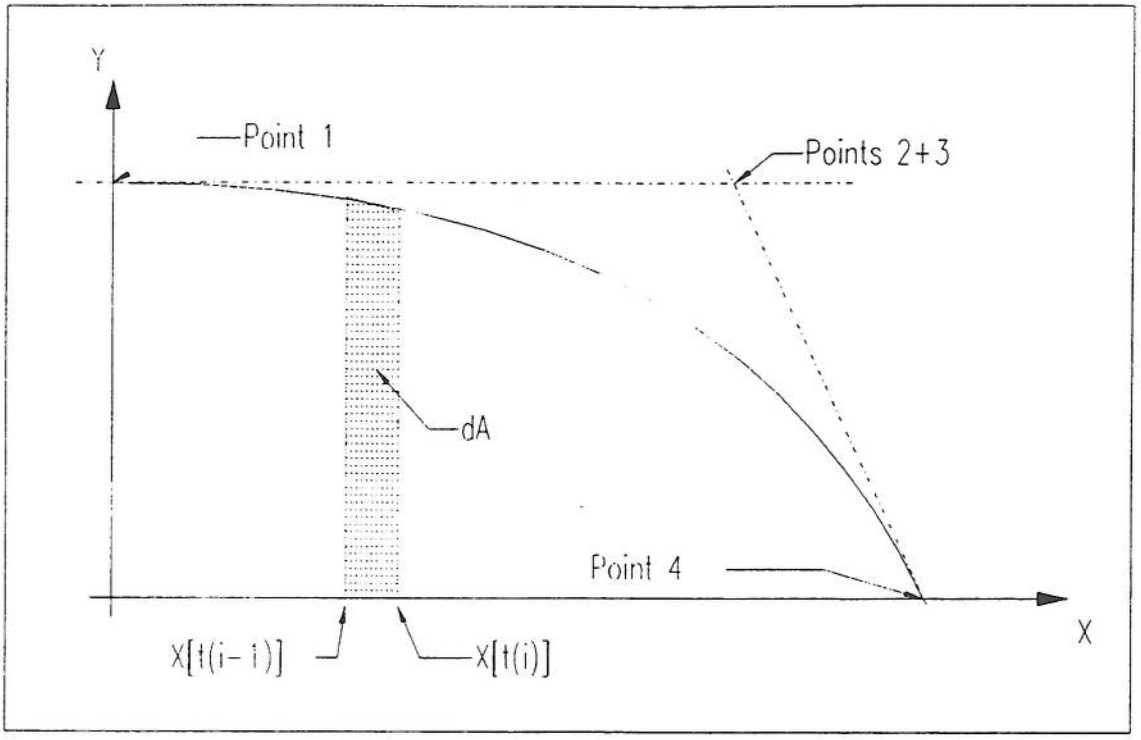

Fig. 71: Geometry Definition for Bezier Splines

Appendix D: SUPERELLIPSES

This appendix describes the algorithm used to fit a superellipse to a given fuselage station.

As described in the main text of this report, a fuselage station making use of superellipses is divided into sections such that the coefficients describe the curve in one quadrant of the Cartesian coordinate system only. The basic superellipse equation is

$$\left(\frac{x}{a}\right)^{2+m} + \left(\frac{y}{b}\right)^{2+n} = 1 \ , \tag{241}$$

and the corresponding geometrical interpretation is given by Figure 72 below. In Equation 241, m and n are parameters which control the shape of the curve in the 1st quadrant of the coordinate system.

An array was defined which contains the coefficients a, b, m, and n of the superellipse as well as the location of the origin. a and b, the semiaxes of the ellipse, are chosen to match the geometry requirements of each individual fuselage station. Table 20 shows how the coefficients are allocated to the array variable fields within the program code.

Field	Function
(1,1)	X-coordinate of origin
(1,2)	Y-coordinate of origin
(2,1)	semiaxis A (x-axis)
(2,2)	semiaxis B (y-axis)
(3,1)	m in exponent of x-coordinate
(3,2)	n in exponent of y-coordinate

Table 20: Definition of superellipse array

In order to evaluate the area enclosed by the curve and the vertical and horizontal axis as well as the perimeter of the superellipse section, Equation 241 is rewritten to obtain

$$y = b \cdot \left[1 - \left(\frac{x}{a}\right)^{2+m}\right]^{\frac{1}{2+n}} \ . \tag{242}$$

By dividing the x-axis into a series of equally spaced intervals, a simple numerical, trapezoidal integration scheme is used to evaluate the enclosed area and the perimeter.

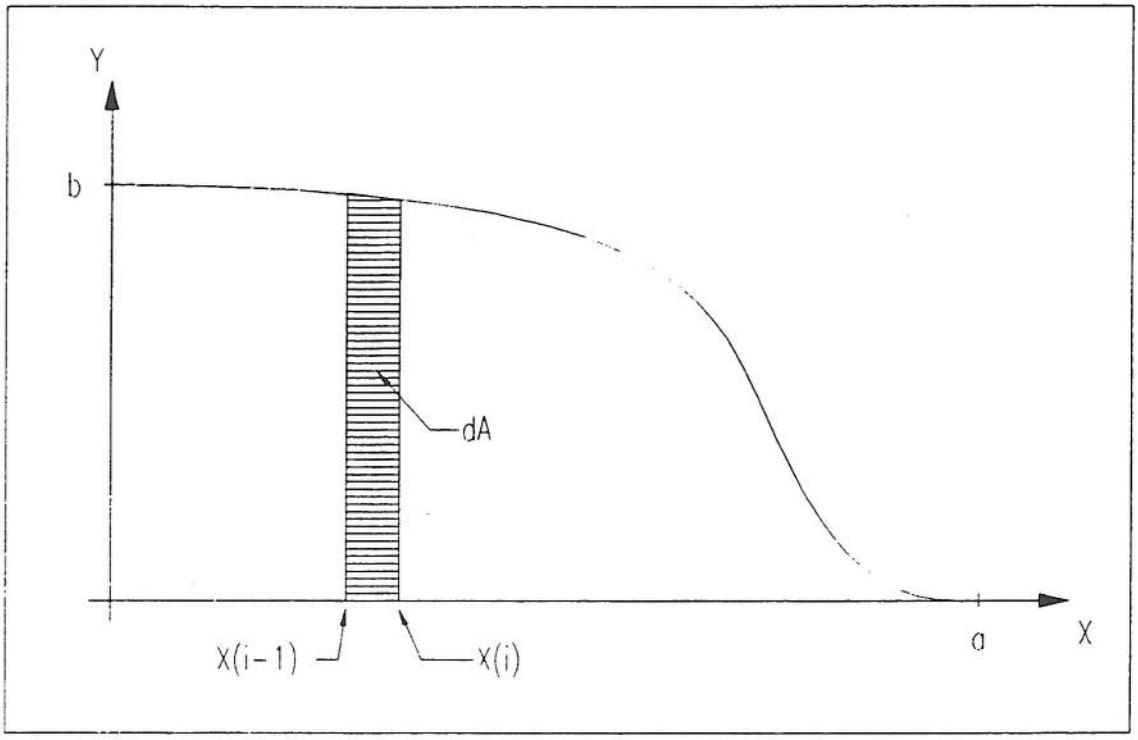

Fig. 72: Schematic Definition of Superellipse Geometry